



# Characterisation of sericitic alteration at the Taca Bajo porphyry Cu deposit, Argentina

by

Sebastian Benjamin Benavides Kolind-Hansen (B.Sc. Geol. Eng.)

CODES ARC Centre of Excellence in Ore Deposits

Submitted in fulfilment of the requirements for the Master of Economic Geology

University of Tasmania, June, 2017

### **Declaration of Originality**

This thesis contains no material which has been accepted for a degree or diploma by the University or any other institution, except by way of background information and duly acknowledged in the thesis, and to the best of my knowledge and belief no material previously published or written by another person except where due acknowledgement is made in the text of the thesis, nor does the thesis contain any material that infringes copyright.

Sebastian Benavides

Date:

### **Authority of Access**

This thesis is not to be made available for loan or copying for two years following the date this statement was signed. Following that time, the thesis may be made available for loan and limited copying and communication in accordance with the Copyright Act 1968.

Sebastian Benavides

Date:

## Acknowledgements

This thesis wouldn't have been possible without the support received from First Quantum Minerals Ltd. I'd like to begin thanking Mike Christie for constantly supporting my professional development ever since I joined FQM and giving me the opportunity to grow as a geologist. I'd also like to thank Tim Ireland for all the technical and professional guidance and editorial support received regarding this manuscript and all other projects I endeavour into. Markku Lappalainen has been key in allowing me enough flexibility and support at work to be able to get the thesis and courses done while working a full-time job.

I'd also like to thank the FQM team involved in Taca Taca Bajo exploration, in particular Guillermo Almando and Santiago Gigola for the discussions, guidance and feedback received, as well as for taking the time to discuss historical data and regional interpretations.

At Utas, I'd like to thank David Cooke, not only for being a great supervisor and providing thorough edits and observations on the manuscript, but also for always being available to guide me in the right direction during my time there. I'd also like to thank Rob Scott for the immense support throughout the whole Master's programme. I am grateful for the assistance provided by Lejun Zhang, Sebastien Meffre, Leonid Danyushevsky, Ivan Belousov, Jay Thompson, Ayesha Ahmed, Karsten Goemann and Sandrin Feig with the operation of laboratory equipment and processing of data.

# Table of Contents

List of Tables .....	iv
List of Figures .....	iv
Abstract.....	vi
1. Introduction .....	1
1.1 Porphyry Copper Deposits .....	1
1.2 Sericitic Alteration in Porphyry Copper Deposits .....	2
1.3 Sericite Description and Chemistry.....	4
1.4 Objective .....	6
2. Taca Taca Bajo Porphyry Copper Deposit .....	10
2.1 Location.....	10
2.2 Exploration History .....	11
2.3 Regional Geology and Structural Setting .....	12
2.3.1 Tectonic and Metallogenic Setting .....	12
2.3.2 Geology of the Puna Region.....	15
2.4 District Geology.....	17
2.5 Local Geology .....	18
2.5.1 Lithology.....	18
2.5.2 Veining, Alteration and Mineralisation.....	22
2.5.3 Paragenesis .....	25
3. Phyllitic Alteration at Taca Taca Bajo .....	27
3.1 Methodology.....	27
3.1.1 Sampling.....	27
3.1.2 Spectral Analysis .....	29
3.1.3 Petrography .....	29
3.1.4 Scanning Electron Microprobe (SEM) and Electron Probe Microanalysis (EPMA) .....	29
3.1.5 Laser Ablation Inductively Coupled Plasma Mass Spectrometry (LA-ICPMS).....	30
3.1.6 Potassium Feldspar Staining .....	31
3.1.7 Quartz Cathodoluminescence (CL).....	31
3.2 Sample Descriptions.....	31
3.2.1 Background Samples .....	31
3.2.2 Green Sericite Samples .....	33
3.2.3 Mixed Sericite Samples .....	34
3.2.4 White Sericite Samples .....	37
3.3 Sulfide Characterisation .....	37
3.4 Sericite Characterisation .....	39

3.4.1 Textural Characterisation.....	39
3.4.2 Analytical Characterisation .....	42
3.4.3 High sulfidation overprint .....	47
3.5 Apatite, Monazite and Xenotime Geochronology .....	51
3.6 Quartz Characterisation .....	52
3.6 Phyllitic Overprint on Potassic alteration.....	54
4. Interpretation and Discussion.....	58
4.1 Alteration Paragenesis .....	58
4.2 Deposit scale integration .....	61
4.3 Implications for porphyry ore formation .....	65
4.4 Exploration Implications .....	67
References .....	68
Appendix 1: SEM analytical results and interpreted mineralogy	
Appendix 2: LA-ICPMS normalised analytical results for ablated sericite sites	
Appendix 3: LA-ICPMS normalised analytical results for ablated apatite, xenotime and monazite sites.	

## List of Tables

Table 1.1: Typical substitutions into the muscovite crystal structure and their associated phyllosilicate species.....	7
Table 2.1: Exploration history at Taca Taca Bajo .....	11
Table 3.1: Sample Descriptions and Locations .....	28

## List of Figures

Figure 1.1: Schematic, generalised alteration model for porphyry Cu deposits .....	3
Figure 1.2: Schematic representation of fluid characteristics and alteration products in the life of a single porphyry system .....	5
Figure 1.3: Ideal muscovite arrangement .....	5
Figure 1.4: Phase diagram at 1kbar, showing the stability fields for different silicates with changes in temperature and pH .....	8
Figure 2.1: Location of the Taca Taca District with relation to major cities and deposits in Argentina and Chile .....	10
Figure 2.2: Eocene to early Oligocene belt of Northern Chile and Southern Peru, showing the location of Taca Taca Bajo in relation to contemporary deposits .....	13
Figure 2.3: Miocene metal distribution map in the Puna province .....	14
Figure 2.4: Geology of the Puna region showing the location of Taca Taca Bajo, Modified from Alonso and Viramonte (1987).....	16
Figure 2.5: Geology of the Taca Taca District. ....	18
Figure 2.6: Geological Map of the Taca Taca Bajo deposit.....	19
Figure 2.7: Lithologies of the Taca Taca Bajo deposit.....	20
Figure 2.8: Alteration and veining in Taca Taca Bajo .....	21
Figure 2.9: Cu, Fe and S distribution per lithology at Taca Taca Bajo.....	22
Figure 2.10: A) Alteration zonation interpreted from geochemical assays.....	24
Figure 2.11: Section 7288750N through the Taca Taca Bajo orebody .....	25
Figure 2.12: Schematic paragenetic sequence for the Taca Taca Bajo orebody .....	26
Figure 3.1: Location of drill-holes sampled in this study .....	27
Figure 3.2: Background samples .....	32
Figure 3.3: Green sericite samples.....	34
Figure 3.4: Mixed green and white sericite Samples .....	36
Figure 3.5: White sericite samples.....	38

Figure 3.6: Transmitted light microscope images from laser mounts showing sulfide textural relationships.....	40
Figure 3.7: SEM textural variation in sericite.....	41
Figure 3.8: Chlorite-muscovite-K feldspar-biotite GER (CMKB) diagram showing the different geochemical trends for the variations in sericite texture.....	43
Figure 3.9: Chlorite-muscovite-K feldspar-biotite GER (CMKB) diagram showing the LA-ICPMS geochemistry of sericite sites from samples with logged white, green or mixed sericite. ....	44
Figure 3.10: Chlorite-muscovite-K feldspar-biotite GER (CMKB) diagram coloured by the w2200 scalar on sericite samples .....	45
Figure 3.11: Chlorite-muscovite-K feldspar-biotite GER (CMKB) diagram of sericite analysis coloured by the whole rock Cu (%) assay of the 2-meter interval where it belongs .....	47
Figure 3.12: Trace element geochemistry of analysed sericite samples, coloured by the sericite type logged.....	48
Figure 3.13: Trace element geochemistry of analysed sericite samples, coloured by the sulfide assemblage recognised on the mount.....	49
Figure 3.14: Effect of high sulfidation overprint on granite-hosted sericite trace element geochemistry.....	50
Figure 3.15: Concordia plot for monazite and xenotime U/Pb dating by LA-ICPMS. ....	51
Figure 3.16: Quartz CL images .....	53
Figure 3.17: Background, fresh granite samples after K-staining .....	55
Figure 3.18: Samples with strong muscovite-pyrite assemblage on granite after K-staining .....	56
Figure 3.19: Samples with dominant phengite-chalcopyrite assemblages in granite after K-staining	57
Figure 4.1: Proposed paragenesis of the Taca Taca Bajo orebody. ....	60
Figure 4.2: Deposit scale view of w2200 (sericite composition) scalar on Terraspec ASD data.....	62
Figure 4.3: Zn enrichment in Taca Taca Bajo assay data. ....	63
Figure 4.4: Logged alteration shown in comparison with 0.25% Cu shell and modelled rhyodacite porphyry stock . .....	64
Figure 4.5: Surface projection of the potassic, phengitic and muscovitic alteration overlain on surface geology.....	65

## Abstract

The Taca Taca Bajo porphyry Cu deposit contains 2,165 Mt at 0.57% Cu Eq. It is located in the province of Salta, in north-western Argentina. It was emplaced in the back-arc of the Chilean Eocene-Oligocene porphyry belt, and localised by WNW trending cross-arc lithospheric structures. Multiple phases of syn-mineralization Oligocene ( $29.30 \pm 0.57$  Ma) rhyodacite porphyritic intrusives have been recognized, although most of the mineralisation is hosted in the Taca Taca Silurian granite batholith host.

Green sericite has been observed at Taca Taca Bajo to be spatially associated with Cu mineralisation and thought to be part of the phyllitic assemblage, occurring together with white sericite. A combination of petrography, spectrometry, scanning electron microprobe (SEM) and laser ablation inductively coupled plasma mass spectrometry (LA-ICPMS), has shown that the green sericite in Taca Taca Bajo is phengite, and occurs as fine grained, shaggy replacements of pre-existing secondary biotite and orthoclase. White sericite, on the other hand, occurs as a late, pervasive alteration of coarse, bladed muscovite which overprints and destroys all pre-existing alteration and mineralisation. Spectral data suggests that phengite crystallised at higher temperature and pH than muscovite, and is interpreted to be a temporal transition stage between potassic and phyllitic alteration. Chalcopyrite was introduced during the early potassic and phengite alteration phases. The later muscovitic stages were ore-destructive, with chalcopyrite replaced by pyrite and, as the system cooled, a pyrite – bornite – chalcocite – covellite high sulfidation state assemblage.

Phengite has been reported previously in porphyry Cu deposits, typically as an outer, lower temperature alteration mineral. In the case of Taca Taca Bajo, phengite appears to be analogous to sericite – chlorite – clay (SCC) alteration documented elsewhere, with a compositional variation potentially due to the felsic nature of the host rocks. Using systematic spectral measurements and whole rock assay data, it is possible to map the area where phengite has overprinted pre-existing potassic alteration.

# 1. Introduction

## 1.1 Porphyry Copper Deposits

Porphyry deposits are of paramount importance to economic geology, as they host most of the world's copper and much of the molybdenum and gold resources. They are distributed widely across the world, mostly in convergent margin terranes (Sillitoe, 2010). These deposits are formed within and around causative hypabyssal porphyritic intrusions (Proffett, 2009) and typically represent high tonnage and low grade resources (Seedorff et al. 2005; Sillitoe, 2010).

Spatially, porphyry deposits tend to form in clusters within active to waning magmatic arcs; a characteristic clearly demonstrated in the South American Andes (Haschke et al., 2002; Sillitoe and Perelló, 2005; Singer et al., 2005; Sillitoe, 2010). The position of these clusters are inferred to be controlled by structural permeability and world class deposit clusters tend to be related to long-lived cross-arc lithospheric structures (Richards et al., 2001; Gow and Walshe, 2005; Singer et al., 2005; Palacios et al., 2007; Sillitoe, 2010).

Porphyry Cu deposits are also controlled in time by specific tectonic events. Stress changes in the subduction zone are interpreted as catalysts for porphyry ore formation in zones of compression, crustal thickening, uplift and exhumation (Cooke et al., 2005; Sillitoe, 2010). In the case of Andean deposits, these events are related to the onset of different orogenic events (Noble and McKee, 1999) and to the subduction of aseismic ridges or plateaux (Rosenbaum et al., 2005; Hollings et al., 2005), and/or subduction of major seafloor transforms (Richards and Holm, 2013)

Wall rock alteration around major porphyry copper deposits affects several cubic kilometres of rock (Lowell and Guilbert, 1970; Sillitoe, 2010). For this reason, exploration geologists have typically used alteration models to navigate different types of wall rock alteration in the search of the core of the hydrothermal system. Recent work has been focused on understanding distal alteration patterns at trace level geochemical variations (Chang et al., 2011; Cooke et al., 2015; Halley et al, 2015; Wilkinson et al., 2015).

Veins and alteration assemblages are typically zoned within the causative intrusion and encompassing host rocks, and their relation to sulfide abundance and mineralogy (and hence

to ore) has been the subject of intense research. Recent detailed descriptions of these features are provided by Seedorff et al. (2005, 2008), Sillitoe (2010), and references therein. The alteration model provided by Sillitoe (2010; Fig. 1.1) shows a deep, barren sodic calcic alteration phase, which transitions upwards to a core potassic alteration (main ore contributor) and laterally into propylitic alteration, characterised by chlorite, epidote, albite and actinolite. During the waning stages of the porphyry hydrothermal system these early assemblages are overprinted by cooler, acid fluids, which generate phyllosilicate minerals that define a “phyllitic” alteration zone. This zone is in some cases related to ore, but is much more commonly barren (e.g. Sillitoe and Gappe, 1984).

## 1.2 Sericitic Alteration in Porphyry Copper Deposits

Phyllitic alteration was described by Lowell and Guilbert (1970) as an overprinting alteration assemblage consisting of quartz, sericite, pyrite, hydrated micas, minor chlorite and trace rutile. This alteration assemblage, or variations of it defined by the presence of phyllosilicate minerals has since been recognised as a fairly consistent aspect of the zoned alteration that overprints and surrounds the potassic altered core of porphyry copper hydrothermal systems, though there are substantial variations in terms of the metal input and/or destruction patterns in different deposits (Lowell and Guilbert, 1970; Rusk et al., 2008; Sillitoe, 2010; Perelló et al., 2012). Phyllitic alteration will form at temperatures between 550° C to 250° C, within the muscovite and illite stability field (Seedorff et al., 2005). Sillitoe (2010) divides this acid overprint into two members: sericite – clay - chlorite (SCC) alteration and sericitic alteration (phyllitic).

SCC alteration is common to the upper regions of ore bodies and is commonly related to Cu grades, as it is considered the upward continuation of potassic alteration. This alteration is characterised by replacement of mafic minerals to chlorite and feldspars to sericite, together with pyrite and chalcopyrite deposition (Sillitoe, 2010). Quartz - hematite (after magnetite) – chalcopyrite - pyrite veins with sericite - chlorite halos are common in this alteration assemblage, and they are considered to be the upward continuation of potassic early, dark micaceous veins (Rusk et al., 2008).

Phyllitic alteration overprints potassic and SCC alteration, typically extending from the outer edge of the potassic ore zone, defining a pyrite-rich halo adjacent to propylitic alteration (Sillitoe, 2010). It is characterised by widespread, pervasive white sericite that occurs as halos and coalesced halos to quartz - pyrite veinlets, and typically replaces all pre-existing silicates and sulfides (Lowell and Guilbert, 1970; Sillitoe, 2010).

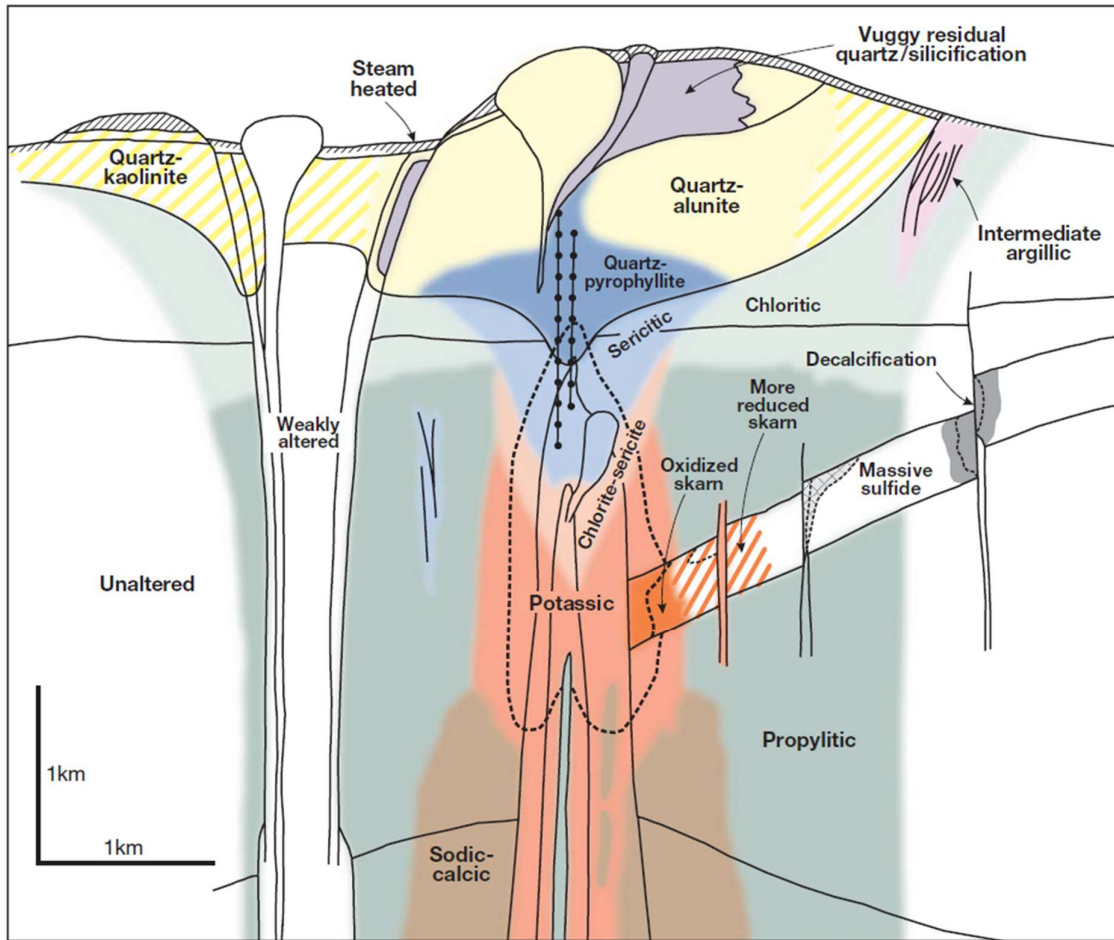


*Figure 1.1: Schematic, generalised alteration model for porphyry Cu deposits. This model is for a telescoped system, but the sericitic and chlorite-sericite overprint on potassic and propylitic alteration is also common without a significant degree of telescoping. (Sillitoe, 2010)*

Less common grey-green sericitic assemblages have been documented in different deposits as part of the phyllitic alteration assemblage. ‘Green sericite’ is somewhat of a bucket terminology in the exploration community. When described and studied, this term encompasses several different textures, compositions and relationships to ore. In Chuquicamata, green sericite occurs within the ore zone and is related to Cu sulfides

(Ossandon et al., 2001); while at Los Pelambres, it is found in the outer phyllitic zones, has a phengite composition and only a minor relationship to Cu sulfides (Perelló et al., 2012). Alva (2011) reported both phengitic green sericite distal to the main ore zone and green-white sericite - chlorite alteration as halos to ore bearing veins in the Highland Valley district. The porphyry model of John et al. (2010) suggest a distal phyllitic assemblage of Fe-rich sericite (phengite) which is also commonly logged as green sericite. This later model matches the systematic increase in 2200 wavelength spectral absorption feature in white micas outboard of porphyry deposits described by Halley et al. (2015).

As the fluids responsible for sericitic alteration cool down, acidity and sulfidation state increases, hence the later stages of sericitic alteration might be stable with high sulfidation sulfide assemblages such as bornite – pyrite – covellite - digenite (Fig. 1.2; Sillitoe, 2010), whereas earlier sericitic assemblages can be stable with respect to chalcopyrite - pyrite.

### 1.3 Sericite Description and Chemistry

Sericite is field terminology for fine grained K-bearing mica and clay (Seedorff et al., 2005), particularly the muscovite compositional variation. It is commonly used given the difficulty of differentiating fine grained muscovite, phengite, illite and paragonite in the field with a hand lens.

Micas are composed of stacked layers of octahedral sheets bound by tetrahedral sheets in a “t-o-t” arrangement (Fig. 1.3; Klein and Dutrow, 2008). The muscovite formula is  $KAl_2(AlSi_3O_{10})(OH)_2$ , where the  $K^+$  cation site is located between each “t-o-t” layer (Deer et al, 2003; Alva, 2011). When Si substitutes for Al in the tetrahedral sites of the  $SiO_5$  sheets, the “t-o-t” layers become more neutral and lack the need of an interlayer cation, forming clays like talc ( $Mg_3Si_4O_{10}(OH)_2$ ) or pyrophyllite ( $Al_2Si_4O_{10}(OH)_2$ ; Klein and Dutrow, 2008).

Illite ( $((K,H_3O)(Al,Mg,Fe)_2(Si,Al)_4O_{10}[(OH)_2,(H_2O)])$ ) is characterised by random, partial substitution of Al by Si in the tetrahedral site, where occasional interlayer cations sites are occupied and molecular water is introduced, producing an alkali-deficient mineral with

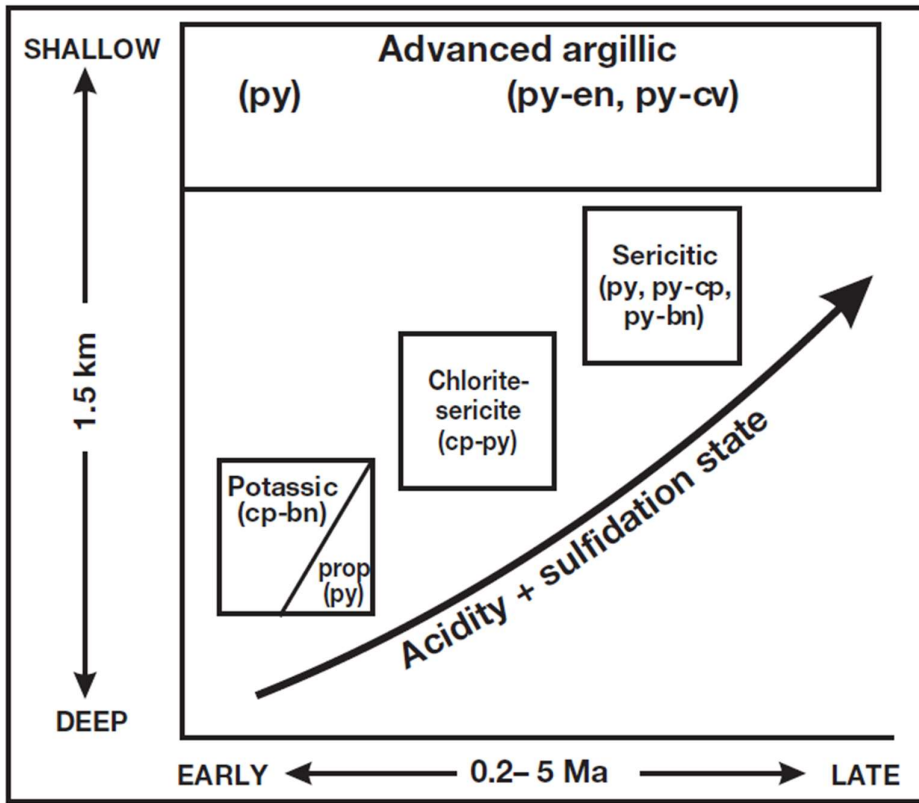


Figure 1.2: Schematic representation of fluid characteristics and alteration products in the life of a single porphyry system. Note the SCC (sericite-chlorite) alteration is stable with chalcopyrite-pyrite and sericitic alteration is stable with regard to pyrite, minor chalcopyrite and high sulfidation assemblages (Sillitoe, 2010).

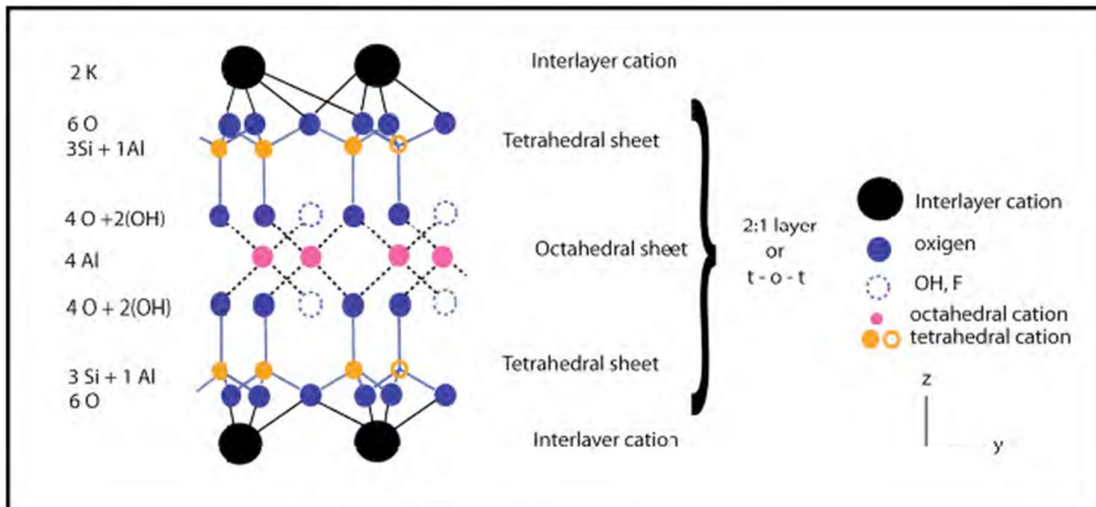


Figure 1.3: Ideal muscovite arrangement. Note the “t-o-t” sheets typical of phyllosilicates, in the case of muscovite bounded by K as an interlayer cation (Alva, 2010; after Deer et al., 2003).

properties of both clay and mica group minerals (Meunier and Velde, 2004; Klein and Dutrow, 2008).

Typical substitutions in the muscovite composition are Na, Rb and Cs for the K<sup>+</sup> interlayer cation site, Mg, Fe<sup>2+</sup>, Fe<sup>3+</sup>, Li, Mn, Ti and Cr for the octahedral Al site and F for the OH site (Klein and Dutrow, 2008; Table 1.1). These element substitutions may occur due to the breakdown of pre-existing muscovite or due to a geochemical input from the pre-existing mineral being altered to sericite. Since different sericite species are stable at different pH and temperature conditions, general paragenetic interpretations can be made.

Potassium feldspar is stable at higher pH and temperature conditions than muscovite (Fig. 1.4). As the hydrothermal system cools and becomes more acid, feldspars can be replaced by muscovite and other K-bearing micas, together with quartz. On the transition towards intermediate argillic alteration, illite is stable at 300-250° C (Seedorff et al., 2005; Alva, 2011).

## 1.4 Objective

Green sericite has been used at the Taca Taca Bajo porphyry Cu deposit, Argentina, to describe a grey-green mica that occurs commonly within the ore zone. This particular sericite type shows a strong correlation with chalcopyrite and chalcopyrite - pyrite assemblages and coexists with a white sericite overprint of potassic alteration. Two hypotheses were presented by the company currently exploring the property, First Quantum Minerals (FQM), for the nature of the green sericite. The first hypothesis is that it is of phengite composition and formed synchronous with white sericite, which would be in agreement with the observations made at Los Pelambres (Perelló et al., 2012) and with observations made by John et al. (2010). The disagreement lies that in both of these cases, phengite is characterised as a distal, lower temperature mica that is not related to ore deposition, whereas the opposite relationship is in fact observed in Taca Taca Bajo. The second hypothesis is that the green sericite is a mixture of fine grained muscovite and chlorite, as part of a transition from potassic to phyllitic

Structure	Substitution	Species	Formula	Remarks
Interlayer cation: K <sup>+</sup>	K <sup>+</sup> = Na <sup>+</sup>  K <sup>+</sup> = Ca <sup>2+</sup> K <sup>+</sup> = Ba <sup>2+</sup>  K <sup>+</sup> = Rb <sup>+</sup> , Cs <sup>+</sup> , Sr <sup>2+</sup> , Ti <sup>3+</sup>  K <sup>+</sup> = NH <sub>4</sub> <sup>+</sup> K <sup>+</sup> = □	Paragonite  Margarite Oellacherite  Illite	NaAl <sub>2</sub> □AlSi <sub>3</sub> O <sub>10</sub> (OH) <sub>2</sub> K<0.15; Ca<0.11  CaAl <sub>2</sub> □(Al <sub>2</sub> Si <sub>2</sub> O <sub>10</sub> (OH) <sub>2</sub> [Ba <sub>0.5</sub> (Na,K) <sub>0.5</sub> ]Al <sub>2</sub> (Si <sub>2.5</sub> Al <sub>1.5</sub> O <sub>10</sub> ) (OH) <sub>2</sub>  Rb may be up 1%; Rb may be up to 5%; Sr reported 0.0025-0.013%  Rare; the presence of hydronium is not well documented.  Deficient K-bearing mica	Commonly low. If Na ≈ 1 pfu, it is considered to be a Na-rich muscovite or paragonite.  If Ca is close to 1 pfu Ba substitution can be considerable; named when Ba-rich mica >11%
Tetrahedral cation: <sup>[4]</sup> AlSi <sub>3</sub>	[ <sup>4</sup> ]Al <sup>3+</sup> = Si <sup>4+</sup>			
Octahedral cation: <sup>[6]</sup> Al	Al <sup>3+</sup> = Fe <sup>2+</sup> , Fe <sup>3+</sup>  1.-phengite substitution: Fe <sup>2+</sup> +Si <sup>4+</sup> = <sup>[6]</sup> Al <sup>3+</sup> + <sup>[4]</sup> Al <sup>3+</sup>  2.-ferrimuscovite substitution: Fe <sup>3+</sup> = <sup>[6]</sup> Al <sup>3+</sup>  3.- Fe couple with Ti: Fe <sup>2+</sup> +Ti <sup>4+</sup> =2 <sup>[6]</sup> Al <sup>3+</sup>  4.- <sup>[4]</sup> Fe <sup>3+</sup> = <sup>[4]</sup> Al <sup>3+</sup>  5.- (Fe <sup>2+</sup> ) <sup>[6]</sup> +H <sup>+</sup> =(Fe <sup>3+</sup> ) <sup>[6]</sup> + □ Al <sup>3+</sup> = Mg <sup>2+</sup> Phengite substitution: <sup>[4]</sup> (Mg <sup>2+</sup> , F <sup>-</sup> ) <sup>[2]</sup> = <sup>[4]</sup> Al <sup>3+</sup> , <sup>[6]</sup> Al <sup>3+</sup>  Al <sup>3+</sup> = Cr <sup>3+</sup> Al <sup>3+</sup> = Li <sup>+</sup> Al <sup>3+</sup> = Ti <sup>4+</sup> Al <sup>3+</sup> = Mn <sup>2+</sup> Al <sup>3+</sup> = V <sup>3+</sup> Al <sup>3+</sup> = Ni <sup>2+</sup>	Phengite  Fuchsite  Lepidolites	K <sub>2</sub> (Fe <sup>3+</sup> Al <sub>3</sub> )(Al <sub>2</sub> Si <sub>6</sub> O <sub>20</sub> )(OH) <sub>2</sub> K(Al,Fe <sup>3+</sup> )Al <sub>1-x</sub> (Mg,Fe <sup>2+</sup> ) <sub>x</sub> [Al <sub>1-x</sub> Si <sub>3+x</sub> O <sub>10</sub> ](OH) <sub>2</sub> K(Li,Al) <sub>3</sub> (Si,Al) <sub>4</sub> O <sub>10</sub> (F,OH) <sub>2</sub>	X = 1-3  If Cr>6%; commonly in ultramafic rocks Commonly <0.1 wt% Lepidolite if Li > 3.6% Comonly ≈ 0.08 pfu. Ti > 0.05 pfu is common in metamorphic rocks.  Commonly < 1 wt% V-rich muscovite Maximum 2 wt% in Fuchsite
Anion Site: (OH)	OH <sup>-</sup> = (□)  OH = F <sup>-</sup> , O, Cl <sup>-</sup>	Vacancies	KV <sub>2</sub> □[AlSi <sub>3</sub> O <sub>10</sub> ](OH) <sub>2</sub>	Principal substituents for the OH  Minor substitution

Table 1.1: Typical substitutions into the muscovite crystal structure and their associated phyllosilicate species. Redrafted from Alva (2010); after Bailey (1984), Muñoz (1984), Guidotti (1984), Deer et al. (1992), Dahl et al. (1993), Guidotti and Sassi (1998), Deer et al. (2003) and Rieder (2001).

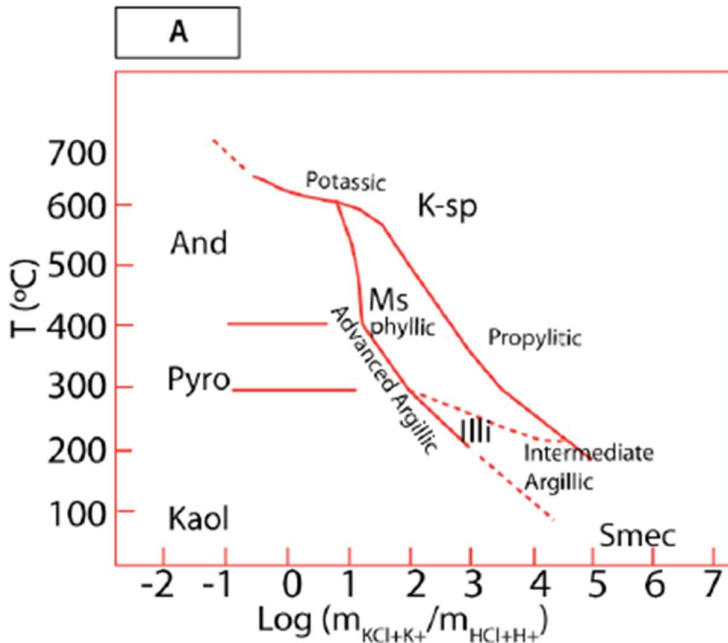


Figure 1.4: Phase diagram at 1kbar, showing the stability fields for different silicates with changes in temperature and pH. Potassic alteration occurs at the K-feldspar stability field and as the system cools, muscovite becomes stable and replaces K-feldspar and plagioclase. If fluids become buffered by wallrock interaction, they will transition to intermediate argillic as they cool, if they are not buffered, they will eventually become stable with advanced argillic alteration. Redrafted by Alva (2010) after Seedorff et al. (2005).

alteration (Fig. 1.2). Prior to this study, this was the main working hypothesis at Taca Taca Bajo, although the chlorite had not been identified through petrography or other means.

The first objective of this study is to understand compositional and textural differences between the logged green and white sericite and their relationships with potassic alteration and main stage mineralisation. It is hoped that this will allow for better understanding of the ore controls at Taca Taca Bajo, and also for development of a more accurate paragenetic sequence.

The second objective is to use petrographic analysis to extrapolate to material classification at the deposit scale. It may be that a better understanding on sulfide and silicate speciation, and relationships to gangue mineralogy may prove helpful when the project reaches a production stage. This study therefore combines two-meter interval assay data with point

spectrometry data with trace element geochemistry to model different sericite appearances at a deposit scale.

The final objective of this study is to contribute to the current understanding of the grey-green sericite reported by Sillitoe (2010) which has been reported in several deposits but within different regions in the deposit model. This further understanding will provide future explorers with more information to make accurate interpretation when encountering green sericite in porphyry copper deposits.

## 2. Taca Taca Bajo Porphyry Copper Deposit

### 2.1 Location

The Taca Taca Bajo deposit is located in the Salta province, 230 kilometres west of the city of Salta, in the Puna region of north-western Argentina (Fig. 2.1). The deposit is located 25 kilometres from the Chilean border and roughly 150 kilometres east-southeast of the La Escondida porphyry Cu deposits in Chile. The closest town and accommodation is Tolar Grande, which is located on the opposite edge of the Salar de Arizaro, 35 kilometres east of Taca Taca Bajo.

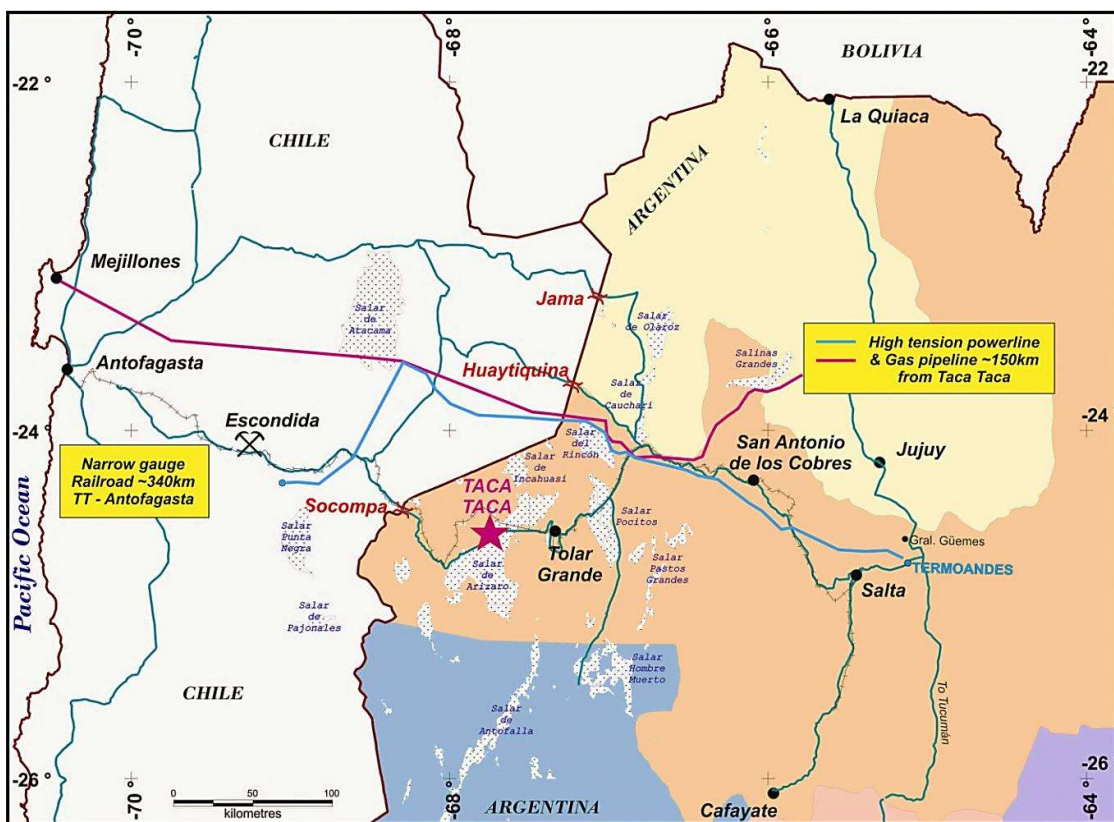


Figure 2.1: Location of the Taca Taca District with relation to major cities and deposits in Argentina and Chile (Scott et al., 2013).

## 2.2 Exploration History

The porphyry deposit was discovered by Fabricaciones Militares, a state-owned company, in 1967 and has since been explored by Falconbridge Argentina S.A., Gatro Argentina Minera S.A., BHP Minerals, Corriente Resources, Rio Tinto, Global Copper, Lumina Copper and its current owner, First Quantum Minerals Ltd (Almadox, 2015). Though the project was drilled by many companies through that time, geological models, adverse commodity prices and varying exploration strategies had a strong influence on the lack of definition of an economic resource at Taca Taca Bajo until 2010, when Lumina Copper had enough economic intercepts to plan a starter pit and pursue definition of the current sulfide indicated resource of 2,165 Mt at 0.57% CuEq (0.44% Cu, 0.08 g/t Au, 0.013% Mo; cut-off grade of 0.3%; Scott et al., 2013).

Overall, Taca Taca Bajo has a modern exploration history spanning at least 45 years, during which time 163,537 meters have been drilled in 400 drill holes (Table 2.1; Almadox, 2015).

COMPANY	YEAR	TARGET	ACTIVITIES	TOTAL METRES DRILLED
FABRICACIONES MILITARES	1967	Cu Porphyry	First mapping	
FALCONBRIDGE	1975	Cu Porphyry	3 short holes	529
GENCOR	1994	Au structures – Cu Porphyry	18 short holes	1,603
BHP	1996-1997	Supergene enrichment blanket	33 diamond drill holes - mapping -geophysic -	11,483
CORRIENTE	1998-1999	Exotic Cu and Cu-Au structures	93 holes	7,674
RIO TINTO	1999	In-situ Copper oxides	7 RC holes	3,338
GLOBAL COPPER	2002	Supergene enrichment blanket	No field work	
RIO TINTO	2008	High-grade hypogene mineralization	8 diamond drill holes	4,877
LUMINA COPPER/CORRIENTE ARG.	2010-2012	Supergene enrichment and high-grade deep <del>hypogene</del> mineralization.	273 diamond drill holes + RC holes	134,033
				Total drilled: 163,537 m

Table 2.1: Exploration history at Taca Taca Bajo (Almadox, 2015).

## 2.3 Regional Geology and Structural Setting

### 2.3.1 Tectonic and Metallogenic Setting

The Oligocene porphyry Cu deposits and occurrences in northwestern Argentina are related to the Eocene-Oligocene metallogenic belt of Chile and Peru (Fig. 2.2). An eastern bulge was included in the metallogenic belt by Sillitoe and Perelló (2005) - this was specifically drawn to incorporate Taca Taca Bajo within the magmatic arc. Mineral occurrences in the Puna region occur along WSW-trending lineaments, which are characterised by volcanic breakouts of the main arc that are inferred to have utilised lithospheric-scale cross arc structures (Alonso and Viramonte, 1987; Richards et al., 2000; Chernicoff et al., 2002). Alonso and Viramonte (1987) mapped these lineaments for Miocene volcanic strata and showed the characteristics that defined them (Fig. 2.3). Note that Taca Taca Bajo is not located within one of these lineaments. The structure controlling the emplacement of Taca Taca Bajo does not seem to have been active in the Miocene.

These cross-arc structures has been inferred to control porphyry emplacement by providing crustal permeability that facilitated magma ascent inboard of the active arcs in Chile, into their back arc in Argentina (Alonso and Viramonte, 1987; Richards et al., 2000; Chernicoff et al., 2002). Gigola (2015) interpreted a more subdued WNW structural corridor that connects Taca Taca Bajo and Socompa mineralised centres to the Eocene-Oligocene belt of Northern Chile (i.e. Escondida-Zaldivar cluster). In agreement with this interpretation, Taca Taca Bajo is interpreted to be in the back-arc of the Chilean Eocene-Oligocene porphyry belt (Almandoz et al., 2008), and its location was controlled by a WNW lithospheric cross-arc structure that did not influence later Miocene volcanism.

The location of late Cenozoic magmatism and porphyry Cu deposits east of the magmatic arc (e.g., Bajo de la Alumbra in the Sierra Pampeanas region) has been interpreted to be linked to segments of flat-slab subduction due to the subduction of seamount chains and oceanic plateaus, forming focused, isolated igneous centres (Proffett, 2003). This is potentially also the case for Oligocene magmatism in the Puna region also.

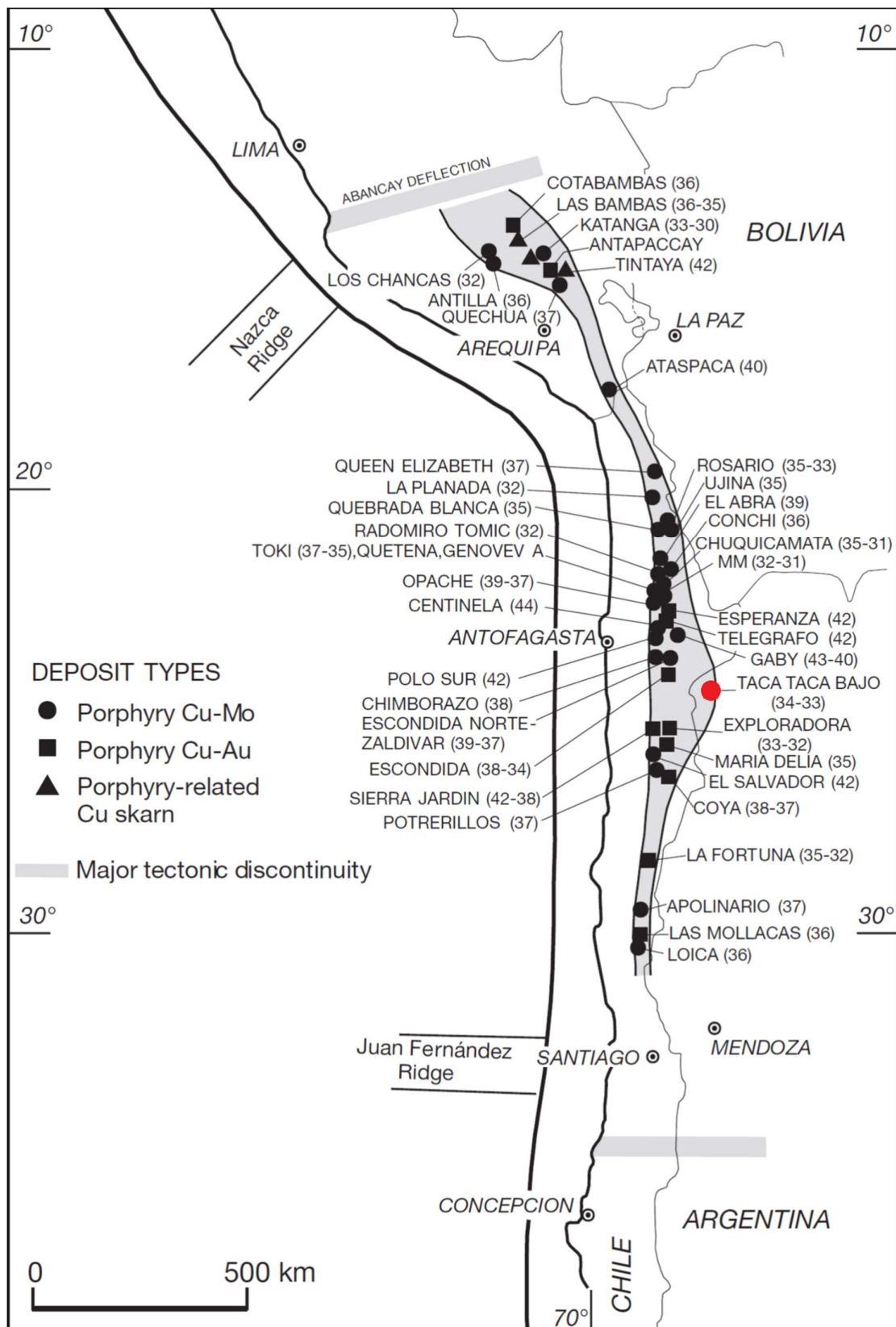


Figure 2.2: Eocene to early Oligocene belt of Northern Chile and Southern Peru, showing the location of Taca Taca Bajo in relation to contemporary deposits. From Sillitoe and Perelló (2005).

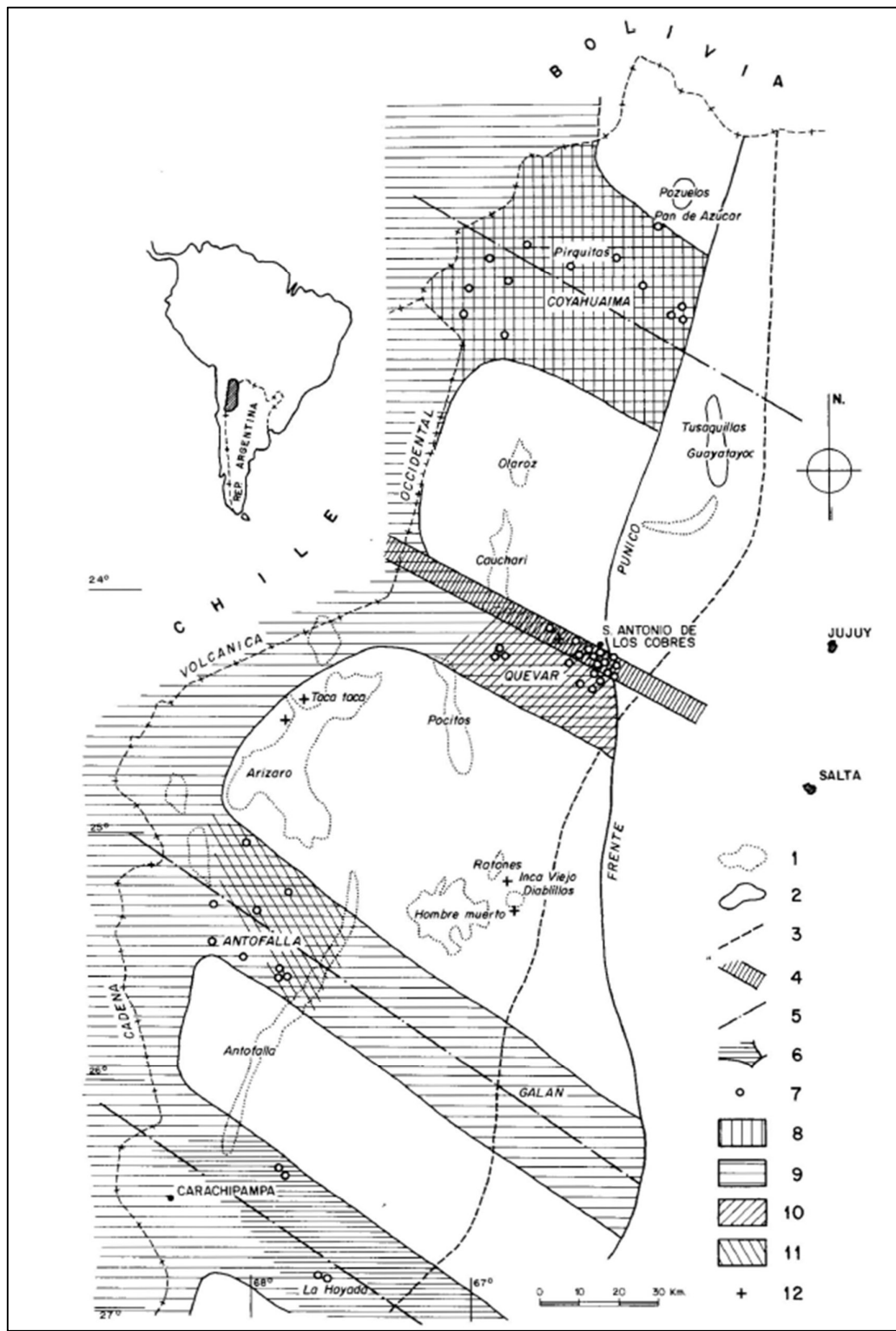


Figure 2.3: Miocene metal distribution map in the Puna province. 1) Salt flats; 2) Lakes; 3) Puna province boundary; 4) Olacapato lineament; 5) WNW-ESE cross-arc lineaments; 6) Region of Miocene volcanism; 7) Deposits and occurrences; 8) Coyahuaima Sn-Ag-Pb-Sb belt; 9) Carachipampa Cu belt; 10) Quevar Ag-Pb-Zn belt; 11) Antofalla-Galán Pb-Ag-Zn belt; 12) Porphyry Cu deposits. From Alonso and Viramonte (1987).

### *2.3.2 Geology of the Puna Region*

The Puna region, host to the Taca Taca Bajo orebody, is a desert on a high elevation (3,000 – 6,000 masl.) depression. This back-arc basin is bound by high angle reverse faults (Turner, 1972). It is flanked on its western side by the volcanic Western Cordillera and on its eastern margin by the Palaeozoic Eastern Cordillera (Alonso and Viramonte, 1987). Prior to its uplift in the Tertiary, this region accumulated sediment as a continental back arc basin since the early Carboniferous. Prior to the Carboniferous, the region underwent continental growth by island arc accretion, and at least two cryptic arc terranes are interpreted to have accreted to the western margin of this part of Gondwana between the Cambrian and Silurian (Ramos and Aleman, 2000).

Outcrops of crystalline basement in the region are scarce and discontinuous. They consist of Precambrian to early Cambrian, medium to high grade metamorphic and metasedimentary rocks, including slates of the Puncoviscana Group and quartzites of the Mesón Group (Fig. 2.4; Turner, 1960; Mangano and Buatois, 2004). The Ordovician was a period of active sedimentation throughout the region, where clastic continental and marine sediments were deposited, together with minor submarine volcanic flows. Some of these units now display low grade metamorphism related to the emplacement of later stocks. Three main calc-alkaline batholiths intruded the previously described strata during the Ordovician-Silurian, one of which is the Taca Taca granite batholith, the host to Taca Taca Bajo (Fig. 2.4; Salfity et al., 1975; Alonso and Viramonte, 1987 and references therein).

Even though there is not much record of later Palaeozoic sedimentation in the area, there are some red sandstones and conglomerates that crop out in the Northern half of the Puna region, including the Cerro Oscuro and Arizaro formations (Fig. 2.4). Along strike to the south and north, the upper Palaeozoic to Mesozoic is marked by the development of deep intracontinental basins in which thick packages of clastic and lesser carbonate sediment accumulated (Salta and Neuquén basins; Alonso and Viramonte, 1987).

There is a marked angular unconformity between all rock units described above, and strata that formed from Tertiary sedimentation and volcanism. Above the unconformity there is a prominent sequence of red sandstones and conglomerates that were deposited during the Eocene. These are overlain by a sequence of evaporites, mudstones and minor intermixed

pyroclastic deposits of mostly Oligocene age, the thickness and composition of which varies considerably along strike. Both these sequences are bulked into the Pastos Grandes group (Fig. 2.4; Schwab, 1985; Alonso and Viramonte, 1987)

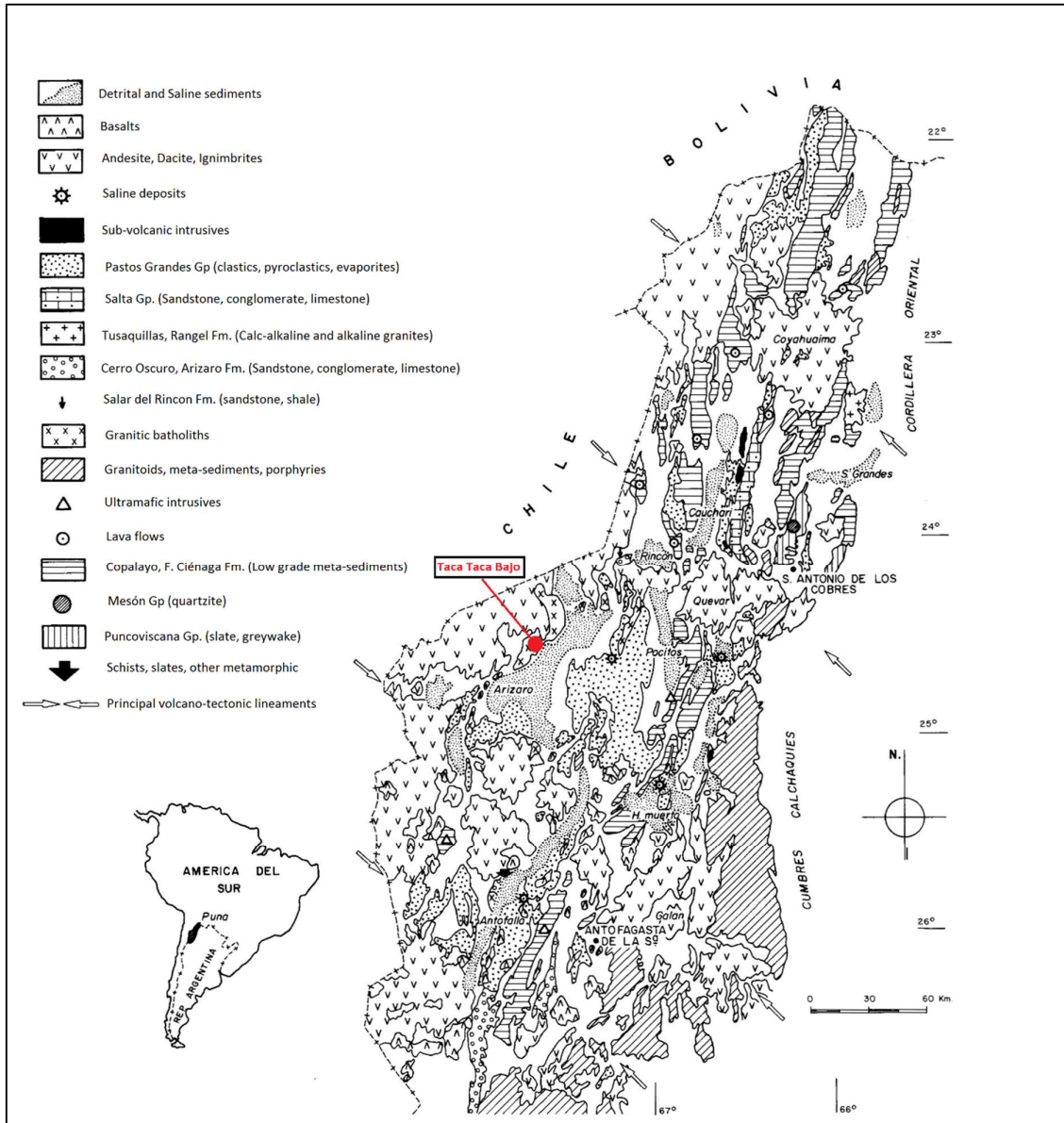


Figure 2.4: Geology of the Puna region showing the location of Taca Taca Bajo, Modified from Alonso and Viramonte (1987).

From the late Oligocene to the Pliocene, voluminous volcanism occurred along the western edge of the Puna, with volcanism extending in linear arrays ESE across the high plateau. Andesite flows, dacite domes, caldera-related ignimbrites and other volcanic features are common in Upper Oligocene to Pliocene stratigraphy of the region (Fig. 2.4). Epiclastic

sedimentation occurred in between these volcanic domains, with accommodation space inferred to have been generated in basins bound by cryptic cross-arc structures. Overall the Tertiary was characterised by rapid shortening and changes in the compressional stresses due to the Inca and Quechua orogenies, in the Eocene-Oligocene and late Miocene, respectively (Salfity and Marquillas, 1994; Sandeman et al., 1995; Oncken et al., 2006). The temporal episodicity of porphyry copper deposit formation has been argued to be controlled by these changes in stress regimes (e.g., Cooke et al., 2005).

During the Quaternary, sedimentary basins were reactivated and locally derived clastic sediments and evaporites accumulated in salt flats (including the Salar de Arizaro, adjacent to Taca Taca Bajo). Localised mafic volcanism also occurred in some regions of the Puna during this time (Alonso and Viramonte, 1987).

## 2.4 District Geology

The geology of the Taca Taca district is dominated by igneous rocks. No true basement is observed in the district, although the oldest units known (Silurian granites, aplites and dolerites of the Taca Taca batholith; Sillitoe, 2008), are regionally distinctive and represent a local basement structurally juxtaposed against younger rocks. The most voluminous package of rocks comprises abundant Permian dacitic volcaniclastic and lesser volcanic sandstones and siltstones. Minor Permian rhyolite dykes intruded the batholith in the vicinity of the Taca Taca Bajo deposit, but are not common in the district. Approximately 5 kilometres northwest of Taca Taca Bajo is Taca Taca Alto, a Permian high sulfidation alteration system ( $257 \pm 18$  Ma; K-Ar on whole rock rhyodacite porphyritic stocks; Zappettini and Blasco, 1998) that was related to Permian magmatism.

Pre-mineral Oligocene dacite to rhyolite volcanic complexes and dykes are inferred to unconformably overlie and intrude Palaeozoic lithologies respectively, but geochronological constraints on these units are weak. Their extent is interpreted to extend throughout most of the covered region (Wood et al., 2015). Volumetrically minor porphyritic rhyodacite dykes (discussed in section 2.4) and rhyolite dykes intruded the Silurian granite.

The other major lithological package in the Taca Taca district are fresh, recent felsic to mafic volcanic flows and complexes which drape over all pre-existing rock types and, together with quaternary colluvium and salt flats, conceal the geology relevant to Oligocene mineralisation. A revised district map was produced by Wood et al. (2015; Fig. 2.5).

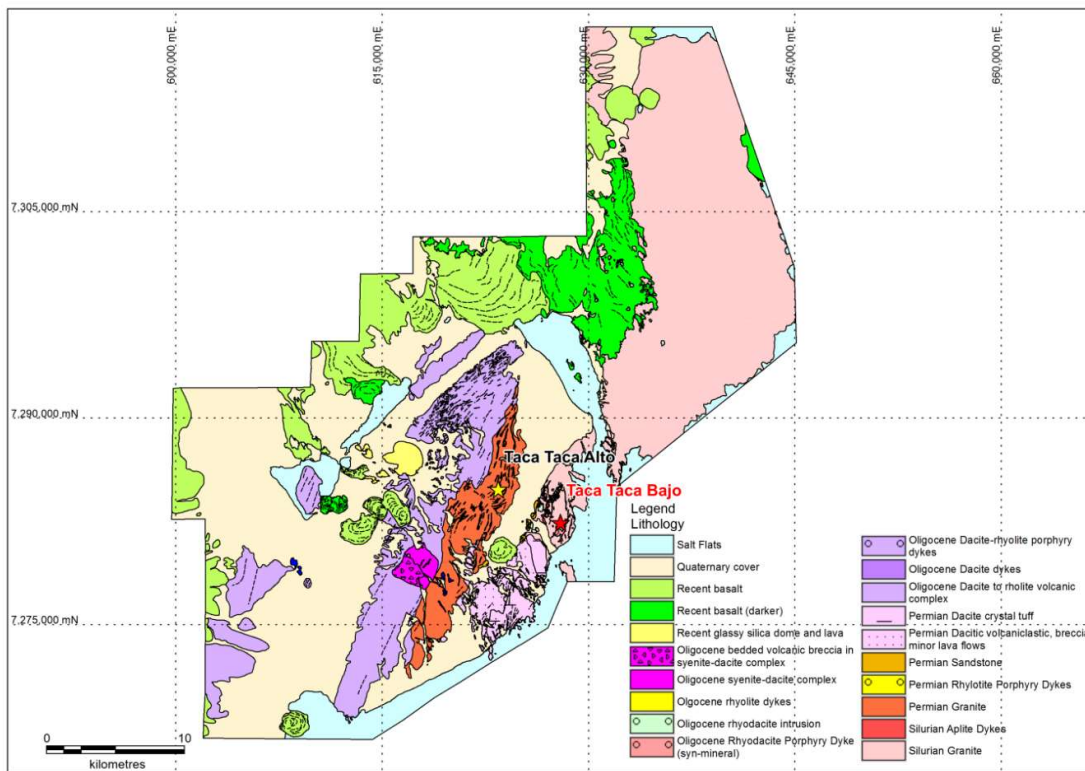


Figure 2.5: Geology of the Taca Taca District (Wood et al., 2015).

## 2.5 Local Geology

### 2.5.1 Lithology

The Taca Taca Bajo porphyry deposit is hosted by the Silurian Taca Taca Batholith. This intrusion is a medium to coarse grained, equigranular, biotite and hornblende-bearing, plagioclase – orthoclase – quartz granite to granodiorite batholith (Fig. 2.7a; Chavez, 2008; Cornejo, 2008; Tripp 2015; Waechter et al., 2015). The batholith was intruded by aplite dykes (Fig. 2.7b) and minor dolerite dykes (Fig. 2.7c), interpreted to be part of the waning stages of batholith emplacement (Sillitoe, 2008). Permian ( $262.4 \pm 2.3$  Ma; U-Pb from zircons, Lumina Copper internal report, 2013), sub-vertical, north-striking rhyolite dykes (Fig. 2.7d) also cut

the Silurian batholith. These dykes have porphyritic textures, with coarse, round quartz phenocrysts in a silicic groundmass and are locally spherulitic (Waechter et al., 2015).

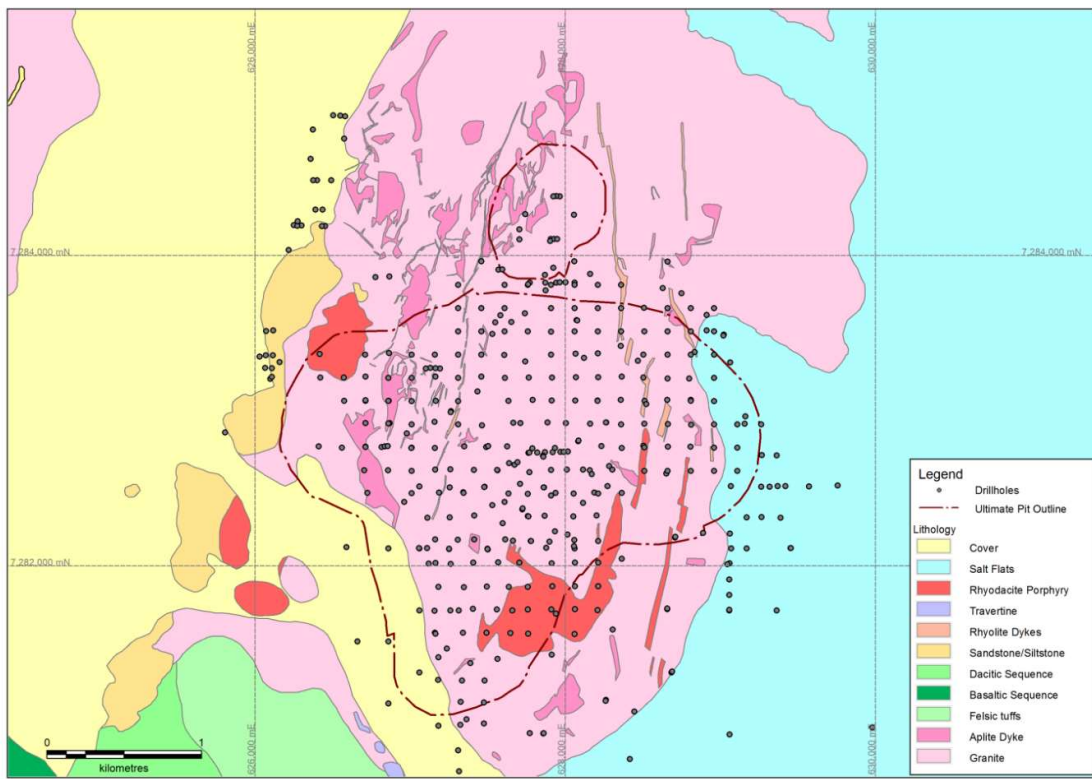
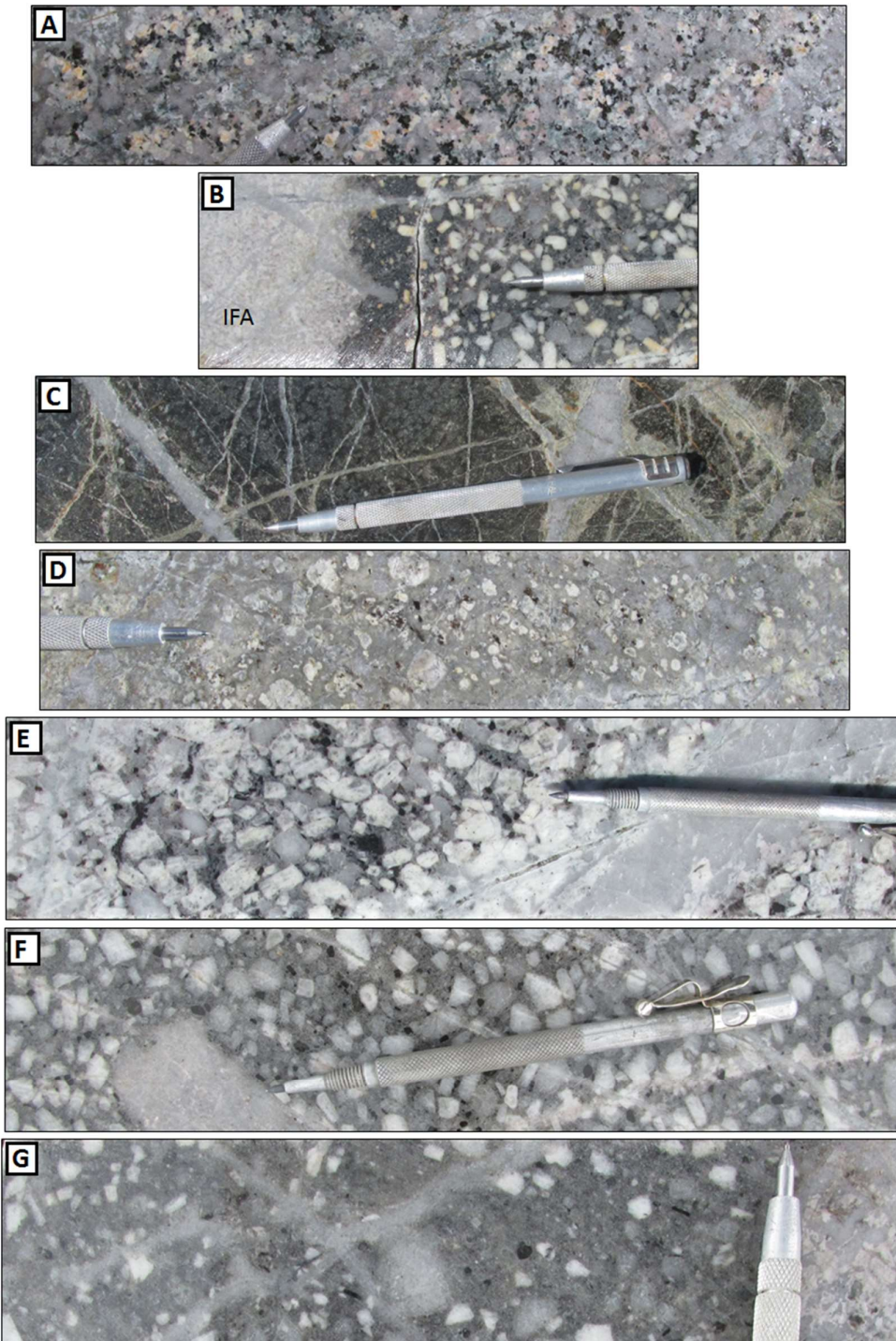


Figure 2.6: Geological Map of the Taca Taca Bajo deposit, modified after Wood et al. (2015).

Three textural variations of Oligocene, syn-mineralisation rhyodacite porphyries have been recognized at Taca Taca Bajo ( $29.30 \pm 0.57$  Ma; U-Pb from zircons; Gigola, 2008). The B1 porphyry is a rhyodacite with coarse porphyritic texture defined by plagioclase and quartz phenocrysts in a shreedy, secondary biotite groundmass (Fig. 2.7e). The B2 porphyry is also early-mineralisation (Fig. 2.7f), but it is distinguished from the B1 porphyry in that it is slightly less crystal-crowded. The late-mineralisation B3 porphyry has similar phenocryst compositions to B1 and B2, but has a less crowded porphyritic texture in an aplitic to secondary biotite-rich groundmass (Fig. 2.7g; Tripp, 2015a; Waechter et al., 2015).

There are no Oligocene post-mineral intrusions in the Taca Taca Bajo project area.



**Figure 2.7: Lithologies of the Taca Taca Bajo deposit.** A) Coarse grained, equigranular Silurian Taca Taca Granitic Batholith; B) Fine grained aplitic dyke truncated by rhyodacite porphyry; C) Silurian dolerite dyke host rock to Oligocene veining and mineralisation D) Permian rhyolite dykes; E) Syn-mineral crowded, coarse grained porphyritic rhyodacite with feldspar and quartz phenocrysts in biotite rich groundmass cut by barren quartz veins and minor quartz-sulfide-sericite vein. F) Syn-mineral moderately crowded, coarse grained feldspar-quartz rhyodacite porphyry with aplite xenoliths. G) Late-mineralisation rhyodacite porphyry with open porphyritic texture of coarse feldspar and quartz phenocrysts in a felsic and shreddy biotite groundmass. Photographs from Waechter et al. (2015).

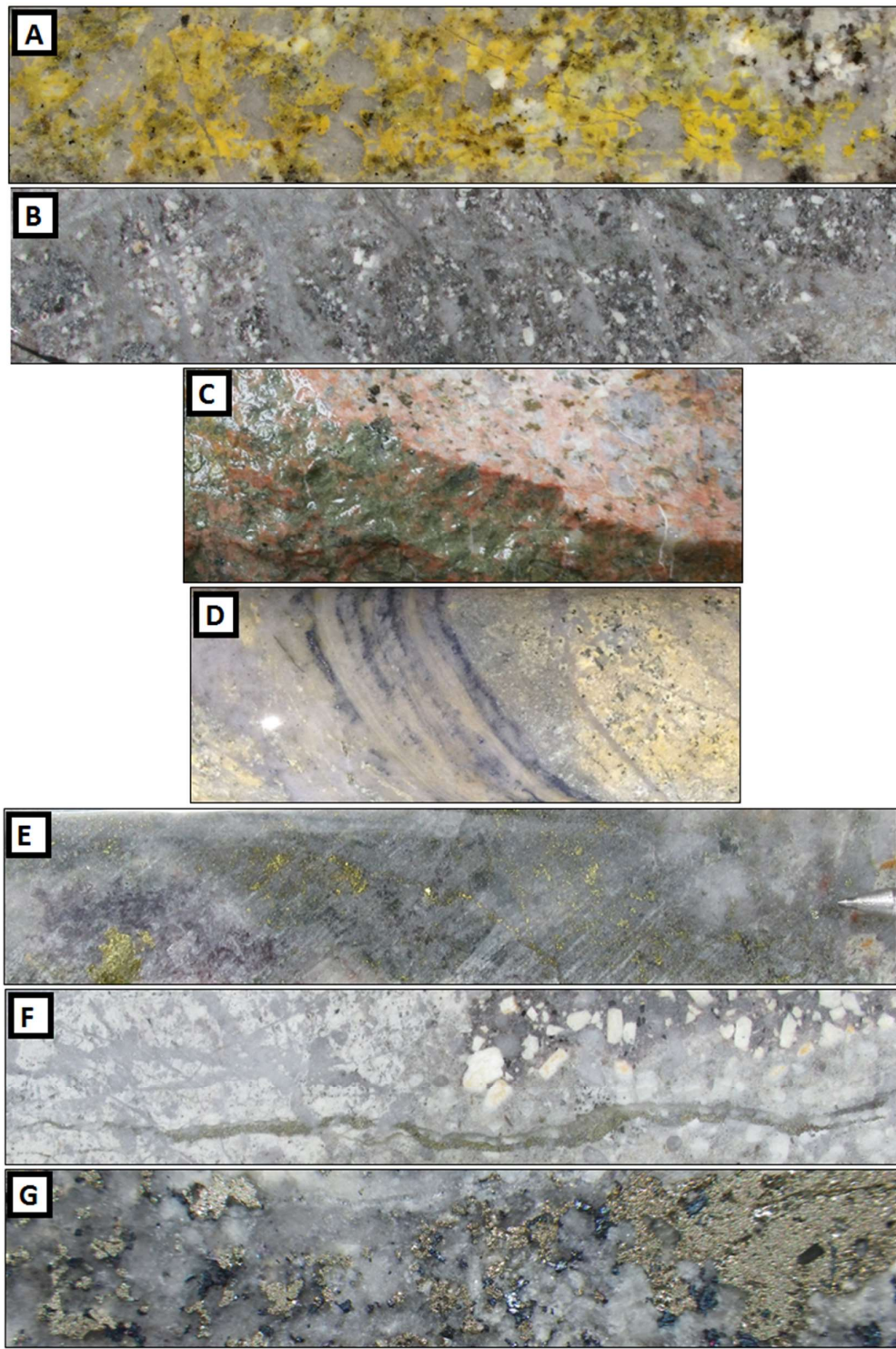


**Figure 2.8: Alteration and veining in Taca Taca Bajo.** A) Proximal granite batholith stained with sodium cobaltinitrate showing potassium feldspar flooding in potassio alteration. B) Shaggy biotite potassio alteration in groundmass of rhyodacite porphyry, cut by barren quartz vein stockwork. C) Epidote vein in granite batholith from distal propylitic alteration. D) Quartz-molybdenite banded vein. E) Pervasive green sericite and chalcopyrite with anhydrite patched in ore zone. F) Quartz-pyrite vein with sericite halo rhyodacite porphyry-aplite contact with barren quartz veins G) High sulfidation overprint of pre-existing sulfides with white sericite alteration. Photographs from Waechter et al. (2015).

### 2.5.2 Veining, Alteration and Mineralisation

The inter-mineralisation porphyritic rhyodacite intrusives and directly adjacent granite show intense potassic alteration, with disseminated biotite in the groundmass (Fig. 2.8a) and weak to strong orthoclase flooding (Fig. 2.8b) and phenocryst replacements (Tripp, 2015a). This potassic core shows weak to moderate development of barren quartz veins and transitions towards thick banded, quartz - molybdenite veins (Fig. 2.8d; Benavides, 2015). Only minor bornite and chalcopyrite is observed and this zone is economically insignificant (Fig. 2.9), but Re-Os geochronology on molybdenite from this vein stage yielded an age of  $29.0 \pm 0.2$  Ma (Gigola, 2008) within analytical uncertainty of the age determinations for the rhyodacite porphyries. The coincidence in time and space of hydrothermal alteration and intrusive activity leads to a conclusion that these are the causative intrusions.

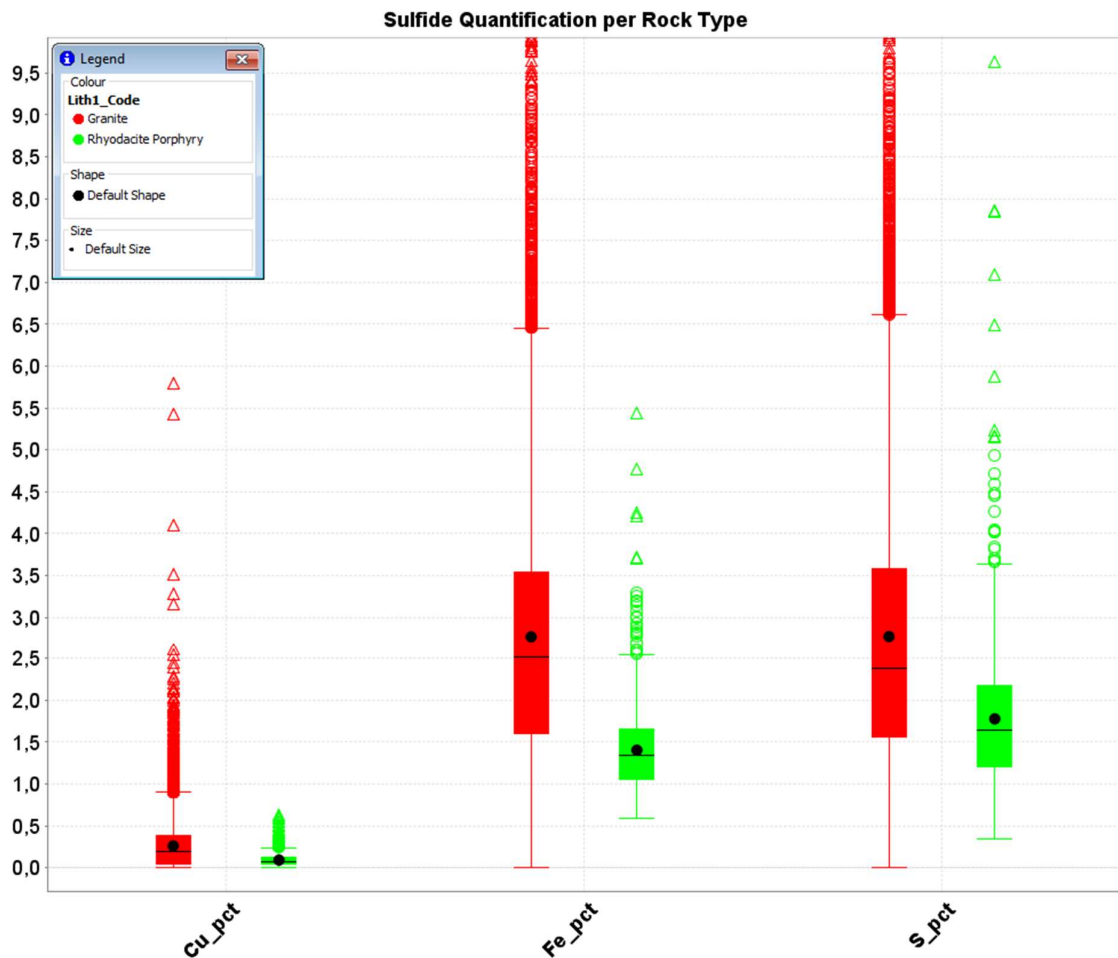


Figure 2.9: Cu, Fe and S distribution per lithology at Taca Taca Bajo. Cu and Fe sulfides were emplaced in the granite host rock preferentially over the rhyodacite porphyritic stock. High S values in the rhyodacitic porphyry are related to anhydrite appearance.

Alteration is strongly zoned outwards (Fig. 2.10a) within the granitic batholith from potassic to sericitic alteration. The sericitic alteration can be broken down into two domains: A) ore-zone phyllitic alteration, and B) pyritic halo. The ore zone phyllitic alteration is characterised by intermixed white sericite and green sericite, which prior to this study, were interpreted to be due to different ratios of white micas intermixed with fine grained chlorite. The green sericite domain is observed to have an affinity with chalcopyrite and minor bornite, hence higher copper grades (Cobeñas and Almandoz, 2015). This alteration assemblage is observed as selvages to rectilinear, thin quartz - sulfide veins and, where more intense, as coalesced selvages forming a pervasive sericitic overprint (Fig. 2.8e; Benavides, 2015). Primary sulfides have been partially overprinted by a high-sulfidation assemblage of chalcocite, bornite, pyrite and minor digenite (Fig. 2.8g). Banded quartz - molybdenite veins are observed on the outer portion of this hypogene ore zone. Outward from this zone, the pyritic halo is composed mainly of white sericite selvages (and coalesced selvages) surrounding quartz - pyrite veins with attendant phyllitic alteration (Fig. 2.8f). The spatial distribution of veins in cross section through the centre of the orebody is shown in Figure 2.11. Distally, the system transitions to a weak-moderate propylitic alteration assemblage, which is characterised by chlorite as thin veinlets and selective replacement of mafic minerals in the granite, as well as rare epidote filling fractures and replacing feldspars and mafic sites (Fig. 2.8c; Tripp, 2015a).

A 150-300 metre leached cap has developed by supergene processes after the deposit was uplifted and exhumed. This domain is depleted in copper but contains sub-economic free gold in undifferentiated limonite. The leached cap is underlain by a narrow oxide zone of inconsistent thickness, characterised by the presence of brochantite, atacamite, malachite and chrysocolla. Copper leached from the oxidised zone was re-precipitated in a supergene enrichment zone which consists mainly of chalcocite with minor digenite, together with structurally controlled supergene alunite and chalcedony (Tripp, 2015b; Waechter et al., 2015). This is the highest grade zone of the deposit. Geochronological results on supergene alunite by K/Ar suggest development of supergene mineral assemblages at 24-21 Ma (Gigola, 2008).

The ore at Taca Taca Bajo is related to an inconsistent supergene enrichment blanket and underlying hypogene mineralisation associated with the inner phyllitic alteration rather than the potassic altered domain (Fig. 2.10b). Among other factors, these complications to the

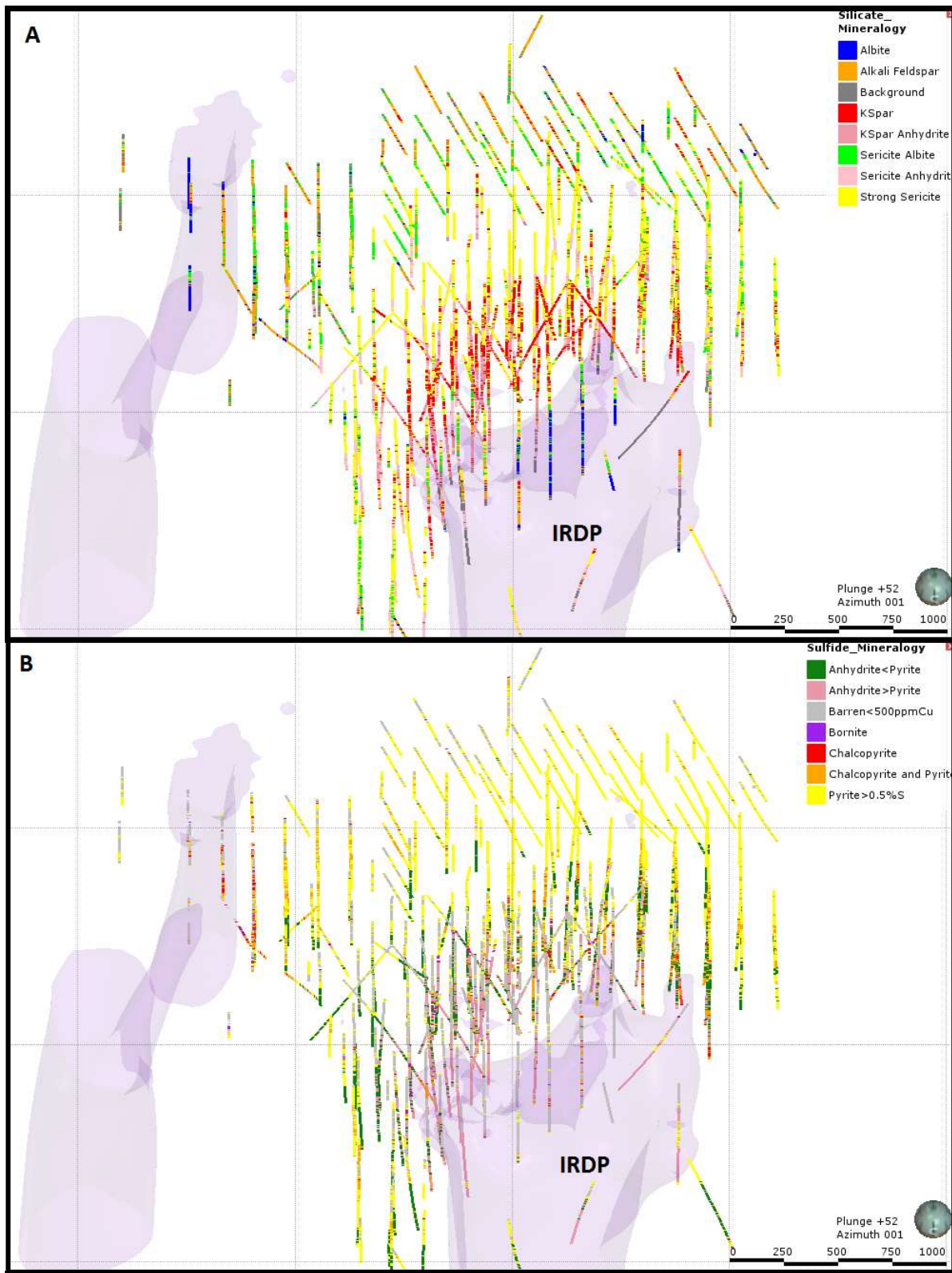


Figure 2.10: A) Alteration zonation interpreted from geochemical assays. This data has been verified and matches logged alteration (Halley, 2015). B) Hypogene mineralisation zonation interpreted from geochemical assays, also verified against paper logs (Halley, 2015). IRDP: Rhyodacite porphyry stock.

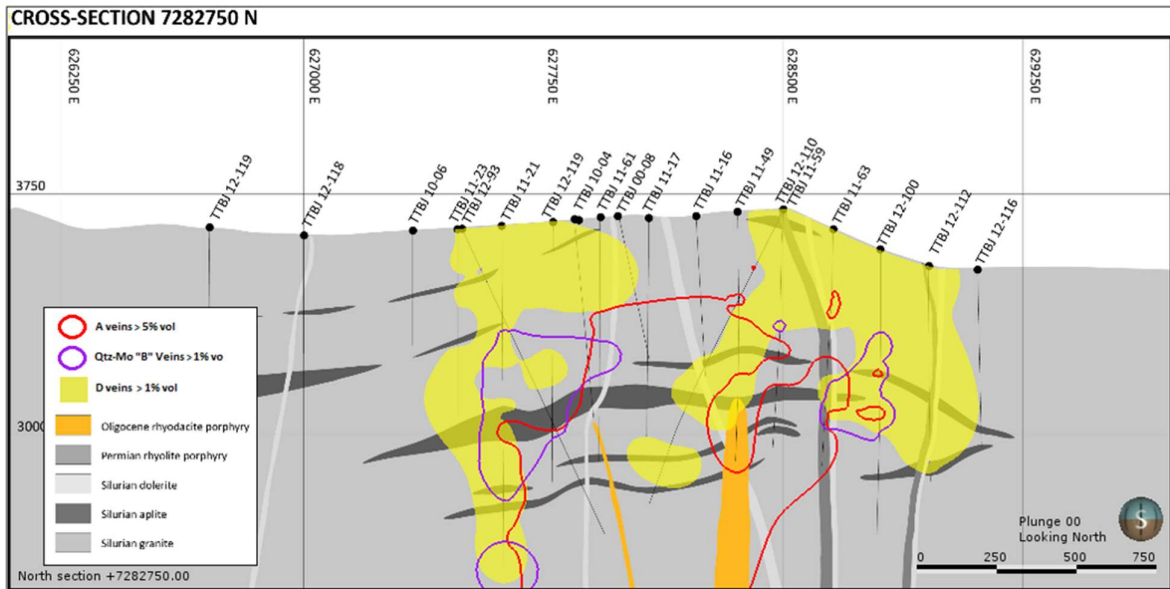


Figure 2.11: Section 7282750N through the Taca Taca Bajo orebody showing the small volume of rhyodacite porphyry and the vein distribution around it. Note that ore in Taca Taca Bajo is related to quartz-sericite-chalcopyrite "D" veins rather than the barren quartz "A" veins. From Benavides (2015).

classical porphyry model of Lowell and Guilbert (1970) led to major difficulties for early explorers at Taca Taca Bajo.

### 2.5.3 Paragenesis

Almandoz (2008) presented the current paragenetic model at Taca Taca Bajo, including all of the lithologies, alteration, veining, hypogene mineralisation and supergene mineralisation (Fig. 2.12). Rhyodacite porphyries intruded the Silurian granites and they are considered the causative intrusions for mineralisation and alteration. Potassic alteration (with very minor disseminated chalcopyrite > bornite) and barren quartz veins are the earliest events observed, followed by molybdenum deposition in banded quartz - molybdenite veins (Almandoz, 2008). This was overprinted by a green sericite alteration event which, prior to this study, was considered to be contemporary with low sulfidation state chalcopyrite - pyrite disseminated in the green sericite halos of quartz veins (Almandoz, 2008). A later high sulfidation state event brought quartz - pyrite veins with white sericite selvages, which replaced the pre-existing chalcopyrite > bornite assemblage by pyrite – bornite – chalcocite - covellite, although it had remained unclear prior to this study as to whether this latest event introduced any additional copper. Supergene enrichment and alteration products occurred roughly 6 to 8 million years later.

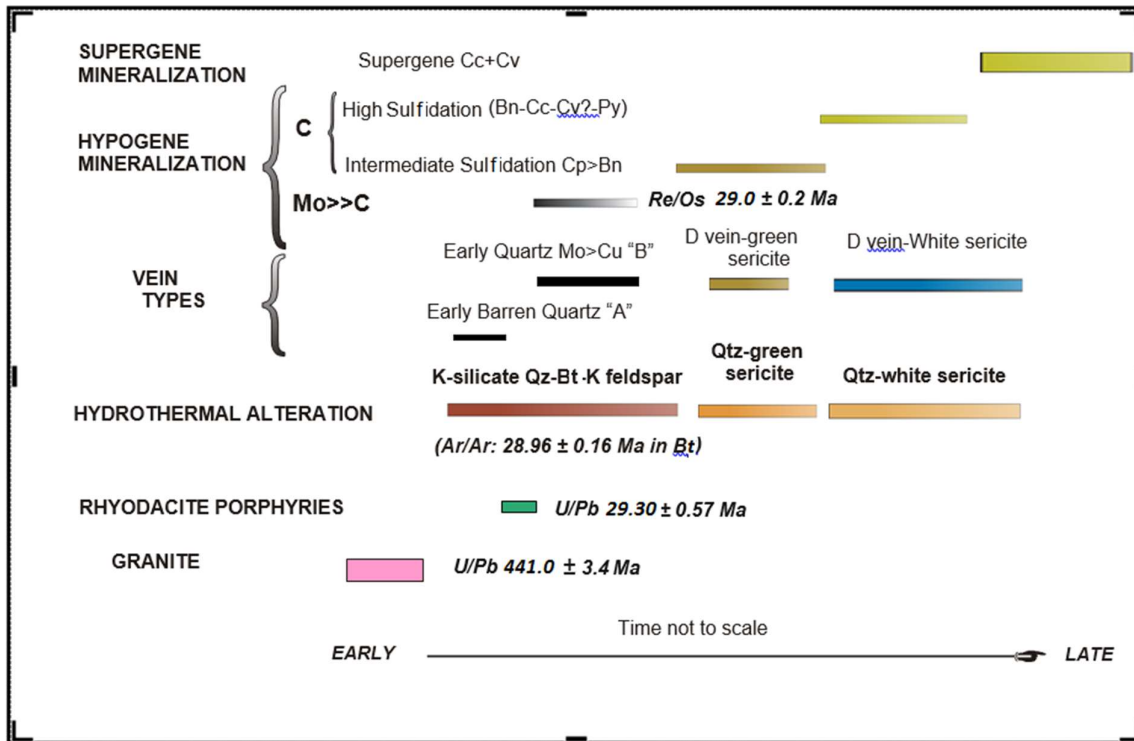


Figure 2.12: Schematic paragenetic sequence for the Taca Taca Bajo orebody. From Almandoz (2008). Cc = chalcocite, Cv = covellite, Py = pyrite, Cp = chalcopyrite, Bn = bornite, Mo = Molybdenite, Qz = quartz; Bt = biotite.

### 3. Phyllitic Alteration at Taca Taca Bajo

#### 3.1 Methodology

##### 3.1.1 Sampling

A total of 24 samples were collected from Taca Taca Bajo for this study; all of them from drill-holes (Fig 3.1). Six of the samples were collected as background control samples: three of fresh host Silurian granitic batholith, one of a potassic-altered variant of this unit, and two of potassic-altered Oligocene rhyodacite porphyry. All other samples display either white sericite, green sericite or a mixture of both, as described during logging (Table 3.1). Twenty-five laser mounts were produced from these samples (TTB\_SB14 had two mounts prepared) at the CODES lapidary (Table 3.2).

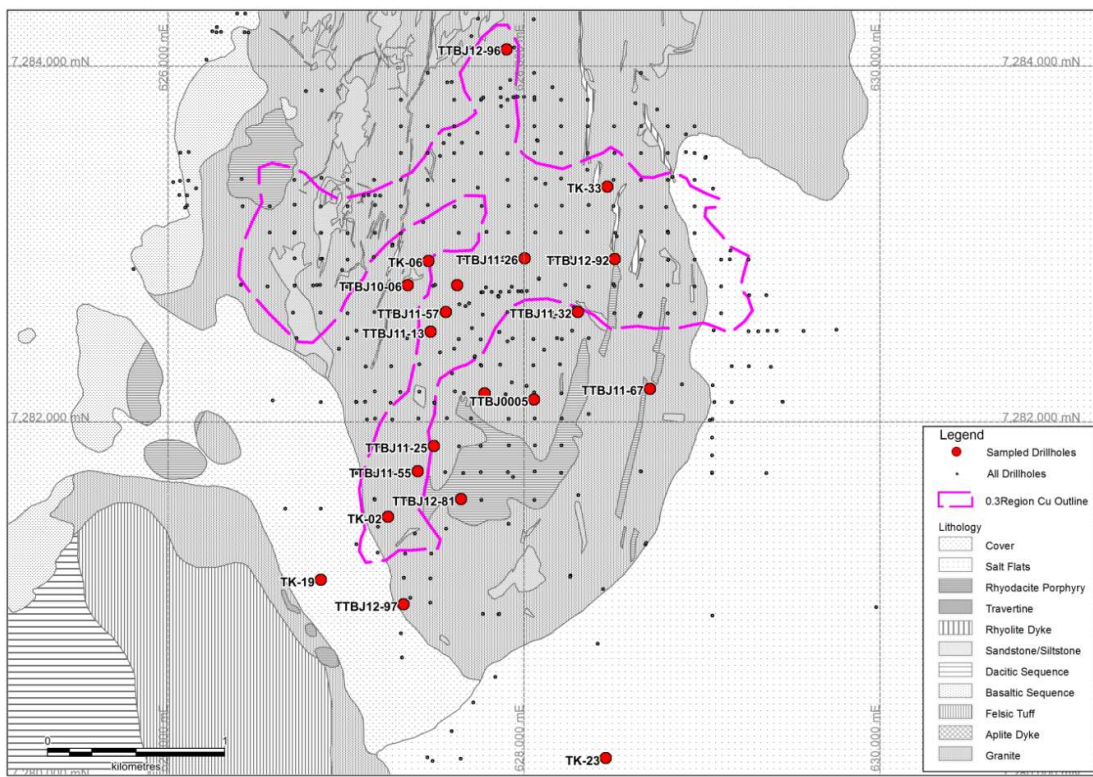


Figure 3.1: Location of drill-holes sampled in this study overlain on 0.3% Cu Indicated & Inferred Resource (Scott et al., 2013) and on surface geology (Wood et al., 2015)

Table 3.1: Sample Descriptions and Locations

Sample ID	Hole ID	Depth (m)	Easting	Northing	Elevation	Lithology	Alteration	Sulfides	Comments
TTB_SB01	TTBJ12-96	285.4	627898	7284096	3290	IGR	Fresh	None	Background Sample
TTB_SB02	TK-19	235.4	626858	7281113	3322	IGR	Fresh	None	Background Sample
TTB_SB03	TK-23	203.5	628459	7280112	3307	IGR	Fresh	None	Background Sample
TTB_SB04	TTBJ11-67	504.3	628494	7282183	3102	IRDP	K-alt	Py > Cpy	Background Sample
TTB_SB05	TTBJ12-83	434.3	627783	7282152	3298	IGR	K-alt	Cpy > Bn, Cc	Background Sample
TTB_SB06	TTBJ11-32	653	628289	7282616	3031	IRDP	K-alt	None	Background Sample
TTB_SB07	TTBJ11-55	540	627404	7281723	3071	IGR	GS-WS	Py, Bn, Cc > Cpy	WS ovp GS veins. HS related to WS
TTB_SB08	TTBJ11-25	369	627496	7281866	3271	IGR	GS	Cpy > Py	5-10 cm. wide K-alt IRDP dykes ovp by PHY.
TTB_SB09	TTBJ11-13	327	627500	7282508	3324	IGR	GS	Cpy	Sericite ovp K-alt IGR
TTB_SB10	TK-02	372.3	627422	7281467	3247	IGR	GS-WS	Py > Cpy	Sulfides and sericite related to vein halo in K-alt IGR
TTB_SB11	TTBJ12-97	642.8	627331	7280977	2898	IGR	WS	Py > Cpy	Pervasive PHY in Py rich halo
TTB_SB12	TTBJ10-06	336.8	627346	7282763	3297	IGR	WS	Py	Pervasive PHY in Py halo
TTB_SB13	TK-33	264.9	628468	7283321	3344	IGR	WS >> GS	Py, Bn, Cc	HS ovp of Cpy.
TTB_SB14a	TTBJ12-81	669.5	627681	7281546	2965	IRDP	GS	Py-Cpy	GS vein cutting K-alt IRDP
TTB_SB14b	TTBJ12-81	669.5	627998	7282107	3084	IRDP	WS	Py > Cpy	WS vein cutting K-alt IRDP
TTB_SB15	TTBJ0005	636.7	628474	7282185	3063	IRDP	WS	Py, Bn, Cc > Cpy	Early Qz and Qz-Mo veins cut but Sulfide-sericite veins
TTB_SB16	TTBJ11-67	548.4	628001	7282909	2948	IRDP	WS	Py	Pervasive PHY ovp of K-alt IRDP
TTB_SB17	TTBJ11-26	715	627463	7282905	3292	IGR	GS >> WS	Py > Cpy	Sulfides and sericite associated to veining
TTB_SB18	TK-06	343	627535	7282477	2743	IGR	WS	Py > Cpy	Sulfides and sericite related to veining
TTB_SB19	TTBJ11-13	909.7	628493	7282183	3100	IGR	GS	Py, Bn, Cc	High grade Cu and Au. GS related to HS minerals (rare)
TTB_SB20	TTBJ11-67	506.7	628505	7282910	3187	IGR	GS-WS	Py, Bn, Cc > Cpy	Pervasive PHY on IGR
TTB_SB21	TTBJ12-92	492.5	627555	7282612	3084	IGR	GS > WS	Cpy > Py	GS dominant, ovp K-alt IGR
TTB_SB22	TTBJ11-57	575.35	627999	7282901	2594	IGR	GS > WS	Py, Bn, Cc > Cpy	GS dominant, ovp K-alt IGR
TTB_SB23	TTBJ11-26	1069.8	627631	7282765	3167	IGR	GS-WS	Cpy > Py	WS veins ovp GS veins
TTB_SB24	TTBJ11-21	485	627898	7284096	3290	IGR	GS	Py, Bn, Cc > Cpy	PHY ovp K-alt IGR

IGR: Granite; IRDP: Rhyodacite Porphyry; WS: White sericite; GS: Green Sericite; K-alt: Potassic alteration; PHY: Phyllitic alteration; Py: Pyrite; Cpy: Chalcopyrite; Bn: Bornite; Cc: Chalcocite; Qz: Quartz; Mo: Molybdenite; ovp: overprint; HS: High sulfidation. Coordinates in UTM WGS84 19S.

### *3.1.2 Spectral Analysis*

Short wave infrared (SWIR) spectral measurements were collected from the mounts using a Terraspec 4 Mineral Spectrometer. The data were processed using The Spectral Geologist (TSG) software together with IoGas Professional to classify results by different mineralogies in relation to their spectral abundances. Sericite samples were then classified by different scalars derived from the SWIR spectra such as the wavelength of the absorption feature near 2200 nm (w2200), and parameters derived from these such as sericite crystallinity. Sericite crystallinity is calculated by dividing the depth of the hull quotient spectrum absorption feature at 2200 wavelength by that of the absorption feature near 1900 nm. The w2200 compares subtle shifts of the exact peak absorption feature at roughly 2200 wavelength, which is a strong absorption feature common to phyllosilicates (Halley, 2012). These can be used as proxies to relative temperature and pH in hydrothermal fluids.

### *3.1.3 Petrography*

Reflected light petrography of the laser mounts was conducted in order to characterise and understand the textural relationships of sulfide species. Further mineral characterisation under transmitted light was not possible due to the thickness of the laser mounts.

### *3.1.4 Scanning Electron Microprobe (SEM) and Electron Probe Microanalysis (EPMA)*

Laser mounts were carbon coated and analysed by SEM/EPMA at the Central Science Laboratory (CSL), University of Tasmania, in order to determine the different mineralogical assemblages, variations in textures, as well as classifying minerals based on their geochemical signatures. A total of 665 analyses were done with the EPMA and the data was interpreted in IoGas Professional to classify each measurement into mineral groups. 144 of those measurements were of pure sericite. SEM backscattered electron imaging was used to define textural variations of sericite and relict alteration textures. With this information, the LA-ICPMS laser points were planned for trace level geochemistry of sericite, apatite, monazite and xenotime sites.

### *3.1.5 Laser Ablation Inductively Coupled Plasma Mass Spectrometry (LA-ICPMS)*

A total of 318 laser spots on sericite sites were analysed with a 20-micron beam. The primary standard was a NIST612 sample and secondary standards were BCR-2 and GSD-1G, all of which were analysed between samples. Each measurement was reviewed for quality standards and clipped or discarded where impurities had been ablated. The data was normalised using an initial assumption of 21% Al for sericite, then converted to total oxide concentrations using the GSD method. A loss on ignition (LOI) of 4.0% was assumed for sericite, and where required, total oxide concentrations were corrected to add to 96%. All values were then converted back to parts per million.

Apatite, monazite and xenotime sites were also ablated for geochemical analysis and U-Pb dating using a 13-micron laser beam and NIST-610 as a primary standard. This was done to attempt to resolve the possibility for overprinting hydrothermal systems complicating the sericite signatures. The ablation process was comparable to that used for the sericite ablation, with the addition of  $^{204}\text{Pb}$ ,  $^{206}\text{Pb}$ ,  $^{207}\text{Pb}$  and  $^{208}\text{Pb}$  to the geochemical measurements. Apatite sites were normalised to 39.36% Ca, monazite to 67.94% Ce and xenotime to 38% Y. For monazite and xenotime measurements, a  $^{140}\text{Ce}$  internal standard was used and the data were then corrected so the total sum of rare earth elements (RRE) balanced against the phosphate ( $\text{PO}_4$ ) component. They were then corrected for the 53% REE molar representation in stoichiometric monazite and xenotime. Technical issues that occurred when analysing the apatite samples prevented proper use of the geochemical or geochronological data, as the spot size on apatite samples was set smaller than the spot size on reference samples. These analyses are hence not reported. Concordia diagrams were generated by Mr. Jay Thompson from UTAS Earth Sciences department to plot the apatite, monazite and xenotime Pb and U isotopic ratios in order to calculate ages and errors.

Only 13 chlorite sites and 7 epidote sites were observed under SEM. They were marked and analysed in the LA-ICPMS with a 20-micron laser beam, using a NIST-612 samples as primary standard between mounts. During early stage data validation, the data were discarded as the fine grained nature of the minerals did not allow for quantification of the chemistry of these minerals.

### *3.1.6 Potassium Feldspar Staining*

Following mount preparation, the offcut core samples were stained with sodium cobaltinitrite to demonstrate the distribution and abundance of potassium feldspar alteration in the samples. The objective of this is to discriminate phyllitic alteration overprinting potassian alteration from that affecting common orthoclase-bearing granite. This procedure was done with the help of Dr. Lejun Zhang from the ARC TMVC Research Hub.

### *3.1.7 Quartz Cathodoluminescence (CL)*

CL imaging of quartz was done on 14 samples where hydrothermal quartz was observed to be intimately related to sericite alteration. The imagery was collected using a Cameca cathodoluminescence detector attached to an FEI Quanta 600 environmental scanning electron microprobe (SEM) at the CSL. Polished mounts were examined using the instrument at an accelerating voltage of 15 kV and beam current of ~3 nA. This procedure was carried out by Dr. Lejun Zhang from the ARC TMVC Research Hub. The aim was to highlight internal textures in quartz to observe differences which might permit differentiation of different stages of phyllitic alteration and/or reversal relationships in the temperature gradient, which would suggest overprinting of another system.

## 3.2 Sample Descriptions

### *3.2.1 Background Samples*

TTB\_SB01: Medium to coarse-grained, equigranular granite from the Silurian batholith. Plagioclase is slightly altered to clays while biotite and hornblende are slightly altered to chlorite. Major components: 5-10% mafics (biotite and hornblende), 30% plagioclase, 30% orthoclase, 30% quartz (Fig. 3.2a).

TTB\_SB02: Medium to coarse-grained, equigranular granite from the Silurian batholith. Plagioclase is slightly altered to clays (greenish) while biotite and hornblende are fresh. There is red staining of orthoclase. Major components: 5-10% mafics (biotite and hornblende), 30% plagioclase, 30% orthoclase, 30% quartz (Fig. 3.2b).

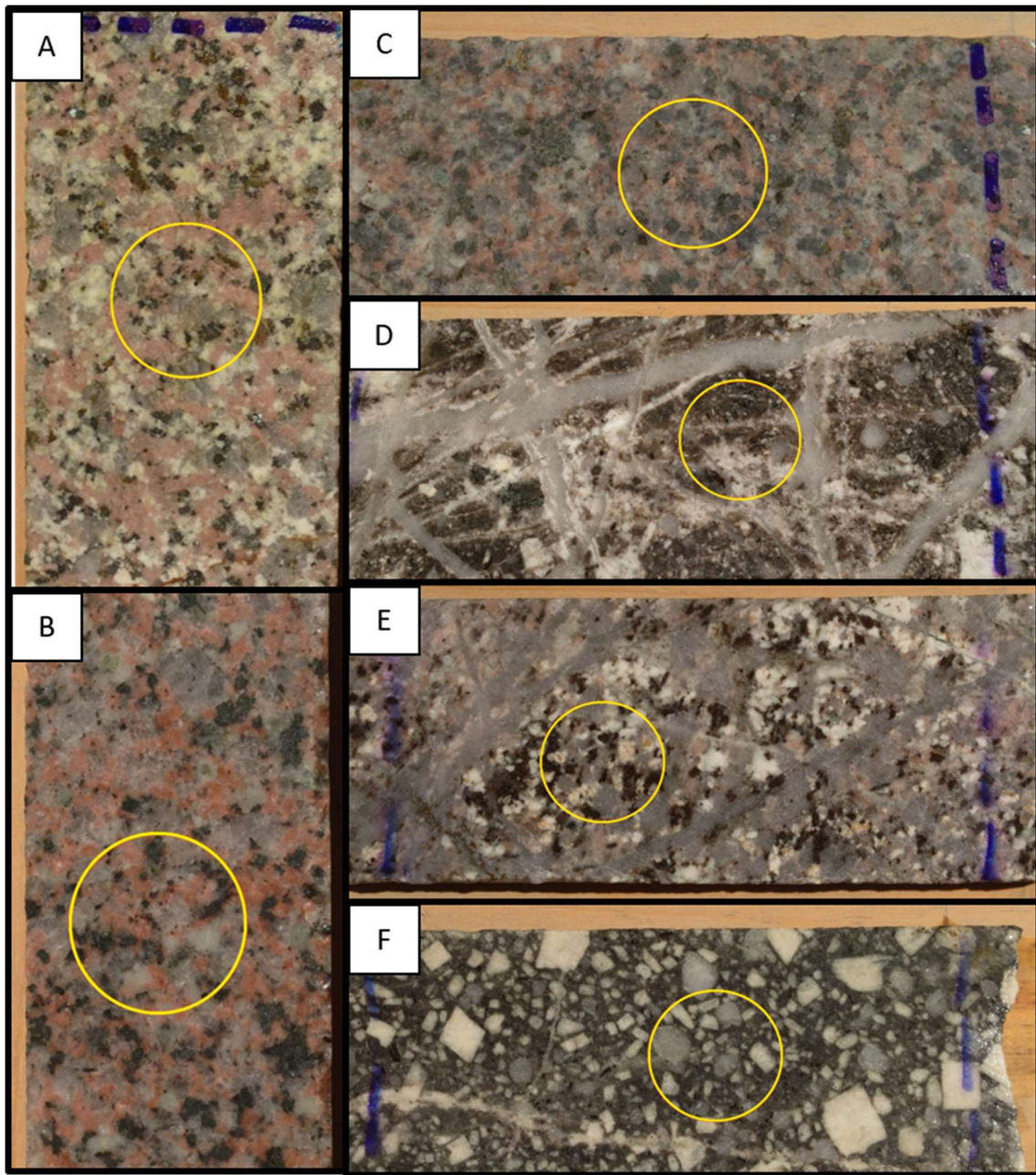


*Figure 3.2: Background samples. Yellow circle is 1-inch laser mount location. Descriptions in section 3.2.1. A) TTB\_SB01; B) TTB\_SB02; C) TTB\_SB03; D) TTB\_SB04; E) TTB\_SB05; F) TTB\_SB06*

TTB\_SB03: Medium-grained, equigranular granite from the Silurian batholith. Biotite and hornblende are slightly weathered to clays, while quartz, orthoclase and plagioclase are fresh. Major components: 10% mafics (biotite and hornblende), 30% plagioclase, 30% orthoclase, 30% quartz (Fig. 3.c).

TTB\_SB04: Coarse-grained porphyritic rhyodacite porphyry with strong pervasive secondary biotite altering the groundmass (roughly 50%). Medium to coarse plagioclase and quartz

phenocrysts (20%) are observed. Very erratic chalcopyrite is disseminated in the groundmass. It is cut by a barren quartz vein stockwork (0.5 centimetres thick on average, 30% of rock) and very minor quartz-pyrite-sericite vein stringers in adjacent core, though not in sample, cross cut all previously described veining (Fig. 3.2d).

TTB\_SB05: Medium-grained, equigranular potassic altered granite from the Silurian batholith host, cut by barren quartz veins (0.4 cm thick on average, 30%). Secondary biotite alteration (roughly 15%) is replacing mafic sites. Weak quartz-pyrite veins with sericite selvages and sulfide stringers are reopening barren quartz veins. The mount was sampled away from these late stage veins (Fig. 3.2e).

TTB\_SB06: Coarse-grained, crowded rhyodacite porphyry. Plagioclase and quartz phenocrysts (40%) are within a groundmass completely replaced by secondary, shreddy biotite. Very minor barren quartz veins present in this sample (Fig. 3.2f).

### *3.2.2 Green Sericite Samples*

TTB\_SB08: Equigranular granite with pervasive green sericite alteration. Relict potassic alteration displays secondary biotite replacing mafics. Relict quartz from granite host is observed. Sulfides are dominated by chalcopyrite with very minor pyrite replacements. This sample is adjacent to a 5-10-centimetre-wide rhyodacite porphyry dyke (Fig. 3.3a).

TTB\_SB09: Equigranular granite with pervasive green sericite alteration. Patches of relict potassic alteration on granite display secondary biotite replacing mafic sites. Quartz-chalcopyrite-green sericite veins crosscut early barren quartz veins (Fig. 3.3b).

TTB\_SB17: Pervasive green sericite alteration in equigranular granite. Patches of green sericite and chalcopyrite appear to be replacing mafic sites. Minor white sericite and pyrite is observed replacing chalcopyrite (Fig. 3.3c).

TTB\_SB19: Strong pervasive green sericite alteration in equigranular granite host. Veins and disseminations of bornite-pyrite are replacing chalcopyrite. Relict quartz from granite host is observed (Fig. 3.3d).

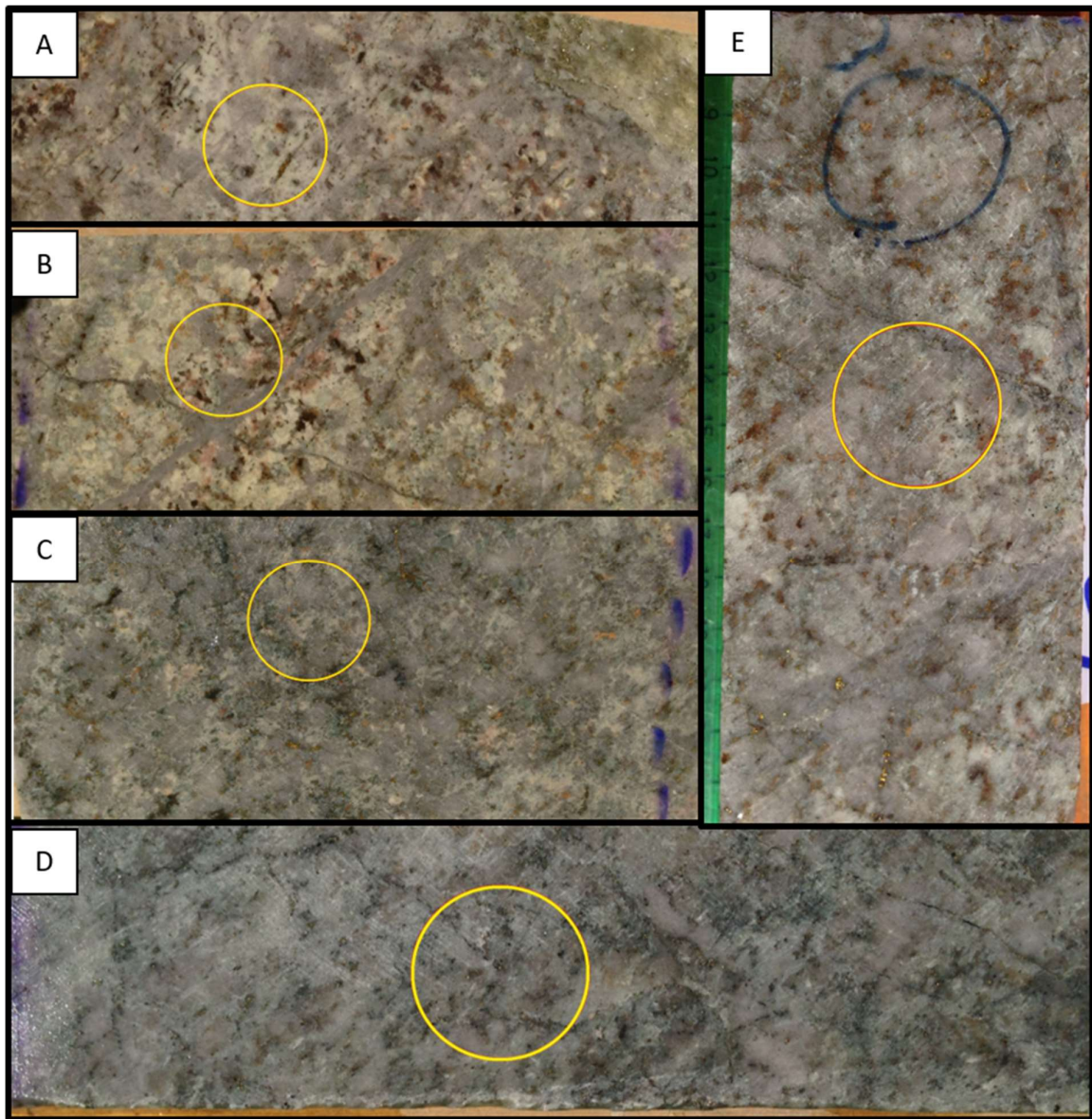


Figure 3.3: Green sericite samples. Yellow circle is 1-inch laser mount location. Descriptions in section 3.2.2 A) TTB\_SB08; B) TTB\_SB09; C) TTB\_SB17; D) TTB\_SB19; E) TTB\_SB24

TTB\_SB24: Equigranular granite with pervasive green sericite alteration as patches around relict secondary biotite sites. Chalcopyrite is disseminated within green sericite patches and in quartz-chalcopyrite veins display weak high sulfidation replacement by pyrite-bornite (Fig. 3.3e).

### 3.2.3 Mixed Sericite Samples

TTB\_SB07: Granite sample with pervasive green sericite and white sericite alteration. Chalcopyrite is disseminated within green sericite patches replacing relict biotite sites and

appears to be overprinted by bornite-pyrite. Replacement fronts on sulfides suggest that the high sulfidation overprint is related to white sericite alteration as a later event (Fig. 3.4a).

TTB\_SB10: Orthoclase-biotite altered granite cut by quartz – chalcopyrite – pyrite - bornite veins with white and green sericite selvages, which have re-opened barren quartz veins. Different sericite types appear to be coexisting in vein selvages (Fig. 3.4b).

TTB\_SB14: Porphyritic rhyodacite with strong secondary biotite replacement of groundmass, cut by two distinct vein types: quartz – pyrite >> chalcopyrite veins with green sericite selvage and quartz veins with white sericite selvages. Two mounts were created from this sample, TTB\_SB14a from a green sericite selvage and TTB\_SB14b from a white sericite selvage (Fig. 3.4c).

TTB\_SB16: Pervasive green and white sericite alteration on potassic altered rhyodacite porphyry (as observed on adjacent rocks). A relict coarse-grained, crowded porphyritic texture is almost completely replaced and pyrite is observed in veins and patches. The mount was made on the white sericite domain (Fig. 3.4d).

TTB\_SB20: Pervasive white and green sericite alteration on granite. Relict quartz crystals and barren quartz veins cut by quartz, pyrite ± bornite veins with white sericite ± green sericite selvages. Green sericite is also observed as patches with disseminated sulfides (Fig. 3.4e).

TTB\_SB21: Potassic altered granite with secondary biotite and orthoclase cut by quartz-chalcopyrite>>pyrite veins with green sericite selvages. Minor white sericite overprint and everything is cross-cut by late gypsum veins. The mount was located on the transition zone between potassic altered granite and vein selvage (Fig. 3.4f).

TTB\_SB22: Pervasive green > white sericite overprint of potassic altered granite. Sericite occurs as coalesced selvages to quartz, pyrite ± bornite veins that reopened and cross cut barren quartz veins (Fig. 3.4g).

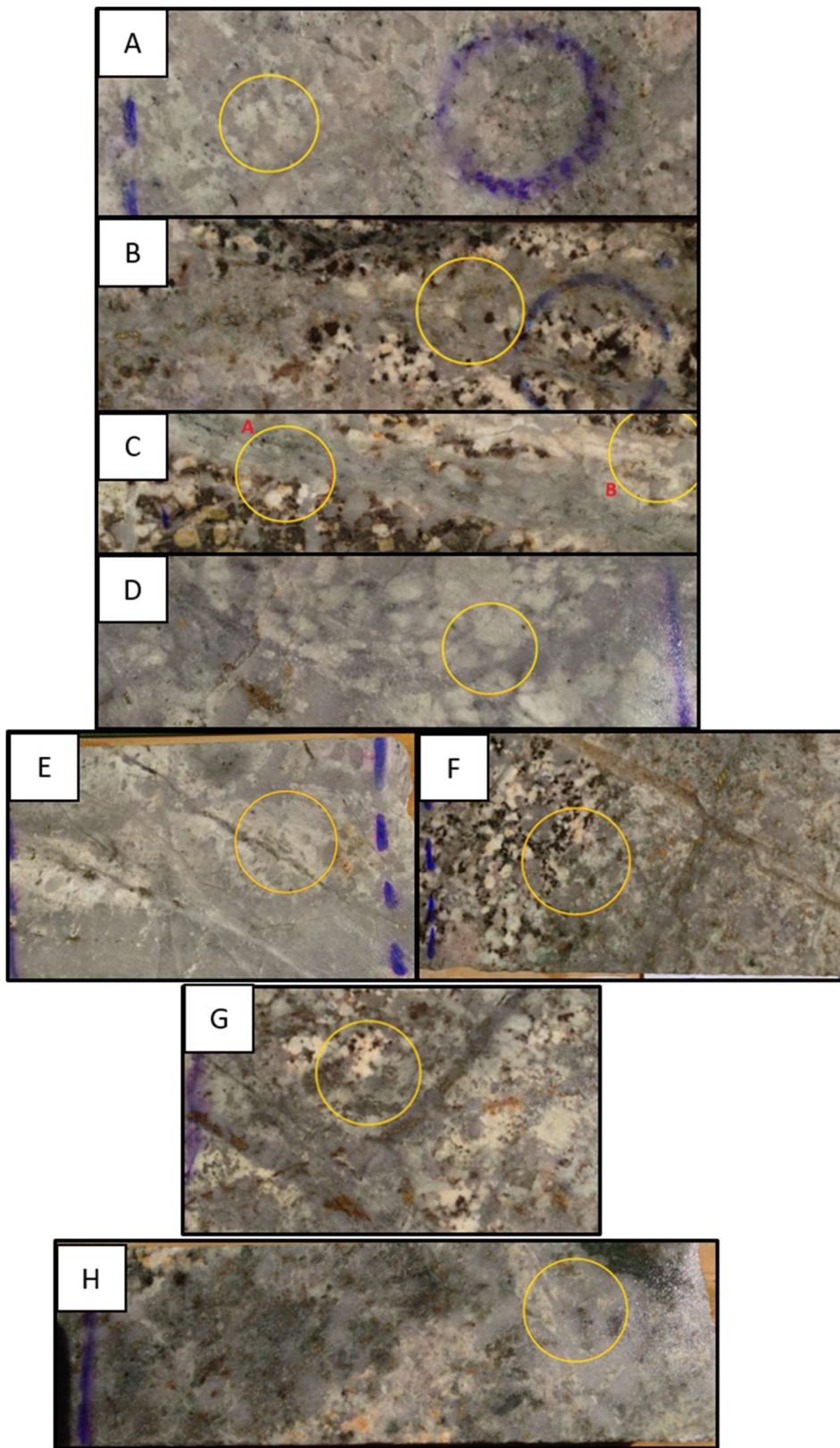


Figure 3.4: Mixed green and white sericite Samples. Yellow circle is 1-inch laser mount location. Descriptions in section 3.2.3.  
A) TTB\_SB07; B) TTB\_SB10; C) TTB\_SB14 with both mounts; D) TTB\_SB16; E) TTB\_SB20; F) TTB\_SB21; G) TTB\_SB22; H)  
TTB\_SB23

TTB\_SB23: Granite with relict potassic alteration overprinted by strong patches of green sericite and disseminated chalcopyrite, pyrite and minor bornite. Later overprint of white sericite is observed as selvage to quartz ± sulfide veins. Minor anhydrite observed. The mount was located on the contact of white sericite selvage with green sericite patches (Fig. 3.4h).

### 3.2.4 White Sericite Samples

TTB\_SB11: Equigranular granite with relict potassic alteration and barren quartz veins, overprinted by white sericite alteration as selvages to quartz, pyrite veins. White sericite selvages coalesce to form roughly 10 centimetres of pervasive white sericite alteration with only relict quartz crystals. The mount was taken within this pervasive alteration (Fig. 3.5a).

TTB\_SB12: Equigranular granite with pervasive white sericite alteration as coalesced selvages to quartz-pyrite veins. Roughly 10% pyrite content is observed in veins and selvages (Fig. 3.5b).

TTB\_SB13: Equigranular granite with pervasive white sericite alteration (minor green sericite) Quartz-bornite-pyrite veins crosscut relict quartz crystals. The greenish tint is from copper oxides after bornite (Fig. 3.5c).

TTB\_SB15: Potassic altered rhyodacite porphyry with barren quartz veins, cut by a quartz-molybdenite vein. Overprinted by minor fine, discontinuous pyrite-bornite>>chalcopyrite stringers and pervasive white sericite (Fig. 3.5d).

TTB\_SB18: Equigranular granite with relict potassic alteration cut by quartz – pyrite >> chalcopyrite vein stockwork and pervasive white sericite alteration. Pyrite is observed in veins (5%; Fig. 3.5e).

## 3.3 Sulfide Characterisation

Petrographic investigation of each mount was used to refine the sulfide mineralogy observed in logging, and to reveal significant textural information. Background samples tend to lack sulfides, but samples TTB\_SB04 and TTB\_SB05 from the potassic altered rhyodacite porphyry display minor disseminated chalcopyrite that is partly replaced by pyrite and by pyrite-bornite-chalcocite, respectively.

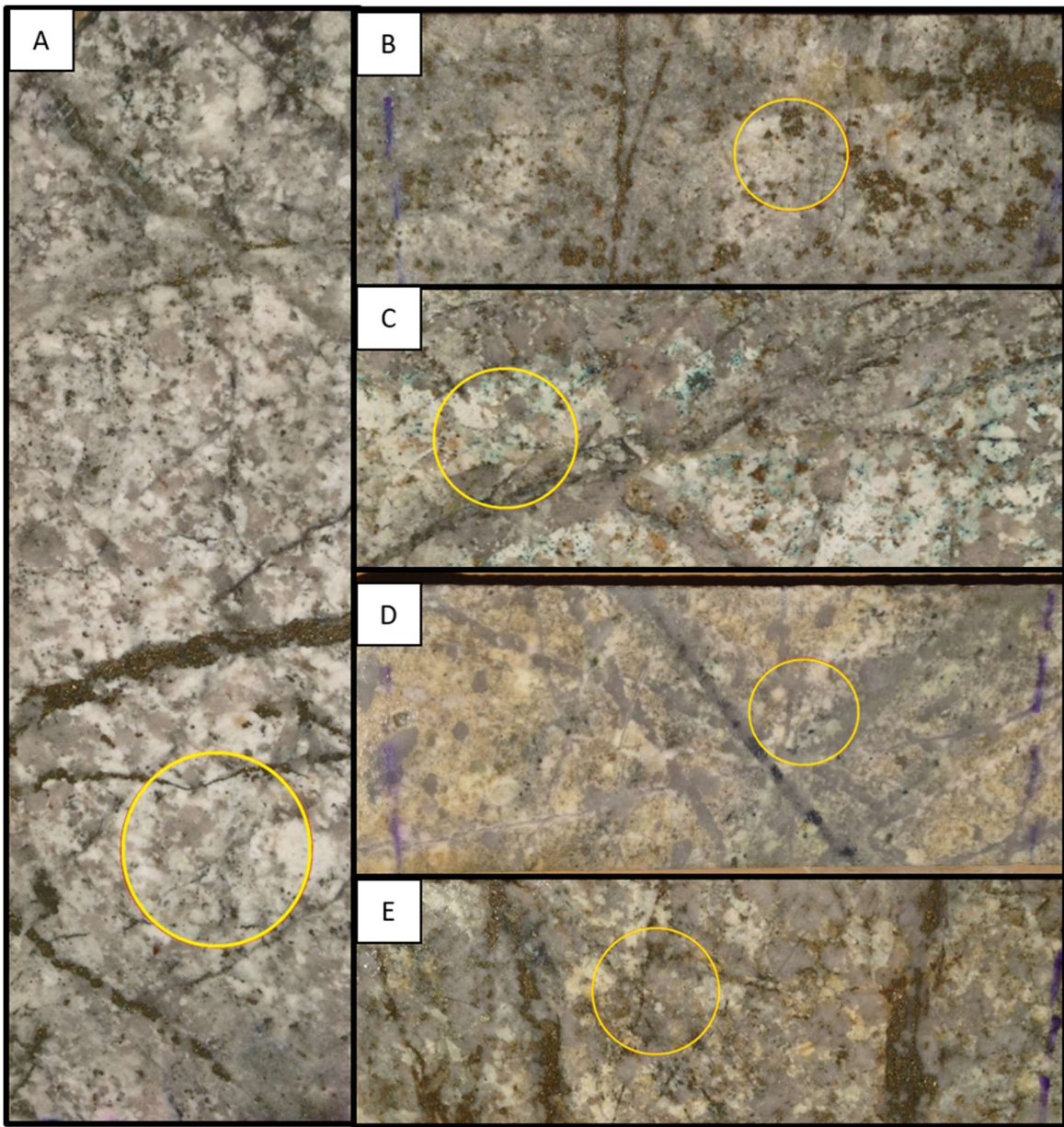


*Figure 3.5: White sericite samples. Yellow circle is 1-inch laser mount location. Descriptions in section 3.2.4 A) TTB\_SB11; B) TTB\_SB12; C) TTB\_SB13; D) TTB\_SB15; E) TTB\_SB18*

With a few exceptions (e.g., TTB\_SB14a, which was adjacent to a white sericite vein), the samples that had been logged as pure\* green sericite (\*in the sense that all the sericite was green, rather than any mixture of green and white; Table 3.1) contain a sulfide assemblage comprising either pure chalcopyrite (Fig. 3.6a) or chalcopyrite partly replaced by pyrite, bornite, chalcocite  $\pm$  digenite as a high-sulfidation overprint (Fig. 3.6b). In samples logged as having a pure white sericite phyllitic alteration facies, pyrite is the dominant sulfide species although in some cases relict chalcopyrite was observed (Fig. 3.6c). These samples are

interpreted as either replacement of chalcopyrite by pyrite or belong to the outer pyritic halo where no primary chalcopyrite has been observed.

The samples logged with proportions of both green and white sericite types show replacement of chalcopyrite by pyrite broadly proportional to the ratio of white to green sericite. This can be observed texturally in almost all samples (Fig. 3.6d through 3.6f).

Three main associations can be distinguished between the logged sericite components and observed sulfides:

1. There is a strong correlation between green sericite occurrence and chalcopyrite.
2. White sericite is always present in some degree in those samples in which pyrite has replaced chalcopyrite. White sericite is always present in samples in which pyrite is the only sulfide.
3. White sericite has a strong correlation with the presence of high sulfidation sulfide assemblage.

No paragenetic evidence has been observed that distinguishes the pyrite-only and the high sulfidation sulfide assemblages, as pyrite is stable under both conditions.

## 3.4 Sericite Characterisation

### *3.4.1 Textural Characterisation*

Examination of sericite textures under SEM revealed that there are two different morphological populations of sericite-group minerals. The dominant sericite morphology in most samples takes the form of coarse (50-100 µm) euhedral blades (Fig. 3.7a-b) and it can be observed in samples with logged white sericite, green sericite or mixtures of both types. Fine grained (1-2µm), shreddy sericite (Fig. 3.7c-d-e) is also observed in several samples from each sericite colour group, although it appears preferentially in green sericite or mixed samples. The shreddy sericite morphology is uncommon in white sericite samples.

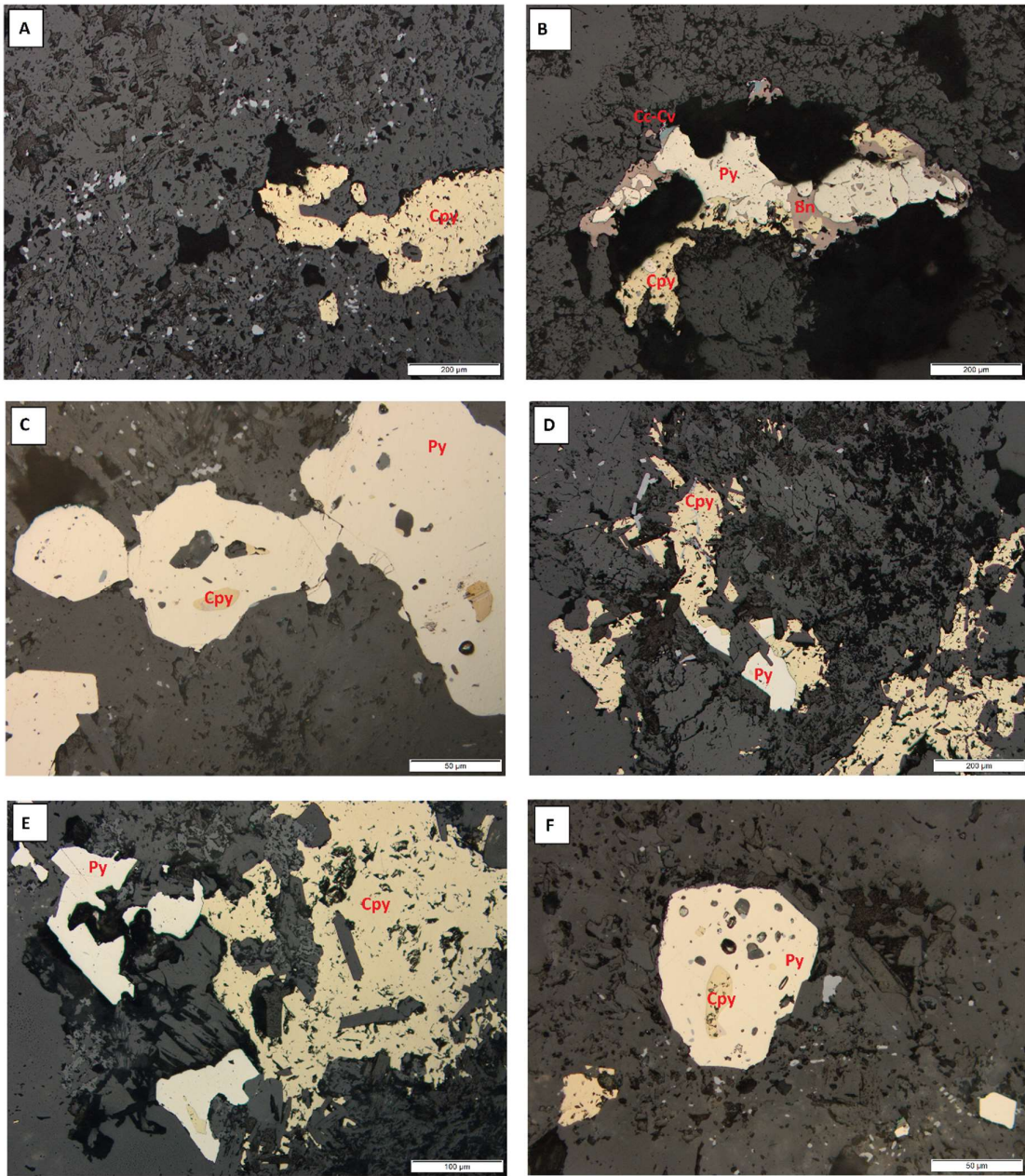


**Figure 3.6:** Transmitted light microscope images from laser mounts showing sulfide textural relationships. A) TTB\_SB08. Disseminated chalcopyrite together in pervasive green sericite sample. B) TTB\_SB15. High sulfidation replacement of chalcopyrite on sample with white sericite overprint of potassic rhyodacite porphyry. C) TTB\_SB18. Relict chalcopyrite cores in potassic altered granite with pervasive white sericite-pyrite overprint. D) TTB\_SB23. Weak pyrite replacement of chalcopyrite at the contacts of a white sericite vein selvage and green sericite + potassic altered granite. E) TTB\_SB17. Moderate replacement of chalcopyrite by pyrite on predominant green sericite sample with minor white sericite. F) TTB\_SB21. Strong pyrite replacement of chalcopyrite, leaving only a chalcopyrite core. Mixed sericite overprint in potassic altered granite. Legend: Py: Pyrite, Cpy: Chalcopyrite, Bn: Bornite, Cc: Chalcocite, Cv: Covellite.

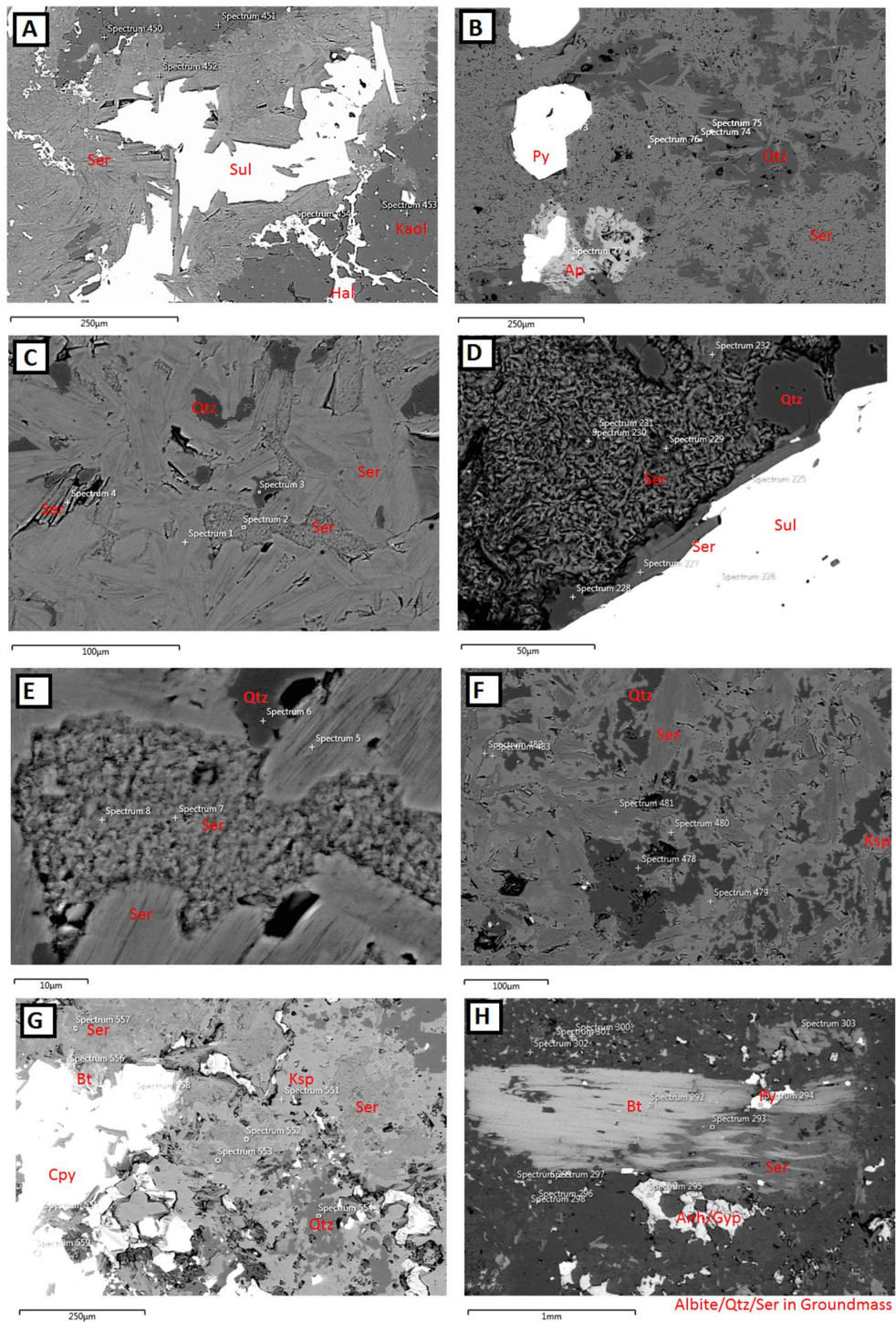


**Figure 3.7: SEM textural variation in sericite.** A) TTB\_SB23. Coarse, bladed sericite in vein selvage to sulfide-bearing micro veinlet. B) TTB\_SB12. Pervasive coarse, bladed sericite with relict quartz from granite. C) TTB\_SB07. Pervasive coarse, bladed sericite with relict patches of quartz and fine grained shreddy sericite. D) TTBJ\_SB11. Fine grained shreddy sericite and quartz cut by quartz-sulfide-coarse, bladed sericite vein. Shreddy sericite appears to be within relict mafic site of granite E) TTB\_SB07. Close-up of sericite contacts from (C) shows that pervasive coarse grained sericite is leaving patches of pre-existing fine, shreddy sericite and quartz. F) TTB\_SB21. Moderate pervasive coarse, bladed sericite overgrowing potassic alteration with orthoclase flooding. G) TTB\_SB17 Moderate, patchy sericite overprint on orthoclase-biotite altered granite with chalcopyrite. H) TTB\_SB14b. Sericite replacing biotite phenocryst in white sericite overprint of rhyodacite porphyry.

Fine-grained, shreddy sericite has a patchy appearance. It resembles the morphology of classical secondary biotite alteration in porphyry systems (e.g., Titley and Beane, 1981) and here seems to have nucleated in the ferromagnesian sites of the potassically-altered protolith (Fig. 3.7g). The euhedral bladed sericite has a more pervasive nature and is interpreted to destroy pre-existing textures, including the fine grained, shreddy sericite (Fig. 3.7e). In samples where phyllitic alteration is less intense, coarse sericite blades are correspondingly less pervasive, revealing the pre-existing alteration assemblages. In sample TTB\_SB21, that relict texture is intense pervasive orthoclase alteration, among which only patches of quartz remain from the granite protolith (Fig. 3.7f-g).

In TTB\_SB14b, where a white sericite vein cuts the biotite rich rhyodacite porphyry, the partial replacement of a euhedral, primary biotite grain by sericite can be observed (Fig. 3.7h). To judge by the amount of secondary biotite alteration in the background samples, an attractive explanation for the shreddy sericite is that it represents a texture-preserving replacement of shreddy, secondary biotite alteration, potentially after a step through shreddy chlorite, which is commonly observed in western Pacific porphyry systems (Cooke et al., 1998).

### *3.4.2 Analytical Characterisation*

Electron microprobe data (Appendix 1) from analysed sericite sites show that the coarse, bladed sericite has muscovite compositions, whereas the fine grained, shreddy sericite is elevated in Fe and Mg (and K), and plots on a trend between sericite and biotite in a chlorite – muscovite – K-feldspar – biotite general element ratio (CMKB) diagram (e.g., Fig. 3.8). The  $(\text{Fe}+\text{Mg})/\text{Al}$  values in the trend suggest a relatively more phengitic composition of the shreddy sericite. These data are not definitive due to analytical limitations of this technique, but the trends suggest compositional distinction between the two populations.

Laser spots were planned to ablate fine, shreddy sericite agglomerations and coarse, bladed sericite, respectively, and were selected to target the purest end member morphology types available. However, due to the resolution limitations of the LA-ICPMS microscope, there is a degree of uncertainty how much of each type was ablated where both coexist. Because of this, the data are presented in Appendix 2 honouring the proportions of green and white sericite components as originally logged.

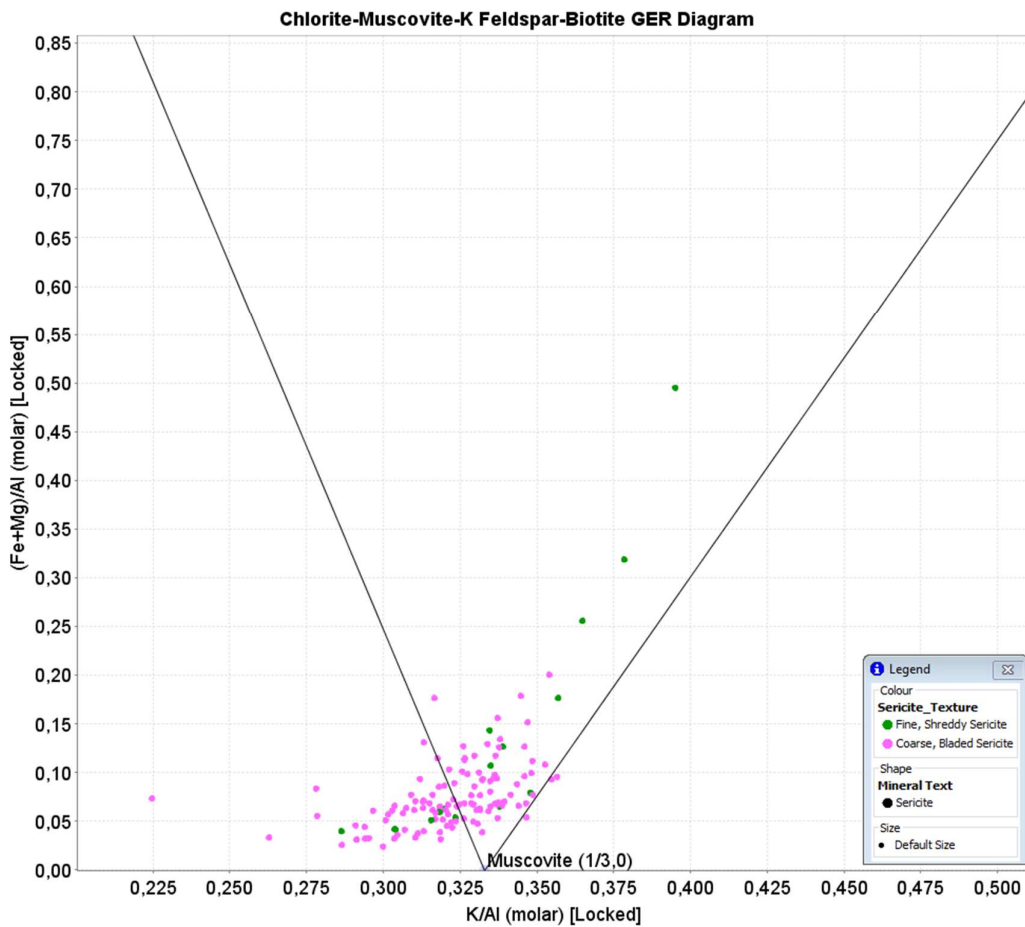


Figure 3.8: Chlorite-muscovite-K feldspar-biotite GER (CMKB) diagram showing the different geochemical trends for the variations in sericite texture. Analytical data from EPMA.

After data validation, reduction and corrections, the measurements from samples with pure white sericite plot in the same region of the CMKB diagram as the coarse grained, bladed sericite as analysed by SEM (Fig. 3.9). The samples logged with mixed colour sericite or pure green sericite plot on two different trends, one identical to the fine grained shreddy sericite observed in the EPMA and another minor trend with elevated K, trending towards orthoclase. Together these data suggest that the logged white sericite is muscovite (Figs. 3.8 and 3.9), which occurs pervasively in the rocks as coarse grained blades overprinting all pre-existing textures. The logged green sericite is therefore considered to be phengite that occurs as a fine grained, shreddy replacement of pre-existing mineral sites, most commonly secondary and primary biotite, and locally also orthoclase.

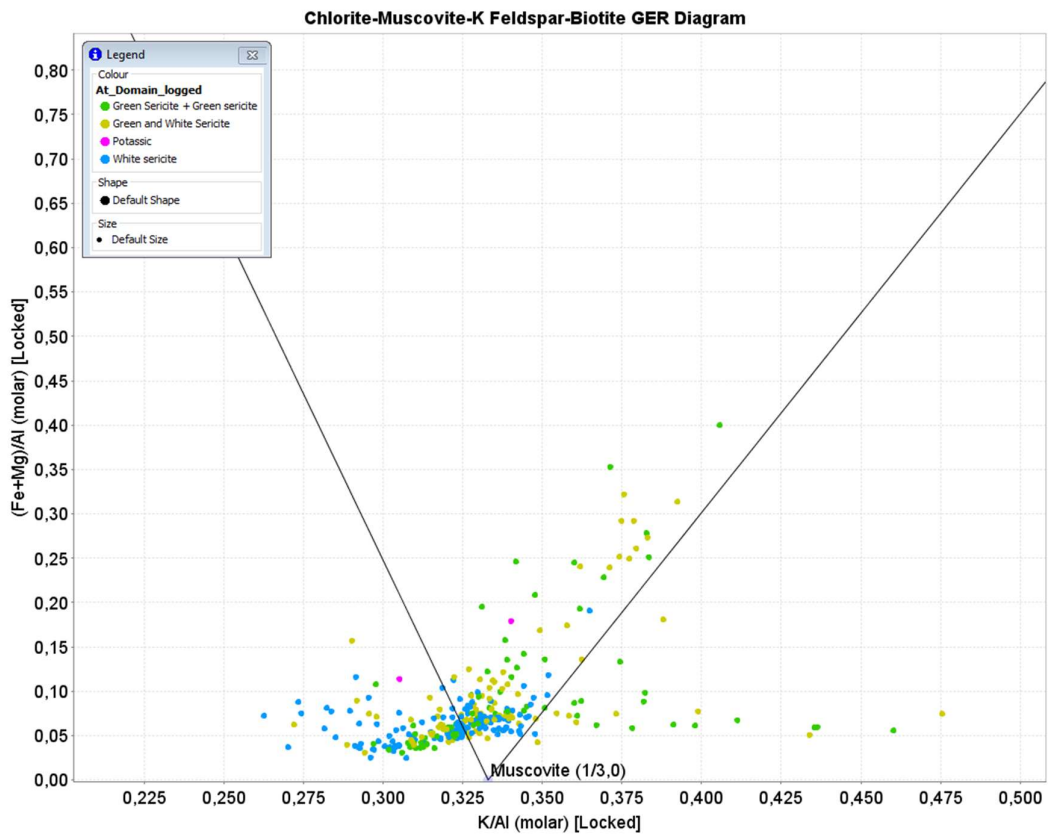


Figure 3.9: Chlorite-muscovite-K feldspar-biotite GER (CMKB) diagram showing the LA-ICPMS geochemistry of sericite sites from samples with logged white, green or mixed sericite.

The interpretation of phengite is confirmed by the SWIR spectral data (Fig. 3.10). There is a clear trend from shorter wavelengths of the w2200 scalar at the muscovitic composition, to longer wavelengths among phengitic compositions. This suggests that the muscovite formed at lower pH conditions than the phengite, and that the phengite probably formed by replacement of other silicates, at higher temperature and pH (e.g. Cohen, 2011; Halley, 2012). The sericite crystallinity scalar is calculated by dividing the hull quotient spectrum depth at w2200 by that at hqd1900, but no consistent relationship was observed between crystallinity, and composition, colour or morphology. In contrast, the backscattered electron imagery permits unambiguous recognition of the crystallinity differences between the muscovite and phengite at Taca Taca Bajo (Fig. 3.7).

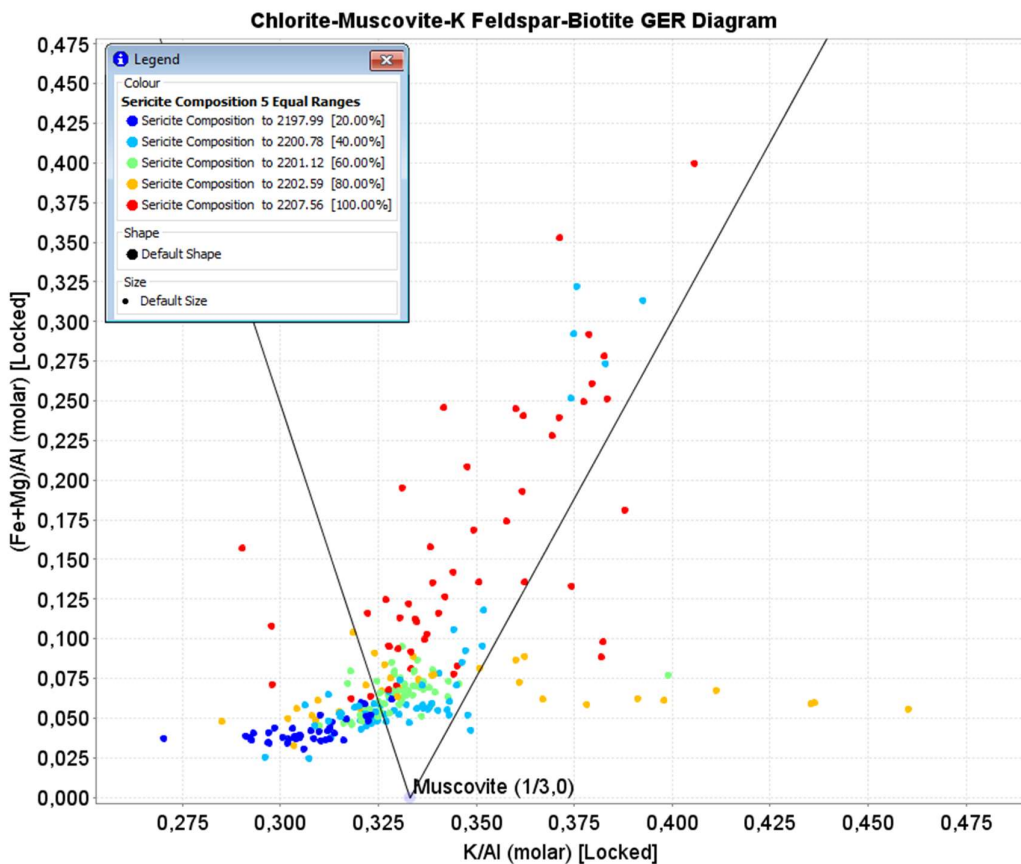


Figure 3.10: Chlorite-muscovite-K feldspar-biotite GER (CMKB) diagram coloured by the w2200 scalar on sericite samples. The population extending onto the biotite trend tend to have a longer wavelength 2200 absorption feature.

This study of sericite permits some discussion of the paragenesis of copper mineralisation at Taca Taca Bajo. To resolve this, it is necessary to address the high sulfidation state sulfide and alteration assemblage. Since some samples show partial replacement of chalcopyrite by pyrite, bornite, chalcocite  $\pm$  digenite, it was not possible to understand whether a sample containing only the high sulfidation assemblage formed by direct precipitation of these minerals, or by replacement of chalcopyrite, or replacement of other sulfides. Hence, to understand the relationship between copper grade and the muscovite and phengite alteration facies, it was necessary to consider only those samples without a high sulfidation overprint. Figure 3.11 shows the CMKB diagram coloured by the Cu grade in the two-meter interval from which the individual samples were selected. These assays are assumed to be representative of the smaller samples investigated here by micro-analytical techniques. The assays were conducted by ALS Chemex and provided to this study by FQM. The relationship

between sericite type and sulfides observed from hand specimens, where Cu sulfides were related to the green sericite, is also observed from the WR assays. Samples that have phengitic sericite show elevated Cu grades, whereas the samples with muscovitic sericite tends to be below 0.1% Cu. This, together with the petrographic observations (section 3.2) suggests that the phengite is either intimately associated with the deposition of chalcopyrite or did not corrode or destroy pre-existing chalcopyrite. In contrast, muscovite is associated with pyrite after replacement of chalcopyrite.

Trace element compositions of sericite were analysed from the granite-protolith samples only, as under-sampling of mineralised porphyritic rhyodacite was unavoidable due to the nature of this porphyry deposit (Fig. 2.9). As with the copper grades, the samples with high sulfidation state sulfide assemblages must be treated separately to understand their chemical input. Samples with alteration logged as green sericite or mixed sericite (which contain some phengite) are enriched in Li, Zn, Mn and Ni, whereas they exhibit bimodal behaviour with V, Ba and to a lesser degree Sn, and Sr (Fig. 3.12). The consistent enrichments could be due to hydrothermal input (i.e. related to phengite precipitation), whereas the bimodality of the other elements notable in this alteration facies could be related to partial geochemical conservation of the original trace element composition of biotite or orthoclase during replacement by phengite. Similar patterns are observed when the data are treated in terms of the observed sulfide assemblage. Samples that contain chalcopyrite have a gross correlation to the phengite samples (Figs. 3.12 and 3.13) in their trace element geochemistry, i.e., these are the same samples that have elevated Li, Zn, Mn and Ni. An imperfect negative correlation exists between phengite abundance and with the Cu and Pb content of sericite (Fig. 3.13).

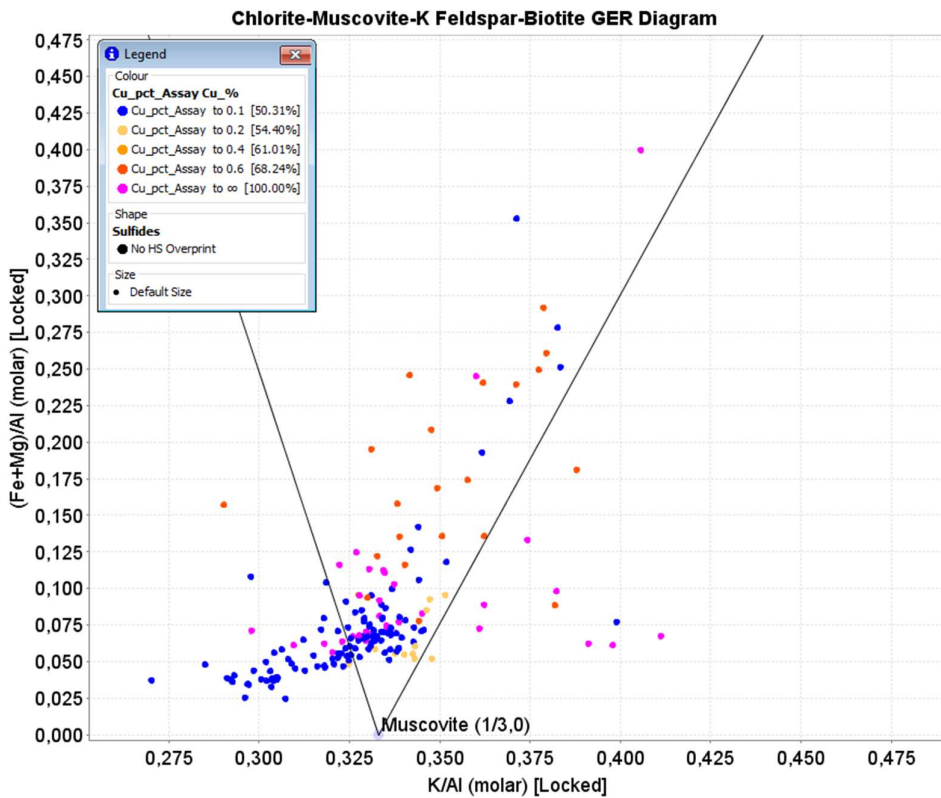


Figure 3.11: Chlorite-muscovite-K feldspar-biotite GER (CMKB) diagram of sericite analysis coloured by the whole rock Cu (%) assay of the 2-meter interval where it belongs.

### 3.4.3 High sulfidation overprint

A similar analysis was conducted including samples in which the high sulfidation assemblage is present. Samples in which there is a higher degree of replacement of primary sulfides by the high sulfidation assemblage, are dominated by sericite with compositions closer to muscovite. This phenomenon is observed in the Ba, Li and Ni trends (Fig. 3.14) and a comparable macroscopic relationship between white sericite and the high sulfidation sulfide assemblage has long been observed by the exploration geologists at Taca Taca Bajo. These observations are consistent with the interpretation of a fundamental relationship between the muscovite phase of phyllitic alteration and high sulfidation state replacement of chalcopyrite. These are interpreted to be part of the same event, as discussed in section 3.3.

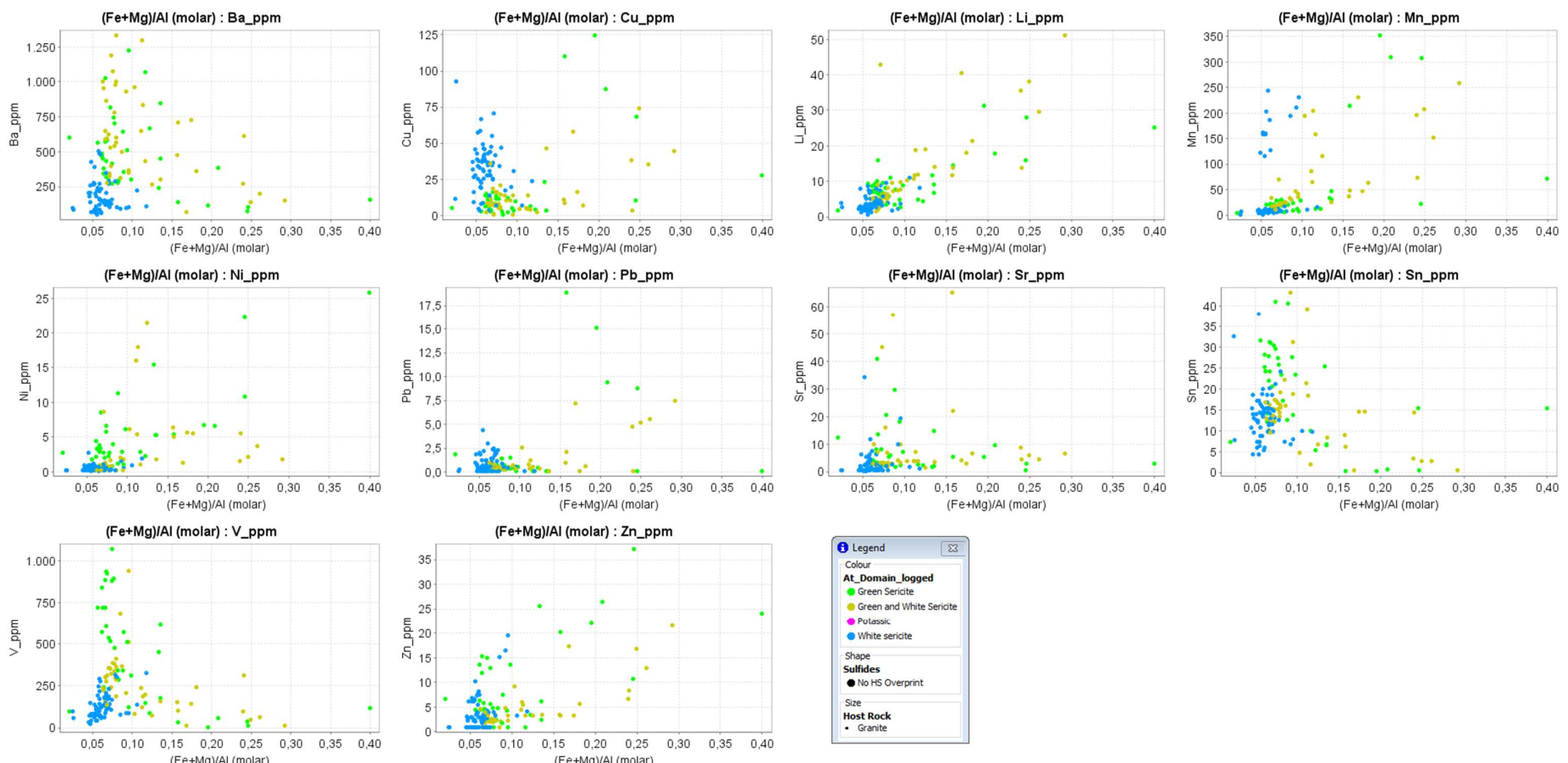


Figure 3.12: Trace element geochemistry of analysed sericite samples, coloured by the sericite type logged. Data has been filtered to show only samples in granite and without high sulfidation overprint.

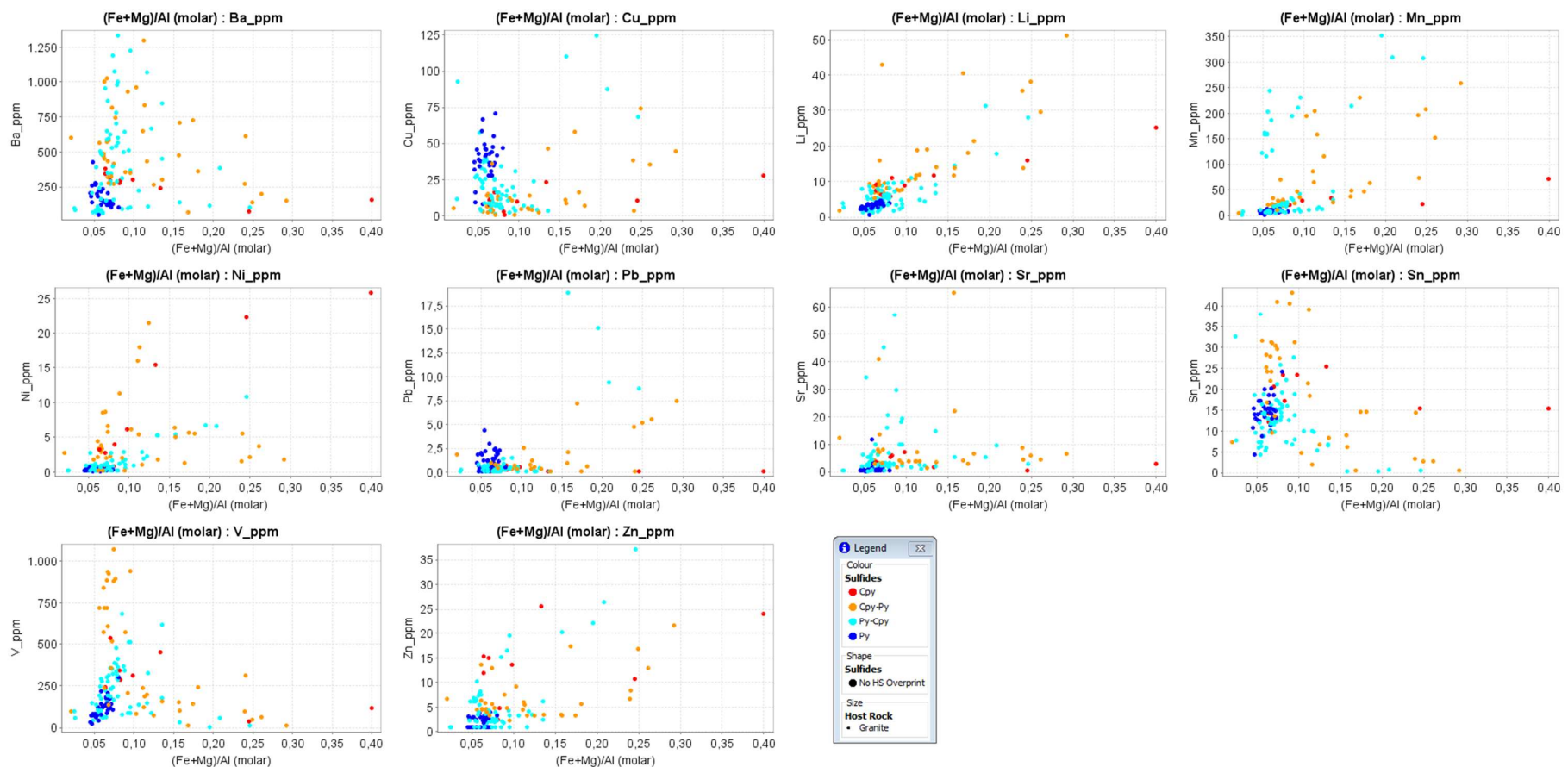


Figure 3.13: Trace element geochemistry of analysed sericite samples, coloured by the sulfide assemblage recognised on the mount. Data has been filtered to show only samples in granite and without high sulfidation overprint. All data located in Appendix 2.

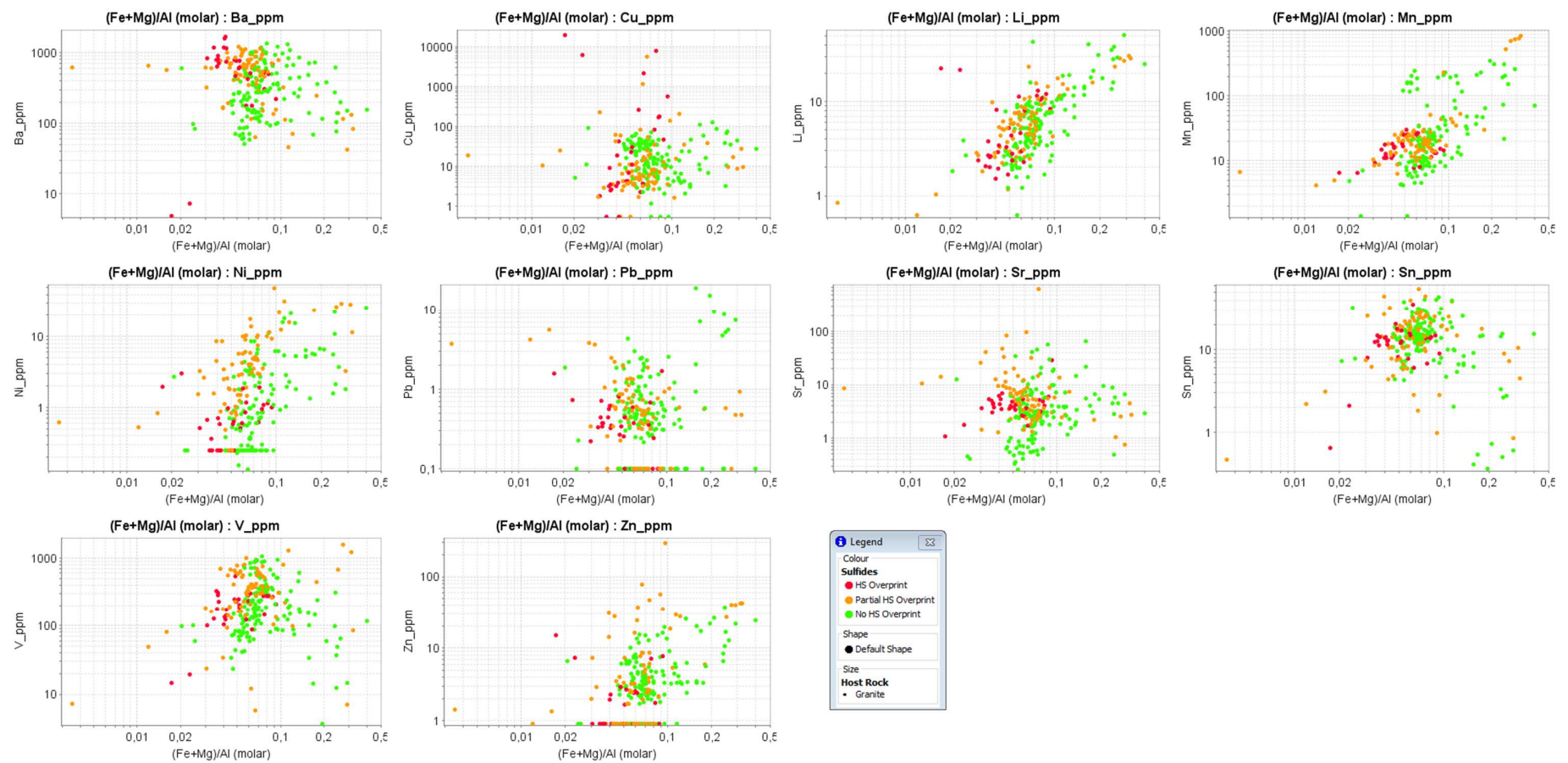


Figure 3.14: Effect of high sulfidation overprint on granite-hosted sericite trace element geochemistry. All data located in Appendix 2.

### 3.5 Apatite, Monazite and Xenotime Geochronology

The observations presented above of two distinct sericite populations place no constraints on the absolute timing of the two events. In the greater Taca Taca district there is a Permian high sulfidation epithermal alteration system (Taca Taca Alto) located ~5 kilometres northwest of the Oligocene intrusions at Taca Taca Bajo (Zappettini and Blasco, 1998). Reconnaissance geochronology was therefore undertaken to validate or discard the hypothesis that the two sericite generations reflect an Oligocene hydrothermal overprint superimposed on an older Permian alteration system (Appendix 3). Also, this part of the study could be used to further constrain geochemical zonation in apatite that might clarify possible overprints between potassic and phyllitic alteration. (e.g., Mao Mao et al., 2016)

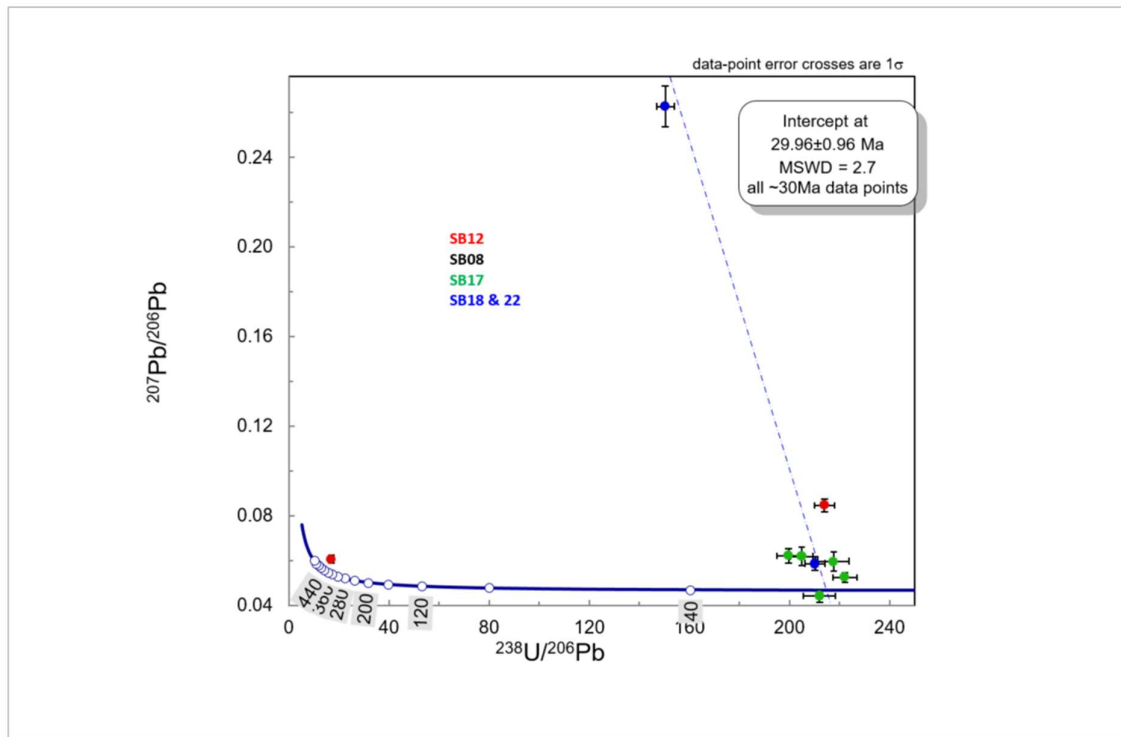


Figure 3.15: Concordia plot for monazite and xenotime U/Pb dating by LA-ICPMS. The data results in an average age of  $29.96 \pm 0.96$  Ma, reinforcing pre-existing dating that suggested the barren Oligocene porphyry as the causative intrusion of the alteration cell and mineralisation. All data located in Appendix 3.

Only one sample submitted for laser ablation analysis of apatite contained radiogenic Pb (TTB\_SB01, a background control sample), and technical issues with the LA-ICPMS analysis did not allow for robust results from apatite samples. Hydrothermal monazite and xenotime U-

Pb geochronology successfully yielded a Concordia age of  $29.96 \pm 0.96$  Ma, within error of existing geochronological results for Taca Taca Bajo. There is no suggestion of pre-existing Permian hydrothermal phosphates or reset phosphates other than one Devonian xenotime grain that plausibly belongs to the Silurian granite emplacement and has been partially reset (Fig. 3.15). This result implies that either A) there is only one phase of hydrothermal alteration related to the rhyodacite porphyry at 30-29 Ma; or B) the Oligocene event completely reset all pre-existing alteration. In both cases, sericite geochemistry would not be affected by pre-existing events, and as there is no other evidence of the latter, interpretation of both sericite generations being products of the Oligocene hydrothermal activity is considered the simplest explanation.

### 3.6 Quartz Characterisation

Quartz CL images display common hydrothermal and magmatic textures. Isolated magmatic quartz grains from granite display as round, CL-bright features. These grains are overgrown by CL-grey quartz and are cut by CL-grey and CL-dark fractures (eg. TTB\_SB07). These overgrowths and fracture-filling of weakly to non-fluorescent quartz are interpreted as late, lower temperature and lower pressure quartz (by analogy with Rusk and Reed, 2002). Hydrothermal features observed are euhedral growth zones, CL-gray patches, CL-dark patches and streaks, healed fractures with non-luminescent intensity, cobweb-like networks and jigsaw puzzle pieces.

Several quartz types have been recognized at Taca Taca Bajo, and their sulfide affinities recorded (Fig. 3.16):

- Early stage, rounded, CL-bright, igneous quartz, observed in sample TTB\_SB07 and TTB\_SB18 (Fig. 3.16c,e).
- Coarse grained, CL-gray quartz with growth textures. This is seen in veins and as overgrowth to igneous quartz. It is commonly intergrown with chalcopyrite and minor pyrite. Pyrite in cracks and cavities within coarse grained quartz are common features. This can be observed in samples TTB\_SB07, TTB\_SB08, TTB\_14B, TTB\_SB17, TTB\_SB18, TTB\_SB19, TTB\_SB20, TTB\_SB22 and TTB\_SB24 (Fig. 3.16a,b,c,d,e,g).
- Coarse grained, isolated, CL-gray quartz associated with chalcopyrite, observed in sample TTB\_SB08 (Fig. 3.16b,d).

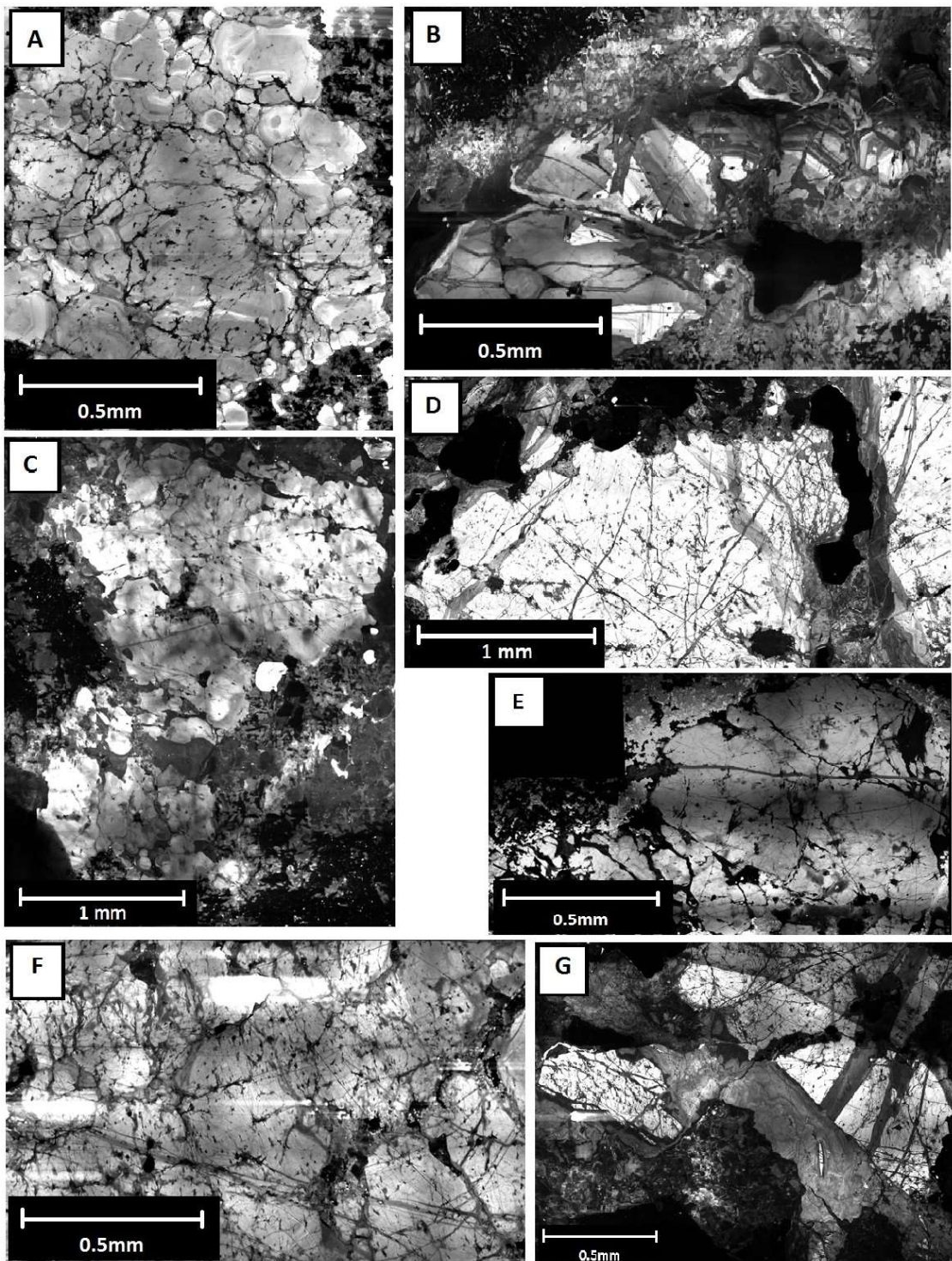


*Figure 3.16: Quartz CL images A) Fine grained quartz intergrown within quartz grains with associated pyrite; from TTB\_SB20, B) Coarse grained quartz with euhedral growth textures and associated chalcopyrite in vein; from TTB\_SB08, C) Isolated coarse grained, CL-gray quartz with chalcopyrite; from TTB\_SB08, D) CL-bright igneous quartz cut by CL-gray fine grained quartz. Pyrite associated to fine grained quartz in fractures; from TTB\_SB18, E) CL-gray, embayed quartz grain with CL-gray, fine grained quartz intermixed with sericite and disseminated chalcopyrite; from TTB\_SB13, F) Coarse, CL-gray quartz cut by darker CL quartz fractures and rimmed with dissolution textures. Pyrite and chalcopyrite intergrown with coarse grained quartz; from TTB\_SB24, G) CL-bright coarse grained quartz with dissolution, overgrowths and fractures of CL-gray quartz associated with py; from TTB\_SB18*

- Fine grained CL-gray quartz associated with sericite and chalcopyrite and/or pyrite. This can be seen in TTB\_SB13, TTB\_SB17, TTB\_SB18, TTB\_SB20 and TTB\_SB20 (Fig. 3.16a,c,e,f).
- Fine grained CL-gray quartz cutting through all previous quartz as fracture fill, this can be observed in sample TTB\_SB24 (Fig 3.16g).

At least 4 stages of quartz growth and dissolution can be recognized. These follow a simple cooling pattern from CL-bright cores to later darker CL features. This observation suggests that a simple paragenesis from hotter fluids at higher pressure to cooler fluids at lower pressure through time is applicable and no overprinting systems are interpreted.

### 3.6 Phyllitic Overprint on Potassic alteration

Potassium staining was done on all samples to study the degree of relict potassic alteration on the granitic batholith prior to the sericitic overprint and its relationship to ore grade mineralisation. Background samples of granite (TTB\_SB01, TTB\_SB02, TTB\_SB03) provided visual identification of igneous orthoclase contents in the unaltered granite host (Fig. 3.17). Samples with predominant muscovite-pyrite assemblages, either from the outer phyllitic halo or due to very strong overprint of the muscovite-high sulfidation assemblage, contain minor or no relict orthoclase. This alteration destroyed feldspar and can be observed in TTB\_SB11, TTB\_SB12, TTB\_SB13 and TTB\_SB18 (Fig. 3.18). Samples with predominant phengite-chalcopyrite assemblages show moderate to intense relict orthoclase flooding that was overprinted by sericitic alteration. This can be observed in samples TTB\_SB08, TTB\_SB09, TTB\_SB10, TTB\_SB17, TTB\_SB22 and TB\_SB24 (Fig.3.19). These observations suggest an intimate spatial relationship between potassic alteration, ore deposition and phengitic alteration.

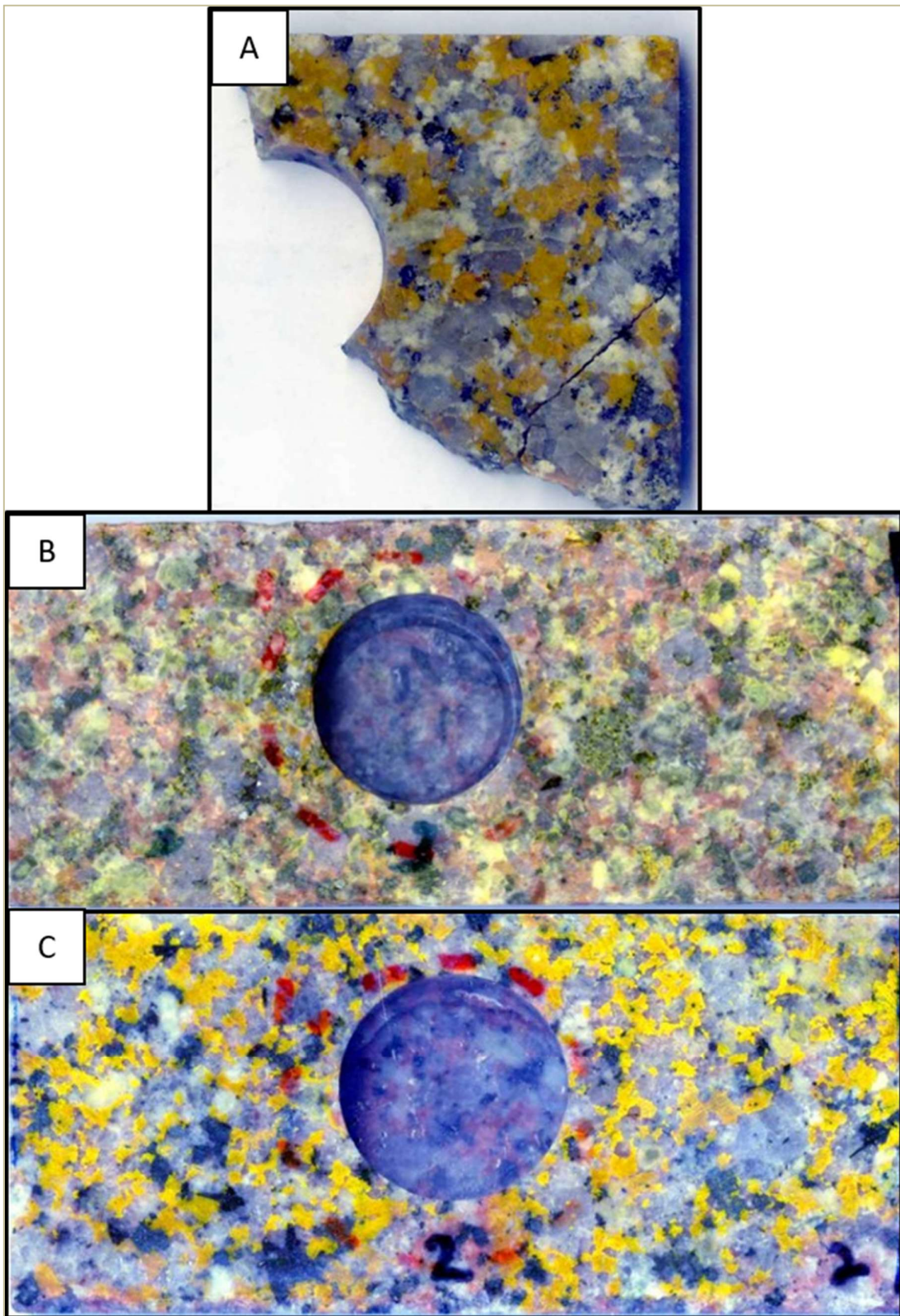


Figure 3.17: Background, fresh granite samples after K-staining. A) TTB\_SB01, B) TTB\_SB02, C) TTB\_SB03

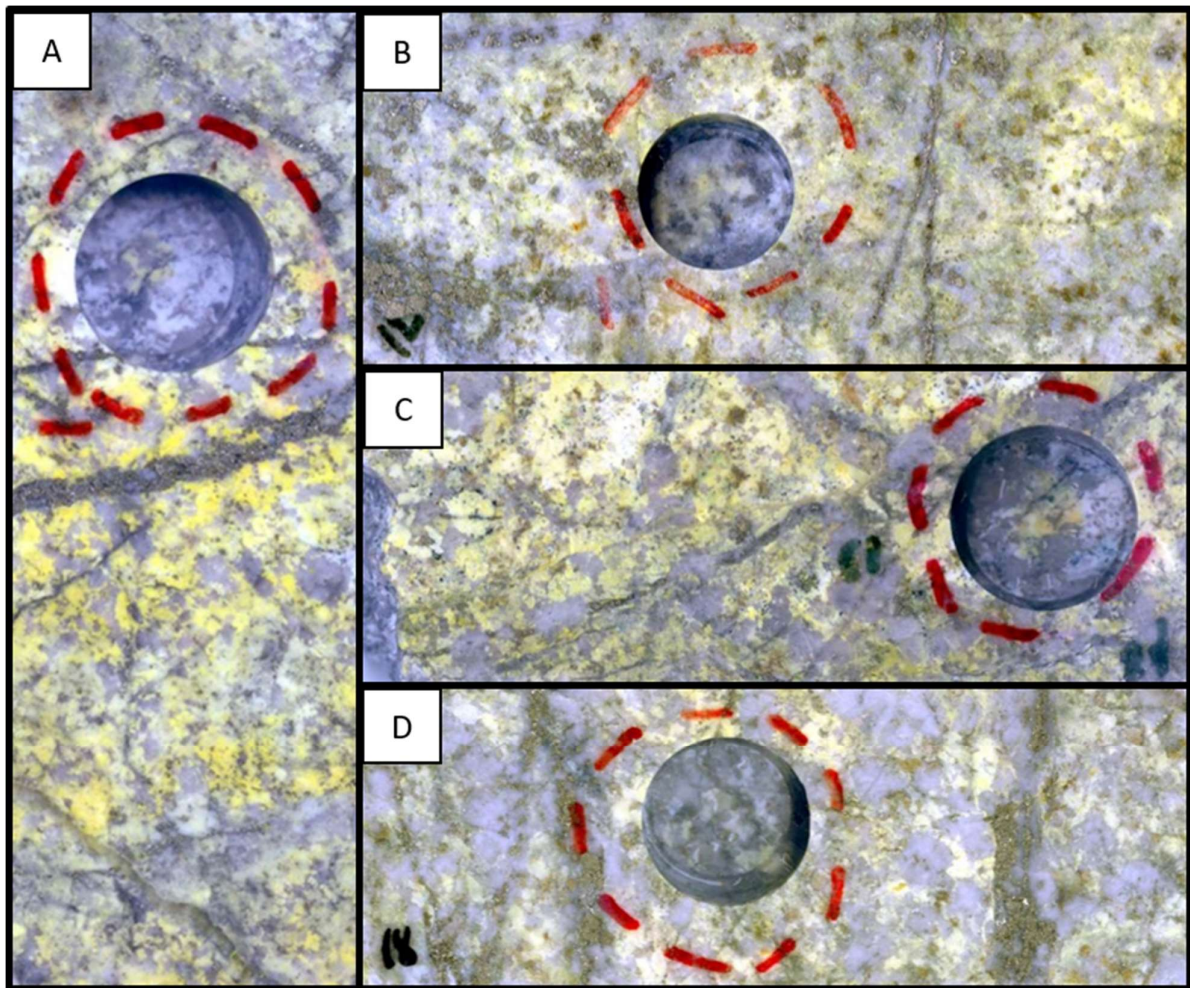


Figure 3.18: Samples with strong muscovite-pyrite assemblage on granite after K-staining. Note the orthoclase destruction caused by strong muscovitic alteration. A) TTB\_SB11, B) TTB\_SB12, C) TTB\_SB13, D) TTB\_SB18

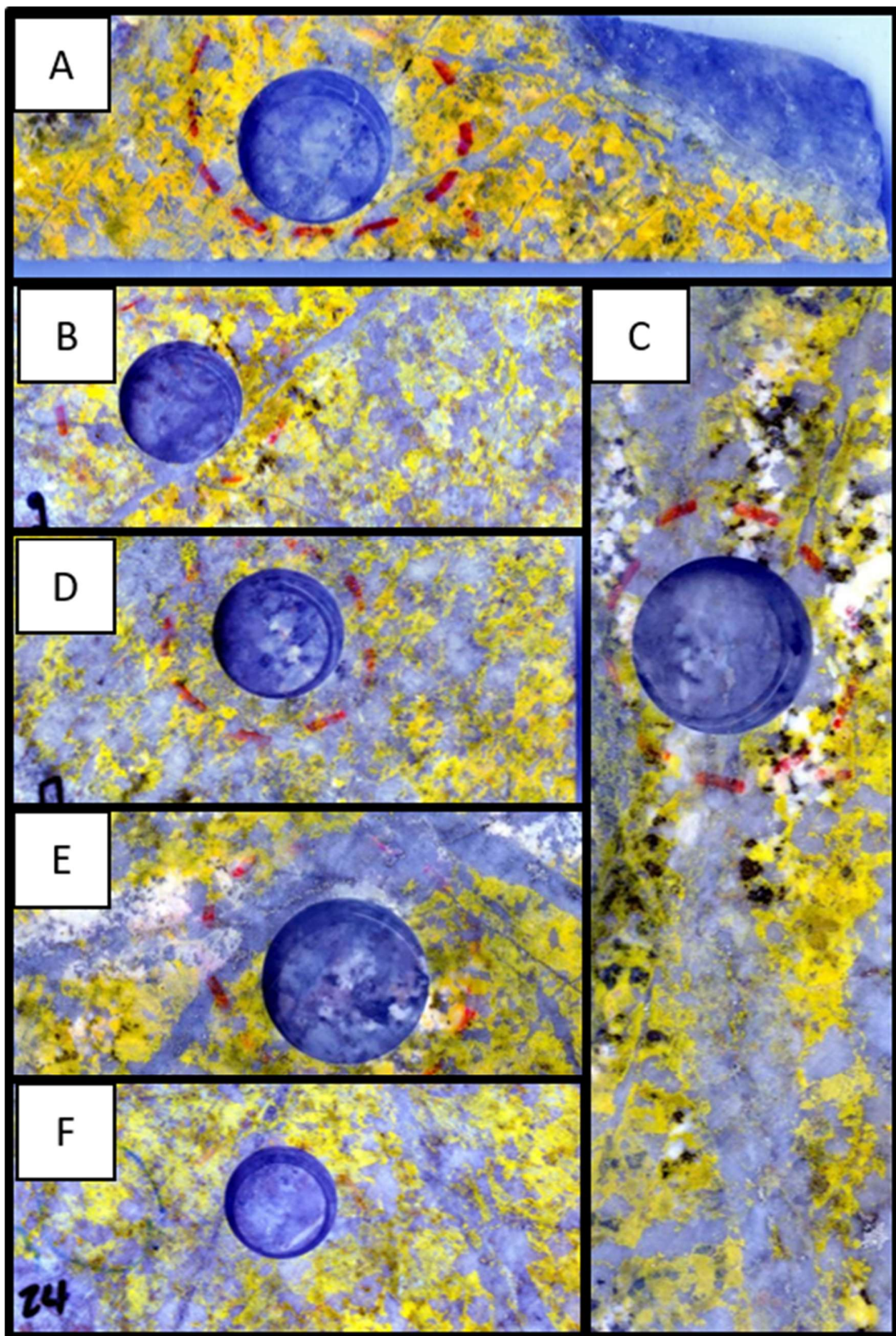


Figure 3.19: Samples with dominant phengite-chalcopyrite assemblages in granite after K-staining. Note the relict, moderate to strong, pervasive orthoclase alteration being overprinted by phengitic (+/- minor muscovitic) alteration. A) TTB\_SB08, B) TTB\_SB09, C) TTB\_SB10, D) TTB\_SB17, E) TTB\_SB22, F) TB\_SB24

## 4. Interpretation and Discussion

### 4.1 Alteration Paragenesis

The data presented in this study support pre-existing interpretations which suggested that all of the hydrothermal alteration at Taca Taca Bajo formed during the early Oligocene. These results are consistent with the interpretation that the Oligocene rhyodacite porphyry phases emplaced at this time were causative to the hydrothermal alteration. Molybdenite Re/Os dating ( $29 \pm 0.2$  Ma, Gigola, 2008) also suggests that mineralisation was related to this magmatic - hydrothermal event. The causative intrusives have undergone intense potassic alteration, with fine grained, pervasive, shreedy biotite replacing the groundmass, and have been cut by a barren quartz vein stockwork (e.g. Fig. 3.2d-f). The spatial dislocation between the potassic core and Cu mineralisation described by Waechter (2016) is interpreted following the scheme of Proffett (2009) as evidence that Taca Taca Bajo was emplaced relatively deep by comparison with classical porphyry systems (>5 km). The hydrothermal assemblage is therefore inferred to have been driven by reactions between wallrock and a single phase, low salinity magmatic fluid.

Background samples show only minor disseminated chalcopyrite in the biotite-rich groundmass of the rhyodacite porphyry dykes, although this scarcely causes enrichment at the scale of assay intervals. Potassic alteration in the granite adjacent to the causative intrusions is characterised by strong orthoclase flooding and secondary biotite replacing primary ferromagnesian minerals, together with barren quartz veins (e.g. Fig 3.19).

The potassic-altered granite has been overprinted by phyllitic alteration. The early stages of phyllitic alteration are characterised by quartz-chalcopyrite veins with phengite selvages, which commonly overlap to yield near-pervasive phengite alteration (e.g. Fig. 3.3). Within the selvages, phengite has replaced pre-existing biotite-altered ferromagnesian sites and occurs in the orthoclase altered matrix. There is a strong positive correlation between disseminated or patchy chalcopyrite and phengite alteration in the wall rock. The mineralisation style is typical of potassic and sericite-chlorite-clay (SCC) type alteration in that Cu sulfide deposition occurs in the selvage of veins, rather than exclusively within the vein fill (Rusk et al., 2008; Sillitoe, 2010). This suggests two non-exclusive possibilities: A) the patchy, disseminated

chalcopyrite was deposited during potassic alteration and survived the phengite overprint; or B) the phengite event marks the transition from potassic to phyllitic alteration, analogous to SCC alteration although with a different composition, and copper was introduced during this stage. The variation in composition is potentially due to the bulk felsic composition of the wallrocks, where the abundant K and scarce Fe would favour phengite formation over chlorite. Chalcopyrite also occurs in thin, rectilinear quartz veins with phengite haloes that overprint potassic alteration (e.g. Fig 3.3b). This observation demands that at least some chalcopyrite was introduced during the phengitic event. Exactly when copper was added as disseminated, patchy chalcopyrite that coexists with fine grained, shaggy phengite that replaced ferromagnesian sites (e.g. Fig. 3.7g) cannot be resolved between the potassic and phengite events. Spectral data (Fig. 3.10) suggests that the fluids that produced phengite-dominated green sericite alteration were less acidic than those that produced later white sericite, supporting the idea that phengite alteration formed during the transition from potassic to phyllitic alteration.

Textures observed in the SEM backscattered electron images (Fig. 3.7) suggest that phengite replaced biotite and, to a lesser degree, orthoclase in the granite. This is consistent with the LA-ICPMS data, where phengite samples follow biotite and orthoclase compositional trends rather than pure phengite trends in CMKB diagrams (Fig. 3.9). The trace element composition of the phengite therefore permits an interpretation that Fe, Mg, K contamination of the sericite occurred by inheritance from pre-existing minerals. Phengitic alteration is also observed as selvages to CL-grey quartz (with growth textures) ± chalcopyrite veins, which confirms that chalcopyrite was also deposited at least partly independent of replacement reactions during phengite alteration.

Textural relationships (Fig. 3.7) and phyllosilicate variation between muscovite and phengite suggest a paragenetically later overprint of phengite by low-pH fluids (main phyllitic phase; Fig. 3.10) that destroyed the original rock texture and replaced the pre-existing secondary mineral assemblage with muscovite.

Whereas the phengitic phyllitic alteration was either copper-additive or at the very least not ore-destructive, the more acidic muscovite alteration caused partial to full replacement of chalcopyrite by pyrite (ore destruction). This relationship is seen in the hand lens scale, as

well as at the microscopic scale (Fig. 3.6). Where muscovite alteration is weaker or appears transitional from phengite alteration, ore minerals and phengite are still fully or partially preserved, explaining the spatial relationship between Cu grades and phengite occurrence.

The high sulfidation assemblage of pyrite, bornite, chalcocite ± covellite, digenite is intimately associated with muscovite, and relates to the late stages of phyllitic alteration. Quartz CL imaging records a general down-temperature path during hydrothermal quartz deposition. The hydrothermal cell is therefore interpreted to have become more acidic upon cooling, with a concomitant increase in the sulfidation state (Fig. 1.2; e.g., Sillitoe, 2010). The strong relationship between muscovite and high sulfidation assemblage suggests that the silicate and sulfide assemblages record alteration by a single fluid. Where this fluid encountered chalcopyrite, it was initially replaced by the high sulfidation assemblage, and upon continued alteration Cu was remobilised and removed. This change in sulfidation state is transitional and associated to the intensity of the late stages of the hydrothermal paragenesis. The original paragenetic sequence presented by Almandoz (2008), has therefore only been slightly modified to reflect the variations presented in this study (Fig. 4.1).

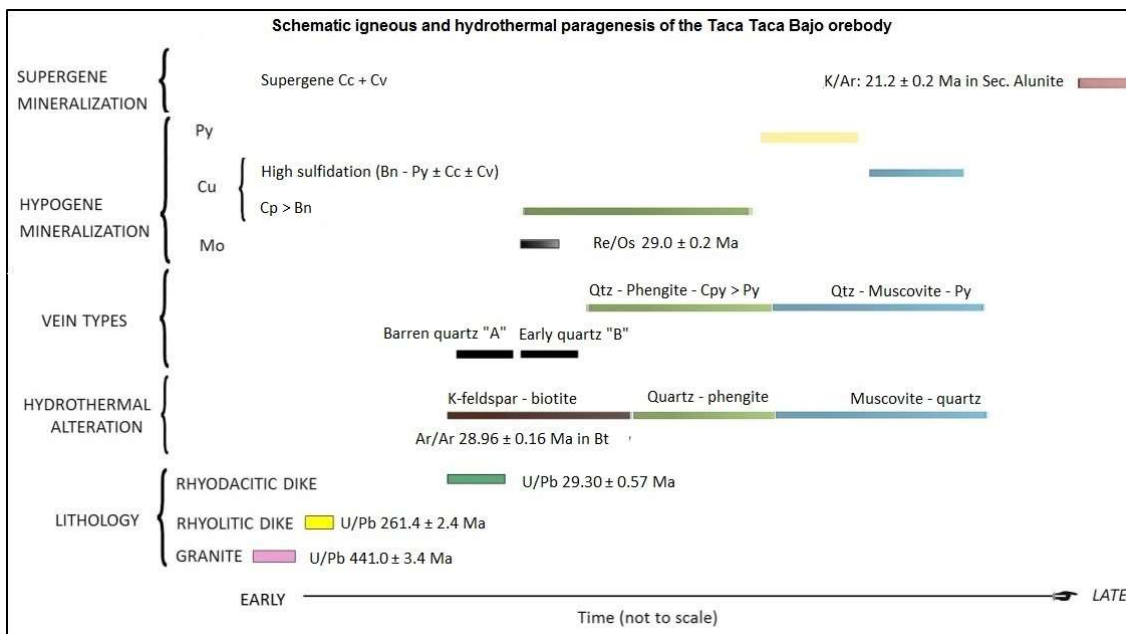


Figure 4.1: Proposed paragenesis of the Taca Taca Bajo orebody (Modified after Almandoz, 2008). Cc = chalcocite, Cv = covellite, Py = pyrite, Mo = molybdenite, Bn = bornite, Cpy = chalcopyrite, Qtz = quartz.

## 4.2 Deposit scale integration

The detailed petrographic and microanalytical results presented here permit some extrapolation to the deposit as a whole. The best data for this purpose is the Terraspec ASD data collected by FQM geologists in 2014, as this is a deposit-wide dataset but the spectrometer has a limited field of view and hence partly avoids possible issues related to whole-rock contamination. For the spectrometry to be considered representative a large quantity of data is required. The dataset at Taca Taca Bajo comprises downhole data from 68 drill holes from in and around the 0.25% Cu shell, along which spectra were collected every 2m.

Considering only the sericite-bearing samples, the w2200 scalar (sericite composition) shows a clear trend from longer wavelength within the 0.25% Cu grade shells, to shorter wavelengths in the more distal zones of the ore zone and into the pyritic shell (Fig. 4.2). The results of this study suggest that that the high wavelength sericite samples are phengite. The distribution of phyllosilicates with the spectral character of phengite could therefore be interpreted to mark the minimum original volume of potassic alteration prior to phyllitic overprint, as phengite is observed to nucleate on secondary biotite and orthoclase flooded granite. The spectral zonation is opposite to the model suggested by Halley et al. (2015), but in detail does not contradict that model, as the w2200 wavelength shift is due to a change of mineral composition, rather than variations within the same mineral species. Nonetheless, the recognition of ‘inverse’ w2200 zonation among the greater group of pale phyllosilicate minerals is relevant to exploration for porphyry deposits.

The variability observed in the microscopic scale can also be observed in the deposit scale, where the phengite domain also incorporates muscovite samples. This is due both to the overprinting nature of phengitic and muscovitic alteration and to the limitations of interval spectral sampling. On both drill core and laser mounts, it is observed that muscovite and sericite commonly coexist, which is due to variable intensity of the overprint by muscovite. This relationship is also observed in the deposit scale, though phengite is dominant adjacent to the rhyodacite porphyry stock and muscovite is dominant outside the 0.25% Cu grade shell.

The application of whole rock trace element data to extrapolation from the microscopic to deposit scale has some limitations due to the more diverse mineralogy present in a 2-meter-

wide assay interval, than in targeted microanalysis. This extrapolation is worthwhile, however, as the continuity of the assay database permits a more representative interpretation than the 68 drill holes for which spectral measurements are available. Whole rock Cu and Zn show recognisable patterns at a deposit scale that are also observable on LA-ICPMS phyllosilicate chemistry and petrographic data. At the deposit scale, there is a positive correlation between phengite - chalcopyrite domains and Zn values at trace levels (e.g., Figs. 3.12 and 3.13). Far stronger Zn enrichment occurs on the periphery of the deposit, but there is a region of minor Zn enrichment coincident with the phengite - chalcopyrite ore zone (Fig. 4.3). This could be due to Zn substitution into the chalcopyrite lattice, or to fine sphalerite accompanying this assemblage, although the latter seems unlikely as it has not been observed.

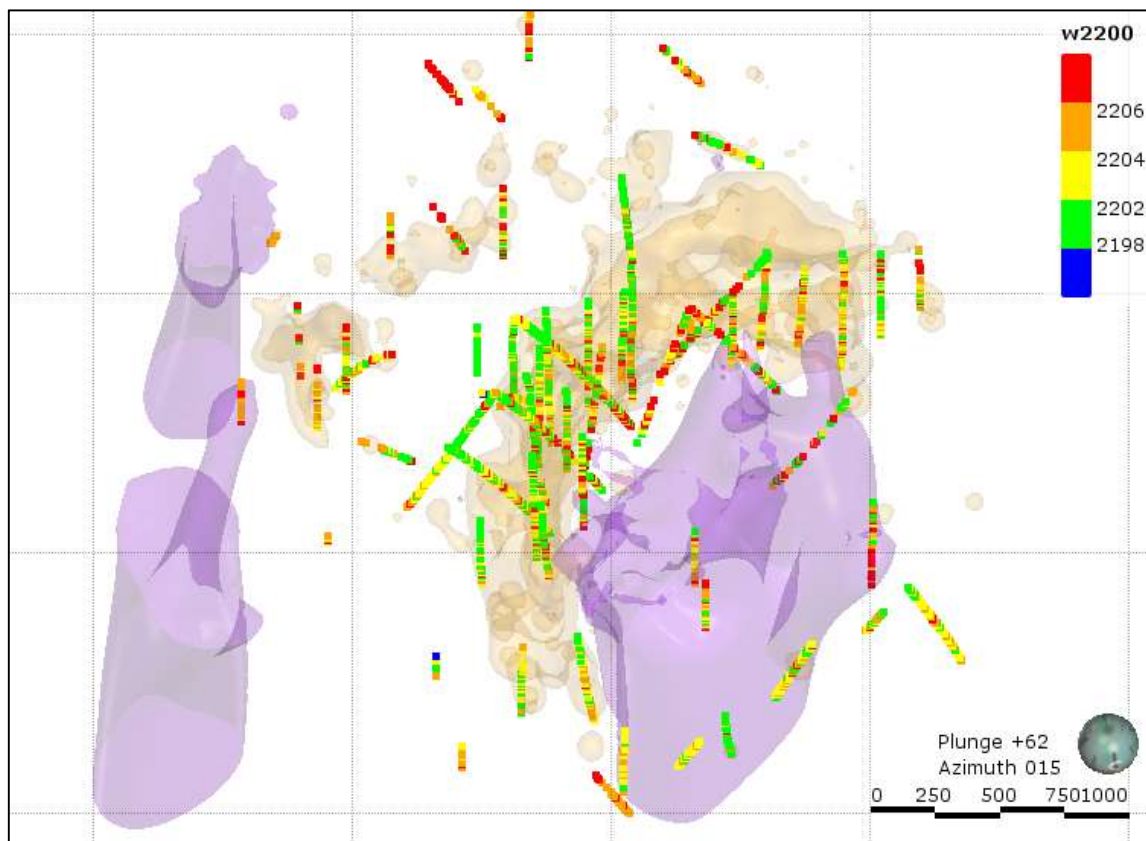


*Figure 4.2: Deposit scale view of w2200 (sericite composition) scalar on Terraspec ASD data. Higher wavelength values interpreted to be the extent of phengite, marking the minimum extent of phengite overprint on potassic alteration. Note the same proximal characteristics are observed on small satellite bodies NW from the main ore zone.*

Alteration logs provided by FQM were revised to evaluate the extent of potassic and phyllitic alteration. Potassic alteration has been recognised in varying intensities, not only in the barren rhyodacite porphyry stocks, but within the main orebody and also in the satellite orebodies roughly 750 metres northwest of central Taca Taca Bajo (Fig. 4.4a). No significant relict potassic alteration has been observed outward of the main orebody (i.e. in the pyritic halo). In contrast, phyllitic alteration has been logged throughout the whole deposit, except for the barren core in the rhyodacite porphyry (Fig. 4.4b). This original logging includes phengite and muscovite alteration, hence it does not discriminate between the ore zone and the pyritic halo, and in fact efforts to log the two separately failed to reveal systematic zonation patterns.

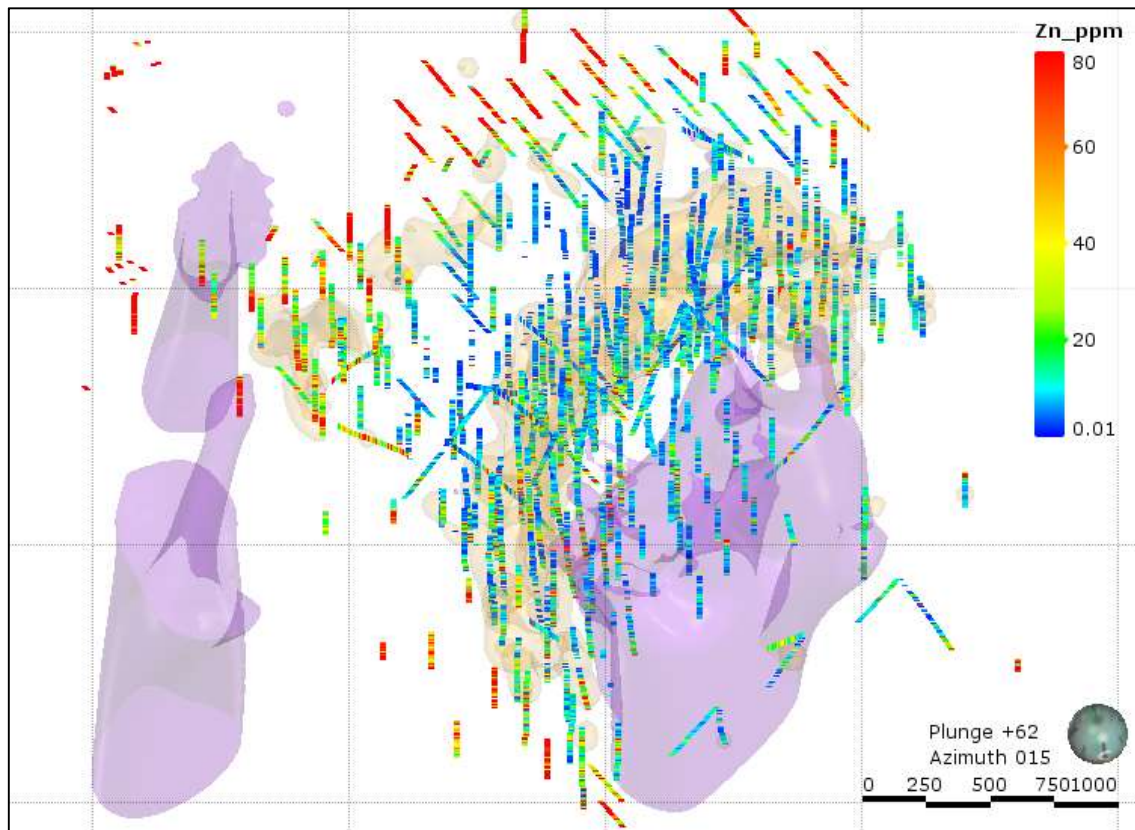


*Figure 4.3: Zn enrichment in Taca Taca Bajo assay data. Strong enrichment is peripheral to the deposit, but a trace level enrichment is observed in the phengite-chalcopyrite domain within the orebody.*

The logged alteration observations, together with the current interpretation of phyllitic alteration overprinting potassic alteration and the modelling of phengite alteration from ASD and assay data, allows an interpretation of the spatial distribution of the main paragenetic stages described above. Potassic alteration extends well into the orebody and is entirely

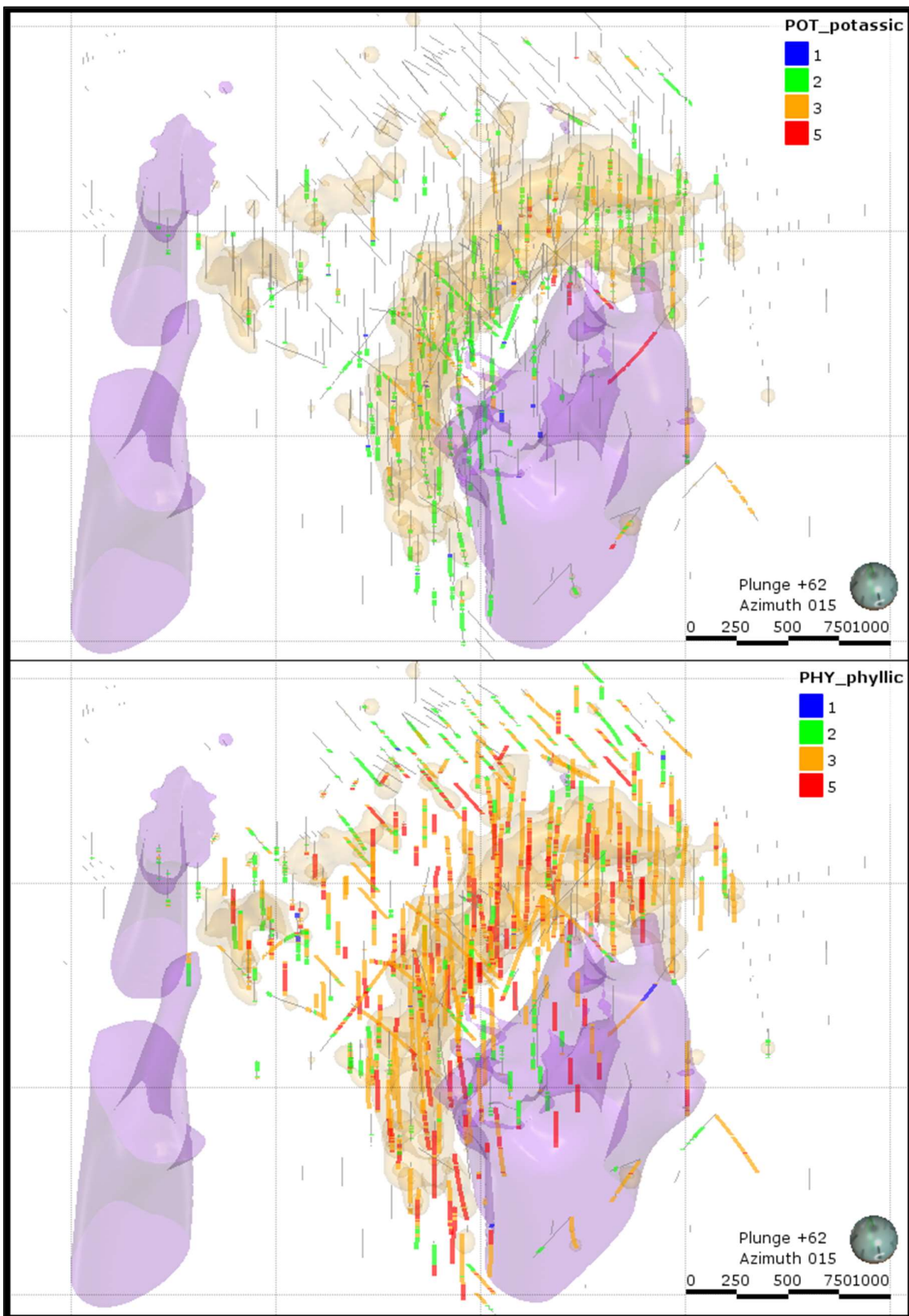


*Figure 4.4: Logged alteration shown in comparison with 0.25% Cu shell (orange) and modelled rhyodacite porphyry stock (purple). All data provided by FQM. A) Logged potassic alteration coloured by intensity (1-5). B) Logged phyllitic alteration (bulking muscovite and phengite alteration), coloured by intensity (1-5).*

contained within the pan view envelope of later muscovite, such that these two alteration minerals have a near concentric distribution (Fig. 4.5). In contrast, phengite overprints potassic alteration only in the N and W quadrants. As the distribution of phengite more closely mimics Cu distribution than the primary potassic alteration distribution, it is likely that Cu introduction occurred mostly during the phengite stage.

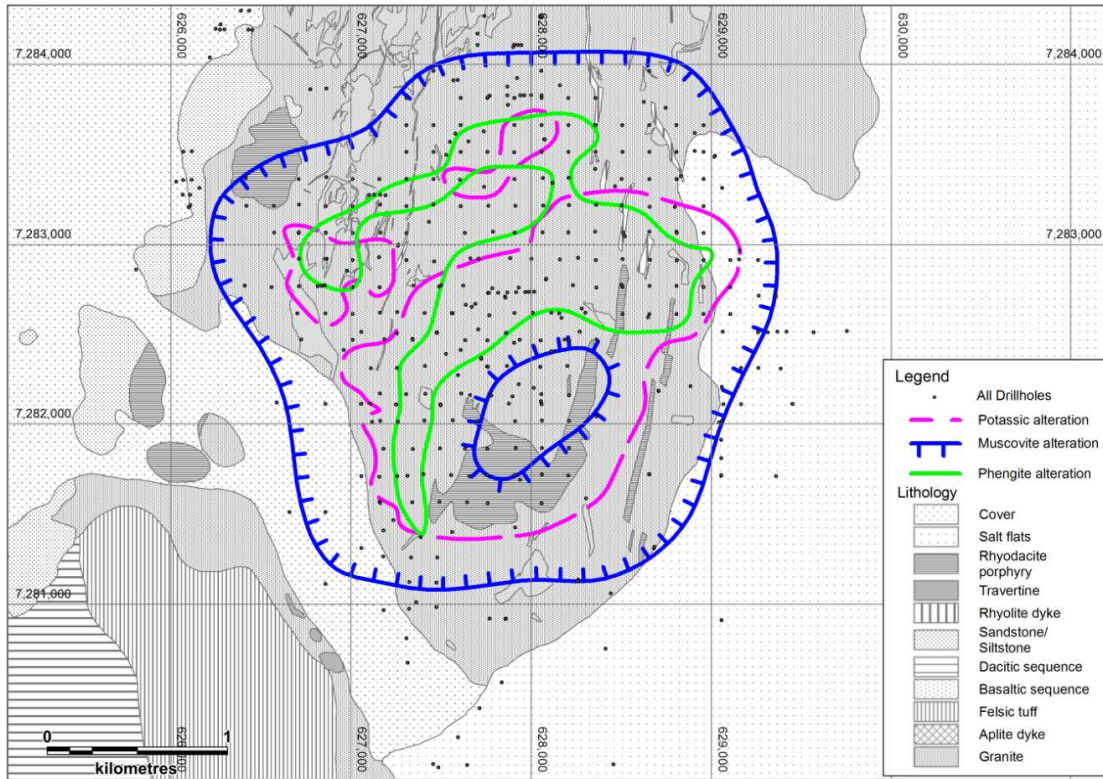


Figure 4.5: Surface projection of the potassic, phengitic and muscovitic alteration overlain on surface geology from Wood et al. (2015).

### 4.3 Implications for porphyry ore formation

As described in Chapter 1, phengitic alteration is typically seen as an outer domain to muscovitic alteration, with which it is commonly grouped in a generalised phyllitic assemblage (John et al., 2010). Green mica, comprising coexisting chlorite and illite intimately associated with Cu sulfides and potassic alteration is considered part of the SCC alteration assemblage; a transitional phase from potassic to phyllitic alteration developed at the higher levels of some porphyry Cu-Au deposits (Sillitoe, 2010). At Taca Taca Bajo, the green mica is phengite rather

than chlorite-sericite, although it is intimately associated with Cu sulfides and potassic alteration as a transitional alteration facies. Alteration at TTB therefore does not fit comfortably into the current porphyry model, although Ossandon (2001) described green micas associated to ore in a similar paragenetic and textural context at Chuquicamata, Chile, raising the possibility that this facies is not unique to TTB. Further understanding of this feature will require studies in different deposits to make analogies and to understand the genetic implications of this feature in porphyry Cu systems.

White mica chemistry and stability in porphyry systems is influenced by temperature and acidity, although it may also be affected by the increased pressure or bulk rock composition, analogous to chlorite supplanting illite at high Fe activity (e.g., Parry et al., 1984; Guidotti and Sassi, 1998; Sassi et al., 1994; Seedorf et al., 2005; Halley et al., 2015).

The author is unaware of any studies that have specifically addressed this variety of controls on potassic white mica mineralogies and compositions outside of the metamorphic environment, i.e. at conditions relevant to porphyry copper alteration systems. However, some constraints are possible on the conditions of formation of the Taca Taca Bajo system. The pale phyllosilicates are almost uniformly properly ordered micas, and correspondingly, illite and smectite are scarce. Therefore, the temperature of formation of both the phengite and muscovite stages is above the thermal threshold for illite stability (Meunier and Velde, 2004). This is consistent with interpretations that envisage formation of the Taca Taca Bajo alteration system at greater depth than classical porphyry copper systems. Why phengite is so abundant at Taca Taca Bajo, and is so closely related to copper distribution remains unexplained, but it is easy to imagine future studies that either a) consider phyllosilicate composition and mineralogy at a range of relevant pressures and bulk compositions, or b) compare the deep hypogene paragenesis of various porphyry Cu deposits emplaced into felsic host rocks, such as parts of Collahuasi, Chile, hosted by Permian rhyolitic strata, or several of the deposits in SW Arizona emplaced into Mesoproterozoic A-type granites.

#### 4.4 Exploration Implications

Characterising, and recognising the variation among porphyry Cu alteration and mineralisation facies is fundamental for successful exploration. Despite a series of well-documented similarities, every porphyry deposit is different in some way, so making analogies between field observations and recognised patterns elsewhere is important in the correct interpretation of limited exploration data.

Taca Taca Bajo is a rare example of a porphyry copper deposit with abundant phengite alteration directly associated with hypogene mineralisation. Exploration models for porphyry copper deposits therefore must permit the occurrence of phengite as a transitional phase between potassic and muscovitic phyllitic alteration, as well as the more conventional description of this mineral as a distal expression of phyllitic alteration. At Taca Taca Bajo, the phengitic stage overprints the outer potassic alteration with an asymmetric distribution, and hence the permeability controls on phengite distribution are inferred to be the primary control on grade distribution. Phengite alteration did not develop in a central ‘core’ of potassic alteration and abundant early quartz veins, and is only weakly developed on the S and E quadrants of the greater potassic alteration domain. At the level of present exposure there is no sense that the phengite stage at TTB is some relict of a shallow analogue of potassic alteration akin to SCC alteration, but instead forms part of a distinct lateral zonation pattern (Fig. 4.5).

Further studies in similar deposits need to be carried out to better understand the relationships between magmatic hydrothermal processes and their mineralogical manifestations, i.e., whether this style of alteration is a persistent feature of deeply emplaced porphyry copper systems in which alteration is mostly caused by a single-phase moderately saline fluid. Conventional fluid inclusion petrography studies, investigation of the inclusion chemistry, and titanium geothermometry on quartz (e.g. Huang and Audétat, 2012) in the different hydrothermal phases documented in this study may provide further constraints on the processes related to development of Taca Taca Bajo and comparable mineral deposits. I hope that those constraints prove useful to explorers looking to recognize and delineate similar systems.

## References

- Almundoz, G., 2015, The history of porphyry copper-gold-molybdenum exploration at Lumina Copper's Taca Taca project: FQM Internal Report, 1 p.
- Almundoz, G., Vasquez, P., Zulliger, G., Gali, S. and Orts, S., 2008, Taca Taca Bajo project, Argentina: Internal Report, 38 p.
- Alonso, R. N. and Viramonte, J. G., 1987, Geología y metalogenia de la Puna: Estudios Geológicos 43, p. 393-407.
- Alva, T. R., 2011, Variation in hydrothermal muscovite and chlorite composition in the Highland Valley porphyry Cu-Mo district, British Columbia, Canada: MSc. Thesis, Vancouver, The University of British Columbia, 225 p.
- Bailey, S.W., 1984, Classification and structures of the micas and crystal chemistry of the true micas: Reviews in Mineralogy, Mineralogical Society of America, v.13, p. 1-60.
- Benavides, S., 2015, Vein density and distribution in Taca Taca: FQM Internal Report, 1 p.
- Chang, Z., Hedenquist, J. W., White, N. C., Cooke, D. R., Roach, M., Deyell, C. L., Garcia, J., Gemmell, J. B., McKnight, S., Cuson, A. L., 2011, Exploration tools for linked porphyry and epithermal deposits: Example from the Mankayan intrusion-centered Cu-Au district, Luzon, Philippines: Economic Geology, v. 106, p. 1365-1398.
- Chavez, W. X., 2008, Comentarios generales - Petrografía de muestras de la serie RT-PC-: FQM Internal Report, 16 p.
- Chernicoff C. J., Richards, J. P., Zappettini, E. O., 2002, Crustal lineament control on magmatism and mineralization in northwestern Argentina: geological, geophysical, and remote sensing evidence: Ore Geology Reviews 21, p. 127-155.
- Cobeñas, C., Almundoz, G., 2015, Alteration and SWIR mineralogy patterns in the Taca Taca Cu-Mo porphyry: FQM Internal Report, 1 p.

Cohen, J.F., 2011, Mineralogy and geochemistry of hydrothermal alteration at the Ann Mason porphyry copper deposit, Nevada: Comparison of large-scale ore exploration techniques to mineral chemistry: MSc thesis, Corvallis, Oregon State University, 111 p.

Cooke, D. R., Heithersay, P. S., Wolfe, R. and Losada Calderón, A., 1998, Australian and western Pacific porphyry Cu-Au deposits: AGSO Journal of Australian Geology & Geophysics, 17(4), 97-104 p.

Cooke, D.R., Hollings P. and Walshe J.L., 2005, Giant porphyry deposits: Characteristics, distribution, and tectonic controls: Economic Geology 100<sup>th</sup> Anniversary Volume, p. 801-818.

Cooke, D.R., Wilkinson, J. J., Baker, M., Agnew, P., Martin, H., Chang, Z., Chen, H., Gemmell, J. B., Wilkinson, C. C., Inglis, S., Danyushevsky, L., Gilbert, S., Hollings, P., 2015, Using mineral chemistry to detect the location of concealed porphyry deposits – an example from Resolution, Arizona: International Applied Geochemistry Symposium 2015, 6 p.

Cornejo, P., 2008, TCT petrographic descriptions: FQM Internal Report, 48 p.

Dahl, P.S., When, D.C., and Feldmann, S.G., 1993, The systematics of trace-element partitioning between coexisting muscovite and biotite in metamorphic rocks from the Black Hills, South Dakota, USA: Geochimica et Cosmochimica Acta 57, p. 2487-2505.

Deer, W.A., Howie, R.A., and Zussman, J., 1992, An introduction to the rock-forming minerals: 2nd edition, p. 279-297.

Deer, W.A., Howie, R.A., and Zussman, J., 2003, Rock-forming minerals, sheet silicates: Micas, v3A, 2nd edition, p. 1-308.

Gigola, S., 2008, Taca Taca Bajo radiometric ages: A tentative interpretation with new data: FQM Internal Report, 5 p.

Gigola, S., 2015, Metallogenic context and W-NW corridor proposal for the Taca Taca district: FQM Internal Report, 1 p.

Gow, P. A. and Walshe J. L., 2005, The role of pre-existing geologic architecture in the formation of giant porphyry-related Cu+ or -Au deposits; examples from New Guinea and Chile: Economic Geology, v. 100, p. 819-833.

Guidotti, C.V., 1984, Micas in metamorphic rocks: Reviews in Mineralogy, Mineralogical Society of America, v.13, p. 357-467.

Guidotti, C.V., and Sassi, F., 1998, Petrogenetic significance of Na-K white mica mineralogy: Recent advances for metamorphic rocks: European Journal of Mineralogy, v. 10, p. 815-854.

Halley, S., 2012, Calculating spectral scalars to map hydrothermal mineral systems: Mineral Mapping Internal Report, 68 p.

Halley, S., 2015, Taca Taca: Predicting 3D mineralogy from the assay results: FQM Internal Report, 1 p.

Halley, S., Dilles J. H. and Tosdal, R. M., 2015, Footprints: Hydrothermal alteration and geochemical dispersion around porphyry copper deposits: SEG Newsletter, January 2015, p. 1; 12-17.

Haschke, M. R., Scheuber, E., Gunther, A. and Reutter, K. J., 2002, Evolutionary cycles during the Andean orogeny: repeated slab breakoff and flat subduction?: Terra Nova, 14, p. 49-55.

Hollings, P., Cooke, D. R. and Clark, A. H., 2005, Regional geochemistry of Tertiary igneous rocks in central Chile; implications for the geodynamic environment of giant porphyry copper and epithermal gold mineralization: Economic Geology, v. 100, p. 887-904.

Huang, H. and Audentát, A., 2012, The titanium-in-quartz (TitaniQ) thermobarometer: A critical examination and re-calibration: Geochimica et Cosmochimica Acta 84, p. 75-89.

John, D.A., Ayuso, R. A., Barton, M. D., Blakely, R. J., Bodnar, R. J., Dilles, J. H., Gray, F., Graybeal, F. T., Mars, J. C., McPhee, D. K., Seal, R. R., Taylor, R. D. and Vikre, P. G., 2010, Porphyry copper deposit model: Chapter B of Mineral Deposit Models for Resource Assessment: U.S. Geological Survey Scientific Investigations Report 2010-5070-B, 169 p.

Klein, C. and Dutrow, B., 2008, Crystal chemistry of rock-forming silicates: 23rd edition, Manual of Mineral Science, p. 434-482.

Lowell, J. D. and Guilbert J. M., 1970, Lateral and vertical alteration-mineralization zoning in porphyry ore deposits: Economic Geology, v. 62, p. 373-408.

Mangano, M. G. and Buatois, L. A., 2004, Integración de estratigrafía secuencial, sedimentología e icnología para un análisis cronoestratigráfico del Paleozoico inferior del noroeste argentino: Revista de la Asociación Geológica Argentina, 59 (2), p. 273-280.

Mao Mao, Rukhlov, A. S., Rowing, S. M., Spence, J. and Coogan, L. A., 2016, Apatite trace element compositions: A robust new tool for mineral exploration: Economic Geology, v. 111, p. 1187-1222.

Meunier, A. and Velde B., 2004, Illite: Origins, evolution and metamorphism: Springer-Verlag Berlin Heidelberg, 289 p.

Muñoz, J.L., 1984, F-OH and Cl-OH exchange in micas with applications to hydrothermal ore deposits in micas: Reviews in Mineralogy, Mineralogical Society of America, v.13, p. 469-491.

Noble, D.C., and McKee, E.H., 1999, The Miocene metallogenic belt of central and northern Peru: Society of Economic Geologists Special Publication 7, p. 155-194.

Oncken, O., Hindle, D., Kley, J., Elger, K., Victor, P. and Schemmann, K., 2006, Deformation of the central Andean upper plate system – Facts, fiction, and constraints for plateau models: The Andes, Active Subduction Orogeny, Frontiers in Earth Sciences, p. 03-27.

Ossandón G., Fréraut, R., Gustafson L. B., Lindsay D. D. and Zentilli, M., 2001, Geology of the Chuquicamata mine: A progress report: Economic Geology, v. 96, p. 249-270.

Palacios, C., Ramirez, L., Townley, B., Solari and M., Guerra, N., 2007, The role of the Antofagasta–Calama lineament in ore deposit deformation in the Andes of northern Chile: Mineralium Deposita, v. 42, p. 301-308.

Parry, W. T., Ballantyne, J. M. and Jacobs, D. C., 1984, Geochemistry of hydrothermal sericite from Roosevelt Hot Springs and the Tintic and Santa Rita porphyry copper systems: Economic Geology, v. 79, 72-86 p.

Perelló, J., Sillitoe R. H., Mpodozis, C., Brockway, H. and Posso, H., 2012, Geologic setting and evolution of the porphyry copper-molybdenum and copper-gold deposits at Los Pelambres, central Chile: Economic Geology, Special Publication 16, p. 79-104.

Proffett, J. M., 2003, Geology of the Bajo de la Alumbrera porphyry copper-gold deposit, Argentina: Economic Geology, v. 98, 1535-1574 p.

Proffett, J. M., 2009, High Cu grades in porphyry Cu deposits and their relationship to emplacement depth of magmatic sources: Geology, August 2009; v. 37; n. 8, p. 675-678.

Ramos, V. A. and Alemán, A., 2000, Tectonic evolution of the Andes: Tectonic Evolution of South America, p. 635-685.

Richards, J. P., 2000, Lineaments revisited: SEG Newsletter, July 2000, p. 1; 14-20.

Richards, J. P., Boyce A. J. and Pringle M. S., 2001, Geologic evolution of the Escondida area, northern Chile: A model for spatial and temporal localization of porphyry Cu mineralization: Economic Geology, v. 96, p. 271-305.

Richards, S. W. and Holm, R. J., 2013, Tectonic preconditioning and the formation of giant porphyry deposits: Economic Geology, Special Publication 17, p. 265-276.

Rieder, M., 2001, Mineral nomenclature in the mica group: the promise and the reality: European Journal of Mineralogy, v. 13, p. 1009-1012.

Rosenbaum, G., Giles, D., Saxon, M., Betts, P.G., Weinberg R.F. and Duboz, C., 2005, Subduction of Nazca ridge and Inca plateau: Insights into the formation of ore deposits in Peru: Earth and Planetary Science Letters 239, p. 18-32.

Rusk, B. G. and Reed, M. H., 2002, Scanning electron microscope-cathodoluminescence analysis of quartz reveals complex growth histories in veins from the Butte porphyry copper deposit, Montana: Geology, August 2002; v. 30; n. 8, p. 727-730.

Rusk, B. G., Reed, M. H. and Dilles, J. H., 2008, Fluid inclusion evidence for magmatic-hydrothermal fluid evolution in the porphyry copper-molybdenum deposit at Butte, Montana: Economic Geology, v. 103, p. 307-334.

Salfity, J. A. and Marquillas, R. A., 1994, Tectonic and sedimentary evolution of the Cretaceous-Eocene Salta group basin: Cretaceous Tectonics of the Andes, p. 266-315.

Salfity, J., Omarini, R., Baldis, B. and Gutierrez, R., 1975, Consideraciones sobre la evolución geológica del Precámbrico y Paleozoico del Noroeste Argentino: II Congreso Iberoamericano de Geología Económica, Actas IV, p. 341-353.

Sandeman, H. A., Clark, A. H. and Farrar, E., 1995, An integrated tectono-magmatic model for the evolution of the southern Peruvian Andes (13-20°S) since 55 Ma: International Geology Review, v. 37, p. 1039-1073.

Sassi, F. P., Guidotti, C. V., Rieder, M., De Pieri, R., 1994, On the occurrence of metamorphic 2M\ phengites: some thoughts on polytypism and crystallization conditions of 3 T phengites: European Journal of Mineralogy, v. 6, 151-160 p.

Schwab, K., 1985, Basin formation in a thickening crust. The intermontane basins in the Puna and Cordillera Oriental: IV Congreso Geológico Chileno, p. I:2-139/2-159.

Scott, K., Elfen, S. C., Sim, R., Davis, B. M. and Rose, W. L., 2013, Taca Taca copper/gold molybdenum project, Preliminary economic assessment report: 2317-RPT-003, 233 p.

Seedorff, E., Barton, M. D., Stavast W. J. and Maher, D. J., 2008, Root zones of porphyry systems: Extending the porphyry model to depth: Economic Geology, v. 103, p. 939-956.

Seedorff, E., Dilles, J. H., Proffett, J. M., Einaudi, M. T., Zurcher, L., Stavast, W. J., Johnson D. A. and Barton, M. D., 2005, Porphyry deposits: characteristics and origin of hypogene features: Economic Geology 100<sup>th</sup> Anniversary Volume, p. 251-298.

Sillitoe, R. H. and Gappe, I. M., 1984, Philippine porphyry copper deposits: Geologic settings and characteristics: Bangkok, Thailand, United Nations. ESCAP, CCOP Technical Publication 14, 89 p.

Sillitoe, R. H. and Perelló J., 2005, Andean copper province: Tectonomagmatic settings, deposit types, metallogeny, exploration and discovery: Economic Geology 100<sup>th</sup> Anniversary Volume, p. 845-890.

Sillitoe, R. H., 2008, Geological model of the Taca Taca Bajo porphyry copper prospect, northwestern Argentina: Internal Report, 11 p.

Sillitoe, R. H., 2010, Porphyry copper systems: Economic Geology, v. 105, p. 003-041.

Singer, D.A., Berger, V.I., Menzie, W.D. and Berger, B.R., 2005, Porphyry copper deposit density: Economic Geology 100<sup>th</sup> Anniversary Volume, p. 491-514.

Titely, S. R. and Beane, R. E., 1981, Porphyry copper deposits: Economic Geology 75<sup>th</sup> Anniversary Volume, 214-269 p.

Tripp, G., 2015a, Taca Taca geological overview: FQM Internal Report, 1 p.

Tripp, G., 2015b, Taca Taca mineralization: FQM Internal Report, 1 p.

Turner, J.C.M., 1960, Estratigrafía de la sierra de Santa Victoria y adyacencias: Boletín de la Academia Nacional de Ciencias de Córdoba, 41, p. 163-196.

Turner, J.C.M., 1972, Puna. Geología regional Argentina: Academia Nacional de Ciencias, p. 91-117.

Waechter, F., 2016, A deep source for magmatic-hydrothermal fluids at Taca Taca Bajo: Gordon Research Conference, 2016, 1 p.

Waechter, F., Almandoz, G. and Gigola, S., 2015, Rocks of the Taca Taca orebody: FQM Internal Report, 1 p.

Wilkinson, J. J., Chang, Z., Cooke, D. R., Baker, M. J., Wilkinson, C. C., Inglis, S., Chen, H. and Gemmell, J. B., 2015, The chlorite proximitor: A new tool for detecting porphyry ore deposits: Journal of Geochemical Exploration 152, p. 10-26.

Wood, D., Waechter, F., Almandoz, G., Cobeñas, G. and Gigola, S., 2015, Taca Taca regional geology: FQM Internal Report, 1 p.

Zappettini, E. and Blasco, G., 1998, Hoja Geológica 2569-II, Socompa, Provincia de Salta, República Argentina: Instituto de Geología y Recursos Minerales, SEGEMAR, Argentina, 65 p.

## Appendix 1: SEM analytical results and interpreted mineralogy

Table A1.1: SEM analytical results and interpreted mineralogy

Sample	Sample ID	Mineral	O_pct	F_pct	Na_pct	Mg_pct	Al_pct	Si_pct	P_pct	S_pct	Cl_pct	K_pct	Ca_pct	Sc_pct	Ti_pct	V_pct	Cr_pct	Mn_pct	Fe_pct	Co_pct
SB08	2.5	Cpy	0.00	0.00	0.00	0.00	0.00	0.00	0.00	32.54	0.00	0.00	0.00	0.00	0.00	0.00	0.00	0.00	29.22	0.00
SB08	2.6	Qtz	54.54	0.00	0.00	0.00	0.00	45.46	0.00	0.00	0.00	0.00	0.00	0.00	0.00	0.00	0.00	0.00	0.00	0.00
SB08	2.7	K-spar	47.63	0.00	1.09	0.00	10.00	29.13	0.00	0.00	0.00	12.14	0.00	0.00	0.00	0.00	0.00	0.00	0.00	0.00
SB08	2.8	K-spar	47.00	0.00	0.61	2.37	9.78	27.36	0.00	0.00	0.00	12.13	0.00	0.00	0.00	0.00	0.00	0.00	0.00	0.75
SB08	5.1	K-spar	47.59	0.00	0.52	0.00	9.66	29.30	0.00	0.00	0.00	12.93	0.00	0.00	0.00	0.00	0.00	0.00	0.00	0.00
SB08	5.11	Ser	49.23	0.00	0.36	0.61	18.56	21.06	0.00	0.00	0.00	8.91	0.00	0.00	0.24	0.00	0.00	0.00	0.00	1.05
SB08	5.12	Mon + Ap	28.28	0.00	0.00	0.00	0.00	0.00	12.58	0.00	0.00	0.23	0.54	0.00	0.00	0.00	0.00	0.00	0.00	0.00
SB08	5.13	Ser	48.41	0.00	0.38	0.57	18.86	21.40	0.00	0.00	0.00	9.06	0.00	0.00	0.24	0.00	0.00	0.00	0.00	1.08
SB08	5.14	Mon + Ap	32.95	4.96	0.51	0.00	0.19	0.56	17.86	0.86	0.00	0.55	41.56	0.00	0.00	0.00	0.00	0.00	0.00	0.00
SB08	5.15	Ser	48.75	0.00	0.31	0.75	18.56	21.40	0.00	0.00	0.00	9.05	0.00	0.00	0.25	0.00	0.00	0.00	0.91	0.00
SB08	5.16	Ser	48.41	0.00	0.38	0.72	18.54	21.54	0.00	0.00	0.00	9.12	0.00	0.00	0.24	0.00	0.00	0.00	0.00	1.05
SB08	5.9	FeOx	42.48	0.00	0.00	0.00	0.00	0.00	0.00	0.00	0.00	0.13	0.14	0.00	0.00	0.00	0.00	2.34	54.91	0.00
SB08	6.17	K-spar	47.45	0.00	1.12	0.00	9.98	29.26	0.00	0.00	0.00	12.20	0.00	0.00	0.00	0.00	0.00	0.00	0.00	0.00
SB08	6.18	Ser	48.91	0.00	0.42	0.63	18.66	21.16	0.00	0.00	0.00	9.03	0.00	0.00	0.31	0.00	0.00	0.00	0.88	0.00
SB08	6.19	Mon + Ap	47.81	0.81	0.56	0.23	17.95	0.00	8.82	4.76	0.53	0.21	1.01	0.00	0.00	0.00	0.00	0.00	0.00	0.00
SB08	6.2	Qtz	54.35	0.00	0.00	0.00	0.00	45.65	0.00	0.00	0.00	0.00	0.00	0.00	0.00	0.00	0.00	0.00	0.00	0.00
SB08	6.21	Bad Spectra	15.50	0.00	0.00	0.00	4.20	7.88	0.00	0.00	0.00	3.04	0.00	0.00	0.00	0.00	0.00	0.00	69.39	0.00
SB08	6.22	Py	0.00	0.00	0.00	0.00	0.00	0.00	53.23	0.00	0.00	0.00	0.00	0.00	0.00	0.00	0.00	0.00	46.25	0.00
SB08	6.23	Hal	22.04	0.00	19.09	1.58	9.63	14.91	0.00	0.43	24.89	5.42	0.42	0.00	0.00	0.00	0.00	0.60	0.00	0.00
SB08	6.24	Mon + Ap	38.30	4.65	0.59	0.00	0.00	0.15	17.05	0.92	0.00	0.19	38.15	0.00	0.00	0.00	0.00	0.00	0.00	0.00
SB08	6.25	FeOx	43.53	0.00	0.00	0.00	0.00	0.00	0.00	0.00	0.00	0.22	1.10	0.00	0.00	0.00	0.00	2.68	52.47	0.00
SB08	6.26	Ser	48.65	0.00	0.53	0.66	18.37	21.02	0.00	0.00	0.43	8.74	0.00	0.00	0.32	0.16	0.00	0.00	1.12	0.00
SB08	6.27	K-spar	47.39	0.00	1.19	0.00	9.83	29.55	0.00	0.00	0.00	12.04	0.00	0.00	0.00	0.00	0.00	0.00	0.00	0.00
SB08	7.28	Qtz	54.29	0.00	0.00	0.00	0.00	45.18	0.00	0.00	0.00	0.00	0.00	0.00	0.00	0.00	0.00	0.00	0.00	0.00
SB08	7.29	Cpy	0.00	0.00	0.00	0.00	0.00	0.00	0.00	32.28	0.00	0.00	0.00	0.00	0.00	0.00	0.00	0.00	29.82	0.00
SB08	7.3	K-spar	47.51	0.00	0.94	0.00	9.81	29.39	0.00	0.00	0.00	12.35	0.00	0.00	0.00	0.00	0.00	0.00	0.00	0.00
SB08	7.31	K-spar	47.49	0.00	0.74	0.00	11.19	28.13	0.00	0.00	0.00	12.17	0.00	0.00	0.00	0.00	0.00	0.00	0.28	0.00
SB08	7.32	Ser	49.29	0.00	0.37	0.48	19.37	20.96	0.24	0.00	0.00	8.79	0.00	0.00	0.00	0.00	0.00	0.00	0.50	0.00
SB08	7.33	Cpy	0.00	0.00	0.00	0.00	0.00	0.00	0.00	32.58	0.00	0.00	0.00	0.00	0.00	0.00	0.00	0.00	29.30	0.00
SB08	7.34	Hal	3.23	0.00	33.59	0.14	5.42	6.56	0.00	0.00	46.21	2.71	0.00	0.00	0.00	0.00	0.00	0.00	0.32	0.00
SB08	7.35	K-spar + Ser	46.80	0.00	0.57	0.10	8.10	21.70	0.00	0.00	0.77	10.99	0.00	0.00	8.85	0.56	0.00	0.00	0.37	0.00
SB08	7.36	K-spar	47.33	0.00	0.32	0.00	9.75	29.28	0.00	0.00	0.00	13.31	0.00	0.00	0.00	0.00	0.00	0.00	0.00	0.00
SB08	7.37	Ser	49.24	0.00	0.43	0.51	19.01	20.62	0.00	0.00	0.00	8.70	0.00	0.00	0.24	0.00	0.00	0.00	1.25	0.00
SB08	7.38	Cpy	0.00	0.00	0.00	0.00	0.00	0.00	32.48	0.00	0.00	0.00	0.00	0.00	0.00	0.00	0.00	0.00	29.42	0.00
SB08	8.39	Ser	49.23	0.00	0.42	0.65	18.52	20.93	0.00	0.00	0.00	9.09	0.00	0.00	0.00	0.00	0.00	0.00	1.17	0.00
SB08	8.4	K-spar	47.20	0.00	0.41	0.00	9.62	29.76	0.00	0.00	0.00	13.01	0.00	0.00	0.00	0.00	0.00	0.00	0.00	0.00
SB08	8.41	Ser	48.67	0.00	0.50	0.46	19.61	20.20	0.00	0.00	0.00	9.09	0.00	0.00	0.00	0.00	0.00	0.00	1.47	0.00
SB08	8.42	Ser	50.00	0.00	0.48	0.54	18.46	20.85	0.00	0.00	0.00	8.65	0.00	0.00	0.20	0.00	0.00	0.00	0.81	0.00
SB08	8.43	Ser	48.99	0.00	0.36	0.42	19.09	20.83	0.23	0.00	0.00	9.11	0.00	0.00	0.00	0.00	0.00	0.00	0.97	0.00
SB08	8.44	K-spar	47.45	0.00	0.77	0.00	9.86	29.28	0.00	0.00	0.00	12.64	0.00	0.00	0.00	0.00	0.00	0.00	0.00	0.00
SB08	8.45	Ser	49.05	0.00	0.40	0.52	19.04	20.47	0.00	0.00	0.00	9.01	0.00	0.00	0.00	0.00	0.00	0.00	1.51	0.00
SB08	8.46	Ser	47.08	0.00	0.45	0.60	19.47	21.61	0.00	0.00	0.00	9.53	0.00	0.00	0.00	0.00	0.00	0.00	1.26	0.00
SB08	9.47	Qtz	54.47	0.00	0.00	0.00	0.00	45.53	0.00	0.00	0.00	0.00	0.00	0.00	0.00	0.00	0.00	0.00	0.00	
SB08	9.48	Ser	48.94	0.00	0.51	0.61	18.28	21.08	0.00	0.00	0.20	8.92	0.00	0.00	0.28	0.00	0.00	0.00	1.18	0.00
SB08	9.49	K-spar	47.78	0.00	0.74	0.00	9.81	29.01	0.00	0.00	0.00	12.66	0.00	0.00	0.00	0.00	0.00	0.00	0.00	0.00
SB08	9.5	Ser	49.14	0.00	0.39	0.51	18.35	20.55	0.00	0.00	0.00	8.97	0.00	0.00	0.41	0.22	0.00	0.00	1.47	0.00
SB08	9.51	Hal	1.82	0.00	30.59	0.00	0.74	1.86	0.00	0.00	62.21	0.60	0.00	0.00	0.00	0.00	0.00	0.00	0.31	0.00
SB08	9.52	Bad Spectra	28.73	0.00	0.00	0.00	1.57	2.79	0.00	0.00	0.00	1.83	0.00	0.00	55.18	6.76	0.00	0.00	3.14	0.00

Table A1.1: SEM analytical results and interpreted mineralogy

Table A1.1: SEM analytical results and interpreted mineralogy

Table A1.1: SEM analytical results and interpreted mineralogy

Sample	Sample ID	Mineral	O_pct	F_pct	Na_pct	Mg_pct	Al_pct	Si_pct	P_pct	S_pct	Cl_pct	K_pct	Ca_pct	Sc_pct	Ti_pct	V_pct	Cr_pct	Mn_pct	Fe_pct	Co_pct	
SB08	10.53	Ser	49.20	0.00	0.37	0.65	18.59	20.89	0.00	0.00	0.00	9.02	0.00	0.00	0.24	0.00	0.00	0.00	1.03	0.00	
SB08	10.54	K-spar	47.44	0.00	0.32	0.00	9.79	29.09	0.00	0.00	0.00	13.36	0.00	0.00	0.00	0.00	0.00	0.00	0.00	0.00	
SB08	10.55	Ser	48.59	0.00	0.35	0.75	18.35	21.87	0.00	0.00	0.00	9.21	0.00	0.00	0.00	0.00	0.00	0.00	0.89	0.00	
SB08	10.56	K-spar	47.78	0.00	0.60	0.00	9.78	29.01	0.22	0.00	0.00	12.60	0.00	0.00	0.00	0.00	0.00	0.00	0.00	0.00	
SB08	10.57	K-spar	47.68	0.00	0.59	0.00	10.09	28.79	0.44	0.00	0.00	12.42	0.00	0.00	0.00	0.00	0.00	0.00	0.00	0.00	
SB08	10.58	K-spar	47.98	0.00	0.62	0.00	9.77	29.23	0.00	0.00	0.00	12.40	0.00	0.00	0.00	0.00	0.00	0.00	0.00	0.00	
SB12	11.59	Py	0.00	0.00	0.00	0.00	0.00	0.00	0.00	53.14	0.00	0.00	0.00	0.00	0.00	0.00	0.00	0.00	46.86	0.00	
SB12	11.6	Py	8.08	0.00	0.00	0.28	0.00	0.00	0.00	47.73	0.00	0.00	0.00	0.00	0.00	0.00	0.00	0.00	0.00	43.92	0.00
SB12	11.61	Py	6.91	0.00	6.68	0.27	0.00	0.15	0.00	41.40	5.56	0.00	0.12	0.00	0.00	0.00	0.00	0.00	0.00	38.90	0.00
SB12	11.62	Py	8.99	0.00	0.00	0.00	0.00	0.00	0.00	46.75	0.00	0.00	0.14	0.00	0.00	0.00	0.00	0.00	0.00	44.13	0.00
SB12	12.63	Py	0.00	0.00	0.00	0.00	0.46	0.00	0.00	52.81	0.00	0.00	0.00	0.00	0.00	0.00	0.00	0.00	0.00	46.73	0.00
SB12	12.64	Qtz	54.42	0.00	0.00	0.00	0.24	45.35	0.00	0.00	0.00	0.00	0.00	0.00	0.00	0.00	0.00	0.00	0.00	0.00	
SB12	12.65	Ser	49.57	0.00	0.44	0.84	17.95	21.04	0.00	0.00	0.26	8.71	0.00	0.00	0.12	0.00	0.00	0.00	1.07	0.00	
SB12	12.66	Rut	42.15	0.00	0.00	0.00	0.27	0.00	0.00	0.00	0.00	0.00	0.00	0.00	56.50	0.00	0.00	0.00	0.75	0.00	
SB12	12.67	Rut	40.53	0.00	0.00	0.00	0.41	0.00	0.00	0.13	0.00	0.00	0.00	0.00	52.73	0.00	0.00	0.00	2.37	0.00	
SB12	12.68	Ser	48.92	0.00	0.60	1.10	17.42	21.49	0.00	0.09	0.85	8.45	0.00	0.00	0.30	0.00	0.00	0.00	0.78	0.00	
SB12	12.69	Mon + Ap	29.35	0.00	0.00	0.00	1.97	2.39	11.39	0.20	0.00	0.32	3.24	0.00	0.00	0.00	0.00	0.00	0.00	0.00	
SB12	12.7	Rut	41.96	0.00	0.00	0.00	0.40	0.10	0.00	0.00	0.00	0.00	0.00	0.00	57.20	0.00	0.00	0.00	0.35	0.00	
SB12	12.71	Rut	39.33	0.00	0.00	0.00	0.48	0.00	0.00	0.00	0.00	0.00	0.00	0.00	52.17	0.72	0.00	0.00	1.91	0.00	
SB12	12.72	Qtz	54.09	0.00	0.00	0.00	0.98	44.46	0.00	0.00	0.46	0.00	0.00	0.00	0.00	0.00	0.00	0.00	0.00	0.00	
SB12	13.73	Py	0.00	0.00	0.00	0.00	0.00	0.00	53.01	0.00	0.00	0.00	0.00	0.00	0.00	0.00	0.00	0.00	46.99	0.00	
SB12	13.74	Qtz	54.57	0.00	0.00	0.00	0.00	45.43	0.00	0.00	0.00	0.00	0.00	0.00	0.00	0.00	0.00	0.00	0.00	0.00	
SB12	13.75	Ser	49.09	0.00	0.25	0.88	17.64	21.55	0.00	0.00	9.07	0.00	0.00	0.00	0.15	0.00	0.00	0.00	1.36	0.00	
SB12	13.76	Ser	49.48	0.00	0.38	0.68	18.32	20.96	0.00	0.00	8.95	0.00	0.00	0.00	0.24	0.00	0.00	0.00	0.99	0.00	
SB12	13.77	Mon + Ap	38.78	5.85	3.06	0.00	0.00	0.00	13.06	4.55	0.00	0.00	34.43	0.00	0.00	0.00	0.00	0.00	0.00	0.27	
SB10	14.78	Py	0.00	0.00	0.00	0.00	0.00	0.00	53.30	0.00	0.00	0.00	0.00	0.00	0.00	0.00	0.00	0.00	46.70	0.00	
SB10	14.79	Cpy	6.20	0.00	0.00	0.00	0.00	0.19	0.00	30.16	0.00	0.00	0.00	0.00	0.00	0.00	0.00	0.00	28.65	0.00	
SB10	14.8	Qtz	54.63	0.00	0.00	0.00	0.00	45.37	0.00	0.00	0.00	0.00	0.00	0.00	0.00	0.00	0.00	0.00	0.00		
SB10	14.81	Rut	41.56	0.00	0.00	0.00	0.00	0.08	0.00	0.00	0.00	0.00	0.10	0.00	56.09	0.47	0.00	0.00	0.70	0.00	
SB10	14.82	Zr	35.46	0.00	0.00	0.00	0.00	14.70	0.00	0.00	0.00	0.00	0.00	0.00	0.00	0.00	0.00	0.00	0.29	0.00	
SB10	14.83	Rut	43.30	0.00	0.00	0.00	0.00	0.00	0.00	0.00	0.00	0.00	0.00	0.00	56.20	0.00	0.00	0.00	0.50	0.00	
SB10	15.85	Qtz	54.82	0.00	0.00	0.00	0.00	45.18	0.00	0.00	0.00	0.00	0.00	0.00	0.00	0.00	0.00	0.00	0.00		
SB10	15.86	Rut	41.60	0.00	0.00	0.00	0.00	0.12	0.00	0.00	0.00	0.00	0.00	0.00	56.62	0.60	0.00	0.00	0.51	0.00	
SB10	15.87	Ser	49.53	0.00	0.30	0.70	18.07	21.02	0.00	0.00	8.67	0.00	0.00	0.45	0.00	0.00	0.00	0.00	1.26	0.00	
SB10	15.88	Ser	49.88	0.00	0.24	0.80	17.94	22.27	0.00	0.00	8.14	0.00	0.00	0.20	0.00	0.00	0.00	0.00	0.54	0.00	
SB10	15.89	K-spar	47.77	0.00	0.71	0.00	9.98	28.71	0.19	0.00	0.00	12.65	0.00	0.00	0.00	0.00	0.00	0.00	0.00		
SB10	15.9	Ser	49.48	0.00	0.24	0.78	17.98	22.20	0.00	0.00	8.36	0.00	0.00	0.27	0.00	0.00	0.00	0.00	0.69	0.00	
SB10	15.91	Rut	41.41	0.00	0.00	0.00	0.16	0.19	0.00	0.00	0.10	0.25	0.00	0.00	52.55	0.00	0.00	0.00	1.78	0.00	
SB10	15.92	Rut	42.81	0.00	0.00	0.00	0.00	0.13	0.00	0.00	0.00	0.17	0.00	0.00	56.12	0.00	0.00	0.00	0.43	0.00	
SB16	16.93	Ser	49.87	0.00	0.57	0.42	19.16	21.07	0.00	0.00	8.42	0.00	0.00	0.18	0.00	0.00	0.00	0.00	0.30	0.00	
SB16	16.94	Qtz	54.45	0.00	0.00	0.00	0.00	45.55	0.00	0.00	0.00	0.00	0.00	0.00	0.00	0.00	0.00	0.00	0.00		
SB16	16.95	Ba	38.26	0.00	0.00	0.00	0.64	0.00	0.00	16.79	0.00	0.21	1.35	0.00	0.00	0.00	0.00	0.00	0.00		
SB16	16.96	Mon + Ap	38.20	4.72	0.20	0.00	0.66	1.03	17.08	0.15	0.00	0.51	36.70	0.00	0.00	0.00	0.00	0.75	0.00		
SB16	16.97	Ser	49.80	0.00	0.62	0.38	19.51	20.84	0.00	0.00	8.24	0.00	0.00	0.21	0.00	0.00	0.00	0.00	0.39	0.00	
SB16	17.1	Cpy	0.00	0.00	0.00	0.00	0.00	0.00	32.44	0.00	0.00	0.00	0.00	0.00	0.00	0.00	0.00	0.00	29.70	0.00	
SB16	17.101	Qtz	54.39	0.00	0.00	0.00	0.00	45.61	0.00	0.00	0.00	0.00	0.00	0.00	0.00	0.00	0.00	0.00	0.00		
SB16	17.102	Ser	49.82	0.00	0.36	0.62	18.77	21.18	0.00	0.00	8.76	0.00	0.00	0.00	0.00	0.00	0.00	0.00	0.48	0.00	
SB16	17.98	Py	0.00	0.00	0.00	0.00	0.00	0.00	53.10	0.00	0.00	0.00	0.00	0.00	0.00	0.00	0.00	0.00	46.90	0.00	

Table A1.1: SEM analytical results and interpreted mineralogy

Table A1.1: SEM analytical results and interpreted mineralogy

Table A1.1: SEM analytical results and interpreted mineralogy

Sample	Sample ID	Mineral	O_pct	F_pct	Na_pct	Mg_pct	Al_pct	Si_pct	P_pct	S_pct	Cl_pct	K_pct	Ca_pct	Sc_pct	Ti_pct	V_pct	Cr_pct	Mn_pct	Fe_pct	Co_pct	
SB16	17.99	Cpy	0.00	0.00	0.00	0.00	0.00	0.00	0.00	32.15	0.00	0.00	0.00	0.00	0.00	0.00	0.00	0.00	29.93	0.00	
SB16	18.103	Bn	0.00	0.00	0.00	0.00	0.00	0.00	0.00	24.58	0.00	0.00	0.00	0.00	0.00	0.00	0.00	0.00	0.00	15.31	0.00
SB16	18.104	Py	0.00	0.00	0.00	0.00	0.00	0.00	0.00	53.15	0.00	0.00	0.00	0.00	0.00	0.00	0.00	0.00	0.00	46.85	0.00
SB16	18.105	Ser	49.18	0.00	0.51	0.46	19.38	21.26	0.00	0.00	0.00	0.00	8.75	0.00	0.00	0.00	0.00	0.00	0.00	0.46	0.00
SB16	18.106	Qtz	54.51	0.00	0.00	0.00	0.00	45.49	0.00	0.00	0.00	0.00	0.00	0.00	0.00	0.00	0.00	0.00	0.00	0.00	0.00
SB16	18.107	Ser	49.62	0.00	0.39	0.51	18.93	21.69	0.00	0.00	0.00	0.00	8.42	0.00	0.00	0.00	0.00	0.00	0.00	0.44	0.00
SB16	18.108	Qtz	54.49	0.00	0.00	0.00	0.00	45.26	0.00	0.00	0.00	0.00	0.00	0.00	0.00	0.00	0.00	0.00	0.00	0.00	0.00
SB16	19.111	Ser	49.04	0.00	0.39	0.58	19.03	21.67	0.00	0.00	0.00	0.00	8.89	0.00	0.00	0.00	0.00	0.00	0.00	0.38	0.00
SB16	19.112	Ser	49.51	0.00	0.61	0.43	19.23	21.08	0.00	0.00	0.00	0.00	8.48	0.00	0.00	0.22	0.00	0.00	0.00	0.43	0.00
SB16	19.113	Qtz	54.32	0.00	0.00	0.00	0.00	45.68	0.00	0.00	0.00	0.00	0.00	0.00	0.00	0.00	0.00	0.00	0.00	0.00	0.00
SB16	19.114	Qtz	54.53	0.00	0.00	0.00	0.00	45.47	0.00	0.00	0.00	0.00	0.00	0.00	0.00	0.00	0.00	0.00	0.00	0.00	0.00
SB20	21.115	Bn	0.00	0.00	0.00	0.00	0.00	0.00	0.00	24.63	0.00	0.00	0.00	0.00	0.00	0.00	0.00	0.00	0.00	11.97	0.00
SB20	21.116	Py	0.00	0.00	0.00	0.00	0.00	0.00	0.00	53.13	0.00	0.00	0.00	0.00	0.00	0.00	0.00	0.00	0.00	46.87	0.00
SB20	21.117	Cpy	0.00	0.00	0.00	0.00	0.00	0.00	0.00	32.67	0.00	0.00	0.00	0.00	0.00	0.00	0.00	0.00	0.00	29.42	0.00
SB20	21.118	Py	0.00	0.00	0.00	0.00	0.00	0.00	0.00	53.08	0.00	0.00	0.00	0.00	0.00	0.00	0.00	0.00	0.00	46.40	0.00
SB20	22.119	Ser	49.03	0.00	0.42	1.61	17.70	21.18	0.00	0.00	0.00	0.00	8.87	0.00	0.00	0.25	0.00	0.00	0.00	0.94	0.00
SB20	22.12	K-spar	47.57	0.00	0.79	0.00	9.76	29.14	0.00	0.00	0.00	12.73	0.00	0.00	0.00	0.00	0.00	0.00	0.00	0.00	0.00
SB20	22.121	Qtz	54.50	0.00	0.00	0.00	0.00	45.50	0.00	0.00	0.00	0.00	0.00	0.00	0.00	0.00	0.00	0.00	0.00	0.00	0.00
SB20	22.122	Ser	49.31	0.00	0.35	1.47	17.69	21.16	0.00	0.00	0.00	8.94	0.00	0.00	0.36	0.00	0.00	0.00	0.72	0.00	
SB20	22.123	K-spar	47.75	0.00	1.24	0.00	10.13	29.02	0.00	0.00	0.00	11.87	0.00	0.00	0.00	0.00	0.00	0.00	0.00	0.00	0.00
SB20	22.124	Ser	49.73	0.00	0.40	0.53	18.39	21.18	0.00	0.00	0.00	8.69	0.00	0.00	0.30	0.00	0.00	0.00	0.79	0.00	
SB20	23.125	Ser	50.04	0.00	0.45	0.55	18.56	20.97	0.00	0.00	0.00	8.53	0.00	0.00	0.14	0.00	0.00	0.00	0.76	0.00	
SB20	23.126	Ser	50.35	0.00	0.51	0.59	18.30	21.29	0.00	0.00	0.00	8.37	0.00	0.00	0.00	0.00	0.00	0.00	0.59	0.00	
SB20	23.127	K-spar	47.80	0.00	0.84	0.00	9.95	28.99	0.00	0.00	0.00	12.42	0.00	0.00	0.00	0.00	0.00	0.00	0.00	0.00	0.00
SB20	23.128	Qtz	55.20	0.00	0.71	0.00	0.64	43.46	0.00	0.00	0.00	0.00	0.00	0.00	0.00	0.00	0.00	0.00	0.00	0.00	0.00
SB20	23.129	K-spar	47.69	0.00	0.86	0.00	9.97	28.84	0.00	0.00	0.00	12.64	0.00	0.00	0.00	0.00	0.00	0.00	0.00	0.00	0.00
SB20	24.13	Anh-Gyp	51.19	0.00	0.00	0.00	0.33	0.00	0.00	21.98	0.00	0.00	26.50	0.00	0.00	0.00	0.00	0.00	0.00	0.00	0.00
SB20	24.131	Ser	49.95	0.00	0.62	0.58	18.54	20.89	0.00	0.00	0.00	8.58	0.00	0.00	0.18	0.00	0.00	0.00	0.67	0.00	
SB20	24.132	Qtz	54.64	0.00	0.00	0.00	0.00	45.36	0.00	0.00	0.00	0.00	0.00	0.00	0.00	0.00	0.00	0.00	0.00	0.00	0.00
SB20	24.133	Ser	49.92	0.00	0.62	0.69	18.51	20.90	0.00	0.00	0.00	8.50	0.00	0.00	0.19	0.00	0.00	0.00	0.66	0.00	
SB20	24.134	Qtz	55.94	0.00	0.00	0.00	0.00	44.06	0.00	0.00	0.00	0.00	0.00	0.00	0.00	0.00	0.00	0.00	0.00	0.00	0.00
SB22	25.135	FeOx	43.62	0.00	0.00	0.00	0.00	0.00	0.36	0.00	0.00	0.00	0.49	0.00	0.00	0.00	0.00	0.00	0.88	54.64	0.00
SB22	25.136	Al-sil	57.85	0.00	0.00	0.00	20.93	21.02	0.00	0.00	0.00	0.00	0.00	0.00	0.00	0.00	0.00	0.00	0.20	0.00	0.00
SB22	25.137	Alb	50.50	0.00	7.76	0.00	10.85	29.68	0.00	0.00	0.00	0.19	1.02	0.00	0.00	0.00	0.00	0.00	0.00	0.00	0.00
SB22	25.138	Ser	49.29	0.00	0.53	0.30	19.01	20.18	0.00	0.00	0.00	8.68	0.00	0.00	0.00	0.00	0.00	0.00	0.00	2.01	0.00
SB22	26.139	Alb	50.00	0.00	7.72	0.00	11.02	29.89	0.00	0.00	0.00	0.23	1.13	0.00	0.00	0.00	0.00	0.00	0.00	0.00	0.00
SB22	26.14	Ser	49.68	0.00	0.71	0.23	19.35	19.95	0.00	0.00	0.15	8.43	0.00	0.00	0.00	0.00	0.00	0.00	0.00	1.50	0.00
SB22	26.141	Hal	4.11	0.00	35.92	0.00	4.12	4.32	0.00	0.00	49.33	0.00	0.00	0.00	0.00	0.00	0.00	0.00	0.31	0.00	0.00
SB22	26.142	Hal	13.54	0.00	26.91	0.26	6.75	12.20	0.00	0.00	36.08	1.28	0.62	0.00	0.00	0.00	0.00	0.00	0.00	1.24	0.00
SB22	26.143	Al-sil	55.82	0.00	0.37	0.00	21.27	22.20	0.00	0.00	0.00	0.22	0.12	0.00	0.00	0.00	0.00	0.00	0.00	0.00	0.00
SB22	27.144	Cpy	0.00	0.00	0.00	0.00	0.00	0.00	0.00	32.30	0.00	0.00	0.00	0.00	0.00	0.00	0.00	0.00	29.48	0.00	0.00
SB22	27.145	Py	0.00	0.00	0.00	0.00	0.00	0.00	0.00	53.13	0.00	0.00	0.00	0.00	0.00	0.00	0.00	0.00	46.87	0.00	0.00
SB22	27.146	Cc	0.89	0.00	0.00	0.00	0.00	0.00	0.00	21.57	0.00	0.00	0.00	0.00	0.00	0.00	0.00	0.00	0.00	3.25	0.00
SB22	27.147	Bn	0.00	0.00	0.00	0.00	0.00	0.00	0.00	23.46	0.00	0.00	0.00	0.00	0.00	0.00	0.00	0.00	0.00	11.69	0.00
SB22	27.148	Cpy	0.00	0.00	0.00	0.00	0.00	0.00	0.00	32.40	0.00	0.00	0.00	0.00	0.00	0.00	0.00	0.00	0.00	29.17	0.00
SB22	27.149	Bn	1.49	0.00	0.00	0.00	0.00	0.00	0.00	27.98	0.00	0.00	0.00	0.00	0.00	0.00	0.00	0.00	0.00	11.12	0.00
SB22	27.15	Bn	0.00	0.00	0.00	0.00	0.00	0.11	0.00	23.70	0.00	0.00	0.00	0.00	0.00	0.00	0.00	0.00	0.00	12.38	0.00
SB22	27.151	Cpy	0.00	0.00	0.00	0.00	0.00	0.00	0.00	32.32	0.00	0.00	0.00	0.00	0.00	0.00	0.00	0.00	0.00	29.52	0.00

Table A1.1: SEM analytical results and interpreted mineralogy

Sample	Sample ID	Mineral	O_pct	F_pct	Na_pct	Mg_pct	Al_pct	Si_pct	P_pct	S_pct	Cl_pct	K_pct	Ca_pct	Sc_pct	Ti_pct	V_pct	Cr_pct	Mn_pct	Fe_pct	Co_pct
SB15	42.25	Ser	48.82	0.00	0.26	1.04	18.27	21.70	0.00	0.00	0.00	9.23	0.00	0.00	0.16	0.00	0.00	0.00	0.53	0.00
SB15	44.251	K-spar	49.50	0.00	0.35	0.90	18.45	22.17	0.00	0.00	0.00	8.63	0.00	0.00	0.00	0.00	0.00	0.00	0.00	0.00
SB15	44.252	Ser	48.88	0.00	0.53	1.50	18.38	20.18	0.00	0.00	0.00	8.90	0.00	0.00	0.16	0.00	0.00	0.00	1.48	0.00
SB15	44.253	K-spar	50.33	0.00	0.29	0.81	18.22	22.10	0.00	0.00	0.00	8.10	0.00	0.00	0.14	0.00	0.00	0.00	0.00	0.00
SB15	44.254	Ser	34.02	0.00	0.34	0.53	10.11	10.21	0.00	13.75	0.00	3.49	0.00	0.00	0.00	0.00	0.00	0.00	27.55	0.00
SB14b	45.255	Alb	50.54	0.00	8.41	0.00	10.23	30.71	0.00	0.00	0.00	0.11	0.00	0.00	0.00	0.00	0.00	0.00	0.00	0.00
SB14b	45.256	Qtz	54.04	0.00	1.20	0.00	1.34	43.21	0.00	0.00	0.00	0.00	0.00	0.00	0.00	0.00	0.00	0.00	0.00	0.00
SB14b	45.257	Ser	49.13	0.00	0.43	0.98	18.65	21.43	0.00	0.00	0.00	8.90	0.00	0.00	0.12	0.00	0.00	0.00	0.36	0.00
SB14b	45.258	Anh-Gyp	48.21	0.00	0.00	0.00	0.00	0.00	0.00	23.13	0.00	0.00	28.67	0.00	0.00	0.00	0.00	0.00	0.00	0.00
SB14b	45.259	Py	0.00	0.00	0.00	0.00	0.00	0.00	53.49	0.00	0.00	0.00	0.00	0.00	0.00	0.00	0.00	0.00	46.51	0.00
SB14b	45.26	Bad Spectra	42.20	0.00	0.00	0.67	14.83	14.65	0.00	0.23	0.00	4.25	0.00	0.00	0.00	0.00	0.00	0.00	23.17	0.00
SB14b	46.261	Py	0.00	0.00	0.00	0.00	0.00	0.00	0.00	53.30	0.00	0.00	0.00	0.00	0.00	0.00	0.00	0.00	46.70	0.00
SB14b	46.262	Py	6.40	0.00	0.00	0.00	0.00	0.00	0.00	48.33	0.00	0.00	0.00	0.00	0.00	0.00	0.00	0.00	45.27	0.00
SB14b	46.263	Py	0.00	0.00	0.00	0.00	0.00	0.00	0.00	51.11	0.00	0.00	0.00	0.00	0.00	0.00	0.00	0.00	48.89	0.00
SB14b	46.264	Py	8.45	0.00	0.00	0.00	0.00	0.00	0.00	47.32	0.00	0.00	0.00	0.00	0.00	0.00	0.00	0.00	44.23	0.00
SB14b	48.266	Py	0.00	0.00	0.00	0.00	0.00	0.00	0.00	53.09	0.00	0.00	0.00	0.00	0.00	0.00	0.00	0.00	46.91	0.00
SB14b	48.267	Qtz	54.60	0.00	0.00	0.00	0.25	45.15	0.00	0.00	0.00	0.00	0.00	0.00	0.00	0.00	0.00	0.00	0.00	0.00
SB14b	48.268	Ser	49.61	0.00	0.33	1.24	18.78	20.59	0.00	0.00	0.00	8.66	0.00	0.00	0.00	0.00	0.00	0.00	0.48	0.00
SB14b	48.269	Anh-Gyp	43.71	0.00	0.00	0.00	0.00	0.00	0.00	24.62	0.00	0.20	31.01	0.00	0.00	0.00	0.00	0.00	0.00	0.00
SB14b	48.27	Hal	22.88	0.00	22.24	0.31	10.29	10.81	0.15	0.00	28.31	4.15	0.00	0.00	0.00	0.00	0.00	0.00	0.00	0.00
SB14b	48.271	Ba	28.56	0.00	0.00	0.00	0.00	3.72	0.00	12.76	0.00	0.00	0.00	0.00	0.00	0.00	0.00	0.00	0.00	0.00
SB14b	49.272	Qtz	54.44	0.00	0.00	0.00	0.00	45.30	0.00	0.00	0.00	0.00	0.00	0.00	0.00	0.00	0.00	0.00	0.00	0.00
SB14b	49.273	Bt	45.58	0.00	0.24	9.87	9.20	17.19	0.00	0.00	0.00	8.15	0.00	0.00	1.97	0.00	0.00	0.00	7.80	0.00
SB14b	49.274	Qtz	54.86	0.00	0.00	0.00	0.00	45.03	0.00	0.00	0.00	0.00	0.10	0.00	0.00	0.00	0.00	0.00	0.00	0.00
SB14b	49.275	Alb	49.70	0.00	6.86	0.00	11.71	28.87	0.00	0.00	0.00	0.18	2.07	0.00	0.00	0.00	0.00	0.00	0.00	0.00
SB14b	49.276	Anh-Gyp	48.17	0.00	0.00	0.00	0.00	0.00	0.00	23.16	0.00	0.00	28.68	0.00	0.00	0.00	0.00	0.00	0.00	0.00
SB14b	49.277	Ser	50.95	0.00	0.38	0.94	16.97	20.31	0.00	0.00	0.00	8.04	0.00	0.00	0.20	0.00	0.00	0.00	1.88	0.00
SB14b	49.278	Calcite	57.59	0.00	0.00	0.32	0.81	1.43	0.00	0.19	0.00	37.08	0.00	0.00	0.00	0.00	0.00	0.67	1.91	0.00
SB14b	49.279	Bt	45.17	0.00	0.00	9.20	8.97	17.08	0.00	0.00	0.00	8.10	0.00	0.00	2.26	0.00	0.00	0.00	9.22	0.00
SB14b	49.28	Anh-Gyp	50.60	0.00	0.00	0.00	0.00	0.00	0.00	21.91	0.00	0.00	27.03	0.00	0.00	0.00	0.00	0.00	0.00	0.00
SB14b	49.281	Ser	48.45	0.00	0.45	0.98	18.08	20.59	0.00	0.00	0.00	8.82	0.00	0.00	0.00	0.00	0.00	0.00	2.14	0.00
SB14b	49.282	Bt	45.73	0.00	0.34	8.93	9.70	18.05	0.00	0.00	0.00	7.78	0.00	0.00	1.67	0.00	0.00	0.19	7.62	0.00
SB14b	49.283	Qtz	54.54	0.00	0.00	0.00	0.00	45.46	0.00	0.00	0.00	0.00	0.00	0.00	0.00	0.00	0.00	0.00	0.00	0.00
SB14b	50.284	Bt	44.86	0.00	0.00	9.03	8.85	17.25	0.00	0.00	0.00	8.00	0.00	0.00	2.35	0.00	0.00	0.20	9.47	0.00
SB14b	50.285	Alb	49.89	0.00	7.23	0.00	11.61	29.19	0.00	0.00	0.00	0.18	1.90	0.00	0.00	0.00	0.00	0.00	0.00	0.00
SB14b	50.286	Qtz	54.71	0.00	0.00	0.00	0.00	45.29	0.00	0.00	0.00	0.00	0.00	0.00	0.00	0.00	0.00	0.00	0.00	0.00
SB14b	50.287	Mon + Ap	39.94	3.09	0.20	0.10	0.08	0.36	17.66	0.00	0.39	0.00	37.40	0.00	0.00	0.00	0.00	0.51	0.27	0.00
SB14b	50.288	Bt + Phosphate	38.07	0.00	0.00	6.74	6.80	11.63	4.70	0.00	0.00	5.23	0.00	0.00	0.88	0.00	0.00	0.00	4.82	0.00
SB14b	50.289	Bt	45.39	0.00	0.00	9.51	9.61	17.33	0.00	0.00	0.00	8.32	0.00	0.00	1.51	0.00	0.00	0.18	8.14	0.00
SB14b	50.29	Anh-Gyp	47.48	0.00	0.00	0.00	0.00	0.00	0.00	23.54	0.00	0.00	28.98	0.00	0.00	0.00	0.00	0.00	0.00	0.00
SB14b	50.291	Alb	50.19	0.00	6.97	0.00	11.69	28.75	0.00	0.00	0.00	0.19	2.21	0.00	0.00	0.00	0.00	0.00	0.00	0.00
SB14b	51.292	Bt	45.55	0.00	0.00	10.62	9.08	17.43	0.00	0.00	0.00	8.09	0.00	0.00	1.96	0.00	0.00	0.21	7.07	0.00
SB14b	51.293	Ser	48.89	0.00	0.24	3.44	16.81	20.60	0.00	0.00	0.00	8.88	0.00	0.00	0.15	0.00	0.00	0.00	0.98	0.00
SB14b	51.294	Py	0.00	0.00	0.00	0.00	0.00	0.00	53.14	0.00	0.00	0.00	0.00	0.00	0.00	0.00	0.00	0.00	46.86	0.00
SB14b	51.295	Anh-Gyp	47.92	0.00	0.00	0.00	0.00	0.00	0.00	23.34	0.00	0.00	28.74	0.00	0.00	0.00	0.00	0.00	0.00	0.00
SB14b	51.296	Alb	50.16	0.00	7.82	0.00	10.99	29.86	0.00	0.00	0.00	0.15	1.02	0.00	0.00	0.00	0.00	0.00	0.00	0.00
SB14b	51.297	Qtz	54.62	0.00	0.25	0.00	0.00	45.14	0.00	0.00	0.00	0.00	0.00	0.00	0.00	0.00	0.00	0.00	0.00	0.00
SB14b	51.298	Ser	49.63	0.00	0.37	1.51	17.67	20.81	0.00	0.00	0.00	8.67	0.00	0.00	0.16	0.00	0.00	0.00	1.17	0.00

Table A1.1: SEM analytical results and interpreted mineralogy

Sample	Sample ID	Mineral	O_pct	F_pct	Na_pct	Mg_pct	Al_pct	Si_pct	P_pct	S_pct	Cl_pct	K_pct	Ca_pct	Sc_pct	Ti_pct	V_pct	Cr_pct	Mn_pct	Fe_pct	Co_pct
SB18	59.352	Ser	48.12	0.00	0.48	0.60	18.85	21.60	0.00	0.29	0.15	9.21	0.00	0.00	0.00	0.00	0.00	0.00	0.70	0.00
SB18	59.353	Py	0.00	0.00	0.00	0.00	0.00	0.00	0.00	53.58	0.00	0.00	0.00	0.00	0.00	0.00	0.00	0.00	46.42	0.00
SB18	59.354	Py	0.00	0.00	0.00	0.00	0.00	0.00	0.00	53.47	0.00	0.00	0.00	0.00	0.00	0.00	0.00	0.00	46.53	0.00
SB18	60.355	Cpy	0.00	0.00	0.00	0.00	0.00	0.00	0.00	32.66	0.00	0.00	0.00	0.00	0.00	0.00	0.00	0.00	29.82	0.00
SB18	60.356	Zr	35.27	0.00	0.00	0.00	0.00	14.83	0.00	0.00	0.00	0.00	0.00	0.00	0.00	0.00	0.00	0.00	0.41	0.00
SB18	60.357	Py	0.00	0.00	0.00	0.00	0.00	0.00	0.00	53.18	0.00	0.00	0.00	0.00	0.00	0.00	0.00	0.00	46.82	0.00
SB18	60.358	Rut	42.22	0.00	0.35	0.00	0.18	0.11	0.00	0.09	0.31	0.00	0.00	0.00	55.63	0.00	0.00	0.00	0.63	0.00
SB18	60.359	Ser	49.61	0.00	0.26	0.89	18.08	21.43	0.00	0.00	0.00	8.38	0.00	0.00	0.17	0.00	0.00	0.00	1.19	0.00
SB18	60.36	Rut	42.14	0.00	0.00	0.00	0.22	0.00	0.00	0.00	0.00	0.00	0.00	0.00	56.51	0.00	0.00	0.00	0.32	0.00
SB18	60.361	FeOx	30.23	0.00	0.00	0.00	0.00	0.10	0.00	2.09	0.00	0.00	0.00	0.00	7.11	1.08	0.56	0.00	58.55	0.00
SB18	60.362	Bt	44.40	0.00	0.22	9.02	9.36	16.85	0.00	0.12	0.00	8.15	0.00	0.00	1.35	0.23	0.17	0.00	10.13	0.00
SB18	60.363	Qtz	54.69	0.00	0.00	0.00	0.00	45.31	0.00	0.00	0.00	0.00	0.00	0.00	0.00	0.00	0.00	0.00	0.00	0.00
SB18	60.364	Ser	48.64	0.00	0.51	0.65	18.51	21.20	0.00	0.00	0.77	8.33	0.00	0.00	0.19	0.00	0.00	0.00	1.21	0.00
SB18	60.365	Cpy	0.00	0.00	0.00	0.00	0.37	0.00	0.00	32.74	0.00	0.00	0.00	0.00	0.00	0.00	0.00	0.00	28.74	0.00
SB18	60.366	Mon + Ap	28.28	0.00	0.00	0.00	0.00	0.00	12.05	0.57	0.00	0.16	1.18	0.00	0.00	0.00	0.00	0.00	0.00	0.00
SB18	61.367	Ser	48.94	0.00	0.29	0.74	17.98	20.62	0.00	0.00	0.00	9.07	0.00	0.00	0.34	0.00	0.00	0.00	2.02	0.00
SB18	61.368	Qtz	54.47	0.00	0.00	0.00	0.00	45.53	0.00	0.00	0.00	0.00	0.00	0.00	0.00	0.00	0.00	0.00	0.00	0.00
SB18	61.369	Ser	49.03	0.00	0.30	0.42	19.09	21.21	0.00	0.00	0.19	9.19	0.00	0.00	0.00	0.00	0.00	0.00	0.56	0.00
SB18	61.37	Py	0.00	0.00	0.00	0.00	0.00	0.00	0.00	53.30	0.00	0.00	0.00	0.00	0.00	0.00	0.00	0.00	46.70	0.00
SB18	62.371	Py	0.00	0.00	0.00	0.00	0.00	0.00	0.00	53.48	0.00	0.00	0.00	0.00	0.00	0.00	0.00	0.00	46.52	0.00
SB18	62.372	Rut	42.68	0.00	0.00	0.00	0.00	1.04	0.00	0.00	0.00	0.16	0.00	0.00	55.87	0.00	0.00	0.00	0.25	0.00
SB18	62.373	Rut	51.22	0.00	0.00	0.25	1.70	1.68	0.00	0.00	0.70	0.00	0.00	0.00	44.20	0.00	0.00	0.00	0.26	0.00
SB18	62.374	Py	0.00	0.00	0.00	0.00	0.00	0.00	0.00	53.44	0.00	0.00	0.00	0.00	0.00	0.00	0.00	0.00	46.56	0.00
SB18	63.376	Ser	49.22	0.00	0.37	0.48	18.86	21.04	0.00	0.00	0.22	9.04	0.00	0.00	0.00	0.00	0.00	0.00	0.76	0.00
SB18	63.377	Ser	48.88	0.00	0.30	1.40	17.84	21.71	0.00	0.00	0.00	9.11	0.00	0.00	0.00	0.00	0.00	0.00	0.76	0.00
SB18	63.378	Qtz	54.53	0.00	0.00	0.00	0.00	45.47	0.00	0.00	0.00	0.00	0.00	0.00	0.00	0.00	0.00	0.00	0.00	0.00
SB18	63.379	Ser	49.38	0.00	0.22	0.83	17.50	21.55	0.00	0.00	0.00	8.72	0.00	0.00	1.33	0.00	0.00	0.00	0.49	0.00
SB19	65.38	Ser	49.72	0.00	0.47	0.27	19.28	20.57	0.00	0.00	0.00	8.67	0.00	0.00	0.30	0.00	0.00	0.00	0.71	0.00
SB19	65.381	Qtz	54.75	0.00	0.00	0.00	0.00	45.25	0.00	0.00	0.00	0.00	0.00	0.00	0.00	0.00	0.00	0.00	0.00	0.00
SB19	65.382	Anh-Gyp	43.32	0.00	0.00	0.00	0.00	0.32	0.00	24.96	0.00	0.00	31.40	0.00	0.00	0.00	0.00	0.00	0.00	0.00
SB19	65.383	Anh-Gyp	48.42	0.00	0.00	0.00	0.00	0.00	0.00	23.02	0.00	0.00	28.56	0.00	0.00	0.00	0.00	0.00	0.00	0.00
SB19	65.384	Anh-Gyp	46.36	0.00	0.00	0.00	0.00	0.00	0.00	23.93	0.00	0.00	29.71	0.00	0.00	0.00	0.00	0.00	0.00	0.00
SB19	65.385	Anh-Gyp	47.25	0.00	0.00	0.00	0.00	0.00	0.00	23.73	0.00	0.00	29.01	0.00	0.00	0.00	0.00	0.00	0.00	0.00
SB19	66.386	FeOx	42.37	0.00	0.00	0.00	0.86	0.90	0.14	0.00	0.00	0.26	0.80	0.00	0.00	0.00	0.00	2.14	52.53	0.00
SB19	66.387	Bn	0.00	0.00	0.00	0.00	0.00	0.00	0.00	23.34	0.00	0.00	0.00	0.00	0.00	0.00	0.00	0.00	11.11	0.00
SB19	66.388	Cc	0.00	0.00	0.00	0.00	0.00	0.00	0.00	21.44	0.00	0.00	0.00	0.00	0.00	0.00	0.00	0.00	2.93	0.00
SB19	66.389	Bn	0.00	0.00	0.00	0.00	0.00	0.00	0.00	23.31	0.00	0.00	0.00	0.00	0.00	0.00	0.00	0.00	11.27	0.00
SB19	66.39	Bn	0.00	0.00	0.00	0.00	0.00	0.00	0.00	23.25	0.00	0.00	0.00	0.00	0.00	0.00	0.00	0.00	11.25	0.00
SB19	66.391	Py	0.00	0.00	0.00	0.00	0.00	0.00	0.00	52.90	0.00	0.00	0.00	0.00	0.00	0.00	0.00	0.00	46.65	0.00
SB19	66.392	Py	0.00	0.00	0.00	0.00	0.00	0.00	0.00	53.25	0.00	0.00	0.00	0.00	0.00	0.00	0.00	0.00	46.75	0.00
SB19	66.393	Py	0.00	0.00	0.00	0.00	0.14	0.73	0.00	54.37	0.00	0.00	0.00	0.00	0.00	0.00	0.00	0.00	44.76	0.00
SB19	66.394	Cc	0.00	0.00	0.00	0.00	0.00	0.11	0.00	20.28	0.00	0.00	0.00	0.00	0.00	0.00	0.00	0.00	0.57	0.00
SB19	67.395	Qtz	54.74	0.00	0.00	0.00	0.00	45.26	0.00	0.00	0.00	0.00	0.00	0.00	0.00	0.00	0.00	0.00	0.00	0.00
SB19	67.396	Ser	49.85	0.00	0.45	0.32	19.17	20.55	0.00	0.00	0.00	8.84	0.00	0.00	0.00	0.00	0.00	0.00	0.82	0.00
SB19	67.397	Ser	49.08	0.00	0.37	0.43	19.16	20.72	0.00	0.00	0.00	8.98	0.00	0.00	0.25	0.00	0.00	0.00	1.01	0.00
SB19	67.398	Anh-Gyp	47.44	0.00	0.00	0.00	0.00	0.00	0.00	23.50	0.00	0.00	29.06	0.00	0.00	0.00	0.00	0.00	0.00	0.00
SB19	67.399	Al-sil	57.89	0.00	0.00	0.00	21.29	20.82	0.00	0.00	0.00	0.00	0.00	0.00	0.00	0.00	0.00	0.00	0.00	0.00
SB19	67.4	Ser	49.25	0.00	0.40	0.49	18.58	21.02	0.00	0.00	0.00	8.90	0.00	0.00	0.13	0.00	0.00	0.00	1.23	0.00

Table A1.1: SEM analytical results and interpreted mineralogy

Table A1.1: SEM analytical results and interpreted mineralogy

Table A1.1: SEM analytical results and interpreted mineralogy

Sample	Sample ID	Mineral	O_pct	F_pct	Na_pct	Mg_pct	Al_pct	Si_pct	P_pct	S_pct	Cl_pct	K_pct	Ca_pct	Sc_pct	Ti_pct	V_pct	Cr_pct	Mn_pct	Fe_pct	Co_pct	
SB19	68.401	Qtz	55.16	0.00	0.00	0.00	0.00	44.84	0.00	0.00	0.00	0.00	0.00	0.00	0.00	0.00	0.00	0.00	0.00	0.00	
SB19	68.402	Anh-Gyp	45.13	0.00	0.00	0.00	0.00	0.00	0.00	24.58	0.00	0.00	30.29	0.00	0.00	0.22	0.00	0.00	0.00	0.78	0.00
SB19	68.403	Ser	49.26	0.00	0.43	0.21	19.71	21.07	0.00	0.00	0.00	8.32	0.00	0.00	0.22	0.00	0.00	0.00	0.00	0.78	0.00
SB19	68.404	Ser	49.89	0.00	0.39	0.24	19.45	20.69	0.00	0.00	0.00	8.32	0.00	0.00	0.26	0.00	0.00	0.00	0.00	0.77	0.00
SB19	68.405	Ser	49.67	0.00	0.39	0.20	19.57	20.84	0.00	0.00	0.00	8.34	0.00	0.00	0.14	0.00	0.00	0.00	0.00	0.84	0.00
SB19	68.406	Ser	49.34	0.00	0.39	0.45	18.77	21.07	0.00	0.00	0.00	8.26	0.00	0.00	0.19	0.00	0.00	0.00	0.00	1.53	0.00
SB19	69.407	Py	0.00	0.00	0.00	0.00	0.00	0.00	0.00	52.85	0.00	0.00	0.00	0.00	0.00	0.00	0.00	0.00	0.00	46.69	0.00
SB19	69.408	Cc	0.00	0.00	0.00	0.00	0.00	0.00	0.00	20.74	0.00	0.00	0.00	0.00	0.00	0.00	0.00	0.00	0.00	0.52	0.00
SB19	69.409	Bn	0.00	0.00	0.00	0.00	0.00	0.00	0.00	23.11	0.00	0.00	0.00	0.00	0.00	0.00	0.00	0.00	0.00	10.54	0.00
SB19	69.411	Cc	0.00	0.00	0.00	0.00	0.00	0.00	0.00	21.12	0.00	0.00	0.00	0.00	0.00	0.00	0.00	0.00	0.00	2.20	0.00
SB19	69.412	Bn	1.30	0.00	0.00	0.00	0.00	0.00	0.00	23.04	0.00	0.00	0.00	0.00	0.00	0.00	0.00	0.00	0.00	10.47	0.00
SB19	69.412	Cc	0.74	0.00	0.00	0.00	0.00	0.19	0.00	21.22	0.00	0.00	0.00	0.00	0.00	0.00	0.00	0.00	0.00	0.48	0.00
SB01	71.413	K-spar	47.55	0.00	1.03	0.00	9.79	29.40	0.00	0.00	0.00	12.23	0.00	0.00	0.00	0.00	0.00	0.00	0.00	0.00	0.00
SB01	71.414	Alb	49.05	0.00	5.14	0.00	13.66	26.65	0.00	0.00	0.00	0.17	5.33	0.00	0.00	0.00	0.00	0.00	0.00	0.00	0.00
SB01	71.415	Alb	50.71	0.00	6.31	0.00	12.34	28.74	0.00	0.00	0.00	0.62	1.28	0.00	0.00	0.00	0.00	0.00	0.00	0.00	0.00
SB01	71.416	Alb	50.20	0.00	7.45	0.00	11.28	29.97	0.00	0.00	0.00	0.21	0.89	0.00	0.00	0.00	0.00	0.00	0.00	0.00	0.00
SB01	72.417	K-spar	47.60	0.00	0.74	0.00	9.69	29.35	0.00	0.00	0.00	12.62	0.00	0.00	0.00	0.00	0.00	0.00	0.00	0.00	0.00
SB01	72.418	Alb	50.32	0.00	6.52	0.00	12.16	28.55	0.00	0.00	0.00	1.48	0.97	0.00	0.00	0.00	0.00	0.00	0.00	0.00	0.00
SB01	72.419	Alb	48.90	0.00	4.86	0.00	14.05	26.05	0.00	0.00	0.00	0.14	6.00	0.00	0.00	0.00	0.00	0.00	0.00	0.00	0.00
SB01	72.42	Bt	42.75	0.00	0.36	6.83	7.34	16.18	0.00	0.00	0.23	6.48	0.00	0.00	2.71	0.11	0.00	0.37	16.63	0.00	
SB01	72.421	Qtz	54.49	0.00	0.00	0.00	0.00	45.51	0.00	0.00	0.00	0.00	0.00	0.00	0.00	0.00	0.00	0.00	0.00	0.00	
SB01	72.422	Mon + Ap	40.48	3.67	0.13	0.00	0.00	0.29	17.12	0.00	0.25	0.00	37.26	0.00	0.00	0.00	0.00	0.00	0.00	0.81	0.00
SB01	72.423	Mon + Ap	40.07	3.55	0.00	0.00	0.00	0.30	17.46	0.00	0.27	0.00	37.85	0.00	0.00	0.00	0.00	0.00	0.00	0.49	0.00
SB01	72.424	K-spar	47.33	0.00	0.29	0.00	9.66	28.95	0.00	0.00	0.00	13.09	0.00	0.00	0.00	0.00	0.00	0.00	0.25	0.00	
SB01	73.425	Qtz	54.56	0.00	0.00	0.00	0.00	45.44	0.00	0.00	0.00	0.00	0.00	0.00	0.00	0.00	0.00	0.00	0.00	0.00	
SB01	73.426	K-spar	47.46	0.00	0.34	0.00	9.71	29.41	0.00	0.00	0.00	13.09	0.00	0.00	0.00	0.00	0.00	0.00	0.00	0.00	
SB01	73.427	Ser	46.72	0.00	0.00	1.18	11.44	10.34	0.00	0.00	0.09	0.11	0.00	0.00	0.00	0.00	0.00	1.47	28.65	0.00	
SB01	73.428	Ser	42.73	0.00	0.00	2.36	11.56	11.25	0.00	0.00	0.10	0.11	0.00	0.00	0.00	0.00	0.00	2.30	29.58	0.00	
SB01	73.429	Chl	48.52	0.00	0.00	8.41	10.64	11.93	0.00	0.00	0.00	0.00	0.00	0.00	0.00	0.00	0.00	1.07	19.43	0.00	
SB01	74.43	FeOx	28.24	0.00	0.00	0.00	0.00	0.10	0.00	0.00	0.00	0.00	0.00	0.00	0.00	0.24	0.00	0.00	71.13	0.00	
SB01	74.431	Mon + Ap	39.71	3.70	0.00	0.00	0.00	0.16	17.62	0.00	0.23	0.00	38.25	0.00	0.00	0.00	0.00	0.00	0.00	0.34	0.00
SB01	74.432	Qtz + FeOx	47.98	0.00	0.59	0.86	11.70	29.33	0.00	0.00	0.24	0.23	0.25	0.00	0.00	0.00	0.00	0.00	0.00	8.82	0.00
SB01	74.433	Alb	49.81	0.00	6.11	0.00	12.42	27.69	0.00	0.00	0.00	0.25	3.72	0.00	0.00	0.00	0.00	0.00	0.00	0.00	0.00
SB01	74.434	Alb	50.15	0.00	6.50	0.00	11.89	27.89	0.00	0.00	0.00	0.27	2.92	0.00	0.00	0.00	0.00	0.00	0.00	0.00	0.00
SB01	74.435	Chl	47.30	0.00	0.00	8.01	11.08	12.52	0.00	0.00	0.00	0.00	0.00	0.00	0.00	0.00	0.00	0.00	1.96	19.13	0.00
SB01	74.436	Bad Spectra	47.69	0.00	4.93	0.00	12.57	27.33	0.00	0.00	0.00	0.28	7.20	0.00	0.00	0.00	0.00	0.00	0.00	0.00	0.00
SB23	75.437	Qtz	54.56	0.00	0.00	0.00	0.00	45.44	0.00	0.00	0.00	0.00	0.00	0.00	0.00	0.00	0.00	0.00	0.00	0.00	
SB23	75.438	Ser	49.39	0.00	0.48	0.61	18.60	20.99	0.00	0.00	0.00	8.43	0.00	0.00	0.19	0.00	0.00	0.00	0.00	1.31	0.00
SB23	75.439	Alb	49.75	0.00	7.64	0.00	10.94	30.18	0.00	0.00	0.00	0.16	0.74	0.00	0.00	0.00	0.00	0.00	0.00	0.00	
SB23	75.44	Ser	49.18	0.00	0.55	0.56	18.68	21.70	0.00	0.00	0.00	8.03	0.00	0.00	0.24	0.00	0.00	0.00	1.06	0.00	
SB23	75.441	Ser	49.37	0.00	0.41	0.63	18.15	20.85	0.00	0.00	0.00	8.49	0.00	0.00	0.19	0.00	0.00	0.00	1.91	0.00	
SB23	75.442	K-spar	47.90	0.00	0.92	0.00	9.80	29.04	0.00	0.00	0.00	12.34	0.00	0.00	0.00	0.00	0.00	0.00	0.00	0.00	
SB23	75.443	Mon + Ap	39.21	3.06	0.42	0.00	0.10	0.29	17.42	0.42	0.00	0.32	38.07	0.00	0.00	0.00	0.70	0.00	0.00	0.00	
SB23	75.444	Ser	48.55	0.00	0.55	2.14	17.61	21.12	0.00	0.00	0.15	8.08	0.00	0.00	0.29	0.00	0.00	0.00	1.51	0.00	
SB23	76.445	Py	0.00	0.00	0.00	0.00	0.00	0.00	0.00	53.12	0.00	0.00	0.00	0.00	0.00	0.00	0.00	0.00	0.00	46.88	0.00
SB23	76.446	Cpy	0.00	0.00	0.00	0.00	0.00	0.00	0.00	32.35	0.00	0.00	0.00	0.00	0.00	0.00	0.00	0.00	0.00	29.09	0.00
SB23	76.447	Cpy	0.00	0.00	0.00	0.00	0.00	0.00	0.00	32.40	0.00	0.00	0.00	0.00	0.00	0.00	0.00	0.00	0.00	29.71	0.00
SB23	76.448	Cpy	0.00	0.00	0.00	0.00	0.00	0.00	0.00	32.59	0.00	0.00	0.00	0.00	0.00	0.00	0.00	0.00	0.00	29.37	0.00

Table A1.1: SEM analytical results and interpreted mineralogy

Sample	Sample ID	Mineral	O_pct	F_pct	Na_pct	Mg_pct	Al_pct	Si_pct	P_pct	S_pct	Cl_pct	K_pct	Ca_pct	Sc_pct	Ti_pct	V_pct	Cr_pct	Mn_pct	Fe_pct	Co_pct	
SB07	102.22	Bt	42.55	1.47	0.00	12.79	8.71	18.62	0.00	0.00	0.00	9.26	0.00	0.00	1.20	0.20	0.00	0.00	5.21	0.00	
SB05	103.23	Qtz	54.47	0.00	0.00	0.00	0.00	45.53	0.00	0.00	0.00	0.00	0.00	0.00	0.00	0.00	0.00	0.00	0.00	0.00	
SB05	103.24	K-spar	47.78	0.00	1.51	0.00	9.88	29.37	0.00	0.00	0.00	11.47	0.00	0.00	0.00	0.00	0.00	0.00	0.00	0.00	
SB05	103.25	Bt	44.87	0.93	0.24	11.86	8.66	17.79	0.00	0.00	0.00	8.31	0.00	0.00	1.58	0.16	0.00	0.00	5.60	0.00	
SB05	103.26	Ser	49.41	0.00	0.29	1.28	17.02	21.56	0.00	0.00	0.00	8.79	0.00	0.00	0.97	0.24	0.00	0.00	0.43	0.00	
SB05	104.27	Ba	27.16	0.00	0.00	0.00	0.00	0.00	0.00	0.00	13.51	0.00	0.00	0.00	0.00	0.00	0.00	0.00	0.00	0.00	
SB05	104.28	Ba	27.36	0.00	0.00	0.00	0.00	0.00	0.00	0.00	13.68	0.00	0.00	0.00	0.00	0.00	0.00	0.00	0.00	0.00	
SB05	104.29	Ba	28.75	0.00	0.00	0.00	0.00	0.00	0.00	0.00	17.45	0.00	0.00	0.33	0.00	0.00	0.00	0.00	0.00	0.00	
SB05	104.3	Ba	31.07	0.00	0.00	0.00	0.71	0.77	0.00	12.70	0.00	0.53	0.00	0.00	0.00	0.00	0.00	0.00	0.00	0.00	
SB05	104.31	Rut	41.07	0.00	0.00	0.00	0.09	0.11	0.00	0.00	0.00	0.00	0.00	0.00	57.10	0.83	0.00	0.00	0.38	0.00	
SB05	104.32	Rut	42.28	0.00	0.00	0.00	0.00	0.00	0.00	0.00	0.00	0.00	0.00	0.00	57.33	0.00	0.00	0.00	0.39	0.00	
SB05	105.33	Qtz	54.30	0.00	0.00	0.00	0.00	45.70	0.00	0.00	0.00	0.00	0.00	0.00	0.00	0.00	0.00	0.00	0.00	0.00	
SB05	105.34	Qtz	52.28	0.00	0.43	0.00	0.00	47.28	0.00	0.00	0.00	0.00	0.00	0.00	0.00	0.00	0.00	0.00	0.00	0.00	
SB05	105.35	K-spar	46.64	0.00	1.68	0.00	9.95	30.11	0.00	0.00	0.00	11.62	0.00	0.00	0.00	0.00	0.00	0.00	0.00	0.00	
SB05	105.36	Bt	44.98	1.16	0.21	12.29	9.03	17.68	0.00	0.00	0.00	8.41	0.00	0.00	1.53	0.00	0.00	0.00	4.72	0.00	
SB05	105.37	K-spar	47.66	0.00	0.64	0.00	9.87	29.00	0.00	0.00	0.00	12.82	0.00	0.00	0.00	0.00	0.00	0.00	0.00	0.00	
SB05	105.38	Bt	44.98	0.77	0.24	11.88	9.65	17.05	0.00	0.00	0.00	8.50	0.00	0.00	1.22	0.27	0.00	0.00	5.42	0.00	
SB05	105.39	Rut	41.35	0.00	0.00	0.00	0.00	0.00	0.00	0.00	0.00	0.00	0.00	0.00	57.03	0.81	0.00	0.00	0.48	0.00	
SB05	105.4	Rut	40.63	0.00	0.00	0.00	0.00	0.12	0.00	0.00	0.00	0.00	0.00	0.00	56.77	0.88	0.00	0.00	0.55	0.00	
SB05	106.41	Cpy	0.00	0.00	0.00	0.00	0.00	0.00	32.34	0.00	0.00	0.00	0.00	0.00	0.00	0.00	0.00	0.00	28.55	0.00	
SB05	106.42	Qtz	54.81	0.00	0.00	0.00	0.00	45.19	0.00	0.00	0.00	0.00	0.00	0.00	0.00	0.00	0.00	0.00	0.00	0.00	
SB05	106.43	K-spar	47.31	0.00	0.57	0.00	9.77	29.24	0.14	0.00	0.00	12.97	0.00	0.00	0.00	0.00	0.00	0.00	0.00	0.00	
SB05	106.44	Ser	49.95	0.00	0.30	0.66	18.88	21.82	0.15	0.00	0.00	7.96	0.00	0.00	0.00	0.00	0.00	0.00	0.27	0.00	
SB05	106.45	Ser	50.49	0.00	0.23	0.79	18.43	22.33	0.00	0.00	0.00	7.43	0.00	0.00	0.00	0.00	0.00	0.00	0.31	0.00	
SB05	106.46	Ser	49.92	0.00	0.29	0.95	18.10	21.80	0.00	0.00	0.00	8.21	0.00	0.00	0.26	0.00	0.00	0.00	0.47	0.00	
SB06	107.47	Qtz	54.77	0.00	0.00	0.00	0.00	45.23	0.00	0.00	0.00	0.00	0.00	0.00	0.00	0.00	0.00	0.00	0.00	0.00	
SB06	107.48	Mon + Ap	39.75	3.55	0.00	0.00	0.00	0.00	17.66	0.00	0.63	0.00	38.00	0.00	0.00	0.00	0.00	0.42	0.00	0.00	
SB06	107.49	Bt	44.19	0.00	0.35	9.06	8.15	17.12	0.00	0.00	0.14	7.62	0.00	0.00	1.90	0.00	0.00	0.24	11.22	0.00	
SB06	107.5	Chl	47.88	0.00	0.00	10.68	10.36	13.25	0.00	0.00	0.12	0.39	0.22	0.00	0.19	0.00	0.00	0.30	16.61	0.00	
SB06	107.51	Alb	49.97	0.00	7.02	0.00	11.80	28.69	0.00	0.00	0.00	0.16	2.36	0.00	0.00	0.00	0.00	0.00	0.00	0.00	
SB06	107.52	Alb	49.30	0.00	4.63	0.00	14.14	25.71	0.00	0.00	0.00	0.14	6.07	0.00	0.00	0.00	0.00	0.00	0.00	0.00	
SB06	107.53	Bt	44.81	0.00	0.34	8.83	8.33	16.90	0.00	0.00	0.16	7.44	0.00	0.00	1.98	0.00	0.00	0.00	11.20	0.00	
SB06	107.54	Chl	46.04	0.00	0.00	12.00	11.20	13.63	0.00	0.00	0.00	0.13	0.00	0.00	0.00	0.00	0.00	0.39	16.60	0.00	
SB06	108.55	Bt	44.98	0.00	0.00	8.46	8.46	16.74	0.00	0.00	0.23	7.65	0.00	0.00	1.78	0.00	0.00	0.00	11.70	0.00	
SB06	108.56	Chl	48.10	0.00	0.00	11.06	10.35	13.46	0.00	0.00	0.12	1.10	0.00	0.00	0.30	0.00	0.00	0.37	15.15	0.00	
SB06	108.57	Chl	48.85	0.00	0.36	11.24	10.35	12.81	0.00	0.00	0.24	0.00	0.00	0.00	0.00	0.00	0.00	0.36	15.80	0.00	
SB06	108.58	Rut	43.88	0.00	0.00	0.53	0.97	1.70	0.00	0.00	0.00	0.37	0.00	0.00	50.85	0.00	0.00	0.00	1.46	0.00	
SB06	108.59	Alb	49.24	0.00	5.04	0.00	14.02	25.87	0.00	0.00	0.00	0.15	5.69	0.00	0.00	0.00	0.00	0.00	0.00	0.00	
SB06	108.6	Alb	49.86	0.00	6.75	0.00	11.91	28.63	0.00	0.00	0.00	0.23	2.63	0.00	0.00	0.00	0.00	0.00	0.00	0.00	
SB06	108.61	Qtz	54.72	0.00	0.00	0.00	0.00	45.28	0.00	0.00	0.00	0.00	0.00	0.00	0.00	0.00	0.00	0.00	0.00	0.00	
SB06	109.62	Alb	49.34	0.00	5.58	0.00	13.21	27.06	0.00	0.00	0.00	0.28	4.52	0.00	0.00	0.00	0.00	0.00	0.00	0.00	
SB06	109.63	Alb	49.87	0.00	6.50	0.00	12.29	28.11	0.00	0.00	0.00	0.25	2.98	0.00	0.00	0.00	0.00	0.00	0.00	0.00	
SB06	109.64	Qtz	54.38	0.00	0.62	0.00	0.00	44.54	0.00	0.00	0.45	0.00	0.00	0.00	0.00	0.00	0.00	0.00	0.00	0.00	
SB06	109.65	K-spar	47.06	0.00	0.89	0.00	9.64	28.30	0.00	0.00	0.00	11.70	0.00	0.00	0.00	0.00	0.00	0.00	0.00	0.00	
SB06	109.66	Bt	43.76	0.00	0.00	7.65	9.18	17.48	0.00	0.00	0.14	8.20	0.00	0.00	1.63	0.00	0.00	0.24	11.72	0.00	
SB13	110.67	Py	0.00	0.00	0.00	0.00	0.00	0.00	52.76	0.67	0.00	0.00	0.00	0.00	0.00	0.00	0.00	0.00	46.57	0.00	
SB13	110.68	Hal	2.53	0.00	39.15	0.00	0.00	0.00	0.00	0.00	0.35	57.79	0.00	0.18	0.00	0.00	0.00	0.00	0.00	0.00	0.00
SB13	111.7	Ser	49.29	0.00	0.35	0.91	17.42	21.04	0.00	0.00	0.00	8.32	0.00	0.00	0.55	0.00	0.00	2.12	0.00	0.00	

Table A1.1: SEM analytical results and interpreted mineralogy

Table A1.1: SEM analytical results and interpreted mineralogy

Table A1.1: SEM analytical results and interpreted mineralogy

Sample	Sample ID	Mineral	O_pct	F_pct	Na_pct	Mg_pct	Al_pct	Si_pct	P_pct	S_pct	Cl_pct	K_pct	Ca_pct	Sc_pct	Ti_pct	V_pct	Cr_pct	Mn_pct	Fe_pct	Co_pct			
SB13	111.71	Qtz	55.14	0.00	0.00	0.00	0.00	44.86	0.00	0.00	0.00	0.00	0.00	0.00	0.00	0.00	0.00	0.00	0.00	0.00			
SB13	111.72	Ser	50.68	0.00	0.35	0.73	17.79	20.64	0.00	0.00	0.24	7.17	0.00	0.00	0.23	0.00	0.00	0.00	0.00	1.39	0.00		
SB13	111.73	Al-sil	56.95	0.00	0.00	0.00	20.37	21.94	0.00	0.00	0.33	0.41	0.00	0.00	0.00	0.00	0.00	0.00	0.00	0.00	0.00		
SB13	111.74	Ser	48.97	0.00	0.35	1.68	17.26	21.31	0.00	0.00	0.00	8.44	0.00	0.00	0.28	0.00	0.00	0.00	0.00	1.71	0.00		
SB13	111.75	Qtz	54.83	0.00	0.00	0.00	0.00	44.92	0.00	0.00	0.00	0.00	0.00	0.00	0.00	0.00	0.00	0.00	0.00	0.24	0.00		
SB13	111.76	Ser	49.16	0.00	0.24	0.89	17.78	21.59	0.00	0.00	0.00	8.44	0.00	0.00	0.30	0.00	0.00	0.00	0.00	1.59	0.00		
SB13	111.77	Py	0.00	0.00	0.00	0.00	0.00	0.00	0.00	53.06	0.00	0.00	0.00	0.00	0.00	0.00	0.00	0.00	0.00	46.94	0.00		
SB13	111.78	Rut	44.26	0.00	0.00	0.00	0.19	0.26	0.00	0.00	0.00	0.27	0.00	0.00	53.99	0.00	0.00	0.00	0.00	0.45	0.00		
SB13	112.79	Ser	49.38	0.00	0.35	1.23	16.95	22.42	0.00	0.00	0.00	8.01	0.00	0.00	0.00	0.00	0.00	0.00	0.00	0.00	1.66	0.00	
SB13	112.8	Al-sil	50.27	0.00	0.00	0.00	22.41	26.79	0.00	0.00	0.25	0.27	0.00	0.00	0.00	0.00	0.00	0.00	0.00	0.00	0.00	0.00	
SB13	112.81	Al-sil	56.62	0.00	0.00	0.00	19.71	22.80	0.00	0.00	0.25	0.62	0.00	0.00	0.00	0.00	0.00	0.00	0.00	0.00	0.00	0.00	
SB13	113.82	Py	0.00	0.00	0.00	0.00	0.33	0.00	0.00	53.11	0.00	0.00	0.00	0.00	0.00	0.00	0.00	0.00	0.00	46.56	0.00		
SB13	113.83	Cpy	0.00	0.00	0.00	0.00	0.40	0.00	0.00	32.58	0.00	0.00	0.00	0.00	0.00	0.00	0.00	0.00	0.00	29.56	0.00		
SB13	114.84	Undefined	55.62	0.00	0.00	0.00	17.95	1.33	6.93	5.88	0.38	1.70	3.38	0.00	0.00	0.00	0.00	0.00	0.00	0.00	0.42	0.00	
SB13	114.85	Undefined	54.84	0.00	0.29	0.00	18.24	0.00	6.79	6.74	0.00	1.89	2.75	0.00	0.00	0.00	0.00	0.00	0.00	0.00	0.56	0.00	
SB13	114.86	Undefined	54.48	0.00	0.22	0.00	18.50	0.00	4.72	9.05	0.26	3.14	1.73	0.00	0.00	0.00	0.00	0.00	0.00	0.00	1.05	0.00	
SB13	114.87	Undefined	56.35	0.00	0.20	0.00	18.89	0.00	2.90	11.45	0.00	4.32	1.01	0.00	0.00	0.00	0.00	0.00	0.00	0.00	1.58	0.00	
SB13	114.88	Undefined	57.03	0.00	0.00	0.00	18.95	0.00	0.33	14.68	0.00	6.08	0.00	0.00	0.00	0.00	0.00	0.00	0.00	0.00	2.93	0.00	
SB13	114.89	Ser	49.39	0.00	0.48	0.44	18.90	20.55	0.00	0.00	0.00	8.71	0.00	0.00	0.22	0.00	0.00	0.00	0.00	1.31	0.00		
SB13	114.9	Ser	50.19	0.00	0.53	0.48	19.20	20.68	0.00	0.21	0.00	7.96	0.00	0.00	0.26	0.00	0.00	0.00	0.00	0.48	0.00		
SB13	114.91	Qtz	53.93	0.00	0.00	0.00	0.00	46.07	0.00	0.00	0.00	0.00	0.00	0.00	0.00	0.00	0.00	0.00	0.00	0.00	0.00		
SB14a	115.92	Ser	49.29	0.00	0.48	1.32	17.82	20.43	0.00	0.00	0.00	8.58	0.00	0.00	0.17	0.00	0.00	0.00	0.00	0.40	0.00		
SB14a	115.93	Alb	50.12	0.00	8.39	0.00	10.47	30.72	0.00	0.00	0.00	0.16	0.14	0.00	0.00	0.00	0.00	0.00	0.00	0.00	0.00	0.00	
SB14a	115.94	Alb	50.21	0.00	8.02	0.00	10.73	30.43	0.00	0.00	0.00	0.16	0.45	0.00	0.00	0.00	0.00	0.00	0.00	0.00	0.00	0.00	
SB14a	115.95	Ba	32.01	0.00	0.00	0.00	0.00	0.00	0.00	16.90	0.00	0.00	0.26	0.00	0.00	0.00	0.00	0.00	0.00	0.00	0.00	0.00	
SB14a	115.96	Ser	49.42	0.00	0.37	2.95	17.16	20.93	0.00	0.00	0.00	8.80	0.00	0.00	0.00	0.00	0.00	0.00	0.00	0.36	0.00	0.00	
SB14a	115.97	Ser	50.27	0.00	0.32	2.54	17.12	20.69	0.00	0.00	0.00	8.56	0.00	0.00	0.00	0.00	0.00	0.00	0.00	0.49	0.00	0.00	
SB14a	116.1	Ba	34.08	0.00	0.00	0.00	0.00	0.00	0.00	17.16	0.00	0.00	0.29	0.00	0.00	0.00	0.00	0.00	0.00	0.00	0.00	0.00	
SB14a	116.98	Ba	28.30	0.00	0.00	0.00	0.00	0.00	0.00	13.69	0.00	0.00	0.00	0.00	0.00	0.00	0.00	0.00	0.00	0.00	0.00	0.00	
SB14a	116.99	Ba	30.64	0.00	0.00	0.00	0.00	0.00	0.00	15.32	0.00	0.00	0.00	0.00	0.00	0.00	0.00	0.00	0.00	0.00	0.00	0.00	
SB14a	117.101	K-spar	47.37	0.00	0.58	0.00	9.85	28.32	0.00	0.00	0.00	12.46	0.00	0.00	0.00	0.00	0.00	0.00	0.00	0.00	0.00	0.00	
SB14a	117.102	Alb	50.42	0.00	7.45	0.00	11.24	29.23	0.00	0.00	0.00	0.17	1.49	0.00	0.00	0.00	0.00	0.00	0.00	0.00	0.00	0.00	
SB14a	117.103	K-spar	47.76	0.00	0.72	0.00	9.76	29.14	0.00	0.00	0.00	12.62	0.00	0.00	0.00	0.00	0.00	0.00	0.00	0.00	0.00	0.00	
SB14a	117.104	Ba	26.20	0.00	0.00	0.00	0.00	0.24	0.00	13.57	0.00	0.00	0.00	0.00	0.00	0.00	0.00	0.00	0.00	0.00	0.00	0.00	
SB14a	117.105	K-spar	45.64	0.00	0.22	0.00	10.36	27.09	0.00	0.00	0.00	11.65	0.00	0.00	0.00	0.00	0.00	0.00	0.00	0.00	0.00	0.00	
SB14a	118.106	Bt	45.99	0.00	0.00	9.86	8.79	17.15	0.00	0.00	0.00	7.90	0.00	0.00	1.99	0.00	0.00	0.00	0.00	8.33	0.00	0.00	
SB14a	118.107	Alb	50.16	0.00	7.40	0.00	11.22	29.52	0.00	0.00	0.00	0.25	1.44	0.00	0.00	0.00	0.00	0.00	0.00	0.00	0.00	0.00	0.00
SB14a	118.108	Qtz	54.88	0.00	0.00	0.00	0.00	45.12	0.00	0.00	0.00	0.00	0.00	0.00	0.00	0.00	0.00	0.00	0.00	0.00	0.00	0.00	
SB14a	118.109	Mon + Ap	39.06	5.46	0.48	1.22	0.00	0.15	16.27	1.00	0.00	0.00	36.34	0.00	0.00	0.00	0.00	0.00	0.00	0.00	0.00	0.00	0.00
SB14a	118.111	Anh-Gyp	50.22	0.00	0.00	0.00	0.00	0.00	0.00	22.49	0.00	0.00	27.29	0.00	0.00	0.00	0.00	0.00	0.00	0.00	0.00	0.00	0.00
SB14a	118.111	Bt	45.34	0.00	0.00	10.55	9.52	17.42	0.00	0.00	0.00	8.11	0.00	0.00	1.59	0.00	0.00	0.21	0.00	6.82	0.00	0.00	

Table A1.1: SEM analytical results and interpreted mineralogy

Table A1.1: SEM analytical results and interpreted mineralogy

## Appendix 2: LA-ICPMS normalised analytical results for ablated sericite sites

Table A2.1: LA-ICPMS normalised analytical results for ablated sericite sites

Sample	Measurement	Host Rock	Alteration	Sulfides	Mineral	Li_ppm	B_ppm	Na_ppm	Mg_ppm	Al_ppm	Si_ppm	K_ppm	Ca_ppm	Ti_ppm	V_ppm	Cr_ppm
SB05	OC10a034	IGR	K-alt	Cpy-HS	Sericite	15.86	6.08	3680.48	23490.20	176398.10	214372.16	86966.88	-1480.89	595.09	444.08	13.11
SB05	OC10a039	IGR	K-alt	Cpy-HS	Sericite	15.41	9.17	2371.03	14716.48	173989.37	222338.20	76942.52	-1891.15	6741.71	1299.36	104.14
SB07	OC10a128	IGR	GS-WS	Cpy-HS	Sericite	2.30	-5.91	3133.25	5231.91	192660.89	211241.92	89938.82	-1542.81	1980.40	558.53	5.02
SB07	OC10a129	IGR	GS-WS	Cpy-HS	Sericite	2.49	-6.47	3035.97	5931.04	187825.05	212678.07	90279.89	-1522.16	2007.39	906.97	7.76
SB07	OC10a130	IGR	GS-WS	Cpy-HS	Sericite	1.18	-8.43	2632.06	4734.45	185429.66	221582.24	86104.90	-1644.01	2354.15	628.18	9.04
SB07	OC10a131	IGR	GS-WS	Cpy-HS	Sericite	2.57	-6.35	3293.87	4874.21	185837.59	216719.93	88600.83	-1842.78	2897.72	783.11	11.75
SB07	OC10a132	IGR	GS-WS	Cpy-HS	Sericite	2.58	-6.35	2600.57	5681.02	188856.75	214397.21	89736.86	-1571.21	1667.09	408.96	11.77
SB07	OC10a133	IGR	GS-WS	Cpy-HS	Sericite	2.93	-7.19	3072.02	5485.14	188361.76	214963.76	88870.12	-1430.85	2253.81	997.96	15.57
SB07	OC10a134	IGR	GS-WS	Cpy-HS	Sericite	2.42	-8.59	3956.60	5475.00	189597.76	213461.85	89746.18	-1407.80	2842.75	638.92	12.55
SB07	OC10a135	IGR	GS-WS	Cpy-HS	Sericite	3.20	-9.53	5166.15	5858.27	185895.60	215200.03	90634.26	-1900.63	2742.75	798.16	7.86
SB07	OC10a136	IGR	GS-WS	Cpy-HS	Sericite	-2.14	-13.71	5840.60	913.05	111315.80	277383.36	119981.02	-2448.80	173.12	49.44	-7.98
SB07	OC10a137	IGR	GS-WS	Cpy-HS	Sericite	1.03	-9.60	5344.59	1183.50	114405.31	276687.76	115335.09	-2028.15	453.88	81.71	-5.64
SB07	OC10a138	IGR	GS-WS	Cpy-HS	Sericite	3.12	-7.19	2487.66	5804.06	186104.50	221763.70	89764.77	-1552.11	1485.84	409.28	-5.41
SB07	OC10a139	IGR	GS-WS	Cpy-HS	Sericite	0.84	-9.41	4571.35	248.49	101787.66	289372.57	116965.55	-3174.65	53.82	7.21	-12.60
SB07	OC10a140	IGR	GS-WS	Cpy-HS	Sericite	7.58	4.58	3495.58	3953.32	193561.18	210379.13	90228.42	-1321.13	1252.65	525.91	-8.36
SB07	OC10a141	IGR	GS-WS	Cpy-HS	Sericite	3.28	10.41	3186.85	3697.19	192406.76	214780.91	89374.21	-1304.56	1408.28	554.00	5.21
SB07	OC10a142	IGR	GS-WS	Cpy-HS	Sericite	6.16	5.25	3180.52	4405.87	191266.29	215532.31	89219.44	-1685.54	1667.05	679.98	-5.91
SB07	OC10a143	IGR	GS-WS	Cpy-HS	Sericite	4.06	5.44	2752.17	4348.38	189023.81	215316.65	90463.16	-1853.52	1682.42	624.38	8.38
SB07	OC10a144	IGR	GS-WS	Cpy-HS	Sericite	3.73	5.65	3016.87	5418.30	188942.01	216839.59	89529.76	-1647.51	2336.44	657.51	-6.78
SB07	OC10a145	IGR	GS-WS	Cpy-HS	Sericite	2.95	4.71	5582.24	4896.47	187598.03	215013.84	87868.87	1083.58	2711.14	771.76	-6.27
SB07	OC10a146	IGR	GS-WS	Cpy-HS	Sericite	9.91	-6.04	3303.07	3837.63	195969.01	213079.16	88879.64	-1355.84	1362.70	693.65	-6.25
SB08	OC10a093	IGR	GS	Cpy-Py	Sericite	7.68	-7.13	7310.52	8798.89	173266.45	221677.04	90960.55	-1501.52	1851.76	569.90	24.57
SB08	OC10a094	IGR	GS	Cpy-Py	Sericite	6.66	-7.59	5075.44	6742.08	186046.14	214913.60	87843.58	-1850.40	2558.58	608.09	13.60
SB08	OC10a095	IGR	GS	Cpy-Py	Sericite	1.83	-12.32	7429.03	1450.70	113038.11	278873.16	110471.17	-2522.03	412.72	97.50	-11.31
SB08	OC10a096	IGR	GS	Cpy-Py	Sericite	6.61	-5.67	6004.12	7591.68	181821.45	216702.71	88333.24	-1258.39	2692.72	879.95	30.17
SB08	OC10a097	IGR	GS	Cpy-Py	Sericite	9.33	-7.71	4178.78	5358.39	189441.39	214805.71	87927.37	-1412.20	1890.73	721.37	11.26
SB08	OC10a098	IGR	GS	Cpy-Py	Sericite	8.68	8.58	5456.09	5710.99	192017.22	210863.00	86141.83	-1629.01	2162.40	840.29	20.69
SB08	OC10a099	IGR	GS	Cpy-Py	Sericite	15.88	-4.02	4181.24	6047.70	184794.96	215371.53	88522.79	-1673.69	2368.32	922.77	15.13
SB08	OC10a100	IGR	GS	Cpy-Py	Sericite	8.17	-7.56	4094.16	6599.24	182850.91	214694.00	89757.17	-1921.89	2484.14	892.56	13.53
SB08	OC10a101	IGR	GS	Cpy-Py	Sericite	9.57	-7.37	4168.14	6612.68	185650.40	212032.61	90189.54	-1477.59	2659.46	1069.06	9.09
SB08	OC10a102	IGR	GS	Cpy-Py	Sericite	7.14	-5.93	7637.84	5459.16	174542.73	214632.69	91301.55	-1587.14	6223.49	518.25	9.72
SB08	OC10a103	IGR	GS	Cpy-Py	Sericite	7.17	-7.49	7504.26	5735.47	168093.75	227028.76	96933.23	-1838.93	2104.64	572.22	9.90
SB08	OC10a104	IGR	GS	Cpy-Py	Sericite	8.05	5.06	6297.99	6693.35	182294.97	219072.55	86912.67	-1391.46	2079.08	883.46	10.00
SB08	OC10a105	IGR	GS	Cpy-Py	Sericite	9.56	-6.42	3802.86	6485.45	187649.54	214128.43	89582.73	-1490.50	1758.07	719.54	7.87
SB08	OC10a106	IGR	GS	Cpy-Py	Sericite	6.95	-6.70	5235.16	5777.14	159307.99	241120.15	90295.76	-1292.17	1667.47	718.60	12.78
SB08	OC10a107	IGR	GS	Cpy-Py	Sericite	10.06	-10.60	4077.24	5871.50	160454.63	235831.95	95627.37	-2000.67	2108.55	936.96	15.46
SB09	OC10a042	IGR	GS	Cpy	Sericite	11.10	7.78	4758.08	6051.08	178968.61	215317.48	89497.06	-1471.15	3570.75	286.54	10.28
SB09	OC10a043	IGR	GS	Cpy	Sericite	5.85	-8.37	4545.07	5033.27	180876.61	210733.15	87376.13	-1298.71	5673.18	342.63	451.36
SB09	OC10a044	IGR	GS	Cpy	Sericite	11.69	-13.59	8943.74	13725.27	169656.97	216212.70	92035.75	-2221.52	2459.71	453.14	53.49

Table A2.1: LA-ICPMS normalised analytical results for ablated sericite sites

Sample	Measurement	Mn_ppm	Fe_ppm	Co_ppm	Ni_ppm	Cu_ppm	Zn_ppm	As_ppm	Sr_ppm	Y_ppm	Zr_ppm	Nb_ppm	Ag_ppm	Sn_ppm	Sb_ppm	Ba_ppm	La_ppm
SB05	OC10a034	29.72	11347.47	0.96	23.73	37.64	6.00	-3.42	2.21	0.02	0.26	1.62	-0.95	17.93	-1.31	244.91	0.03
SB05	OC10a039	34.91	7091.84	2.56	31.48	209.51	28.99	1.59	2.73	-0.11	0.47	3.77	-1.00	39.00	-1.26	45.81	0.09
SB07	OC10a128	19.67	9860.63	0.26	1.00	11.27	2.58	-3.44	4.84	0.04	1.08	8.17	-0.80	22.05	-1.49	1037.50	-0.09
SB07	OC10a129	30.43	12776.39	0.27	-1.46	5.75	3.05	-2.65	4.06	-0.13	0.44	4.36	-0.63	27.76	-1.05	879.05	0.01
SB07	OC10a130	20.10	7717.60	0.27	1.80	3.60	2.93	-2.18	2.30	-0.07	0.48	8.02	-0.74	17.11	-1.02	524.87	-0.15
SB07	OC10a131	17.81	9988.30	0.22	1.50	3.25	-2.69	-1.98	4.01	0.05	0.54	10.25	-0.58	17.14	-1.03	608.96	-0.09
SB07	OC10a132	23.11	11493.25	-0.39	1.90	17.03	2.33	-1.71	8.97	0.01	-0.28	6.46	-0.63	15.90	-0.64	600.65	-0.12
SB07	OC10a133	21.71	9938.85	0.40	1.76	1.69	-1.89	-2.58	7.21	-0.05	0.50	6.21	-0.66	14.80	-0.92	514.49	-0.15
SB07	OC10a134	25.69	7980.52	-0.25	1.79	5.53	-2.46	-1.27	5.18	-0.05	0.72	10.53	-0.64	18.78	-0.87	478.08	-0.15
SB07	OC10a135	23.96	8180.05	0.29	2.85	12.50	3.22	-2.97	4.14	0.07	0.46	7.27	-0.82	20.16	-1.01	451.43	0.02
SB07	OC10a136	4.11	654.48	-0.45	0.53	10.34	-4.16	-2.99	10.43	0.03	0.07	0.72	-0.89	2.21	-1.56	657.80	-0.14
SB07	OC10a137	4.94	1078.91	0.14	0.84	24.80	1.33	-4.02	14.18	-0.16	0.10	1.68	-0.96	3.12	-1.44	563.44	0.04
SB07	OC10a138	24.84	4765.62	-0.31	2.59	28.98	4.01	-1.96	3.49	-0.11	0.33	5.95	-0.69	14.65	-0.92	406.07	-0.10
SB07	OC10a139	6.71	170.15	-0.39	0.62	18.93	1.42	-2.79	8.68	0.02	0.03	0.28	-1.37	0.46	-2.01	617.04	-0.15
SB07	OC10a140	19.83	12559.37	-0.47	0.80	4.99	1.69	-1.87	14.73	-0.05	0.78	4.53	-0.52	10.57	-0.83	981.92	-0.09
SB07	OC10a141	16.17	8601.97	0.35	-0.53	-1.70	-2.27	-1.69	9.57	-0.07	1.18	5.45	-0.65	10.53	-0.99	837.78	0.03
SB07	OC10a142	22.20	7686.51	0.17	1.13	4.22	-2.11	-2.07	8.71	0.03	0.76	9.41	-0.45	14.00	-0.78	689.55	0.05
SB07	OC10a143	20.90	10441.46	0.25	0.70	7.52	-2.95	-2.49	4.72	0.04	0.53	4.98	-0.68	10.77	-0.73	629.46	-0.09
SB07	OC10a144	27.16	6255.47	0.26	1.85	7.44	2.91	-2.29	8.60	-0.05	0.43	10.38	-0.73	17.55	-0.92	425.69	-0.10
SB07	OC10a145	24.51	8168.11	-0.26	0.84	11.32	3.34	-1.67	5.92	0.09	0.35	10.42	-0.59	16.89	-0.84	492.49	-0.15
SB07	OC10a146	18.07	6591.98	0.34	1.57	3.53	-2.65	-1.22	12.55	-0.07	0.58	8.44	-0.59	14.36	-0.84	769.32	0.07
SB08	OC10a093	23.52	11652.53	0.66	11.30	11.85	7.47	-2.55	1.78	0.01	0.46	2.46	1.23	40.59	-0.89	356.30	-0.09
SB08	OC10a094	15.24	10392.78	-0.36	3.42	2.72	4.65	-1.84	3.31	-0.11	1.16	4.76	0.86	31.26	-0.78	436.11	-0.09
SB08	OC10a095	4.86	1470.64	0.24	2.74	5.18	6.65	-2.93	12.50	-0.09	-0.36	0.21	-0.91	7.26	-1.63	604.01	-0.16
SB08	OC10a096	18.61	10462.18	0.60	5.78	13.43	12.91	-2.67	3.24	0.01	-0.28	2.78	2.72	41.09	-0.73	270.09	-0.15
SB08	OC10a097	20.79	9746.18	0.31	1.81	2.90	4.44	-1.93	2.95	-0.05	0.57	3.15	-0.64	31.54	-0.81	564.02	-0.15
SB08	OC10a098	23.30	11266.08	0.42	2.20	6.04	13.55	-1.24	3.75	-0.12	0.94	4.24	2.15	25.29	-0.70	485.92	-0.15
SB08	OC10a099	28.57	12280.77	0.40	0.72	3.24	3.84	-1.89	13.47	-0.05	1.70	7.87	0.98	30.98	-0.93	583.67	-0.15
SB08	OC10a100	25.50	13945.56	0.47	2.23	7.30	4.86	-1.98	2.43	52.66	0.68	3.08	-0.72	27.33	-0.74	743.74	0.04
SB08	OC10a101	29.89	13465.63	0.84	6.64	11.55	5.55	-2.62	2.37	-0.14	0.86	4.62	0.52	29.65	-1.04	414.67	-0.09
SB08	OC10a102	26.91	13635.56	0.29	2.01	7.89	-3.38	-1.84	8.16	-0.05	3.27	16.84	4.76	30.36	0.74	816.32	0.07
SB08	OC10a103	20.23	8164.47	0.41	4.42	13.76	6.37	1.07	3.67	-0.09	0.04	3.60	2.02	28.27	-0.95	467.46	0.04
SB08	OC10a104	21.02	9429.09	0.49	3.80	12.43	5.84	-2.82	6.60	-0.05	0.69	2.60	2.56	27.89	-0.86	573.33	0.03
SB08	OC10a105	20.41	10760.56	0.39	2.90	4.89	2.06	-1.23	8.00	0.02	1.06	3.08	-0.50	21.91	-1.04	1026.53	0.01
SB08	OC10a106	17.59	7261.86	0.51	3.31	14.72	4.44	-2.25	4.22	-0.08	0.35	1.67	2.30	24.26	-1.05	452.03	0.01
SB08	OC10a107	17.15	8921.12	0.37	8.59	10.70	4.35	-2.79	40.98	0.02	0.55	2.14	0.98	24.20	-1.36	317.24	0.03
SB09	OC10a042	20.10	16771.85	0.58	4.03	-1.09	4.72	-2.82	5.86	6.46	1.23	22.32	-0.72	17.23	-0.74	294.55	1.42
SB09	OC10a043	20.48	18872.11	0.76	0.86	2.69	2.37	-1.94	5.53	0.03	1.33	3.19	-0.69	23.49	-0.87	279.45	0.01
SB09	OC10a044	33.60	15239.47	2.95	15.48	23.39	25.55	-5.65	1.77	-0.08	0.52	2.00	-1.31	25.40	-1.70	239.04	-0.15

Table A2.1: LA-ICPMS normalised analytical results for ablated sericite sites

Sample	Measurement	Ce_ppm	Eu_ppm	Gd_ppm	Yb_ppm	Lu_ppm	Hf_ppm	Ta_ppm	Au_ppm	Tl_ppm	Pb_ppm	Bi_ppm	Th_ppm	U_ppm
SB05	OC10a034	-0.12	-0.09	0.08	-0.31	-0.04	0.08	0.07	-0.22	-0.77	0.57	-0.39	-0.10	0.07
SB05	OC10a039	-0.10	-0.07	-0.46	-0.53	-0.04	-0.59	1.57	-0.22	-0.66	-0.42	-0.33	0.13	0.21
SB07	OC10a128	-0.15	0.08	-0.24	-0.38	-0.05	-0.53	0.61	-0.21	-0.44	0.41	-0.28	-0.12	-0.05
SB07	OC10a129	-0.14	-0.13	-0.23	-0.39	-0.05	0.26	0.24	-0.16	-0.56	0.32	-0.26	-0.16	-0.06
SB07	OC10a130	0.05	-0.10	0.14	-0.43	0.01	-0.39	0.72	-0.13	-0.44	0.23	-0.32	0.05	-0.07
SB07	OC10a131	-0.27	-0.14	0.18	-0.18	-0.08	-0.61	1.37	-0.31	0.39	1.12	-0.24	-0.12	-0.12
SB07	OC10a132	0.04	-0.07	-0.46	0.09	0.01	-0.37	0.43	-0.17	0.44	0.59	-0.14	-0.11	-0.08
SB07	OC10a133	0.01	-0.14	-0.55	-0.24	-0.08	-0.59	0.26	-0.30	0.62	0.45	-0.14	-0.13	-0.08
SB07	OC10a134	-0.09	-0.15	-0.25	-0.17	-0.05	-0.54	0.68	-0.28	-0.60	0.45	0.12	-0.06	0.08
SB07	OC10a135	0.06	-0.13	-0.29	0.13	0.01	-0.31	0.21	-0.28	-0.50	0.35	-0.20	-0.06	-0.13
SB07	OC10a136	0.04	-0.23	-0.40	0.03	-0.20	-0.41	0.05	0.13	0.39	4.18	-0.33	-0.09	-0.08
SB07	OC10a137	-0.15	-0.21	-0.99	0.14	0.02	0.09	0.21	-0.33	-0.71	5.57	-0.32	-0.15	-0.15
SB07	OC10a138	0.05	0.05	0.24	-0.37	-0.04	-0.64	0.29	0.02	0.58	-0.43	-0.11	-0.06	0.03
SB07	OC10a139	-0.15	-0.13	-0.46	-0.41	-0.09	-0.46	0.08	-0.51	-0.81	3.68	-0.30	0.04	-0.17
SB07	OC10a140	0.03	0.10	-0.55	0.03	-0.09	-0.27	0.33	-0.24	0.54	1.32	-0.23	-0.08	-0.11
SB07	OC10a141	-0.20	0.06	-0.46	-0.18	-0.06	0.15	0.32	-0.18	-0.45	0.61	-0.12	0.07	-0.07
SB07	OC10a142	0.02	0.07	-0.81	-0.46	-0.04	-0.47	0.44	-0.26	-0.46	0.57	-0.18	-0.13	-0.09
SB07	OC10a143	-0.18	-0.15	-0.57	-0.18	0.01	0.05	0.33	-0.40	-0.49	-0.35	-0.20	-0.13	-0.10
SB07	OC10a144	-0.10	0.01	-0.38	0.10	0.03	-0.58	0.60	-0.41	0.44	0.71	-0.18	0.07	-0.12
SB07	OC10a145	0.03	-0.07	-0.25	0.06	-0.08	-0.27	0.79	-0.30	0.46	0.86	-0.14	-0.11	-0.11
SB07	OC10a146	0.02	-0.11	0.14	-0.39	-0.04	-0.55	0.25	-0.13	0.45	1.05	-0.20	-0.08	-0.12
SB08	OC10a093	0.03	-0.07	-0.25	0.19	-0.05	-0.41	-0.17	-0.21	0.42	0.36	-0.21	-0.08	0.06
SB08	OC10a094	-0.15	-0.14	-0.24	0.14	-0.07	-0.57	0.26	-0.16	-0.43	0.24	0.14	-0.07	-0.08
SB08	OC10a095	-0.34	-0.12	-0.61	-0.31	-0.07	-0.94	0.07	-0.30	-0.81	1.88	-0.24	-0.27	-0.12
SB08	OC10a096	-0.09	-0.13	0.19	-0.29	0.02	0.15	0.27	-0.20	0.40	-0.28	-0.18	-0.12	0.11
SB08	OC10a097	-0.15	0.09	-0.49	-0.17	-0.08	-0.26	0.15	-0.25	0.31	0.32	-0.18	-0.08	-0.11
SB08	OC10a098	-0.17	-0.14	-0.46	-0.24	-0.05	-0.53	0.28	-0.41	-0.42	0.42	-0.18	0.15	-0.08
SB08	OC10a099	0.04	-0.15	-0.46	-0.17	-0.04	0.23	0.36	0.15	0.38	0.48	-0.19	0.04	-0.05
SB08	OC10a100	0.23	0.85	4.29	10.22	1.40	0.17	0.24	-0.28	-0.41	0.26	-0.20	0.92	0.24
SB08	OC10a101	-0.15	-0.07	-0.25	-0.25	-0.06	-0.27	0.49	-0.21	-0.35	0.28	-0.15	-0.13	0.01
SB08	OC10a102	0.06	-0.16	-0.35	-0.49	-0.04	0.13	1.12	-0.24	0.47	0.68	-0.19	-0.17	0.58
SB08	OC10a103	-0.10	-0.16	0.13	-0.38	-0.07	-0.59	0.32	-0.32	0.35	0.25	-0.27	-0.06	0.05
SB08	OC10a104	-0.18	-0.13	0.23	-0.30	-0.08	-0.41	0.31	-0.31	-0.35	0.33	-0.22	0.04	-0.12
SB08	OC10a105	-0.09	-0.09	-0.53	-0.23	-0.04	-0.78	0.28	-0.12	-0.39	0.38	-0.21	0.08	-0.05
SB08	OC10a106	-0.15	0.07	0.09	-0.34	-0.10	-0.41	0.29	-0.42	0.55	0.44	-0.28	-0.16	-0.15
SB08	OC10a107	0.06	0.06	0.09	-0.31	-0.08	-0.41	0.25	-0.26	-0.65	-0.58	-0.27	-0.12	-0.10
SB09	OC10a042	5.19	0.28	1.42	0.73	-0.09	0.17	0.70	-0.22	0.33	0.31	-0.20	-0.05	-0.14
SB09	OC10a043	-0.15	-0.13	-0.38	-0.22	-0.09	-0.25	0.24	-0.48	0.99	0.66	-0.24	-0.05	-0.14
SB09	OC10a044	-0.13	-0.13	0.26	-0.26	-0.06	-0.41	0.08	-0.59	-0.72	-0.68	-0.32	0.11	0.13

Table A2.1: LA-ICPMS normalised analytical results for ablated sericite sites

Sample	Measurement	Host Rock	Alteration	Sulfides	Mineral	Li_ppm	B_ppm	Na_ppm	Mg_ppm	Al_ppm	Si_ppm	K_ppm	Ca_ppm	Ti_ppm	V_ppm	Cr_ppm
SB09	OC10a045	IGR	GS	Cpy	Sericite	8.85	-7.45	4762.85	8332.88	168291.23	225137.98	93228.27	-1729.97	1599.38	312.32	14.23
SB09	OC10a046	IGR	GS	Cpy	Sericite	25.21	-8.34	4099.57	48842.75	154822.65	208276.28	91016.99	-1597.52	741.59	117.48	9.00
SB09	OC10a047	IGR	GS	Cpy	Sericite	6.34	-8.16	5353.06	6004.22	183295.47	215353.71	87559.91	-1382.85	3125.04	537.70	20.18
SB09	OC10a048	IGR	GS	Cpy	Sericite	7.55	9.97	8109.41	5819.90	186351.60	215087.59	87222.31	-1316.85	1538.21	242.10	-6.65
SB09	OC10a049	IGR	GS	Cpy	Sericite	9.20	6.88	5813.48	5576.25	185402.95	216681.86	88533.29	-1412.46	1385.64	233.11	-6.10
SB09	OC10a051	IGR	GS	Cpy	Sericite	15.94	-7.44	3281.07	34180.78	172955.33	210307.19	90228.96	-2042.91	24.70	37.01	-6.81
SB10	OC11a043	IGR	GS-WS	Py-Cpy	Sericite	1.58	-7.28	2387.06	7873.22	180127.78	223432.25	84920.28	-1207.04	3691.37	300.59	49.15
SB10	OC11a044	IGR	GS-WS	Py-Cpy	Sericite	2.05	-9.36	2271.81	8193.43	179169.46	223122.05	86149.35	-1968.66	3880.03	310.84	53.09
SB10	OC11a045	IGR	GS-WS	Py-Cpy	Sericite	2.73	-6.19	2371.85	7809.78	176185.24	227763.92	85360.64	-1685.78	2568.74	356.67	30.28
SB10	OC11a046	IGR	GS-WS	Py-Cpy	Sericite	3.28	-7.97	2880.97	7032.07	185764.45	219336.56	88620.43	-1208.00	1016.98	156.47	-7.34
SB10	OC11a047	IGR	GS-WS	Py-Cpy	Sericite	4.24	-7.24	3031.53	7130.38	182750.19	215433.23	89109.64	5055.50	1933.05	242.27	9.03
SB10	OC11a048	IGR	GS-WS	Py-Cpy	Sericite	5.08	-8.36	3582.18	7419.98	184702.02	217558.86	88766.15	-1289.94	1784.31	230.07	11.49
SB10	OC11a049	IGR	GS-WS	Py-Cpy	Sericite	4.43	-7.50	3778.32	6218.79	179882.13	223603.53	89330.74	-1501.98	1162.47	224.30	-7.53
SB10	OC11a050	IGR	GS-WS	Py-Cpy	Sericite	6.17	4.24	3369.57	7553.49	185770.03	213559.05	89958.22	-1000.75	1612.71	362.76	9.36
SB10	OC11a051	IGR	GS-WS	Py-Cpy	Sericite	5.67	-7.73	3508.62	7058.87	186048.94	213956.90	89145.58	-1561.92	2044.47	387.29	10.01
SB10	OC11a052	IGR	GS-WS	Py-Cpy	Sericite	5.13	-5.60	3658.06	7815.76	185143.60	215702.29	88292.02	-1244.28	1586.32	297.84	-6.79
SB10	OC11a053	IGR	GS-WS	Py-Cpy	Sericite	6.35	-7.31	3555.65	7197.42	185596.43	216737.34	87301.16	-1325.82	1537.14	319.95	10.36
SB10	OC11a054	IGR	GS-WS	Py-Cpy	Sericite	8.13	-8.92	3411.37	6744.14	190853.15	210002.03	87916.34	-1536.66	1259.85	410.71	-7.05
SB10	OC11a055	IGR	GS-WS	Py-Cpy	Sericite	4.62	-7.94	4053.26	6348.06	187766.09	215078.13	86303.19	-1152.34	1164.00	351.55	-5.40
SB10	OC11a056	IGR	GS-WS	Py-Cpy	Sericite	5.58	-7.13	3773.30	7219.52	186143.55	215001.52	88767.50	-1110.50	894.47	285.99	-8.08
SB10	OC11a057	IGR	GS-WS	Py-Cpy	Sericite	5.16	-9.38	4029.60	6182.95	184975.38	218178.37	89203.27	-1291.11	801.30	274.97	-6.12
SB10	OC11a058	IGR	GS-WS	Py-Cpy	Sericite	4.18	6.35	3422.78	7804.65	182739.42	219605.41	88450.08	-1140.31	610.72	189.05	-6.13
SB10	OC11a059	IGR	GS-WS	Py-Cpy	Sericite	6.49	-5.92	3872.01	6654.04	183834.18	217407.80	87650.66	-1428.89	1308.03	380.25	-5.45
SB10	OC11a060	IGR	GS-WS	Py-Cpy	Sericite	5.42	-6.16	3471.58	6162.88	165148.10	229602.15	95474.59	-1806.55	2334.48	337.40	25.48
SB10	OC11a061	IGR	GS-WS	Py-Cpy	Sericite	9.75	-6.79	3778.52	8410.19	185983.40	210337.10	89231.77	-1510.25	1770.24	511.85	-8.01
SB10	OC11a062	IGR	GS-WS	Py-Cpy	Sericite	7.32	-8.82	3379.67	7854.26	181496.72	209315.12	88091.10	13840.26	1276.94	367.61	4.62
SB10	OC11a063	IGR	GS-WS	Py-Cpy	Sericite	9.62	-7.61	4079.75	6509.27	185034.76	212144.09	88066.43	-1475.78	2196.85	683.14	-7.28
SB11	OC10a211	IGR	WS	Py-Cpy	Sericite	1.22	-5.99	1234.90	9564.17	181258.56	227133.38	90139.65	-1628.34	1186.15	67.85	3.83
SB11	OC10a212	IGR	WS	Py-Cpy	Sericite	2.35	-8.36	3035.69	13934.50	179174.08	223492.44	90146.81	-1817.46	1094.20	89.60	-7.08
SB11	OC10a213	IGR	WS	Py-Cpy	Sericite	1.69	11.65	1730.12	12624.59	177638.48	227098.37	89135.66	-1927.30	1209.82	80.15	-6.81
SB11	OC10a214	IGR	WS	Py-Cpy	Sericite	3.64	3.93	4397.96	14409.06	176562.19	224889.12	89940.03	-1883.51	1150.56	87.31	-8.46
SB11	OC10a215	IGR	WS	Py-Cpy	Sericite	2.36	6.66	1730.59	8074.22	182405.06	226206.57	90674.12	-1979.34	1284.58	80.00	-7.96
SB11	OC10a216	IGR	WS	Py-Cpy	Sericite	2.42	-8.47	1255.03	9751.52	181563.48	229318.33	87015.09	-1417.08	755.65	59.13	-5.62
SB11	OC10a223	IGR	WS	Py-Cpy	Sericite	2.40	-7.64	1251.46	8107.79	170576.72	244570.97	80103.51	-1622.49	537.19	41.65	-6.70
SB11	OC10a224	IGR	WS	Py-Cpy	Sericite	1.58	-6.98	1368.05	8753.07	181887.16	227124.47	90295.36	-1755.51	1192.45	77.95	-4.57
SB11	OC10a225	IGR	WS	Py-Cpy	Sericite	1.21	7.33	1869.00	7807.68	183792.94	229123.46	86486.26	-1457.20	529.52	44.19	-5.61
SB11	OC10a226	IGR	WS	Py-Cpy	Sericite	2.12	-6.21	1339.53	8621.69	182421.66	226816.43	89928.09	-2100.94	1165.30	81.23	-8.78
SB11	OC10a227	IGR	WS	Py-Cpy	Sericite	1.88	-7.57	1352.66	8286.34	181478.33	227254.45	91455.07	-1583.29	1185.76	83.98	-6.97
SB11	OC10a228	IGR	WS	Py-Cpy	Sericite	1.96	-7.35	1229.36	8842.01	186216.85	221805.14	91133.43	-2464.84	1606.21	92.90	-6.68

Table A2.1: LA-ICPMS normalised analytical results for ablated sericite sites

Sample	Measurement	Mn_ppm	Fe_ppm	Co_ppm	Ni_ppm	Cu_ppm	Zn_ppm	As_ppm	Sr_ppm	Y_ppm	Zr_ppm	Nb_ppm	Ag_ppm	Sn_ppm	Sb_ppm	Ba_ppm	La_ppm
SB09	OC10a045	29.15	15050.76	1.50	6.19	9.55	13.55	-2.61	7.16	-0.12	0.53	2.09	-0.77	23.49	-1.13	302.73	-0.15
SB09	OC10a046	71.65	15862.51	4.18	25.90	27.52	24.03	1.27	2.89	-0.11	0.22	0.96	-0.93	15.30	-1.04	155.87	0.03
SB09	OC10a047	18.34	12937.16	1.38	2.80	16.17	15.00	-2.58	1.74	0.03	0.47	2.52	-0.65	20.57	-0.89	293.97	-0.17
SB09	OC10a048	15.59	11207.45	1.73	3.31	10.70	11.92	-1.98	2.84	0.05	0.70	2.31	-0.51	12.09	-0.91	344.80	-0.18
SB09	OC10a049	15.42	11773.60	1.65	3.26	7.34	15.31	-2.07	3.47	0.02	0.60	2.38	-0.71	14.13	-0.70	382.20	0.09
SB09	OC10a051	21.68	9203.40	2.12	22.31	10.39	10.68	-2.27	0.48	0.81	-0.39	0.11	-0.90	15.47	-0.87	76.57	-0.09
SB10	OC11a043	17.11	6482.08	0.16	0.98	43.99	-3.50	-1.53	1.64	-0.05	0.41	7.85	-0.63	12.83	-0.68	647.49	-0.15
SB10	OC11a044	18.48	6544.48	-0.29	0.28	9.39	1.79	-2.42	1.66	-0.12	0.29	1.39	-0.64	11.71	-0.80	597.23	-0.20
SB10	OC11a045	17.61	7608.08	0.11	1.07	18.75	2.47	-2.09	1.75	0.06	0.15	1.47	-0.65	11.48	-0.74	623.20	-0.20
SB10	OC11a046	18.26	9204.54	0.21	0.61	6.72	-2.54	-2.26	2.50	0.08	0.07	1.15	-0.53	10.17	-0.75	586.28	0.08
SB10	OC11a047	23.55	11258.04	0.20	1.31	8.02	2.00	-2.04	45.21	4.47	0.53	2.99	-0.77	12.24	-0.80	397.68	2.39
SB10	OC11a048	20.00	10267.38	-0.18	-0.51	1.16	2.20	-1.97	2.02	-0.05	0.45	2.13	-0.48	12.24	-0.70	343.60	-0.09
SB10	OC11a049	17.16	9336.33	0.25	0.56	8.33	-2.02	-1.78	10.05	0.25	0.29	1.79	-0.69	12.96	-0.82	954.49	0.21
SB10	OC11a050	23.95	13365.00	-0.23	0.86	14.64	3.51	-2.92	3.15	-0.05	-0.42	1.94	-0.53	15.50	0.54	1332.39	0.05
SB10	OC11a051	22.44	12719.23	-0.26	0.84	16.11	2.62	-2.32	3.21	0.06	0.47	2.89	-0.50	17.12	-0.55	1077.28	-0.15
SB10	OC11a052	24.65	12208.80	-0.23	0.73	5.84	2.38	-1.42	1.82	-0.05	0.32	2.73	-0.70	14.32	-0.76	980.77	0.02
SB10	OC11a053	20.74	11703.22	-0.35	-1.09	16.00	2.25	-1.62	2.46	-0.10	0.57	2.51	-0.47	17.40	-0.92	1191.03	0.02
SB10	OC11a054	26.53	15985.49	-0.41	1.68	4.86	2.33	-1.93	2.88	0.20	0.96	2.63	-0.65	19.21	-0.99	567.09	0.06
SB10	OC11a055	21.58	13337.63	-0.27	-0.66	6.65	-2.31	-1.58	3.13	20.12	0.63	1.98	-0.35	15.27	-1.03	530.52	266.21
SB10	OC11a056	24.25	14129.41	-0.32	-1.02	5.67	2.29	-1.60	2.03	-0.05	0.41	1.18	-0.63	16.09	-1.03	602.91	0.02
SB10	OC11a057	19.92	11520.05	-0.30	0.97	12.15	-2.71	-1.90	2.51	0.03	-0.22	1.27	-0.77	16.22	-0.87	862.71	0.07
SB10	OC11a058	22.19	12071.51	-0.26	-0.68	21.03	2.52	-2.09	6.91	0.56	0.17	0.67	-0.45	13.41	-0.76	1000.11	0.22
SB10	OC11a059	23.55	14114.11	0.23	0.70	5.28	2.38	-2.30	3.02	-0.14	0.38	1.50	-0.44	16.57	-0.60	542.85	0.03
SB10	OC11a060	21.74	12240.36	-0.35	0.70	7.88	1.97	-1.59	16.15	1.81	1.63	3.99	-0.66	15.21	-0.88	779.03	0.03
SB10	OC11a061	42.00	17358.66	-0.25	1.80	14.07	3.33	-2.01	9.80	0.28	0.77	3.02	-0.49	18.83	-0.82	368.73	0.19
SB10	OC11a062	30.72	14459.22	0.15	-0.68	10.63	2.12	-2.09	56.95	2.64	0.55	1.98	-0.69	16.00	-0.81	497.55	1.28
SB10	OC11a063	33.25	17608.99	0.20	-1.00	13.71	-2.70	-1.38	3.07	0.11	0.87	2.83	-0.36	22.27	-1.20	311.42	-0.18
SB11	OC10a211	186.68	710.56	-0.33	0.89	39.10	8.15	-2.73	1.67	-0.11	-0.46	3.17	-0.60	5.33	-0.58	70.56	-0.32
SB11	OC10a212	210.34	2344.53	-0.51	1.55	19.78	16.47	-1.38	9.92	0.02	0.35	2.17	-0.62	6.85	-0.94	97.07	-0.15
SB11	OC10a213	193.99	2304.83	0.46	-0.85	17.17	15.18	-1.13	2.66	0.04	-0.24	2.56	-0.60	7.38	-0.93	93.39	-0.15
SB11	OC10a214	231.50	1791.38	0.65	0.61	30.86	19.50	-2.10	19.28	0.07	0.86	2.47	-0.60	7.93	-0.87	101.18	-0.10
SB11	OC10a215	162.01	1079.77	0.89	2.73	57.34	6.10	-2.55	34.42	-0.12	0.16	3.05	-0.60	7.26	-1.18	84.77	0.05
SB11	OC10a216	127.10	531.86	0.35	-1.05	37.85	7.44	-1.75	7.42	-0.06	0.21	2.47	-0.69	5.86	-0.80	58.73	0.02
SB11	OC10a223	115.66	500.15	-0.59	-1.40	33.22	6.18	-4.03	5.27	-0.08	0.36	1.34	-1.12	4.27	-1.48	59.84	-0.15
SB11	OC10a224	158.06	630.60	-0.38	-0.60	19.52	6.36	-2.74	2.39	0.03	0.28	2.90	-0.99	7.30	-1.19	61.86	-0.10
SB11	OC10a225	121.99	490.42	-0.59	-1.00	27.84	6.12	-2.67	6.16	0.89	0.20	1.40	-0.86	9.59	-1.34	70.05	5.78
SB11	OC10a226	160.28	895.12	-0.42	1.00	23.65	6.58	-1.85	2.46	0.09	0.28	2.29	-0.72	6.28	-1.37	71.30	0.03
SB11	OC10a227	158.60	528.83	0.31	0.91	25.26	6.79	-3.06	2.46	0.01	-0.47	2.74	-0.77	5.98	-1.06	67.23	0.02
SB11	OC10a228	203.65	1146.17	0.38	-2.82	18.89	10.20	-2.05	3.65	0.07	0.40	2.91	-0.68	10.86	-0.75	85.28	0.10

Table A2.1: LA-ICPMS normalised analytical results for ablated sericite sites

Sample	Measurement	Ce_ppm	Eu_ppm	Gd_ppm	Yb_ppm	Lu_ppm	Hf_ppm	Ta_ppm	Au_ppm	Tl_ppm	Pb_ppm	Bi_ppm	Th_ppm	U_ppm
SB09	OC10a045	0.05	-0.25	-0.27	-0.19	-0.06	-0.29	-0.42	-0.25	-0.56	0.54	-0.22	0.08	0.05
SB09	OC10a046	0.01	-0.07	0.04	0.08	-0.06	-0.41	0.12	-0.39	0.49	-0.31	-0.15	-0.11	0.18
SB09	OC10a047	-0.18	-0.12	-0.23	0.03	-0.09	-0.35	0.35	-0.31	-0.37	-0.21	-0.21	0.05	0.07
SB09	OC10a048	0.01	-0.09	0.12	0.05	-0.09	-0.35	0.49	-0.19	-0.58	-0.29	-0.18	-0.16	-0.06
SB09	OC10a049	0.10	0.02	-0.52	0.11	0.02	-0.35	0.22	-0.16	0.46	0.36	-0.31	-0.05	-0.11
SB09	OC10a051	-0.18	-0.07	-0.57	-0.25	0.01	0.22	-0.18	-0.38	0.34	-0.29	-0.29	-0.14	-0.07
SB10	OC11a043	0.03	-0.16	-0.45	0.12	-0.04	-0.29	0.99	-0.29	-0.33	-0.35	-0.11	-0.12	0.18
SB10	OC11a044	0.08	0.07	-0.27	-0.19	0.01	0.25	0.85	-0.17	-0.40	-0.21	-0.33	-0.09	0.12
SB10	OC11a045	-0.10	0.10	-0.81	-0.31	-0.06	-0.30	0.20	-0.27	0.61	0.22	-0.15	-0.09	0.37
SB10	OC11a046	0.08	-0.16	-1.17	-0.18	-0.06	-0.28	-0.09	0.09	0.40	0.38	-0.13	-0.10	0.16
SB10	OC11a047	5.76	0.39	0.87	-0.39	0.12	-0.41	0.23	-0.16	0.53	0.38	-0.18	-0.16	-0.19
SB10	OC11a048	0.05	-0.07	0.05	-0.37	-0.04	-0.57	0.14	-0.17	0.63	0.50	-0.25	0.03	0.13
SB10	OC11a049	0.24	-0.20	-0.26	-0.46	-0.04	-0.28	0.15	-0.24	-0.31	0.49	-0.21	0.07	-0.07
SB10	OC11a050	-0.15	-0.07	-0.25	-0.18	-0.14	-0.39	0.13	-0.16	0.46	0.27	-0.13	-0.06	-0.10
SB10	OC11a051	0.03	-0.09	-0.50	-0.31	-0.04	-0.41	0.22	0.13	-0.36	0.50	-0.29	-0.06	0.14
SB10	OC11a052	-0.20	-0.13	-0.35	-0.42	-0.12	-0.27	0.14	-0.16	0.30	0.33	0.13	-0.12	0.10
SB10	OC11a053	0.03	-0.07	0.18	-0.31	-0.08	0.19	0.32	-0.25	0.44	-0.44	-0.17	0.09	0.11
SB10	OC11a054	-0.10	0.02	0.09	-0.32	-0.04	-0.29	0.31	-0.27	-0.39	0.26	-0.19	-0.09	0.19
SB10	OC11a055	458.51	4.84	11.70	0.80	0.07	0.18	-0.17	-0.31	-0.37	0.49	0.14	130.89	16.87
SB10	OC11a056	0.05	0.02	-0.36	-0.18	-0.06	0.05	0.12	-0.23	-0.33	0.38	-0.19	-0.06	-0.11
SB10	OC11a057	0.02	-0.10	-0.59	0.03	-0.06	0.10	0.08	-0.26	0.62	0.40	0.17	-0.06	0.09
SB10	OC11a058	0.55	0.09	-0.34	-0.33	-0.04	-0.41	0.18	-0.16	0.45	0.49	-0.30	-0.15	-0.16
SB10	OC11a059	-0.18	-0.09	-0.46	0.06	-0.09	0.09	0.19	-0.16	0.42	0.37	-0.17	0.04	0.09
SB10	OC11a060	0.03	-0.07	0.09	-0.31	-0.13	0.14	0.74	-0.18	-0.57	1.43	-0.23	-0.09	0.24
SB10	OC11a061	0.44	-0.07	0.36	-0.18	-0.08	0.10	0.18	-0.16	0.40	0.46	-0.24	-0.06	0.15
SB10	OC11a062	3.45	0.30	-0.25	0.11	-0.07	0.14	0.21	-0.23	0.36	0.51	-0.21	-0.13	0.08
SB10	OC11a063	-0.18	-0.07	-0.35	-0.18	-0.04	-0.28	-0.09	-0.16	0.29	0.31	-0.13	-0.08	0.08
SB11	OC10a211	0.02	-0.16	-0.28	-0.33	-0.04	0.15	0.19	-0.15	0.84	0.45	-0.25	0.06	0.11
SB11	OC10a212	0.02	-0.15	-0.28	-0.20	-0.04	0.05	0.11	-0.15	0.74	0.64	-0.21	-0.06	0.31
SB11	OC10a213	-0.10	-0.11	0.05	0.03	-0.07	0.15	-0.22	0.09	1.03	0.42	-0.25	-0.09	0.16
SB11	OC10a214	-0.10	-0.08	-0.29	-0.59	-0.05	0.10	0.06	-0.56	0.88	0.56	-0.19	-0.19	0.29
SB11	OC10a215	0.07	0.05	-0.29	-0.20	-0.06	-0.31	0.10	-0.21	0.89	0.48	-0.19	-0.15	0.11
SB11	OC10a216	-0.21	0.03	0.10	-0.46	0.02	-0.41	-0.10	-0.50	-0.62	0.49	-0.29	-0.13	0.23
SB11	OC10a223	-0.31	-0.16	0.05	-0.35	-0.14	0.15	-0.21	-0.48	0.63	0.67	-0.33	-0.07	0.27
SB11	OC10a224	0.05	0.04	-0.29	-0.20	0.02	0.16	0.13	-0.44	0.93	0.38	-0.16	0.13	0.26
SB11	OC10a225	13.49	0.17	0.75	-0.20	-0.10	-0.31	0.02	-0.28	0.80	-0.35	-0.22	1.23	0.65
SB11	OC10a226	-0.20	-0.15	-0.57	-0.33	-0.04	-0.41	-0.14	-0.28	0.73	-0.34	-0.25	-0.13	0.23
SB11	OC10a227	-0.20	0.02	0.15	-0.33	-0.04	-0.41	-0.10	-0.36	0.55	0.55	-0.22	-0.09	0.24
SB11	OC10a228	-0.15	0.05	-0.67	-0.51	0.05	-0.41	-0.11	0.09	0.75	0.51	-0.45	0.08	0.11

Table A2.1: LA-ICPMS normalised analytical results for ablated sericite sites

Sample	Measurement	Host Rock	Alteration	Sulfides	Mineral	Li_ppm	B_ppm	Na_ppm	Mg_ppm	Al_ppm	Si_ppm	K_ppm	Ca_ppm	Ti_ppm	V_ppm	Cr_ppm
SB11	OC10a229	IGR	WS	Py-Cpy	Sericite	1.98	-7.85	1185.25	9029.91	176386.59	234599.90	84896.19	-1748.97	1377.77	68.88	-6.39
SB12	OC11a064	IGR	WS	Py	Sericite	3.81	-6.54	2416.82	9806.12	179726.80	222117.83	88267.02	-1214.09	2423.82	300.55	79.90
SB12	OC11a071	IGR	WS	Py	Sericite	4.50	-7.44	3702.50	7805.59	184482.86	216292.97	89689.66	-1523.36	2911.87	179.05	31.66
SB12	OC11a072	IGR	WS	Py	Sericite	3.95	-12.63	3695.96	8117.20	180661.68	220256.88	90488.71	-1694.51	2310.10	140.61	30.58
SB12	OC11a073	IGR	WS	Py	Sericite	3.84	5.91	3146.76	6655.55	184140.11	216873.45	90573.74	-1644.98	2624.62	104.85	19.27
SB12	OC11a074	IGR	WS	Py	Sericite	2.67	-7.90	2774.66	6297.63	159628.59	250349.41	75890.39	-1472.16	1958.20	86.63	-8.18
SB12	OC11a075	IGR	WS	Py	Sericite	3.63	5.56	3573.33	7657.46	180915.83	220838.25	88610.21	-1547.36	2663.43	170.00	26.81
SB12	OC11a076	IGR	WS	Py	Sericite	3.91	4.75	3366.89	7407.91	187214.57	215957.98	89548.00	-1355.08	1839.68	207.16	15.26
SB12	OC11a077	IGR	WS	Py	Sericite	3.21	11.03	3616.92	7027.43	178427.54	224408.08	88667.16	-1401.21	1024.74	107.73	6.10
SB12	OC11a078	IGR	WS	Py	Sericite	3.66	8.27	3206.67	6424.28	187288.06	216433.42	89913.10	-1356.15	1613.50	133.66	7.90
SB12	OC11a079	IGR	WS	Py	Sericite	3.85	5.33	3462.46	6664.45	188150.73	215555.18	89307.51	-1393.52	1618.61	175.50	14.71
SB12	OC11a080	IGR	WS	Py	Sericite	4.60	3.69	4834.00	6847.47	184809.67	217411.96	90126.27	-1281.48	1155.20	116.21	7.38
SB12	OC11a081	IGR	WS	Py	Sericite	-1.25	-7.05	2583.72	4294.04	175830.90	234438.80	82027.70	-1427.05	521.78	42.27	-6.06
SB12	OC11a082	IGR	WS	Py	Sericite	3.43	-7.69	3077.87	6773.84	187327.15	216244.53	90163.87	-1422.92	1604.47	181.19	-7.25
SB12	OC11a083	IGR	WS	Py	Sericite	2.42	-7.80	3042.55	6166.60	181563.17	213864.23	89086.74	16300.73	988.71	79.09	-11.35
SB12	OC11a084	IGR	WS	Py	Sericite	2.65	6.34	4254.11	5140.83	192124.31	216504.89	88588.06	-1067.36	979.00	72.18	-9.11
SB12	OC11a085	IGR	WS	Py	Sericite	3.38	-6.56	4299.41	6492.83	189976.47	216770.11	88847.13	-1402.27	971.25	115.71	-7.78
SB12	OC11a086	IGR	WS	Py	Sericite	3.59	9.30	4803.57	5810.02	190046.51	214964.53	89604.42	-1462.68	1444.43	124.60	-6.82
SB12	OC11a087	IGR	WS	Py	Sericite	2.54	11.39	3481.74	6377.45	186523.28	218771.83	89271.58	-1108.96	1427.67	143.55	-7.02
SB12	OC11a088	IGR	WS	Py	Sericite	3.03	7.73	4466.51	6769.65	187102.41	217722.95	89670.38	-1269.76	1096.19	121.49	-4.88
SB12	OC11a089	IGR	WS	Py	Sericite	2.76	5.05	3371.68	5860.36	191119.93	217453.24	88824.91	-1301.88	1056.01	82.71	-8.10
SB12	OC11a090	IGR	WS	Py	Sericite	2.04	-11.39	2806.13	6888.54	188322.75	221457.37	87426.90	-1414.13	909.06	61.51	-7.01
SB12	OC11a091	IGR	WS	Py	Sericite	2.16	-7.80	4561.51	5770.17	183890.37	221355.92	89556.58	-1698.99	1768.93	69.14	-7.69
SB12	OC11a092	IGR	WS	Py	Sericite	2.63	-7.73	5018.71	5849.04	188487.07	217775.27	88716.89	-1287.78	1526.45	81.89	-7.49
SB12	OC11a093	IGR	WS	Py	Sericite	3.33	-7.20	4373.95	6054.92	188546.90	217644.85	89579.15	-1389.28	1214.83	71.22	-6.73
SB12	OC11a094	IGR	WS	Py	Sericite	2.20	4.97	3109.78	5513.48	191103.26	217083.20	88069.21	-1758.94	1776.07	74.39	7.25
SB12	OC11a095	IGR	WS	Py	Sericite	2.98	-14.96	1775.32	2471.79	88827.52	341699.85	40683.48	-2801.40	380.81	23.24	-14.66
SB12	OC11a096	IGR	WS	Py	Sericite	2.16	-13.31	3786.12	5197.32	162828.44	254525.78	73156.49	-1554.09	259.24	33.58	-7.03
SB12	OC11a097	IGR	WS	Py	Sericite	3.03	4.87	2655.08	6607.61	180328.25	228390.01	84967.67	-1346.52	854.29	122.85	-7.84
SB12	OC11a098	IGR	WS	Py	Sericite	4.55	23.83	2932.93	7251.85	187835.52	216280.83	89389.79	-1051.56	1307.01	176.08	-8.57
SB12	OC11a099	IGR	WS	Py	Sericite	4.39	14.14	4069.79	7330.51	186258.61	216710.85	90116.36	-1419.12	892.33	119.86	-7.08
SB12	OC11a100	IGR	WS	Py	Sericite	4.27	9.79	5234.70	6981.93	187476.24	215112.02	90089.40	-1276.61	1188.84	145.23	7.33
SB12	OC11a101	IGR	WS	Py	Sericite	4.19	-7.92	4391.64	6756.91	186655.94	216833.04	90281.48	-1494.52	1089.31	131.43	-9.42
SB12	OC11a102	IGR	WS	Py	Sericite	3.70	7.32	4365.69	6019.92	189598.91	214199.81	89737.39	-1420.69	1696.14	218.65	8.87
SB13	OC10a053	IGR	WS	HS	Sericite	8.41	19.01	6303.42	9797.87	197154.47	201554.77	84416.22	-1915.81	1944.84	207.95	-7.36
SB13	OC10a054	IGR	WS	HS	Sericite	10.86	7.35	8206.56	6655.78	182607.35	212487.27	86645.49	-1410.62	3043.43	275.14	7.47
SB13	OC10a055	IGR	WS	HS	Sericite	11.27	6.62	9454.39	6033.90	183679.79	225873.55	74942.65	-1692.13	1293.78	121.47	7.26
SB13	OC10a057	IGR	WS	HS	Sericite	12.08	6.51	13881.04	7221.56	181246.58	210327.24	86137.07	-1288.52	2512.59	269.52	-6.20
SB13	OC10a058	IGR	WS	HS	Sericite	10.43	6.21	16483.07	6608.00	182920.73	208580.41	85297.46	-1871.94	2688.79	278.74	12.66

Table A2.1: LA-ICPMS normalised analytical results for ablated sericite sites

Sample	Measurement	Mn_ppm	Fe_ppm	Co_ppm	Ni_ppm	Cu_ppm	Zn_ppm	As_ppm	Sr_ppm	Y_ppm	Zr_ppm	Nb_ppm	Ag_ppm	Sn_ppm	Sb_ppm	Ba_ppm	La_ppm
SB11	OC10a229	244.02	602.26	-0.21	1.17	31.66	7.38	1.69	6.21	-0.12	0.64	4.02	-0.83	8.70	-1.33	88.24	0.05
SB12	OC11a064	8.10	7339.17	0.98	0.30	46.67	3.31	-2.27	0.62	0.08	1.13	5.23	-0.53	24.11	-1.03	101.80	0.03
SB12	OC11a071	5.99	8702.61	0.95	-0.74	34.71	-2.72	-4.66	2.51	0.08	0.53	4.98	-0.93	18.54	-1.57	116.60	-0.16
SB12	OC11a072	8.41	8145.08	1.60	-1.31	70.51	3.91	-2.93	1.22	1.39	0.75	5.30	-0.75	14.74	-1.19	105.71	-0.15
SB12	OC11a073	8.11	10060.82	1.11	-0.55	27.59	2.70	2.04	0.55	-0.13	0.36	6.15	-0.68	11.30	-0.95	148.53	-0.15
SB12	OC11a074	7.51	7226.51	1.07	0.37	36.25	-2.64	-2.20	0.55	0.26	0.30	3.72	-0.74	9.89	-1.26	118.66	-0.11
SB12	OC11a075	8.33	8299.57	1.90	-0.78	54.97	-2.83	-2.56	0.57	-0.11	0.55	4.38	-0.61	15.14	-1.37	120.47	0.02
SB12	OC11a076	11.57	8911.75	1.16	0.36	43.91	2.75	-2.51	0.95	0.07	0.50	4.01	-0.67	20.10	-0.68	140.09	-0.13
SB12	OC11a077	9.31	10886.12	1.50	0.61	41.58	-2.21	-1.58	0.57	0.08	-0.46	2.97	-0.64	13.07	-0.75	128.22	-0.10
SB12	OC11a078	10.01	9740.99	1.18	-0.70	27.66	2.22	-1.83	0.66	0.08	0.55	4.55	-0.44	15.44	-0.86	142.19	-0.09
SB12	OC11a079	9.97	9805.88	0.98	0.14	36.46	1.73	-1.99	0.94	-0.05	0.62	3.76	-0.56	16.86	-0.60	145.71	0.03
SB12	OC11a080	11.08	10370.81	1.95	0.44	47.61	3.17	-1.86	0.80	0.37	0.34	3.76	-0.67	13.01	-1.16	119.83	-0.15
SB12	OC11a081	5.49	10437.37	0.23	0.15	7.76	-2.47	-1.69	0.53	0.35	0.08	2.64	-0.61	8.73	-1.13	50.46	0.08
SB12	OC11a082	8.19	9481.33	1.36	0.29	43.09	3.08	-2.11	0.93	0.15	0.37	3.90	-0.61	18.56	-1.04	145.88	0.08
SB12	OC11a083	6.81	7869.94	0.99	-1.38	40.97	3.81	-2.29	11.85	2.52	0.16	3.80	-0.54	13.45	-1.32	123.19	0.95
SB12	OC11a084	9.00	6431.49	1.45	0.38	31.65	3.04	-2.01	0.69	0.07	0.30	3.80	-0.67	15.34	-1.04	179.83	-0.21
SB12	OC11a085	9.66	6931.22	2.24	-1.04	66.80	2.47	-1.93	0.72	0.10	0.34	3.81	-0.44	14.30	-1.00	221.16	-0.19
SB12	OC11a086	13.04	8114.85	2.53	0.23	58.60	-2.51	-2.62	0.86	0.16	0.31	4.40	-0.47	17.20	-0.98	179.59	-0.10
SB12	OC11a087	8.49	7923.69	1.81	0.29	49.36	-2.88	-1.80	0.51	0.09	-0.43	4.16	-0.59	15.69	-0.86	215.48	-0.26
SB12	OC11a088	10.97	7819.76	2.72	-0.53	45.99	2.92	-2.03	2.84	0.57	0.50	3.55	-0.42	14.37	-0.59	234.19	0.02
SB12	OC11a089	4.12	5684.97	1.37	0.70	45.66	-2.85	-1.88	1.00	0.14	0.56	4.31	-0.48	13.06	-0.74	426.58	0.02
SB12	OC11a090	-2.77	4389.52	0.57	-1.23	34.37	2.99	1.33	0.36	-0.09	-0.23	3.29	-0.43	17.11	-1.07	274.47	0.02
SB12	OC11a091	7.02	6302.16	0.90	0.69	38.83	2.88	-2.29	0.33	0.03	0.35	4.70	-0.62	12.48	-0.78	276.09	-0.33
SB12	OC11a092	7.82	6364.42	1.38	0.53	42.78	-2.24	-1.88	0.48	0.04	0.58	3.73	-0.52	13.94	-1.12	267.94	-0.15
SB12	OC11a093	9.45	6831.12	1.09	-0.72	37.55	-3.43	-1.57	0.64	-0.10	0.29	4.05	-0.56	12.32	-0.74	202.36	0.03
SB12	OC11a094	4.23	6048.00	0.94	-0.52	16.10	-2.30	-1.71	0.54	-0.10	0.50	5.85	-0.56	13.94	-1.40	257.95	-0.09
SB12	OC11a095	4.28	2933.51	0.68	-1.82	9.25	2.67	-5.12	0.87	10.48	0.22	1.50	-0.91	4.38	-1.46	138.60	-0.20
SB12	OC11a096	8.85	3332.03	1.59	-0.75	37.21	-3.81	-2.67	0.63	0.16	0.24	1.22	-0.76	10.66	-1.33	205.07	0.04
SB12	OC11a097	5.79	7333.57	1.29	0.57	42.30	-3.09	-1.74	3.17	0.17	-0.51	2.99	-0.49	15.17	-0.91	153.70	-0.10
SB12	OC11a098	9.80	9583.87	1.35	-1.03	27.80	-2.89	-2.12	1.11	0.05	0.43	3.25	-0.67	14.17	-0.65	206.61	0.02
SB12	OC11a099	13.45	10348.13	1.86	-0.52	36.22	2.68	-2.39	0.96	0.17	-0.22	2.82	-0.62	13.50	-1.09	143.22	0.02
SB12	OC11a100	11.55	9748.23	1.23	-0.53	30.81	2.31	-2.15	0.94	0.11	0.34	2.88	-0.41	15.44	-0.98	146.13	0.02
SB12	OC11a101	9.48	9428.88	1.18	-1.25	34.74	2.82	1.12	0.94	0.17	0.32	3.10	-0.46	14.48	-1.07	145.08	-0.10
SB12	OC11a102	10.96	9246.73	1.01	-1.09	46.21	-1.82	-2.24	1.45	0.08	0.38	4.79	-0.44	19.91	-1.18	156.63	0.03
SB13	OC10a053	14.43	15368.32	0.61	1.01	574.73	7.68	-2.46	29.18	-0.09	-0.39	2.40	-1.35	8.99	-1.00	219.08	0.25
SB13	OC10a054	13.00	15720.84	-0.19	1.08	174.65	1.76	-2.44	4.09	0.04	0.57	3.45	-0.56	14.23	-0.83	496.45	0.04
SB13	OC10a055	7.66	8089.27	-0.24	0.52	259.70	-2.79	-1.99	2.62	0.05	0.18	2.04	-0.84	7.69	-0.81	177.16	-0.15
SB13	OC10a057	15.27	16254.50	0.17	1.15	47.35	-2.46	-2.10	5.89	0.02	-0.40	3.85	-0.60	14.72	-1.07	683.23	0.14
SB13	OC10a058	13.26	15247.33	0.31	0.96	167.36	-2.06	-2.59	4.89	0.09	0.31	3.37	-0.64	13.49	-0.92	544.58	0.03

Table A2.1: LA-ICPMS normalised analytical results for ablated sericite sites

Sample	Measurement	Ce_ppm	Eu_ppm	Gd_ppm	Yb_ppm	Lu_ppm	Hf_ppm	Ta_ppm	Au_ppm	Tl_ppm	Pb_ppm	Bi_ppm	Th_ppm	U_ppm
SB11	OC10a229	-0.32	0.06	-0.87	-0.29	-0.05	-0.32	0.10	-0.16	0.88	0.69	-0.24	-0.07	0.08
SB12	OC11a064	0.06	-0.21	-0.28	-0.20	-0.06	-0.31	0.12	0.10	0.69	0.48	0.47	-0.19	0.38
SB12	OC11a071	-0.13	-0.86	-0.27	0.03	-0.09	-0.41	0.23	0.08	-0.47	2.08	0.89	-0.06	0.28
SB12	OC11a072	0.05	-0.16	-0.60	0.41	0.01	-0.33	0.58	-0.41	0.72	1.10	1.15	0.58	0.19
SB12	OC11a073	-0.10	0.04	-0.61	-0.27	-0.09	-0.31	0.60	-0.29	0.52	0.86	8.81	-0.13	0.19
SB12	OC11a074	0.03	-0.08	-0.30	-0.30	0.01	-0.33	0.30	-0.39	-0.64	0.75	0.56	-0.15	-0.15
SB12	OC11a075	0.02	-0.15	-0.56	-0.27	0.05	-0.41	0.35	-0.31	0.48	1.71	4.36	-0.07	0.15
SB12	OC11a076	-0.15	0.03	0.14	-0.31	-0.08	0.24	0.30	-0.12	0.52	1.43	1.16	-0.06	0.16
SB12	OC11a077	-0.10	0.07	0.19	0.13	-0.09	-0.41	0.23	-0.13	0.59	2.29	3.20	0.07	0.09
SB12	OC11a078	0.06	-0.09	0.09	-0.49	-0.08	0.10	0.25	-0.25	0.72	0.55	0.90	-0.06	0.09
SB12	OC11a079	-0.09	0.04	-0.40	-0.17	0.01	-0.26	0.24	-0.19	0.77	1.06	1.25	0.04	0.08
SB12	OC11a080	0.11	0.02	-0.36	-0.18	-0.04	-0.29	-0.27	-0.21	0.61	2.46	2.07	0.12	-0.14
SB12	OC11a081	-0.29	-0.11	-0.29	-0.59	0.03	0.15	-0.21	-0.14	0.49	-0.44	-0.31	-0.11	0.10
SB12	OC11a082	-0.20	-0.07	0.27	-0.18	-0.09	-0.28	0.28	-0.12	0.66	0.94	0.78	0.09	0.14
SB12	OC11a083	2.82	0.13	1.00	-0.59	-0.13	-0.44	0.26	-0.35	-0.52	1.20	1.01	-0.16	0.19
SB12	OC11a084	0.03	0.01	0.05	-0.26	-0.09	-0.29	0.22	-0.17	-0.49	1.84	1.33	-0.09	0.12
SB12	OC11a085	-0.09	-0.14	0.09	-0.18	-0.07	-0.29	0.26	-0.21	-0.39	2.18	1.78	-0.10	0.15
SB12	OC11a086	-0.21	0.04	0.10	-0.18	-0.04	0.20	0.33	-0.17	0.55	4.35	21.63	-0.21	-0.16
SB12	OC11a087	-0.19	-0.10	-0.26	0.12	-0.11	-0.28	0.42	-0.12	-0.46	1.24	1.05	-0.06	0.12
SB12	OC11a088	0.12	0.06	-0.27	-0.37	-0.10	0.15	0.33	-0.33	0.47	2.98	3.28	0.08	0.14
SB12	OC11a089	0.03	-0.07	-0.37	-0.19	-0.09	-0.59	0.23	-0.30	-0.36	0.39	0.77	-0.12	-0.15
SB12	OC11a090	-0.15	0.03	-0.67	0.13	0.06	-0.31	0.29	-0.33	-0.34	-0.22	0.79	0.09	-0.08
SB12	OC11a091	-0.15	0.01	-0.61	-0.22	-0.08	-0.41	0.43	-0.37	0.64	1.81	1.18	0.07	0.15
SB12	OC11a092	-0.19	-0.15	0.14	0.19	-0.04	0.05	0.22	-0.27	0.42	1.98	1.45	-0.08	0.10
SB12	OC11a093	-0.09	0.02	0.05	0.03	-0.06	0.15	0.22	-0.27	0.51	1.22	0.88	0.11	-0.13
SB12	OC11a094	-0.15	-0.07	-0.36	0.06	-0.04	0.15	-0.27	-0.20	0.57	-0.29	-0.31	-0.23	0.13
SB12	OC11a095	0.23	0.12	0.85	0.52	0.08	0.15	0.15	-0.61	-0.81	0.69	0.55	-0.28	0.24
SB12	OC11a096	-0.13	0.01	-1.32	-0.31	-0.08	-0.41	-0.13	-0.35	-0.58	0.97	1.34	-0.09	0.16
SB12	OC11a097	-0.35	-0.20	-0.28	-0.39	-0.06	0.10	0.19	-0.26	0.68	-0.33	0.44	-0.09	-0.19
SB12	OC11a098	0.14	-0.13	-0.36	-0.25	-0.07	0.10	0.32	0.11	0.42	0.82	0.59	-0.06	0.22
SB12	OC11a099	-0.19	-0.10	0.23	-0.51	-0.04	-0.29	0.18	-0.17	0.64	1.91	1.07	-0.17	0.10
SB12	OC11a100	-0.15	-0.07	-0.58	0.09	0.03	0.05	0.34	-0.17	0.42	2.40	1.10	-0.15	0.08
SB12	OC11a101	-0.09	-0.07	-0.26	0.16	-0.08	0.10	0.21	-0.40	0.48	1.42	1.46	-0.06	0.12
SB12	OC11a102	-0.12	0.03	0.18	0.09	-0.05	0.19	0.13	-0.20	0.67	1.17	1.27	0.01	-0.13
SB13	OC10a053	0.16	0.04	-0.44	-0.31	-0.11	-0.48	0.40	-0.37	0.71	1.68	-0.26	1.01	-0.19
SB13	OC10a054	0.01	-0.14	-0.41	-0.49	-0.07	0.31	0.43	-0.26	0.82	0.24	-0.16	-0.12	0.16
SB13	OC10a055	-0.09	0.06	0.05	-0.36	0.01	-0.28	0.41	-0.24	-0.44	-0.32	-0.24	0.20	-0.07
SB13	OC10a057	0.12	0.06	0.12	-0.37	-0.09	-0.26	0.50	-0.20	0.59	-0.32	-0.15	0.20	0.24
SB13	OC10a058	0.01	-0.13	-0.46	-0.38	-0.06	0.18	0.38	-0.26	0.74	-0.27	-0.21	0.21	0.20

Table A2.1: LA-ICPMS normalised analytical results for ablated sericite sites

Sample	Measurement	Host Rock	Alteration	Sulfides	Mineral	Li_ppm	B_ppm	Na_ppm	Mg_ppm	Al_ppm	Si_ppm	K_ppm	Ca_ppm	Ti_ppm	V_ppm	Cr_ppm
SB13	OC10a059	IGR	WS	HS	Sericite	11.55	9.67	16728.72	6314.06	182691.23	212575.78	80744.04	-1548.68	2522.09	274.26	7.30
SB13	OC10a060	IGR	WS	HS	Sericite	22.43	22.51	1574.02	2238.78	169432.02	275558.47	15123.96	-1759.15	18.29	14.52	-6.27
SB13	OC10a061	IGR	WS	HS	Sericite	21.90	18.44	4759.82	3099.84	182752.97	257585.12	34508.76	-1674.43	61.54	19.55	-5.08
SB13	OC10a062	IGR	WS	HS	Sericite	13.15	11.56	4723.11	7608.33	178596.62	226678.47	73424.74	-1942.78	1102.37	145.27	-8.55
SB13	OC10a063	IGR	WS	HS	Sericite	8.08	7.94	3330.31	6225.49	163914.15	249835.28	70810.48	-1920.64	726.60	87.08	-4.94
SB14a	OC10a108	IRDP	GS	Py-Cpy	Sericite	16.19	6.60	1952.74	37041.30	161101.52	220408.14	89340.21	-1817.13	196.90	136.01	-9.63
SB14a	OC10a109	IRDP	GS	Py-Cpy	Sericite	10.72	4.77	2012.42	32206.96	169379.32	217330.38	90645.51	-1958.36	176.29	121.41	-8.16
SB14a	OC10a110	IRDP	GS	Py-Cpy	Sericite	12.42	-7.85	2735.65	20580.13	181255.92	214160.42	90386.14	-1755.75	1012.17	79.14	-9.34
SB14a	OC10a112	IRDP	GS	Py-Cpy	Sericite	4.71	-7.70	12253.87	13007.70	153023.36	254398.51	66021.10	-1842.57	582.83	58.33	-9.63
SB14a	OC10a113	IRDP	GS	Py-Cpy	Sericite	5.37	-13.49	2160.95	11870.68	117348.35	298179.51	58153.90	-2513.17	645.29	31.82	-9.60
SB14a	OC10a114	IRDP	GS	Py-Cpy	Sericite	9.81	-11.20	2693.98	27856.74	173009.79	216616.72	90690.91	1569.30	190.60	75.10	-7.21
SB14a	OC10a116	IRDP	GS	Py-Cpy	Sericite	22.82	5.46	2789.50	47355.93	165090.59	204573.10	88827.13	-1334.37	888.57	193.09	6.32
SB14a	OC10a119	IRDP	GS	Py-Cpy	Sericite	8.05	-7.53	2794.91	13164.38	179150.80	220531.70	87423.05	2864.00	918.43	194.47	5.06
SB14a	OC10a120	IRDP	GS	Py-Cpy	Sericite	16.01	-9.39	3200.52	32917.97	166426.64	213112.11	92466.66	-2013.04	757.06	134.40	-7.48
SB14b	OC11a028	IRDP	WS	Py-Cpy	Sericite	1.88	-7.68	4902.04	6940.79	181414.16	232498.47	79375.48	-1956.83	250.21	48.86	-5.76
SB14b	OC11a030	IRDP	WS	Py-Cpy	Sericite	2.52	6.59	3460.00	7323.62	194832.75	220854.52	80489.03	-1839.07	147.39	30.27	-7.65
SB14b	OC11a033	IRDP	WS	Py-Cpy	Sericite	6.69	-8.22	3591.80	6897.23	194849.63	214900.97	86989.30	-1385.99	594.94	416.71	-6.72
SB14b	OC11a034	IRDP	WS	Py-Cpy	Sericite	1.52	-7.09	3817.22	4515.98	196612.32	215906.24	86440.07	-1695.29	1049.75	456.53	-9.28
SB14b	OC11a035	IRDP	WS	Py-Cpy	Sericite	6.52	-6.04	3769.45	11676.00	181966.98	208017.87	88049.50	8457.87	2242.07	195.95	-7.43
SB14b	OC11a036	IRDP	WS	Py-Cpy	Sericite	18.52	-7.69	3706.26	14553.39	191798.91	209250.32	88548.96	-1633.14	518.04	130.81	-8.99
SB14b	OC11a037	IRDP	WS	Py-Cpy	Sericite	3.89	-7.60	3612.87	6372.92	193683.16	215773.10	86728.67	-1361.25	1100.16	353.33	-7.26
SB14b	OC11a038	IRDP	WS	Py-Cpy	Sericite	8.17	-7.33	3384.85	11301.65	187721.85	215347.83	88842.99	-1218.78	998.28	271.72	-8.28
SB14b	OC11a039	IRDP	WS	Py-Cpy	Sericite	16.84	-10.20	3337.43	12434.13	189980.85	212347.89	89218.33	-1379.35	725.48	219.41	-9.36
SB14b	OC11a040	IRDP	WS	Py-Cpy	Sericite	9.47	-8.82	3183.64	9803.81	190067.73	215721.31	88641.74	-1421.96	874.02	301.89	-6.67
SB14b	OC11a041	IRDP	WS	Py-Cpy	Sericite	2.97	-8.05	2853.68	7920.62	182185.23	231450.60	80287.82	-1802.71	386.69	80.98	-6.22
SB14b	OC11a042	IRDP	WS	Py-Cpy	Sericite	2.73	-5.81	3110.17	7627.03	188038.09	222368.23	85852.26	-1433.36	490.22	89.76	-6.04
SB15	OC11a152	IRDP	WS	Cpy-HS	Sericite	10.71	12.90	4410.94	9834.66	168656.33	234753.40	70767.66	-2882.12	1069.04	210.51	-11.78
SB15	OC11a153	IRDP	WS	Cpy-HS	Sericite	5.43	5.27	2185.70	9761.52	181590.30	219091.29	83898.73	-1491.16	1455.86	280.78	9.13
SB15	OC11a154	IRDP	WS	Cpy-HS	Sericite	9.76	8.28	2033.72	11075.57	182003.98	223636.21	74467.91	-1541.10	1207.19	242.07	9.11
SB15	OC11a155	IRDP	WS	Cpy-HS	Sericite	5.37	-8.11	2123.95	10739.79	183660.06	222711.37	88328.13	-1578.69	1542.12	460.84	10.10
SB15	OC11a156	IRDP	WS	Cpy-HS	Sericite	3.58	6.20	2189.52	9758.62	185068.03	223361.63	87008.02	-1563.04	1441.32	537.46	7.20
SB15	OC11a157	IRDP	WS	Cpy-HS	Sericite	4.45	-11.70	2171.73	9369.97	184202.07	224963.34	86231.64	-1573.06	1265.82	411.58	7.14
SB15	OC11a158	IRDP	WS	Cpy-HS	Sericite	4.71	7.12	2102.66	10340.95	181936.00	224648.16	88529.04	-1669.65	1501.08	513.12	12.09
SB15	OC11a159	IRDP	WS	Cpy-HS	Sericite	4.91	8.28	2151.35	9427.43	184432.16	221663.97	88323.95	-1086.99	2499.55	507.25	12.13
SB15	OC11a160	IRDP	WS	Cpy-HS	Sericite	5.71	6.67	1900.13	13648.36	178467.65	225390.71	85272.84	-1380.70	1337.66	384.60	28.29
SB15	OC11a161	IRDP	WS	Cpy-HS	Sericite	5.62	3.69	1966.83	18588.67	165747.06	219324.53	87629.49	-2013.28	1507.99	300.37	6.88
SB15	OC11a162	IRDP	WS	Cpy-HS	Sericite	4.79	-6.61	2225.58	11693.48	183910.81	222148.54	86981.68	-1485.95	1371.69	246.10	-6.86
SB15	OC11a163	IRDP	WS	Cpy-HS	Sericite	9.84	5.05	10020.49	9514.34	176455.29	236615.44	67181.80	-2155.05	843.61	285.98	-8.32
SB15	OC11a164	IRDP	WS	Cpy-HS	Sericite	11.91	10.40	2195.95	10552.44	186811.51	227034.19	74283.73	-1628.51	1094.54	318.05	6.89

Table A2.1: LA-ICPMS normalised analytical results for ablated sericite sites

Sample	Measurement	Mn_ppm	Fe_ppm	Co_ppm	Ni_ppm	Cu_ppm	Zn_ppm	As_ppm	Sr_ppm	Y_ppm	Zr_ppm	Nb_ppm	Ag_ppm	Sn_ppm	Sb_ppm	Ba_ppm	La_ppm
SB13	OC10a059	11.37	14095.99	-0.28	0.61	84.62	-2.58	-2.54	5.19	-0.05	0.71	3.19	-0.81	13.55	-1.10	501.64	-0.09
SB13	OC10a060	6.53	925.23	0.31	1.95	19766.20	15.08	-2.72	1.07	1.08	0.63	0.20	-0.62	0.65	-1.17	4.91	0.02
SB13	OC10a061	6.41	1642.95	0.19	3.05	6216.65	7.35	-1.70	1.75	0.08	0.22	0.50	-0.76	2.09	-0.73	7.29	0.09
SB13	OC10a062	14.42	11085.82	0.36	1.94	7916.19	7.11	-2.36	3.19	-0.12	0.21	1.51	-0.73	6.76	0.61	306.99	-0.15
SB13	OC10a063	8.01	7095.80	-0.33	1.17	2151.18	-3.46	-1.66	1.70	0.03	0.25	1.14	-0.61	5.97	-1.44	176.04	0.02
SB14a	OC10a108	156.48	7653.03	1.44	4.64	109.76	18.53	-2.83	6.17	0.10	-0.99	3.15	-1.04	4.48	-1.65	150.08	0.04
SB14a	OC10a109	106.16	5985.81	0.44	-1.70	41.77	6.68	-2.35	6.65	0.53	0.36	2.46	-0.64	3.72	-1.01	117.44	0.09
SB14a	OC10a110	67.83	6066.81	0.32	1.19	8.23	6.45	-2.26	4.05	-0.08	0.45	5.92	-0.64	3.57	-1.03	398.63	-0.14
SB14a	OC10a112	50.23	4305.44	-0.52	1.00	6.52	3.88	-3.20	21.29	0.08	0.08	7.47	-0.84	2.30	-1.01	626.24	0.05
SB14a	OC10a113	44.12	3449.95	-0.48	-0.88	13.65	4.39	-4.06	2.94	0.08	-0.71	5.41	-1.03	1.65	-1.43	472.88	0.02
SB14a	OC10a114	90.55	5049.77	0.60	1.59	52.29	9.68	-1.50	42.82	1.14	0.12	1.75	-0.66	2.94	-0.88	173.88	0.45
SB14a	OC10a116	334.97	11706.97	0.46	4.72	40.71	32.45	-2.42	12.17	0.04	0.25	2.33	-0.63	3.36	-0.87	423.00	-0.20
SB14a	OC10a119	76.80	6609.98	-0.29	-0.84	12.42	9.00	-1.78	50.30	0.40	-0.48	4.17	-0.93	4.22	-1.06	1580.22	0.19
SB14a	OC10a120	215.90	10937.70	0.35	2.77	7.51	26.68	-2.92	5.74	-0.15	0.32	3.22	-0.92	6.66	-0.93	562.15	-0.15
SB14b	OC11a028	22.19	2787.68	0.19	0.93	10.56	3.46	-5.00	8.38	-0.13	1.09	2.26	-0.95	1.99	-1.25	1046.97	-0.15
SB14b	OC11a030	24.37	2553.27	-0.31	-1.61	21.03	4.86	-3.02	9.28	0.27	-0.28	0.66	-0.82	1.91	-1.89	1182.61	-0.13
SB14b	OC11a033	43.94	4936.21	0.43	0.72	9.16	4.11	-2.22	18.88	-0.05	0.53	3.01	-0.75	6.79	-1.13	1148.04	-0.10
SB14b	OC11a034	17.16	2927.45	-0.28	1.15	22.80	-2.15	-2.74	14.27	0.42	0.47	3.72	-0.68	7.50	-1.08	1198.53	-0.15
SB14b	OC11a035	80.84	6665.25	0.21	-1.42	7.17	8.27	5.69	140.04	135.76	44.10	7.70	-0.62	7.01	-1.10	1612.14	2548.78
SB14b	OC11a036	92.18	7791.19	0.27	1.73	5.11	12.71	-2.05	17.17	-0.15	2.02	3.17	-0.61	6.60	-0.99	757.77	0.07
SB14b	OC11a037	35.57	4884.39	-0.26	-0.52	8.78	2.47	-1.34	7.76	-0.05	0.61	3.64	-0.75	8.93	-1.23	1112.30	0.10
SB14b	OC11a038	67.85	6619.44	-0.24	1.48	7.86	6.53	1.98	8.11	0.08	0.23	4.54	-0.55	5.81	-1.04	848.59	0.05
SB14b	OC11a039	76.92	7222.53	-0.30	1.42	5.49	6.80	-2.22	16.02	-0.11	0.69	3.87	-0.66	8.10	-0.89	801.00	0.02
SB14b	OC11a040	54.28	5353.45	0.27	-1.15	11.61	5.47	-2.28	11.74	-0.07	0.74	3.06	-0.65	10.02	-0.74	853.73	0.05
SB14b	OC11a041	24.33	2935.94	-0.37	1.43	48.99	-3.70	-2.36	6.60	-0.12	0.36	1.44	-0.64	4.54	-1.23	1124.66	0.03
SB14b	OC11a042	25.93	3524.35	-0.39	4.17	120.27	6.14	-2.94	9.03	0.12	0.49	2.36	-0.50	4.01	-0.74	1518.69	0.02
SB15	OC11a152	57.14	4575.03	25.60	26.97	16742.57	65.21	-3.83	1.02	0.06	-0.39	3.84	-0.75	11.21	-1.98	26.52	-0.17
SB15	OC11a153	55.57	4158.09	32.33	18.29	13165.25	36.63	-2.52	1.27	-0.08	0.22	5.13	-0.54	9.45	0.92	53.17	0.02
SB15	OC11a154	75.11	5078.75	17.28	19.17	11879.59	51.38	-1.64	1.58	-0.10	1.31	3.98	-0.61	9.28	-0.84	65.79	0.46
SB15	OC11a155	74.25	2324.48	1.04	6.12	67.69	16.77	-2.39	0.95	0.02	-0.48	4.44	-0.62	3.53	-0.92	74.69	-0.15
SB15	OC11a156	69.24	1804.30	0.64	5.58	54.22	10.38	-2.50	0.90	0.04	0.21	3.74	-0.65	2.83	-1.08	61.82	0.02
SB15	OC11a157	60.93	2277.69	1.00	5.16	60.72	10.01	-1.78	1.12	-0.06	0.37	5.36	-0.53	2.42	-1.02	82.30	0.02
SB15	OC11a158	70.58	2042.26	0.77	5.69	59.37	13.87	1.63	1.14	0.05	0.13	3.20	-0.77	2.64	-0.89	63.87	0.02
SB15	OC11a159	69.33	2103.28	0.65	5.06	51.13	14.92	-2.58	1.01	0.08	0.43	6.85	-0.58	4.88	-0.90	70.76	-0.15
SB15	OC11a160	58.73	5075.82	1.85	10.46	34.59	18.65	-2.11	0.96	0.04	0.56	2.40	-0.55	2.14	-1.26	75.15	0.03
SB15	OC11a161	94.10	22766.42	4.95	11.59	21.52	13.25	-1.70	1.32	0.02	0.15	7.16	-0.59	2.44	-0.82	358.23	-0.15
SB15	OC11a162	84.59	3415.18	1.29	6.72	21.00	14.62	-1.46	0.64	0.11	-0.50	4.90	-0.66	4.60	-0.91	82.79	0.02
SB15	OC11a163	75.10	4599.87	2.78	8.50	76.00	38.09	2.83	3.45	-0.06	0.12	2.76	-0.41	3.67	-0.82	91.18	-0.11
SB15	OC11a164	64.55	4781.71	4.91	13.69	76.82	61.35	1.56	1.16	-0.14	0.42	4.93	-0.80	5.16	-0.64	65.65	0.07

Table A2.1: LA-ICPMS normalised analytical results for ablated sericite sites

Sample	Measurement	Ce_ppm	Eu_ppm	Gd_ppm	Yb_ppm	Lu_ppm	Hf_ppm	Ta_ppm	Au_ppm	Tl_ppm	Pb_ppm	Bi_ppm	Th_ppm	U_ppm
SB13	OC10a059	0.07	-0.06	-0.24	-0.32	-0.04	0.18	0.34	-0.12	0.71	0.36	-0.19	0.17	0.12
SB13	OC10a060	-0.10	-0.15	-0.29	-0.20	-0.05	-0.41	-0.10	-0.23	-0.47	1.56	-0.15	0.18	-0.14
SB13	OC10a061	0.18	-0.14	0.04	-0.31	0.01	-0.41	0.04	-0.13	0.41	0.73	-0.10	-0.14	0.12
SB13	OC10a062	0.04	-0.15	-0.63	-0.20	-0.05	-0.31	0.13	0.06	0.78	0.67	-0.27	0.21	0.12
SB13	OC10a063	0.01	-0.08	-0.40	-0.28	-0.08	-0.68	-0.20	-0.27	0.60	-0.33	-0.19	0.15	0.11
SB14a	OC10a108	0.02	-0.13	-0.42	-0.40	0.04	-0.41	0.19	-0.52	-0.97	0.58	-0.31	0.38	0.49
SB14a	OC10a109	0.48	0.04	-0.46	-0.28	0.03	-0.41	-0.24	-0.24	0.55	-0.28	-0.22	0.16	0.29
SB14a	OC10a110	0.05	-0.16	-0.27	0.25	-0.04	0.10	0.40	-0.49	-0.46	0.46	-0.27	0.14	0.33
SB14a	OC10a112	0.12	-0.12	-0.46	-0.55	-0.07	0.21	0.33	-0.84	-0.56	0.81	-0.25	-0.07	-0.23
SB14a	OC10a113	-0.15	-0.11	-0.95	-0.60	-0.09	0.05	0.22	-0.65	0.37	0.41	-0.29	-0.19	-0.19
SB14a	OC10a114	1.54	-0.15	0.37	0.21	0.01	-0.41	-0.21	-0.20	0.43	0.39	-0.33	0.10	0.16
SB14a	OC10a116	0.04	-0.07	-0.28	0.12	-0.14	-0.30	0.15	-0.19	0.71	0.65	-0.37	-0.06	0.21
SB14a	OC10a119	0.42	-0.29	0.50	-0.21	0.05	0.05	0.36	-0.20	0.58	0.59	-0.10	-0.07	0.22
SB14a	OC10a120	0.08	-0.13	-0.34	0.05	0.01	-0.37	0.21	-0.28	-0.64	-0.51	-0.25	0.08	-0.09
SB14b	OC11a028	0.03	-0.17	0.21	0.03	-0.05	-0.65	0.22	-0.34	0.66	0.94	-0.36	-0.07	0.10
SB14b	OC11a030	0.05	-0.13	-0.34	-0.34	-0.05	-0.75	0.05	-0.49	-0.70	0.83	-0.36	-0.12	-0.21
SB14b	OC11a033	-0.15	-0.12	-0.65	-0.27	-0.10	0.11	0.05	-0.33	-0.39	1.34	-0.35	-0.06	0.13
SB14b	OC11a034	-0.15	0.07	0.05	-0.43	-0.04	0.17	0.41	-0.21	-0.57	1.27	-0.28	0.03	0.07
SB14b	OC11a035	4497.36	62.26	141.90	3.38	0.34	1.81	-0.20	-0.36	-0.51	1.54	-0.30	400.74	166.97
SB14b	OC11a036	0.05	-0.14	-0.27	0.07	-0.06	-0.41	0.23	-0.23	-0.46	0.83	-0.23	0.06	0.32
SB14b	OC11a037	0.08	-0.15	0.19	-0.41	0.01	0.10	0.10	-0.26	-0.45	0.86	-0.18	-0.06	-0.17
SB14b	OC11a038	0.02	0.04	-0.36	0.19	-0.04	-0.41	0.14	-0.39	0.31	0.30	-0.28	-0.10	0.08
SB14b	OC11a039	0.03	-0.07	0.10	-0.19	-0.09	0.10	0.15	-0.29	0.52	1.00	-0.31	0.13	0.13
SB14b	OC11a040	0.02	-0.14	-0.63	-0.19	-0.07	0.25	0.10	-0.17	-0.46	1.02	0.22	-0.12	0.18
SB14b	OC11a041	0.03	0.07	-0.29	0.05	-0.05	-0.32	-0.23	-0.13	0.68	0.61	-0.28	0.10	-0.13
SB14b	OC11a042	-0.15	-0.07	-0.61	-0.39	-0.04	0.11	0.21	-0.28	-0.60	0.72	-0.19	0.06	-0.10
SB15	OC11a152	-0.15	0.04	0.56	-0.33	-0.12	-0.72	0.37	-0.23	0.84	1.55	-0.22	0.10	-0.31
SB15	OC11a153	0.04	0.04	-0.40	-0.33	-0.13	0.23	0.44	-0.37	-0.47	1.99	-0.33	-0.15	0.11
SB15	OC11a154	0.94	-0.19	-0.26	-0.18	-0.04	-0.57	-0.26	-0.41	-0.44	1.14	-0.31	0.65	0.19
SB15	OC11a155	-0.11	0.03	-0.64	0.10	-0.05	-0.32	0.35	-0.42	0.56	-0.39	-0.37	0.11	-0.13
SB15	OC11a156	0.02	0.04	0.11	-0.29	-0.07	-0.41	0.24	-0.20	0.48	-0.46	-0.24	0.17	0.28
SB15	OC11a157	0.07	-0.15	-0.40	-0.20	-0.05	-0.41	0.37	-0.31	-0.53	0.41	-0.20	-0.15	0.37
SB15	OC11a158	0.03	-0.24	0.21	-0.50	-0.14	0.22	0.25	0.20	-0.55	-0.34	-0.21	0.08	0.28
SB15	OC11a159	-0.11	-0.23	-0.30	-0.46	-0.07	-0.33	1.58	-0.29	0.40	-0.37	-0.21	0.13	0.33
SB15	OC11a160	-0.15	0.05	-0.29	0.03	0.02	-0.41	0.26	0.08	0.70	-0.47	-0.22	0.12	0.29
SB15	OC11a161	-0.21	-0.08	-0.40	-0.49	-0.10	0.10	0.73	-0.34	0.77	-0.20	-0.19	-0.09	0.18
SB15	OC11a162	-0.15	0.09	-0.66	-0.50	-0.07	-0.33	0.49	-0.38	0.53	0.36	-0.34	-0.15	0.15
SB15	OC11a163	-0.21	0.03	-0.41	-0.31	0.02	-0.33	0.26	-0.46	0.61	0.65	-0.26	-0.12	0.24
SB15	OC11a164	0.03	-0.08	0.05	-0.38	-0.09	-0.32	0.64	-0.14	-0.36	-0.31	-0.19	-0.07	-0.10

Table A2.1: LA-ICPMS normalised analytical results for ablated sericite sites

Sample	Measurement	Host Rock	Alteration	Sulfides	Mineral	Li_ppm	B_ppm	Na_ppm	Mg_ppm	Al_ppm	Si_ppm	K_ppm	Ca_ppm	Ti_ppm	V_ppm	Cr_ppm
SB15	OC11a165	IRDP	WS	Cpy-HS	Sericite	4.46	5.66	2255.36	11186.21	180421.89	227459.54	85372.73	-1289.98	1167.05	334.43	10.13
SB15	OC11a166	IRDP	WS	Cpy-HS	Sericite	5.78	7.71	2124.77	10245.17	184266.49	223634.53	84392.86	-1327.07	2006.44	328.03	9.98
SB15	OC11a167	IRDP	WS	Cpy-HS	Sericite	3.79	4.90	1974.97	10060.52	183983.82	223418.37	86259.43	-1186.24	2344.94	538.84	22.56
SB15	OC11a168	IRDP	WS	Cpy-HS	Sericite	4.23	11.46	1955.44	10613.93	183965.53	223215.41	88248.14	-1613.71	1349.35	417.12	10.20
SB15	OC11a169	IRDP	WS	Cpy-HS	Sericite	4.03	7.38	2059.89	10808.54	185319.32	222318.37	87155.05	-1530.14	1312.24	271.99	-6.90
SB15	OC11a170	IRDP	WS	Cpy-HS	Sericite	6.62	5.52	2182.72	11503.95	184519.54	221365.13	87117.76	-1284.32	1310.99	198.69	-7.47
SB15	OC11a171	IRDP	WS	Cpy-HS	Sericite	9.12	7.03	2034.74	16088.99	178874.88	224570.52	83492.72	-1535.38	1156.92	232.43	-7.75
SB15	OC11a172	IRDP	WS	Cpy-HS	Sericite	13.49	12.11	1950.73	13138.55	187913.32	224797.45	74452.84	-1160.66	973.73	315.46	7.12
SB15	OC11a173	IRDP	WS	Cpy-HS	Sericite	12.12	7.19	1709.39	16835.99	179618.03	228397.37	75862.87	-1490.66	908.23	248.35	-7.01
SB15	OC11a175	IRDP	WS	Cpy-HS	Sericite	5.04	5.17	11612.95	8150.51	171782.09	236457.39	72825.21	-1734.02	1574.03	246.00	17.02
SB16	OC10a230	IRDP	GS-WS	Py	Sericite	4.15	-5.38	4840.73	5684.45	189306.53	222224.32	83141.49	-1447.09	1156.69	216.96	-6.56
SB16	OC10a232	IRDP	GS-WS	Py	Sericite	4.30	-7.84	5262.68	4648.46	193141.72	216656.70	85378.52	-1120.33	1635.64	318.36	-7.01
SB16	OC10a233	IRDP	GS-WS	Py	Sericite	12.59	-22.78	2336.63	2347.86	96786.46	335831.79	37903.21	-7031.23	722.45	99.40	-22.39
SB16	OC10a234	IRDP	GS-WS	Py	Sericite	5.17	3.91	4638.76	4960.17	193235.02	217439.13	85365.92	-1647.74	1317.46	245.48	-5.22
SB16	OC10a235	IRDP	GS-WS	Py	Sericite	4.32	-5.81	5480.38	4412.63	197521.08	214390.94	83787.73	-1696.41	1340.53	205.15	-5.97
SB16	OC10a236	IRDP	GS-WS	Py	Sericite	4.15	-7.13	7021.46	4539.49	191509.96	218897.69	83852.23	-1665.26	1232.28	136.30	6.68
SB16	OC10a237	IRDP	GS-WS	Py	Sericite	3.28	-6.33	5440.15	4310.70	194264.08	217941.19	83568.53	-1719.01	1212.22	161.90	-6.06
SB16	OC10a238	IRDP	GS-WS	Py	Sericite	5.52	-7.35	5876.82	4544.39	192837.27	217037.36	85189.84	-1637.98	1403.88	181.48	-5.43
SB16	OC10a239	IRDP	GS-WS	Py	Sericite	4.27	3.69	6523.35	4483.69	193231.92	216573.58	84160.82	-1391.05	1582.55	268.63	13.09
SB16	OC10a240	IRDP	GS-WS	Py	Sericite	6.01	-7.95	5255.58	4593.26	191000.36	218398.58	84436.73	-1638.10	2122.38	246.44	7.73
SB16	OC10a241	IRDP	GS-WS	Py	Sericite	5.26	3.65	5540.65	5287.95	190403.80	217403.07	86270.87	-1415.03	1941.85	230.38	8.76
SB16	OC10a242	IRDP	GS-WS	Py	Sericite	3.99	-5.79	4103.77	5519.92	185385.38	228405.99	80203.75	-1600.88	935.33	193.05	-4.50
SB16	OC10a243	IRDP	GS-WS	Py	Sericite	4.18	-7.91	4607.77	5349.89	197259.55	215606.18	83780.69	-1794.15	900.42	178.29	-4.48
SB16	OC10a244	IRDP	GS-WS	Py	Sericite	3.36	5.47	3957.72	4963.91	179242.95	238598.85	75629.46	-1607.66	413.17	91.48	-5.56
SB16	OC10a245	IRDP	GS-WS	Py	Sericite	2.29	-5.83	5068.24	5122.79	194759.15	219917.57	82453.49	-1848.49	439.27	74.57	-7.36
SB16	OC10a246	IRDP	GS-WS	Py	Sericite	2.35	6.01	4465.67	5070.32	191674.20	221605.30	84367.98	-1305.86	490.42	89.99	-6.63
SB16	OC10a247	IRDP	GS-WS	Py	Sericite	4.25	-5.26	5229.92	4401.01	193343.20	217457.58	85157.93	-1293.68	1273.26	320.06	-6.21
SB16	OC10a248	IRDP	GS-WS	Py	Sericite	1.45	-6.14	5635.76	4125.13	193312.20	218620.13	83241.03	-1730.36	1380.01	191.57	-6.06
SB16	OC10a249	IRDP	GS-WS	Py	Sericite	4.48	-6.05	5037.45	4515.86	194411.09	216646.24	85534.99	-1296.53	970.45	254.62	-6.21
SB16	OC10a250	IRDP	GS-WS	Py	Sericite	3.25	-6.32	5174.43	4524.54	192127.01	218744.44	84891.57	-1729.63	1148.23	318.04	-6.13
SB17	OC10a147	IGR	GS	Py-Cpy	Sericite	14.41	21.70	2451.69	15420.57	167790.91	227113.83	82255.79	-1945.63	186.93	33.47	-5.97
SB17	OC10a148	IGR	GS	Py-Cpy	Sericite	17.85	15.85	2542.93	20696.53	163977.89	222875.14	82625.35	-1340.33	501.36	59.08	-8.42
SB17	OC10a149	IGR	GS	Py-Cpy	Sericite	31.36	30.72	2683.52	18727.75	168022.76	221648.53	80597.23	-1965.62	7.66	3.73	-6.80
SB17	OC10a150	IGR	GS	Py-Cpy	Sericite	3.49	-8.65	4614.18	3487.40	181765.55	212511.20	90651.73	-1785.88	2692.49	476.14	-7.77
SB17	OC10a151	IGR	GS	Py-Cpy	Sericite	3.42	-8.24	4085.42	3739.50	149094.29	249875.87	82498.39	-2200.62	1375.68	341.80	-4.93
SB17	OC10a152	IGR	GS	Py-Cpy	Sericite	28.07	21.09	2390.10	26649.21	166289.09	217301.64	82328.70	-1404.56	16.78	12.37	-6.91
SB17	OC10a153	IGR	GS	Py-Cpy	Sericite	4.85	-6.72	4088.94	6391.04	176882.52	215945.58	87246.52	-1147.18	396.67	148.46	-6.78
SB17	OC10a154	IGR	GS	Py-Cpy	Sericite	4.45	-7.62	3490.03	6085.05	152811.96	248045.47	73685.16	-1652.96	264.65	87.00	-6.22
SB17	OC10a155	IGR	GS	Py-Cpy	Sericite	2.67	-6.40	3833.94	4979.50	166695.72	233605.16	79154.78	-1877.45	1261.16	124.16	-8.50

Table A2.1: LA-ICPMS normalised analytical results for ablated sericite sites

Sample	Measurement	Mn_ppm	Fe_ppm	Co_ppm	Ni_ppm	Cu_ppm	Zn_ppm	As_ppm	Sr_ppm	Y_ppm	Zr_ppm	Nb_ppm	Ag_ppm	Sn_ppm	Sb_ppm	Ba_ppm	La_ppm
SB15	OC11a165	78.89	2328.12	1.31	4.70	27.70	18.89	-1.57	0.90	-0.06	0.25	3.44	-0.66	2.42	-1.44	62.56	-0.11
SB15	OC11a166	72.00	3031.51	3.05	9.03	31.97	37.30	-1.64	1.66	0.58	0.13	6.24	-0.60	4.56	-0.92	71.40	-0.21
SB15	OC11a167	68.04	1531.84	0.78	4.58	45.58	14.92	-1.69	3.11	0.16	0.47	4.83	-0.68	2.24	-1.06	54.88	-0.15
SB15	OC11a168	56.92	2001.81	0.55	14.94	163.92	13.14	-2.95	0.92	0.07	0.42	2.71	-0.67	4.38	-0.79	52.84	0.05
SB15	OC11a169	55.16	2405.54	1.05	10.55	88.99	14.72	-1.71	0.87	0.26	0.04	2.72	-0.41	6.24	-1.15	40.67	-0.20
SB15	OC11a170	62.80	4053.71	0.84	9.46	103.46	16.25	-3.11	2.19	0.06	-0.47	4.44	-0.79	8.51	-0.97	54.73	-0.10
SB15	OC11a171	87.22	4780.20	1.11	9.90	197.56	19.55	-1.95	1.01	0.03	0.40	5.23	0.25	9.16	-0.88	56.51	-0.15
SB15	OC11a172	70.85	4044.69	2.62	11.38	126.28	36.39	-2.32	2.31	-0.11	0.20	3.47	-0.65	6.27	-0.78	38.66	0.05
SB15	OC11a173	94.39	4516.57	2.34	12.18	121.18	38.69	-2.27	2.11	0.13	-0.46	4.10	-0.41	6.88	-0.93	40.86	0.10
SB15	OC11a175	39.41	3865.46	3.20	7.12	991.70	18.50	-1.13	21.20	0.07	0.27	5.59	-0.57	10.64	-1.29	70.98	0.19
SB16	OC10a230	6.36	3974.34	-0.27	0.61	5.47	2.22	-1.94	5.51	-0.11	1.25	5.00	-0.48	16.92	-0.70	700.07	0.03
SB16	OC10a232	5.29	4746.96	0.24	1.52	5.48	3.22	-3.37	9.76	0.01	0.82	6.61	-0.49	18.65	-0.66	1037.02	-0.09
SB16	OC10a233	7.92	2054.37	-0.67	-3.31	4.12	-9.81	-9.68	4.20	0.05	1.78	3.63	-2.48	5.90	-2.57	432.96	-0.41
SB16	OC10a234	7.89	4326.84	-0.36	0.82	7.10	-2.01	-2.48	11.18	0.09	2.91	6.75	-0.67	17.40	-0.86	1163.73	0.05
SB16	OC10a235	6.84	4589.84	0.46	4.51	27.98	3.35	-1.62	10.63	0.03	0.94	6.12	-0.61	13.63	-0.90	954.44	-0.15
SB16	OC10a236	5.95	4140.11	-0.48	3.60	17.62	3.69	-1.97	12.86	0.03	2.17	7.56	-0.66	16.99	-1.14	1328.16	-0.15
SB16	OC10a237	6.84	4073.56	0.19	-0.58	3.26	-3.06	-1.23	11.26	-0.11	3.04	6.48	-0.75	15.49	-0.56	1228.10	-0.22
SB16	OC10a238	6.22	4755.18	1.03	4.27	35.84	9.02	-1.57	11.00	0.01	2.28	6.30	-0.36	16.90	-1.09	1198.91	0.08
SB16	OC10a239	6.15	4826.53	-0.35	0.83	5.62	2.97	-2.17	9.29	0.05	2.08	6.30	-0.51	16.60	-0.79	1062.05	-0.15
SB16	OC10a240	9.28	4880.25	0.73	7.00	37.15	7.59	1.16	16.44	-0.11	1.90	4.67	-0.54	14.79	-0.82	760.23	0.16
SB16	OC10a241	6.78	5109.39	-0.27	4.10	8.17	-2.57	-1.83	13.51	0.01	2.09	3.13	-0.73	11.82	-0.57	679.04	-0.15
SB16	OC10a242	9.15	4105.10	0.66	2.63	25.01	3.83	-1.78	4.07	-0.08	0.61	4.88	-0.62	14.77	-0.71	373.01	-0.23
SB16	OC10a243	11.96	4254.44	0.57	1.96	12.34	4.93	-3.28	6.41	0.03	0.48	5.15	-0.55	11.53	-0.66	527.84	0.06
SB16	OC10a244	7.37	2964.08	-0.32	-1.30	11.73	-3.11	-2.02	3.82	-0.12	0.55	3.51	-0.79	7.64	-0.91	395.21	-0.15
SB16	OC10a245	5.38	3363.67	-0.27	0.99	19.30	-3.20	-1.72	3.71	-0.09	0.81	4.37	-0.53	5.75	-0.73	419.22	-0.10
SB16	OC10a246	7.84	3690.67	0.37	1.05	13.28	3.82	-2.51	5.28	0.01	1.12	4.65	-0.80	7.40	-0.97	487.21	0.02
SB16	OC10a247	7.02	4656.82	-0.28	0.84	9.31	2.82	-1.21	11.77	-0.05	0.64	5.87	-0.59	17.98	-0.83	992.00	0.03
SB16	OC10a248	7.57	4244.93	-0.25	0.57	2.10	-2.18	-3.09	11.00	0.04	2.23	6.89	-0.41	16.68	-1.02	1274.10	-0.19
SB16	OC10a249	4.85	4815.30	-0.42	-0.79	8.47	3.20	-2.35	17.27	0.04	1.49	4.99	-0.38	20.73	-0.93	1212.63	-0.15
SB16	OC10a250	6.40	4760.45	-0.27	1.79	7.00	1.76	-1.23	10.79	-0.06	1.12	5.15	-0.68	16.58	-0.81	943.81	-0.15
SB17	OC10a147	213.77	19370.94	1.48	5.36	110.28	20.21	-2.04	5.51	0.11	-0.39	0.05	-0.53	0.41	-0.72	140.35	0.06
SB17	OC10a148	309.12	23255.74	1.38	6.62	87.29	26.42	2.47	9.49	1.57	0.10	0.14	-0.50	0.72	-0.75	382.98	-0.19
SB17	OC10a149	352.01	24883.29	5.09	6.71	124.68	22.01	-2.26	5.29	-0.09	-0.21	0.02	-0.62	0.36	-0.78	116.15	-0.13
SB17	OC10a150	6.76	21263.88	0.35	2.74	11.56	-3.31	-2.73	20.66	0.38	0.93	5.93	-0.78	25.82	0.51	703.62	0.17
SB17	OC10a151	9.44	18704.79	-0.32	1.25	2.02	1.82	-1.88	29.76	0.72	0.41	2.35	-0.78	12.64	-0.80	643.91	0.30
SB17	OC10a152	307.46	23406.85	3.72	10.80	68.14	37.15	-2.25	2.80	-0.12	0.10	0.05	-0.71	0.50	0.68	104.49	0.11
SB17	OC10a153	13.45	27838.14	0.49	2.88	6.54	-2.55	-2.32	2.67	0.01	0.33	2.79	-0.50	10.05	-0.59	1071.34	0.03
SB17	OC10a154	12.36	24670.66	-0.36	2.28	4.24	3.37	-4.04	2.27	-0.19	0.09	1.06	-0.79	5.32	-0.96	667.53	0.02
SB17	OC10a155	8.23	21498.17	0.34	1.09	3.37	-2.99	-1.87	2.44	0.06	0.43	3.49	-0.64	13.76	-0.76	1224.57	-0.15

Table A2.1: LA-ICPMS normalised analytical results for ablated sericite sites

Sample	Measurement	Ce_ppm	Eu_ppm	Gd_ppm	Yb_ppm	Lu_ppm	Hf_ppm	Ta_ppm	Au_ppm	Tl_ppm	Pb_ppm	Bi_ppm	Th_ppm	U_ppm
SB15	OC11a165	-0.11	-0.18	-0.30	-0.61	-0.05	0.05	0.20	-0.43	0.53	0.26	-0.26	-0.10	0.22
SB15	OC11a166	0.35	-0.16	0.10	-0.29	-0.12	0.05	0.63	-0.14	-0.43	-0.31	-0.23	0.06	0.30
SB15	OC11a167	0.13	-0.16	-0.30	0.07	0.03	-0.73	0.56	-0.21	0.59	0.43	0.12	-0.17	0.42
SB15	OC11a168	0.14	-0.08	0.15	0.14	-0.05	-0.65	0.10	0.18	0.51	0.67	-0.14	-0.15	0.41
SB15	OC11a169	0.29	0.02	-0.53	-0.19	0.01	0.16	0.18	-0.30	0.53	-0.30	-0.15	0.08	0.24
SB15	OC11a170	0.10	0.02	-0.28	-0.40	-0.12	-0.31	0.31	-0.41	-0.46	-0.34	-0.23	-0.14	0.15
SB15	OC11a171	0.07	-0.17	-0.29	0.10	-0.10	-0.45	0.33	0.18	0.59	-0.29	-0.27	-0.07	0.15
SB15	OC11a172	-0.20	-0.07	-0.27	0.07	-0.04	0.10	0.29	-0.44	0.56	-0.36	-0.18	-0.09	0.09
SB15	OC11a173	0.10	-0.07	-0.39	-0.19	-0.04	0.10	0.16	-0.14	0.78	-0.39	-0.22	0.10	0.10
SB15	OC11a175	0.54	0.09	-0.68	-0.43	-0.05	-0.34	0.35	-0.21	-0.55	0.86	0.10	-0.17	0.12
SB16	OC10a230	-0.15	-0.07	-0.37	0.03	-0.04	0.15	0.49	-0.23	-0.47	-0.30	-0.18	-0.06	0.02
SB16	OC10a232	-0.09	0.08	-0.51	0.13	0.02	-0.28	0.37	-0.32	-0.45	-0.34	-0.23	-0.06	-0.07
SB16	OC10a233	0.07	-0.66	-2.26	-0.31	0.03	-0.41	-0.88	-1.80	-1.36	-0.78	-0.39	-0.42	-0.50
SB16	OC10a234	-0.09	-0.22	-0.37	0.10	-0.07	0.15	0.81	-0.43	-0.46	0.44	-0.22	-0.13	-0.07
SB16	OC10a235	0.07	0.06	0.10	-0.36	-0.10	0.15	0.51	-0.19	-0.40	1.85	-0.16	-0.14	-0.05
SB16	OC10a236	0.02	-0.14	-0.27	0.03	-0.07	0.15	1.03	-0.36	0.49	0.75	-0.22	0.04	0.04
SB16	OC10a237	-0.15	-0.07	-0.55	-0.54	-0.10	0.11	0.51	-0.20	-0.43	0.53	-0.14	-0.15	0.04
SB16	OC10a238	-0.09	-0.16	-0.59	-0.19	-0.07	-0.29	1.05	-0.28	-0.52	0.58	-0.21	-0.08	-0.12
SB16	OC10a239	-0.10	0.02	0.05	-0.19	-0.08	0.21	0.80	-0.34	-0.39	0.54	-0.17	-0.12	-0.09
SB16	OC10a240	0.32	-0.14	-0.27	-0.31	-0.04	0.10	0.40	-0.34	0.63	0.35	-0.22	-0.12	0.04
SB16	OC10a241	-0.13	-0.12	-0.54	-0.19	-0.09	0.46	0.19	-0.43	-0.57	0.74	-0.17	-0.10	-0.12
SB16	OC10a242	0.02	0.04	-0.63	-0.20	-0.06	-0.41	0.43	-0.38	0.45	-0.33	-0.12	-0.09	-0.06
SB16	OC10a243	-0.10	-0.08	-0.29	-0.28	-0.10	-0.41	0.38	-0.33	-0.58	-0.36	-0.21	-0.06	0.06
SB16	OC10a244	-0.11	-0.13	0.32	-0.36	-0.10	-0.33	0.22	-0.27	-0.42	0.29	-0.25	0.08	0.04
SB16	OC10a245	0.02	-0.18	-0.46	-0.43	-0.09	-0.41	0.18	0.09	0.42	-0.50	-0.37	-0.14	-0.09
SB16	OC10a246	0.02	-0.14	-0.27	-0.27	0.04	0.10	0.24	-0.32	-0.60	-0.38	-0.21	-0.13	-0.05
SB16	OC10a247	-0.10	-0.14	-0.60	-0.19	-0.09	-0.41	0.20	-0.20	-0.38	-0.37	-0.22	0.05	-0.12
SB16	OC10a248	-0.15	0.05	-0.79	0.13	-0.13	0.30	1.18	-0.19	-0.60	-0.31	-0.14	0.04	-0.13
SB16	OC10a249	0.03	-0.12	-0.37	-0.38	-0.04	0.31	0.19	-0.34	0.47	0.59	-0.17	-0.06	0.03
SB16	OC10a250	-0.20	-0.10	-0.46	-0.56	-0.10	-0.41	0.50	-0.72	0.38	-0.63	-0.15	0.03	-0.10
SB17	OC10a147	0.14	-0.10	-0.26	-0.31	-0.04	-0.28	0.05	-0.40	0.81	18.86	-0.18	-0.17	-0.07
SB17	OC10a148	0.18	-0.10	-0.44	0.25	0.05	-0.28	-0.18	-0.22	0.62	9.40	-0.19	-0.12	0.07
SB17	OC10a149	0.33	-0.07	-0.36	-0.36	-0.04	0.04	-0.20	0.13	0.93	15.12	-0.27	0.03	0.08
SB17	OC10a150	0.09	0.18	-0.71	-0.31	-0.14	-0.35	0.33	-0.39	0.70	1.44	-0.23	0.12	-0.15
SB17	OC10a151	0.38	0.09	0.08	-0.60	0.03	-0.64	0.15	-0.36	0.35	1.53	-0.14	-0.20	-0.10
SB17	OC10a152	-0.21	-0.13	-0.60	-0.19	-0.08	-0.41	-0.22	0.14	0.70	8.74	-0.26	-0.08	-0.22
SB17	OC10a153	-0.15	0.03	-0.46	0.14	-0.04	0.13	0.18	-0.27	-0.50	-0.37	-0.18	-0.05	0.05
SB17	OC10a154	0.32	-0.11	-0.90	-0.62	-0.05	0.06	0.13	-0.16	0.34	0.42	-0.29	0.06	-0.13
SB17	OC10a155	0.12	0.03	-0.55	-0.19	-0.13	-0.30	0.39	-0.19	0.43	-0.23	-0.21	-0.16	0.08

Table A2.1: LA-ICPMS normalised analytical results for ablated sericite sites

Sample	Measurement	Host Rock	Alteration	Sulfides	Mineral	Li_ppm	B_ppm	Na_ppm	Mg_ppm	Al_ppm	Si_ppm	K_ppm	Ca_ppm	Ti_ppm	V_ppm	Cr_ppm
SB17	OC10a156	IGR	GS	Py-Cpy	Sericite	4.73	-6.00	4547.91	4668.60	180168.05	210505.50	86171.52	1766.04	3872.95	512.14	3.83
SB17	OC10a157	IGR	GS	Py-Cpy	Sericite	9.15	4.04	3644.53	9672.67	175206.41	214033.22	86035.14	2833.12	953.13	176.37	-5.85
SB17	OC10a159	IGR	GS	Py-Cpy	Sericite	6.77	-7.02	3559.18	8281.02	175116.76	210974.97	89002.34	-1630.41	2088.42	614.08	-5.48
SB18	OC10a180	IGR	WS	Py-Cpy	Sericite	6.99	4.97	2068.46	4517.50	128092.01	294347.39	56857.85	-2648.14	543.86	101.72	-6.19
SB18	OC10a181	IGR	WS	Py-Cpy	Sericite	5.78	-9.24	2263.66	7423.99	160670.42	249446.20	76932.48	-1861.75	1040.60	165.55	-6.32
SB18	OC10a182	IGR	WS	Py-Cpy	Sericite	3.86	-9.61	2184.28	2000.76	149649.08	273467.71	66643.93	-2460.27	332.46	99.82	-6.30
SB18	OC10a183	IGR	WS	Py-Cpy	Sericite	5.19	-7.39	2602.44	5637.44	169519.32	243068.86	79689.17	-1908.75	581.90	105.74	-5.43
SB18	OC10a184	IGR	WS	Py-Cpy	Sericite	2.69	-8.66	2462.99	2418.73	154311.72	269438.47	66194.84	-1756.00	306.72	59.68	-8.32
SB18	OC10a185	IGR	WS	Py-Cpy	Sericite	7.28	8.96	3840.46	5451.93	187648.48	213837.45	92101.26	-1527.39	1938.40	277.65	5.57
SB18	OC10a186	IGR	WS	Py-Cpy	Sericite	7.52	7.21	2721.08	5285.68	187223.72	215749.58	91740.36	-1315.29	1912.35	245.96	-6.31
SB18	OC10a187	IGR	WS	Py-Cpy	Sericite	6.63	4.42	3434.91	5403.52	187805.21	214356.82	91514.37	-1622.05	2047.87	292.91	7.53
SB18	OC10a188	IGR	WS	Py-Cpy	Sericite	8.79	5.01	2712.00	7742.65	186120.31	216929.53	90678.16	-1558.23	1285.43	185.41	-5.76
SB18	OC10a189	IGR	WS	Py-Cpy	Sericite	9.49	6.42	8623.99	7724.01	183705.43	211718.98	90661.61	-1125.35	2447.33	314.54	9.34
SB18	OC10a190	IGR	WS	Py-Cpy	Sericite	8.22	5.75	2558.23	14212.45	172504.27	214442.75	87970.26	-1653.09	8319.29	324.83	32.22
SB18	OC10a191	IGR	WS	Py-Cpy	Sericite	8.67	8.51	5595.42	5004.46	188337.06	215023.13	91377.95	-1904.48	818.31	193.84	-5.81
SB18	OC10a192	IGR	WS	Py-Cpy	Sericite	7.91	6.59	8025.17	4570.96	191115.79	214207.63	89521.85	-1777.25	702.07	149.95	-4.99
SB18	OC10a193	IGR	WS	Py-Cpy	Sericite	5.27	-10.55	1598.09	4554.28	117185.05	306483.31	53024.71	-2436.58	458.13	63.53	-9.69
SB18	OC10a194	IGR	WS	Py-Cpy	Sericite	7.90	9.18	2771.77	6943.58	188810.69	215275.51	89658.53	-1321.76	1281.57	193.77	8.51
SB18	OC10a195	IGR	WS	Py-Cpy	Sericite	11.09	10.33	2581.96	11396.87	182560.97	214450.18	91050.24	-1185.19	1151.15	139.12	-4.63
SB18	OC10a196	IGR	WS	Py-Cpy	Sericite	7.52	9.73	2636.49	7353.65	183380.97	218148.32	91684.59	-1423.80	1695.55	231.99	9.40
SB18	OC10a197	IGR	WS	Py-Cpy	Sericite	5.77	4.60	2396.53	5294.16	179418.05	199981.88	83666.90	46943.43	1003.95	139.64	7.20
SB18	OC10a198	IGR	WS	Py-Cpy	Sericite	5.13	-7.99	2370.89	6131.93	184560.43	223387.39	86614.25	-2081.07	916.37	170.47	-7.77
SB19	OC10a065	IGR	GS	HS	Sericite	2.40	-6.96	4237.54	2600.36	198687.80	211099.41	88105.80	-2015.52	1861.35	99.75	17.67
SB19	OC10a066	IGR	GS	HS	Sericite	2.80	-7.44	3888.78	4949.57	190190.61	213759.88	89026.65	-1489.56	2504.37	185.35	21.29
SB19	OC10a067	IGR	GS	HS	Sericite	2.28	-8.16	3678.08	4852.42	187340.54	213323.86	89163.15	-1138.73	2898.20	304.99	8.09
SB19	OC10a068	IGR	GS	HS	Sericite	3.44	-7.18	4063.65	3252.79	191987.09	215433.21	85633.73	-1609.23	2210.41	142.98	7.83
SB19	OC10a069	IGR	GS	HS	Sericite	4.60	3.86	3672.28	4432.67	190024.02	213263.11	88539.85	-1373.16	1822.62	288.19	-6.18
SB19	OC10a070	IGR	GS	HS	Sericite	2.36	-6.45	3733.96	4738.95	191841.34	213903.30	86212.72	-1432.80	2472.40	203.22	19.99
SB19	OC10a071	IGR	GS	HS	Sericite	1.96	-6.40	4847.43	3148.28	192350.05	213114.89	86975.59	-1388.00	2837.12	171.03	-6.24
SB19	OC10a072	IGR	GS	HS	Sericite	2.95	-9.20	3561.81	5526.59	186624.40	216920.40	86708.56	-1764.92	2666.62	231.69	-5.66
SB19	OC10a073	IGR	GS	HS	Sericite	2.91	-8.52	4173.34	2922.87	180143.10	229085.75	80872.26	-1841.84	2107.76	122.30	-6.36
SB19	OC10a074	IGR	GS	HS	Sericite	8.16	-8.03	3726.58	3539.41	186061.08	226997.44	80071.79	-1628.38	770.43	132.58	-5.53
SB19	OC10a075	IGR	GS	HS	Sericite	2.06	-7.83	4768.22	2554.97	197912.15	209719.70	86558.94	-1245.12	2738.12	127.39	14.07
SB19	OC10a076	IGR	GS	HS	Sericite	2.65	-5.81	4187.24	2828.96	192205.26	215604.79	85930.66	-1378.97	2604.92	227.38	24.46
SB19	OC10a083	IGR	GS	HS	Sericite	1.51	-6.90	5655.94	2768.37	193336.70	213728.93	87904.15	-1413.68	1126.79	104.49	8.70
SB19	OC10a084	IGR	GS	HS	Sericite	5.27	-6.19	3799.71	4116.59	194024.38	211134.91	89107.24	-1559.11	1941.99	224.33	-6.06
SB19	OC10a085	IGR	GS	HS	Sericite	3.78	-7.01	4090.35	3093.99	194840.39	213077.29	89269.95	-1897.50	1886.85	174.73	6.08
SB19	OC10a086	IGR	GS	HS	Sericite	3.31	-7.01	4002.32	3830.85	193131.70	212808.74	87647.52	-1492.52	1943.48	244.81	-7.41
SB19	OC10a087	IGR	GS	HS	Sericite	4.39	-8.12	3802.57	4537.57	191744.80	212483.98	89454.73	-1729.61	2234.48	247.79	4.53

Table A2.1: LA-ICPMS normalised analytical results for ablated sericite sites

Sample	Measurement	Mn_ppm	Fe_ppm	Co_ppm	Ni_ppm	Cu_ppm	Zn_ppm	As_ppm	Sr_ppm	Y_ppm	Zr_ppm	Nb_ppm	Ag_ppm	Sn_ppm	Sb_ppm	Ba_ppm	La_ppm
SB17	OC10a156	12.23	24263.88	0.69	2.94	4.88	4.22	-1.59	18.13	0.75	1.15	7.36	-0.65	27.62	-0.66	512.28	0.31
SB17	OC10a157	47.72	26902.64	0.53	5.27	3.09	6.21	0.45	14.73	1.09	0.26	1.57	-0.50	6.51	-0.77	450.15	0.78
SB17	OC10a159	31.10	30160.85	-0.40	5.33	3.52	2.44	-1.53	1.99	-0.05	0.37	0.44	-0.61	6.79	-0.95	849.40	0.01
SB18	OC10a180	4.49	5083.89	0.38	-1.66	8.73	-4.96	-4.62	0.41	-0.08	-0.39	1.58	-1.08	18.80	-1.53	162.59	-0.15
SB18	OC10a181	8.06	7562.38	-0.38	0.61	6.97	-3.66	-2.76	0.48	-0.06	0.37	1.77	-0.82	21.16	-0.97	160.23	-0.11
SB18	OC10a182	-4.01	2996.14	0.47	-0.83	11.31	-3.11	1.91	0.45	-0.11	0.32	1.14	-0.98	32.59	-1.47	96.67	0.09
SB18	OC10a183	6.26	5979.11	0.31	0.50	3.64	2.20	1.19	0.25	0.03	0.24	1.68	-0.53	38.00	-1.02	109.10	-0.11
SB18	OC10a184	6.95	2552.72	0.42	-1.00	92.85	-2.78	-3.03	0.41	0.10	0.12	0.54	-0.65	7.78	-0.99	84.05	0.02
SB18	OC10a185	8.43	10581.81	2.07	-0.73	30.44	5.44	-1.92	4.54	0.08	0.44	3.44	-0.54	13.89	-0.86	482.31	0.02
SB18	OC10a186	9.78	9985.96	1.77	0.48	37.17	3.50	-2.01	5.79	-0.11	0.57	3.17	-0.46	14.14	-0.60	502.65	0.02
SB18	OC10a187	8.32	10199.99	2.02	0.81	38.71	3.95	-2.56	4.92	0.08	0.40	3.05	-0.65	14.23	-1.06	487.60	-0.09
SB18	OC10a188	10.92	9422.64	1.55	-1.06	25.13	3.52	-2.52	2.42	-0.11	0.62	2.74	-0.66	9.83	-0.81	291.92	-0.18
SB18	OC10a189	17.44	11968.14	2.45	-0.89	34.17	3.99	1.08	2.02	0.04	0.43	2.22	-0.47	12.60	-0.58	286.64	-0.15
SB18	OC10a190	16.17	9494.04	1.42	1.96	23.83	4.11	1.84	1.17	0.07	0.77	21.58	-0.56	9.73	-1.09	109.64	-0.10
SB18	OC10a191	9.77	10356.62	1.56	0.58	22.70	2.07	-1.96	3.35	0.19	0.59	2.46	-0.63	16.34	-0.71	242.11	-0.13
SB18	OC10a192	11.60	8032.43	1.45	0.93	26.41	2.28	-1.32	2.14	0.15	0.34	2.22	-0.54	18.63	-0.81	208.46	-0.09
SB18	OC10a193	4.49	5280.70	0.37	0.73	3.45	-4.43	-3.78	2.72	0.83	-0.36	1.31	-1.16	9.68	-1.28	154.14	-0.22
SB18	OC10a194	9.52	10062.62	1.36	0.38	13.69	3.53	-1.79	6.31	0.06	0.67	1.89	-0.60	11.75	-0.58	347.10	-0.09
SB18	OC10a195	10.83	13861.88	1.02	0.93	6.82	3.26	-2.83	1.86	0.20	0.90	1.35	-0.59	9.88	-0.82	221.16	0.03
SB18	OC10a196	10.11	9902.94	1.73	1.07	25.15	4.29	-1.80	2.82	0.12	0.66	2.05	-0.64	11.50	-0.76	273.01	0.38
SB18	OC10a197	5.98	7395.77	-0.31	-0.56	4.79	-2.52	-2.67	2.53	11.59	-0.22	1.82	-0.50	12.01	-0.78	389.55	0.06
SB18	OC10a198	6.74	8404.32	1.36	-1.77	25.37	7.73	-2.20	0.71	0.36	0.35	2.01	-0.65	14.38	-1.24	269.32	0.41
SB19	OC10a065	9.20	6640.12	-0.61	0.52	1.83	-3.07	-2.96	3.67	0.07	0.20	4.07	-0.63	7.95	-0.94	834.95	0.02
SB19	OC10a066	25.41	9079.36	-0.32	-1.09	29.70	2.71	-1.79	4.14	-0.05	0.43	7.36	-0.81	16.88	-0.73	765.49	0.02
SB19	OC10a067	26.57	12824.55	-0.23	0.85	3.75	2.43	-1.99	3.61	0.03	0.41	6.68	-0.63	35.33	-0.84	514.01	-0.24
SB19	OC10a068	15.76	9235.14	-0.25	-1.01	41.53	-2.43	-1.99	6.99	-0.05	0.66	7.20	-0.58	12.82	-0.64	1154.35	-0.09
SB19	OC10a069	26.70	12949.72	-0.37	0.60	4.57	2.43	-2.18	5.36	0.10	0.26	3.97	-0.49	15.69	-0.65	425.22	-0.08
SB19	OC10a070	24.44	9680.90	0.33	0.63	10.94	-2.55	-2.28	3.42	0.13	0.67	7.30	-0.61	12.48	-1.13	607.77	0.09
SB19	OC10a071	16.45	9456.82	0.19	0.58	-1.60	-3.14	-1.45	3.49	-0.10	0.94	7.63	-0.63	11.41	-0.92	736.93	0.02
SB19	OC10a072	25.38	10410.67	0.24	1.84	2.24	2.54	-2.30	2.50	0.02	0.24	8.83	-0.65	14.67	-0.92	725.01	-0.15
SB19	OC10a073	11.92	8735.66	-0.27	-0.55	3.85	-3.82	-2.53	5.34	0.11	0.45	8.63	0.39	12.47	-1.07	1677.51	-0.20
SB19	OC10a074	18.01	7570.61	-0.18	0.71	18.68	2.28	-2.31	4.27	0.11	0.29	3.34	-0.88	14.04	-0.98	1584.75	-0.16
SB19	OC10a075	14.77	8172.53	-0.27	0.67	-1.67	-2.21	-2.42	5.29	-0.05	0.59	9.33	-0.62	12.40	-0.79	1170.92	-0.15
SB19	OC10a076	11.05	8225.05	0.19	-0.71	2.61	-2.83	-1.89	3.76	-0.09	0.37	4.61	-0.63	14.23	-0.98	706.70	-0.15
SB19	OC10a083	10.88	9777.96	0.22	-0.68	3.25	1.93	-4.87	6.21	-0.05	0.75	5.11	-0.77	13.63	-1.08	1189.87	-0.15
SB19	OC10a084	24.98	10312.84	-0.32	-0.99	6.90	-2.34	-2.38	4.74	0.05	0.55	5.13	-0.88	8.12	-1.25	770.45	-0.09
SB19	OC10a085	17.72	7404.34	-0.20	-0.50	8.97	-2.39	-2.41	3.01	-0.05	0.43	5.30	-0.62	12.52	-1.28	637.56	-0.09
SB19	OC10a086	18.25	10207.71	-0.34	0.98	4.34	2.94	-1.59	3.57	0.01	0.73	5.59	-0.55	20.55	-0.70	779.04	0.01
SB19	OC10a087	29.68	9851.14	0.29	0.59	22.94	1.65	-2.36	3.78	0.04	0.39	5.63	-0.81	11.91	-1.05	594.30	0.02

Table A2.1: LA-ICPMS normalised analytical results for ablated sericite sites

Sample	Measurement	Ce_ppm	Eu_ppm	Gd_ppm	Yb_ppm	Lu_ppm	Hf_ppm	Ta_ppm	Au_ppm	Tl_ppm	Pb_ppm	Bi_ppm	Th_ppm	U_ppm
SB17	OC10a156	1.06	0.08	-0.34	-0.17	-0.05	-0.41	0.27	-0.21	-0.57	0.31	-0.24	-0.07	-0.07
SB17	OC10a157	1.98	0.11	0.39	-0.50	0.04	0.13	0.07	-0.12	-0.46	-0.32	-0.17	0.08	0.10
SB17	OC10a159	0.03	-0.16	-0.35	0.03	-0.07	0.09	0.15	-0.13	-0.40	-0.24	0.08	-0.06	0.14
SB18	OC10a180	0.10	-0.15	-0.89	-0.28	-0.09	-0.43	0.14	-0.43	-1.06	-0.42	-0.31	-0.21	-0.08
SB18	OC10a181	0.08	-0.08	0.14	-0.21	-0.05	-0.32	0.22	-0.37	0.38	-0.34	-0.27	0.06	-0.08
SB18	OC10a182	0.02	-0.13	-0.46	0.09	-0.20	-0.95	0.06	-0.21	-0.66	-0.39	-0.28	-0.21	-0.22
SB18	OC10a183	-0.15	0.05	-0.31	-0.48	-0.10	0.10	0.31	-0.27	0.64	-0.24	-0.18	-0.14	0.07
SB18	OC10a184	-0.12	-0.09	-0.69	-0.24	-0.12	0.05	-0.24	-0.58	-0.63	0.23	-0.24	-0.17	-0.14
SB18	OC10a185	-0.09	-0.07	-0.35	-0.39	0.02	-0.60	0.35	-0.18	0.73	0.81	0.10	-0.12	0.11
SB18	OC10a186	0.01	-0.09	-0.49	0.06	-0.04	-0.27	0.33	-0.13	0.74	0.45	-0.19	0.13	0.10
SB18	OC10a187	0.06	-0.07	0.04	-0.24	-0.04	-0.54	0.39	-0.33	0.85	-0.33	-0.12	0.06	0.15
SB18	OC10a188	-0.15	-0.09	-0.25	0.09	-0.04	-0.27	0.75	-0.35	0.81	0.47	-0.21	-0.12	-0.07
SB18	OC10a189	0.13	-0.14	-0.43	-0.18	-0.08	0.14	0.22	-0.25	0.52	0.88	-0.23	0.16	0.30
SB18	OC10a190	0.05	-0.22	0.05	0.03	0.01	0.14	2.81	-0.34	0.83	-0.31	-0.17	0.49	0.42
SB18	OC10a191	-0.18	-0.14	0.23	-0.18	-0.10	0.14	0.31	-0.46	0.54	0.56	-0.24	0.22	0.19
SB18	OC10a192	-0.09	-0.13	-0.43	-0.18	0.01	-0.27	0.26	-0.22	0.38	0.83	-0.24	-0.13	0.13
SB18	OC10a193	-0.22	-0.16	-0.44	0.26	-0.07	-0.94	0.17	-0.54	-0.62	-0.34	-0.44	0.22	0.08
SB18	OC10a194	0.02	-0.19	0.32	-0.18	-0.06	-0.61	0.21	-0.32	0.61	-0.25	-0.18	-0.17	0.10
SB18	OC10a195	0.04	0.05	-0.49	-0.48	-0.04	-0.27	0.23	-0.18	-0.45	-0.33	-0.13	0.34	0.63
SB18	OC10a196	0.41	0.02	-0.58	-0.18	-0.08	-0.28	0.30	-0.14	-0.46	-0.34	-0.19	0.21	0.18
SB18	OC10a197	0.12	0.14	0.56	0.89	0.11	-0.29	0.15	-0.14	-0.72	0.30	-0.29	1.16	0.71
SB18	OC10a198	0.53	0.05	0.32	-0.21	-0.11	-0.65	0.31	-0.22	0.60	-0.46	-0.34	-0.16	-0.18
SB19	OC10a065	-0.15	-0.09	-0.75	-0.18	0.04	0.15	0.22	-0.17	0.58	0.22	-0.29	-0.20	-0.07
SB19	OC10a066	-0.15	-0.14	-0.24	0.03	-0.08	0.09	0.44	-0.30	0.44	0.44	-0.16	-0.05	-0.05
SB19	OC10a067	-0.08	0.03	-0.39	-0.16	0.01	-0.41	0.27	-0.23	0.50	-0.31	-0.19	-0.05	-0.05
SB19	OC10a068	0.02	-0.07	-0.25	0.23	-0.05	-0.37	0.32	-0.27	0.42	0.35	-0.29	-0.06	-0.15
SB19	OC10a069	0.07	-0.06	-0.45	0.03	0.05	-0.68	0.24	-0.28	-0.47	0.59	-0.16	-0.10	-0.10
SB19	OC10a070	0.24	0.03	-0.66	-0.37	0.03	-0.51	0.45	-0.26	-0.40	-0.41	-0.15	-0.18	-0.15
SB19	OC10a071	-0.15	0.03	0.09	0.03	-0.04	-0.26	0.43	-0.26	0.41	0.32	-0.18	-0.12	-0.08
SB19	OC10a072	-0.21	-0.10	-0.46	-0.31	0.02	0.31	0.39	-0.32	-0.52	0.38	-0.32	-0.18	-0.11
SB19	OC10a073	-0.15	0.07	-0.60	-0.48	-0.04	0.19	0.86	-0.29	-0.41	0.62	-0.29	-0.17	-0.05
SB19	OC10a074	0.05	0.06	-0.36	-0.25	0.03	-0.41	0.27	-0.24	-0.61	0.57	-0.26	-0.16	-0.07
SB19	OC10a075	-0.15	-0.06	0.14	-0.37	0.01	0.14	0.39	-0.12	-0.42	0.33	-0.27	-0.05	-0.08
SB19	OC10a076	0.03	0.01	-0.25	-0.24	-0.04	0.05	0.34	-0.31	0.39	0.38	-0.22	-0.08	-0.05
SB19	OC10a083	-0.09	-0.06	-0.53	-0.31	-0.10	0.05	0.17	-0.20	-0.51	0.44	-0.37	0.04	-0.07
SB19	OC10a084	-0.09	0.12	0.09	-0.24	-0.07	0.23	0.50	-0.38	-0.42	0.34	-0.22	-0.12	-0.07
SB19	OC10a085	-0.09	-0.17	-0.46	-0.17	-0.08	0.14	0.34	-0.33	-0.54	0.71	-0.23	-0.14	-0.07
SB19	OC10a086	-0.15	-0.14	0.22	-0.36	-0.05	0.22	0.38	-0.16	0.59	0.80	-0.16	-0.12	0.04
SB19	OC10a087	-0.09	-0.19	-0.68	-0.17	-0.04	-0.58	0.19	0.15	-0.48	0.25	-0.24	-0.05	-0.11

Table A2.1: LA-ICPMS normalised analytical results for ablated sericite sites

Sample	Measurement	Host Rock	Alteration	Sulfides	Mineral	Li_ppm	B_ppm	Na_ppm	Mg_ppm	Al_ppm	Si_ppm	K_ppm	Ca_ppm	Ti_ppm	V_ppm	Cr_ppm
SB19	OC10a088	IGR	GS	HS	Sericite	1.68	-5.14	4104.39	4208.48	188903.96	213092.11	88276.40	-1899.94	4128.29	535.34	-7.52
SB19	OC10a089	IGR	GS	HS	Sericite	2.01	-6.70	4755.62	2803.63	193512.70	212518.71	87375.19	-1696.97	3068.51	284.47	-7.35
SB19	OC10a091	IGR	GS	HS	Sericite	2.69	-7.98	4445.44	2663.39	194978.96	210861.46	87671.12	-1760.14	3349.45	326.57	8.10
SB19	OC10a092	IGR	GS	HS	Sericite	2.56	3.61	4361.34	2548.12	194649.88	210523.60	88166.15	-1575.06	3346.13	309.64	-5.62
SB20	OC10a160	IGR	GS-WS	Cpy-HS	Sericite	28.78	-6.96	2338.58	45951.06	165558.20	210518.86	90105.31	-2199.72	169.71	84.88	-7.59
SB20	OC10a162	IGR	GS-WS	Cpy-HS	Sericite	23.65	11.97	2433.63	36393.32	168487.71	214758.40	91364.51	-1848.98	187.98	669.92	-6.43
SB20	OC10a163	IGR	GS-WS	Cpy-HS	Sericite	30.46	8.53	2895.70	43423.73	161621.05	213043.55	91919.90	-1652.21	554.82	1228.11	-6.44
SB20	OC10a164	IGR	GS-WS	Cpy-HS	Sericite	4.88	-6.12	4389.15	5755.90	190856.96	215708.42	87257.89	-1586.60	1382.10	162.39	-7.18
SB20	OC10a165	IGR	GS-WS	Cpy-HS	Sericite	28.65	15.74	3073.52	38902.83	164381.22	214863.85	91225.94	-1826.24	690.76	1590.09	-4.96
SB20	OC10a172	IGR	GS-WS	Cpy-HS	Sericite	5.87	-5.57	4894.65	6134.21	190746.44	216497.97	87103.95	-1571.46	1095.21	193.23	-5.09
SB20	OC10a173	IGR	GS-WS	Cpy-HS	Sericite	6.42	5.42	4596.65	5358.23	191819.17	215838.32	87660.95	-1587.04	669.27	160.82	-5.64
SB20	OC10a174	IGR	GS-WS	Cpy-HS	Sericite	5.71	-7.38	6513.61	5997.39	187277.20	218815.18	86568.61	-1676.36	493.34	139.91	-5.41
SB20	OC10a175	IGR	GS-WS	Cpy-HS	Sericite	7.75	3.71	4641.66	5776.44	189977.84	214217.77	88087.87	-1292.05	1806.54	312.81	-5.61
SB20	OC10a176	IGR	GS-WS	Cpy-HS	Sericite	5.21	-6.10	5364.38	5590.45	192238.51	215534.32	86963.21	-1340.87	1179.54	227.43	-4.77
SB20	OC10a177	IGR	GS-WS	Cpy-HS	Sericite	5.39	-6.17	5399.77	4624.04	177131.57	230160.27	89456.81	-1426.75	545.44	93.01	-5.79
SB20	OC10a178	IGR	GS-WS	Cpy-HS	Sericite	5.03	-5.40	5283.41	5218.16	191290.31	214419.44	85608.03	4390.26	1543.78	128.86	-8.45
SB20	OC10a179	IGR	GS-WS	Cpy-HS	Sericite	27.13	4.75	2219.24	40109.01	164607.26	214991.49	89422.46	-1808.98	23.71	7.05	-7.48
SB21	OC10a016	IGR	GS-WS	Cpy-Py	Sericite	13.72	4.61	4372.14	22325.40	163594.30	211809.18	85809.47	-1323.82	2071.27	313.64	5.81
SB21	OC10a017	IGR	GS-WS	Cpy-Py	Sericite	13.91	9.89	4484.13	11809.16	137146.77	244119.32	102611.89	-1343.77	875.79	101.05	-10.38
SB21	OC10a018	IGR	GS-WS	Cpy-Py	Sericite	18.02	7.24	3208.93	14643.68	172719.78	211694.18	89534.11	-1444.20	685.81	144.90	-11.43
SB21	OC10a020	IGR	GS-WS	Cpy-Py	Sericite	21.48	9.12	2924.91	15226.51	163695.70	219066.90	92020.46	-1480.74	1005.47	240.46	-6.48
SB21	OC10a021	IGR	GS-WS	Cpy-Py	Sericite	11.74	-11.52	22064.93	12330.47	153515.47	237267.46	64571.99	-1573.13	780.90	153.88	-12.24
SB21	OC10a022	IGR	GS-WS	Cpy-Py	Sericite	51.13	27.81	2806.52	31660.17	160055.25	215127.47	87833.51	-1852.10	38.56	14.46	-6.16
SB21	OC10a023	IGR	GS-WS	Cpy-Py	Sericite	35.64	17.49	3284.10	24847.19	160772.04	220605.68	86458.53	-1731.88	400.50	97.26	-6.87
SB21	OC10a024	IGR	GS-WS	Cpy-Py	Sericite	14.14	-9.48	4028.43	10411.61	164818.55	227241.77	86536.89	-2395.15	719.45	158.77	-6.50
SB21	OC10a025	IGR	GS-WS	Cpy-Py	Sericite	40.60	17.96	2076.92	18330.70	169198.44	223868.90	85637.66	-1495.85	44.32	14.42	-7.35
SB21	OC10a026	IGR	GS-WS	Cpy-Py	Sericite	38.13	22.29	2696.53	27021.13	157813.47	224255.06	86297.51	-1537.27	335.74	49.40	-8.52
SB21	OC10a027	IGR	GS-WS	Cpy-Py	Sericite	29.54	19.17	3239.26	27896.87	161715.38	215404.65	88938.94	-1741.64	589.16	65.16	-10.54
SB22	OC11a109	IGR	GS-WS	Cpy-HS	Sericite	7.88	8.14	3429.02	9181.62	186774.92	215624.92	85170.23	-1650.40	386.90	132.43	-5.30
SB22	OC11a110	IGR	GS-WS	Cpy-HS	Sericite	14.39	-12.56	5774.97	9579.08	186514.70	217601.41	78858.39	2574.31	447.02	103.14	-8.62
SB22	OC11a111	IGR	GS-WS	Cpy-HS	Sericite	23.42	9.29	21551.65	7787.61	172862.38	243041.99	45273.47	5677.10	15.73	5.77	-7.19
SB22	OC11a112	IGR	GS-WS	Cpy-HS	Sericite	10.72	-8.64	8749.16	6794.24	187789.12	224454.69	74047.05	-1997.61	36.38	12.19	-8.86
SB22	OC11a113	IGR	GS-WS	Cpy-HS	Sericite	17.65	7.76	3908.93	7162.01	178952.06	209878.64	86442.59	-1495.65	5299.30	799.35	238.53
SB22	OC11a117	IGR	GS-WS	Cpy-HS	Sericite	5.40	5.30	3284.47	7149.28	174749.56	223535.97	94510.14	-1228.05	1439.35	313.43	7.99
SB22	OC11a118	IGR	GS-WS	Cpy-HS	Sericite	4.06	-7.05	3677.96	7172.27	184078.33	216917.29	90291.08	-1109.82	1490.18	301.72	-8.25
SB22	OC11a119	IGR	GS-WS	Cpy-HS	Sericite	6.14	-6.02	3602.87	6123.76	178153.04	218806.97	92501.99	-1427.05	2825.77	585.79	12.97
SB22	OC11a120	IGR	GS-WS	Cpy-HS	Sericite	4.43	-6.75	3386.89	6841.15	183165.00	217349.41	90191.05	-1458.20	1783.21	382.95	7.00
SB22	OC11a121	IGR	GS-WS	Cpy-HS	Sericite	4.57	-5.53	3444.45	6687.82	184321.50	217826.98	89460.26	-1409.61	1713.59	283.22	-6.51
SB22	OC11a122	IGR	GS-WS	Cpy-HS	Sericite	2.59	-7.45	3530.32	4242.17	194426.97	216701.68	87227.59	-1433.68	766.13	174.89	-7.22

Table A2.1: LA-ICPMS normalised analytical results for ablated sericite sites

Sample	Measurement	Mn_ppm	Fe_ppm	Co_ppm	Ni_ppm	Cu_ppm	Zn_ppm	As_ppm	Sr_ppm	Y_ppm	Zr_ppm	Nb_ppm	Ag_ppm	Sn_ppm	Sb_ppm	Ba_ppm	La_ppm
SB19	OC10a088	16.65	9240.51	0.30	-0.85	4.31	-2.24	-2.45	3.97	-0.05	1.01	8.47	-0.81	17.89	-1.11	465.33	-0.20
SB19	OC10a089	12.60	8174.49	-0.34	-1.01	3.48	-3.32	-2.04	4.30	0.08	0.44	6.94	-0.53	11.22	-1.08	808.57	-0.15
SB19	OC10a091	10.97	8346.61	-0.17	-1.01	3.14	-2.68	-1.88	5.08	0.04	0.33	7.63	-0.80	14.68	-1.32	793.92	0.05
SB19	OC10a092	11.67	8911.08	-0.24	0.37	2.45	-2.35	-2.37	4.54	-0.05	0.51	7.51	-0.62	14.23	-0.81	894.50	0.02
SB20	OC10a160	862.21	4810.91	1.14	11.36	9.53	42.76	-1.79	2.75	0.52	0.11	0.67	-0.60	4.51	-0.89	82.23	-0.30
SB20	OC10a162	531.09	4133.62	0.64	26.35	9.74	26.86	-2.72	1.05	0.04	0.16	0.62	-0.60	8.96	-1.04	138.56	0.02
SB20	OC10a163	788.58	5047.85	1.14	28.54	27.40	42.40	-1.89	4.44	0.06	-0.25	0.65	-0.51	10.39	-0.85	131.45	-0.25
SB20	OC10a164	25.26	7779.29	0.44	1.03	3.68	-2.48	-2.54	6.73	-0.12	1.18	4.46	-0.58	6.66	-0.72	1105.73	-0.13
SB20	OC10a165	706.49	3648.13	0.97	29.73	16.95	40.24	-2.30	2.56	-0.10	0.38	0.86	-0.71	7.23	-0.84	115.28	-0.11
SB20	OC10a172	24.22	6825.17	-0.38	0.87	3.47	1.70	-2.90	6.94	-0.09	0.73	5.05	-1.05	5.80	-1.50	887.74	-0.15
SB20	OC10a173	22.80	7848.45	0.40	-1.06	4.11	-2.54	-2.35	8.02	-0.05	0.59	4.17	-0.66	7.69	-1.18	1207.25	0.05
SB20	OC10a174	27.64	8284.69	0.46	1.25	9.16	2.45	-2.77	7.34	0.07	0.74	5.20	-0.89	5.87	-0.92	1113.91	-0.13
SB20	OC10a175	28.81	9355.49	0.47	1.51	4.98	3.22	-1.90	5.87	0.03	0.19	7.13	-0.75	10.86	-0.56	603.90	0.03
SB20	OC10a176	20.55	6367.80	-0.54	-0.53	3.67	-2.32	-1.30	6.99	0.03	0.57	4.67	-0.60	7.46	-0.52	846.02	-0.19
SB20	OC10a177	24.82	4912.89	-0.22	0.89	11.02	-3.41	-2.29	47.44	0.26	0.44	3.52	-0.73	4.37	-0.78	988.34	0.41
SB20	OC10a178	19.71	5975.44	-0.29	0.49	3.20	-3.21	-2.12	83.31	0.61	0.55	5.30	-0.65	4.81	-1.02	695.99	0.87
SB20	OC10a179	759.73	7393.84	1.05	3.24	8.86	39.89	-1.87	0.75	-0.16	0.07	0.20	-0.80	0.84	-0.95	41.88	-0.14
SB21	OC10a016	73.99	30191.33	-0.24	5.58	3.25	8.36	-2.04	4.44	-0.09	0.34	1.82	-0.88	14.34	-1.08	612.58	-0.15
SB21	OC10a017	48.21	17695.29	-0.44	5.11	8.38	3.29	-4.19	21.96	0.06	-0.53	0.68	-0.81	6.18	-1.12	710.19	-0.16
SB21	OC10a018	46.91	28563.28	-0.40	5.70	16.25	3.32	-2.33	3.08	0.05	0.43	0.93	-0.80	14.56	-1.10	727.34	-0.08
SB21	OC10a020	64.18	26340.08	-0.44	5.55	6.73	5.57	-2.45	6.70	-0.10	0.68	2.07	-0.76	14.64	-0.91	361.01	0.03
SB21	OC10a021	36.50	21553.38	0.32	6.43	10.95	3.49	-3.99	65.28	0.02	-0.23	0.98	-1.08	9.02	-1.21	478.06	0.16
SB21	OC10a022	259.43	24001.56	-0.33	1.82	44.43	21.63	1.85	6.56	0.77	0.44	-0.27	-0.81	0.60	-1.07	149.77	0.58
SB21	OC10a023	196.16	22593.65	0.28	1.58	38.33	6.64	-2.70	8.86	0.36	0.31	0.42	-0.78	3.30	-1.03	270.43	0.01
SB21	OC10a024	25.53	22430.49	0.12	1.82	46.62	3.41	-2.90	3.42	192.88	0.66	0.84	-0.83	8.35	-1.72	302.61	0.17
SB21	OC10a025	231.03	16939.46	-0.25	1.33	58.13	17.33	1.58	4.04	0.46	0.10	-0.12	-0.72	0.54	-1.08	69.58	-0.15
SB21	OC10a026	207.74	19371.03	-0.36	2.14	74.06	16.74	-2.99	5.85	0.58	0.41	0.82	-0.77	2.65	-1.16	137.29	0.03
SB21	OC10a027	152.43	23227.86	-0.29	3.69	35.37	12.85	-2.67	4.52	0.35	0.22	0.93	-0.94	2.78	-1.09	199.88	0.01
SB22	OC11a109	230.31	14837.92	3.34	9.32	3.58	34.79	-5.01	3.03	0.11	-0.52	1.06	-1.05	2.82	-1.56	156.99	0.05
SB22	OC11a110	43.52	12475.94	5.58	11.66	9.35	56.42	-4.73	8.81	-0.08	-0.39	2.09	-1.04	0.98	-1.54	133.88	0.07
SB22	OC11a111	27.90	5979.44	3.32	17.73	25.23	77.57	-2.97	31.56	0.24	-0.39	-0.14	-0.77	1.84	-1.19	63.07	1.00
SB22	OC11a112	34.75	8630.58	2.70	10.32	14.32	36.95	-2.36	6.28	-0.13	-0.39	0.15	-0.82	2.85	-1.14	115.61	0.04
SB22	OC11a113	44.76	22116.16	3.86	22.17	1.65	18.58	-1.69	13.79	0.03	1.10	10.06	-0.62	17.44	-1.11	323.01	-0.09
SB22	OC11a117	15.83	10489.21	-0.25	4.90	7.96	3.93	-2.34	2.63	0.02	0.51	2.44	-0.87	14.59	-0.96	934.27	0.03
SB22	OC11a118	16.76	11003.69	-0.27	5.11	8.11	-3.20	-3.78	2.45	-0.06	0.38	3.12	-0.56	13.95	-1.09	1132.74	-0.21
SB22	OC11a119	20.01	12500.86	0.47	4.70	7.75	2.43	0.92	5.12	-0.11	1.00	4.70	-0.68	24.00	-0.85	464.12	0.02
SB22	OC11a120	19.03	11835.12	-0.29	4.78	4.01	2.65	-1.94	2.21	0.02	0.57	3.57	-0.55	12.32	0.44	820.69	0.05
SB22	OC11a121	17.61	10434.52	0.27	4.06	3.40	1.96	-2.05	2.17	-0.12	0.43	2.76	-0.63	11.72	-1.04	1029.44	0.12
SB22	OC11a122	13.57	6272.06	0.41	4.57	43.23	14.33	-2.86	1.27	-0.08	0.50	3.33	-0.63	44.10	-0.91	167.13	-0.22

Table A2.1: LA-ICPMS normalised analytical results for ablated sericite sites

Sample	Measurement	Ce_ppm	Eu_ppm	Gd_ppm	Yb_ppm	Lu_ppm	Hf_ppm	Ta_ppm	Au_ppm	Tl_ppm	Pb_ppm	Bi_ppm	Th_ppm	U_ppm
SB19	OC10a088	0.01	-0.17	-0.42	0.03	-0.08	0.28	0.30	-0.23	0.73	0.27	-0.20	-0.09	-0.13
SB19	OC10a089	-0.09	-0.07	-0.35	-0.17	-0.13	-0.27	0.22	-0.27	-0.46	0.37	-0.23	-0.17	-0.07
SB19	OC10a091	0.06	-0.16	0.14	-0.38	-0.04	-0.53	0.24	-0.27	0.37	0.44	-0.21	-0.06	-0.07
SB19	OC10a092	-0.09	0.03	-0.49	-0.31	-0.04	0.09	0.18	-0.36	0.44	0.34	-0.28	0.04	-0.08
SB20	OC10a160	0.59	-0.13	-0.41	0.28	0.05	-0.44	-0.17	-0.47	-0.46	0.48	-0.20	0.35	0.27
SB20	OC10a162	-0.11	-0.16	-0.46	-0.21	-0.05	-0.33	0.03	-0.40	-0.50	0.58	-0.19	0.25	0.25
SB20	OC10a163	0.05	-0.11	0.21	-0.43	-0.09	-0.41	0.07	-0.26	0.68	0.93	-0.19	0.16	0.28
SB20	OC10a164	0.02	-0.10	0.05	0.06	-0.06	0.20	-0.18	-0.39	0.49	0.97	-0.15	-0.13	-0.14
SB20	OC10a165	0.05	-0.18	0.05	-0.21	-0.11	-0.33	0.16	-0.34	0.41	-0.55	-0.20	0.21	0.28
SB20	OC10a172	-0.13	-0.18	-0.26	-0.18	-0.04	0.10	-0.29	-0.34	-0.59	0.58	-0.25	0.06	-0.12
SB20	OC10a173	0.02	-0.20	-0.26	-0.18	-0.06	-0.28	0.24	-0.31	-0.47	0.70	-0.25	-0.08	-0.11
SB20	OC10a174	0.06	-0.10	-0.26	-0.18	0.02	0.20	0.14	-0.37	-0.38	1.37	-0.20	-0.06	-0.10
SB20	OC10a175	0.05	0.05	-0.43	-0.36	-0.06	-0.41	0.19	-0.18	0.51	0.68	-0.21	-0.11	0.06
SB20	OC10a176	0.03	-0.20	0.09	-0.18	-0.08	-0.28	0.23	-0.31	0.42	0.86	-0.24	-0.08	-0.11
SB20	OC10a177	0.74	0.11	0.10	-0.27	-0.04	-0.29	0.24	-0.33	-0.48	2.45	-0.14	-0.08	-0.05
SB20	OC10a178	1.63	-0.14	-0.84	-0.41	-0.10	-0.29	0.30	-0.33	-0.51	0.59	-0.17	-0.08	-0.07
SB20	OC10a179	-0.20	0.03	-0.28	-0.20	-0.11	0.05	0.04	-0.24	0.61	0.48	-0.13	0.56	0.50
SB21	OC10a016	-0.16	-0.19	-0.50	-0.16	-0.07	-0.34	0.17	-0.33	0.40	-0.28	-0.21	0.06	0.09
SB21	OC10a017	-0.11	0.06	-0.54	-0.49	-0.11	-0.35	-0.22	0.11	-0.71	2.06	-0.42	-0.15	0.62
SB21	OC10a018	-0.08	0.04	-0.68	0.10	-0.05	0.16	-0.19	-0.39	0.44	-0.36	-0.21	0.12	0.28
SB21	OC10a020	-0.12	0.02	0.15	-0.47	-0.05	0.04	-0.19	-0.42	-0.60	0.58	-0.35	0.26	0.83
SB21	OC10a021	0.16	-0.17	-0.28	-0.19	-0.07	-0.41	0.08	-0.13	0.52	0.94	-0.22	-0.09	0.21
SB21	OC10a022	0.90	0.02	-0.26	-0.25	-0.06	0.04	-0.09	-0.37	0.95	7.43	-0.15	0.46	1.11
SB21	OC10a023	0.03	0.02	-0.57	-0.18	0.07	-0.28	-0.18	-0.17	0.64	4.74	-0.21	0.28	0.67
SB21	OC10a024	1.20	4.26	17.20	15.94	2.34	0.28	0.07	-0.31	0.36	-0.41	-0.21	4.96	2.00
SB21	OC10a025	0.05	0.06	0.04	-0.35	0.01	0.13	-0.21	-0.26	0.64	7.15	-0.25	0.22	0.78
SB21	OC10a026	0.03	0.03	-0.36	0.34	-0.06	-0.28	-0.21	-0.35	0.77	5.16	-0.23	0.62	1.20
SB21	OC10a027	-0.18	-0.15	0.12	-0.18	0.01	-0.27	0.19	-0.25	0.69	5.56	-0.29	0.19	0.51
SB22	OC11a109	-0.11	0.10	-0.70	0.19	-0.07	-0.35	0.14	-0.38	-0.55	-0.31	-0.40	-0.15	-0.15
SB22	OC11a110	-0.14	-0.14	-0.46	-0.31	-0.17	-0.43	0.28	-0.57	-0.90	-0.34	-0.44	-0.32	-0.11
SB22	OC11a111	3.42	0.18	-1.04	0.13	-0.16	0.05	-0.21	-0.36	-0.48	0.39	-0.20	-0.09	0.17
SB22	OC11a112	0.04	-0.24	0.23	-0.38	0.03	-0.35	-0.16	-0.21	-0.62	-0.58	-0.27	-0.07	-0.09
SB22	OC11a113	-0.12	0.08	-0.34	-0.17	0.01	0.04	0.27	-0.11	-0.56	1.01	-0.22	-0.12	-0.12
SB22	OC11a117	-0.15	0.07	-0.40	0.16	-0.06	-0.31	0.32	-0.30	0.49	0.55	-0.27	0.07	-0.11
SB22	OC11a118	0.08	-0.08	-0.62	-0.47	-0.09	-0.43	0.30	-0.34	-0.51	-0.35	-0.23	-0.20	-0.13
SB22	OC11a119	0.03	-0.07	0.09	-0.19	-0.04	-0.30	0.35	0.10	0.42	0.48	-0.42	-0.06	0.07
SB22	OC11a120	-0.15	0.09	-0.38	0.13	-0.04	0.15	0.30	-0.22	-0.39	-0.33	-0.22	-0.06	-0.08
SB22	OC11a121	-0.10	-0.10	-0.38	-0.31	-0.12	0.25	0.29	-0.18	-0.59	-0.43	-0.28	-0.11	0.02
SB22	OC11a122	0.09	-0.15	-0.39	-0.19	-0.04	-0.41	0.22	-0.34	-0.40	0.26	0.14	-0.14	-0.09

Table A2.1: LA-ICPMS normalised analytical results for ablated sericite sites

Sample	Measurement	Host Rock	Alteration	Sulfides	Mineral	Li_ppm	B_ppm	Na_ppm	Mg_ppm	Al_ppm	Si_ppm	K_ppm	Ca_ppm	Ti_ppm	V_ppm	Cr_ppm
SB22	OC11a123	IGR	GS-WS	Cpy-HS	Sericite	2.87	-8.97	3091.76	5290.11	195529.16	220361.12	81789.95	-1818.79	487.92	34.21	-7.48
SB22	OC11a124	IGR	GS-WS	Cpy-HS	Sericite	5.30	-5.89	3133.10	6804.86	190767.59	215869.85	87765.67	-1424.71	1189.20	376.57	6.93
SB22	OC11a125	IGR	GS-WS	Cpy-HS	Sericite	5.14	-6.30	2830.15	8177.28	192641.37	213872.62	86204.50	-1363.65	1296.32	416.02	-6.75
SB22	OC11a126	IGR	GS-WS	Cpy-HS	Sericite	2.70	4.59	2953.25	4397.20	198836.58	217799.78	84779.17	-1679.90	201.40	23.70	-7.75
SB22	OC11a127	IGR	GS-WS	Cpy-HS	Sericite	4.33	4.69	4909.78	5411.81	191979.07	215138.88	86037.12	5240.11	901.06	143.23	-7.90
SB22	OC11a128	IGR	GS-WS	Cpy-HS	Sericite	5.68	-6.50	3695.66	5394.37	179380.38	218349.55	90438.26	-1206.37	3196.41	694.71	-7.87
SB22	OC11a129	IGR	GS-WS	Cpy-HS	Sericite	6.07	-11.54	3053.60	6471.38	170885.51	173609.59	73190.00	93364.53	3966.57	542.34	8.97
SB22	OC11a130	IGR	GS-WS	Cpy-HS	Sericite	6.94	-6.04	3257.46	6513.79	184445.67	215203.85	90758.19	-1473.99	2514.11	567.43	-6.58
SB22	OC11a131	IGR	GS-WS	Cpy-HS	Sericite	11.19	4.91	3197.58	6544.28	190751.58	210844.50	90147.49	-1366.42	1780.33	560.38	-6.35
SB22	OC11a132	IGR	GS-WS	Cpy-HS	Sericite	4.58	-9.78	3058.57	6460.61	179033.17	221324.64	93571.47	-1187.85	1803.39	402.67	9.15
SB22	OC11a133	IGR	GS-WS	Cpy-HS	Sericite	7.67	2.37	3342.67	5545.26	183790.32	213047.70	90732.67	-1236.57	3812.16	620.83	20.82
SB22	OC11a134	IGR	GS-WS	Cpy-HS	Sericite	13.59	8.82	2742.75	17629.78	182804.41	217094.44	89454.66	-1722.21	302.55	98.61	-6.20
SB22	OC11a135	IGR	GS-WS	Cpy-HS	Sericite	11.56	-6.36	2874.87	13013.45	186798.08	210117.35	91808.74	-1651.91	1244.06	220.26	-7.54
SB22	OC11a136	IGR	GS-WS	Cpy-HS	Sericite	15.59	-7.55	3546.63	6130.92	188169.59	210898.92	89655.17	-1791.00	2174.62	758.50	7.48
SB22	OC11a137	IGR	GS-WS	Cpy-HS	Sericite	3.09	-6.13	2868.66	6873.93	187119.29	220202.81	86435.31	-1679.06	429.54	206.58	-6.99
SB22	OC11a138	IGR	GS-WS	Cpy-HS	Sericite	4.44	-7.13	2814.02	7086.20	184091.93	216827.69	88711.20	-1402.31	1242.15	371.70	4.26
SB22	OC11a139	IGR	GS-WS	Cpy-HS	Sericite	4.26	7.55	3627.13	5689.45	159937.62	240423.82	79332.84	-1767.45	1312.35	309.45	-9.93
SB22	OC11a140	IGR	GS-WS	Cpy-HS	Sericite	2.23	-9.69	4443.03	3148.58	133120.17	263328.09	102571.47	-2026.93	643.76	190.75	-9.92
SB22	OC11a141	IGR	GS-WS	Cpy-HS	Sericite	4.94	3.96	3258.93	7242.96	178436.20	222345.62	91679.61	-1584.54	935.79	375.87	-5.88
SB22	OC11a148	IGR	GS-WS	Cpy-HS	Sericite	2.86	-11.00	5769.52	1634.18	126872.96	265135.42	110292.04	-1897.74	842.57	183.35	-8.08
SB22	OC11a149	IGR	GS-WS	Cpy-HS	Sericite	5.80	-7.05	4230.66	3475.46	159897.11	236866.35	100533.30	-2155.64	1361.13	582.61	-9.81
SB22	OC11a150	IGR	GS-WS	Cpy-HS	Sericite	1.81	-7.04	6458.76	2298.87	127183.68	265080.50	108302.92	1212.85	647.81	161.14	-10.93
SB22	OC11a151	IGR	GS-WS	Cpy-HS	Sericite	3.59	-9.25	4234.31	6230.21	145883.53	243827.44	100499.79	-2039.65	3801.11	364.51	16.73
SB23	OC10a199	IGR	GS-WS	Cpy-Py	Sericite	9.03	-6.88	5263.22	5954.77	160209.39	248876.91	76065.94	-1992.02	934.84	135.86	4.67
SB23	OC10a200	IGR	GS-WS	Cpy-Py	Sericite	11.69	-5.46	4780.58	6929.62	181296.21	211843.89	87857.69	-1564.15	336.44	122.21	-6.93
SB23	OC10a201	IGR	GS-WS	Cpy-Py	Sericite	5.21	-9.03	5716.63	5663.85	190207.73	212553.24	87673.30	-1705.84	1524.44	235.68	-6.10
SB23	OC10a203	IGR	GS-WS	Cpy-Py	Sericite	10.78	-6.32	4443.97	10673.04	179250.23	216206.13	86986.28	-1293.02	1594.78	238.53	7.03
SB23	OC10a204	IGR	GS-WS	Cpy-Py	Sericite	42.93	-9.83	4647.16	4604.52	189264.39	215061.00	81712.72	-1688.28	1194.63	355.18	-9.63
SB23	OC10a205	IGR	GS-WS	Cpy-Py	Sericite	7.74	-6.05	4736.15	4623.09	184300.56	210619.84	87532.16	-1389.34	922.81	938.67	7.06
SB23	OC10a206	IGR	GS-WS	Cpy-Py	Sericite	18.88	8.11	4064.42	11338.96	181815.75	215395.37	87056.67	-1248.16	339.97	185.35	15.68
SB23	OC10a207	IGR	GS-WS	Cpy-Py	Sericite	19.04	8.20	4339.05	15815.22	185861.12	211786.38	88059.14	-1573.64	77.79	75.08	-6.03
SB23	OC10a208	IGR	GS-WS	Cpy-Py	Sericite	10.38	22.62	3324.38	10883.93	180569.18	218779.93	88280.92	-1508.62	328.27	84.88	-6.29
SB23	OC10a209	IGR	GS-WS	Cpy-Py	Sericite	7.49	4.59	6710.35	5347.09	180557.66	215814.47	87221.82	-1629.28	335.77	208.25	-5.92
SB23	OC10a210	IGR	GS-WS	Cpy-Py	Sericite	11.83	5.59	4038.80	12072.46	179608.48	219049.29	83874.54	-1753.91	710.61	199.55	10.40
SB24	OC10a003	IGR	GS	Cpy-HS	Sericite	7.21	-9.28	4316.44	5839.55	172375.04	221476.73	91660.37	9240.11	2176.92	413.48	91.74
SB24	OC10a004	IGR	GS	Cpy-HS	Sericite	9.33	-7.29	3971.44	6616.22	176464.69	217515.83	89699.67	-1212.07	4302.10	377.55	184.56
SB24	OC10a005	IGR	GS	Cpy-HS	Sericite	5.11	4.38	5911.26	2763.36	128313.08	264071.61	107700.71	-2207.05	453.78	188.82	-8.21
SB24	OC10a008	IGR	GS	Cpy-HS	Sericite	8.82	-8.52	5044.35	4320.81	157705.70	238621.88	99697.16	-1445.48	719.54	325.20	-9.88
SB24	OC10a009	IGR	GS	Cpy-HS	Sericite	7.18	-8.17	5871.38	4915.83	158837.56	237186.98	100206.41	-1823.17	782.26	336.17	-8.33

Table A2.1: LA-ICPMS normalised analytical results for ablated sericite sites

Sample	Measurement	Mn_ppm	Fe_ppm	Co_ppm	Ni_ppm	Cu_ppm	Zn_ppm	As_ppm	Sr_ppm	Y_ppm	Zr_ppm	Nb_ppm	Ag_ppm	Sn_ppm	Sb_ppm	Ba_ppm	La_ppm
SB22	OC11a123	12.29	3946.68	1.14	8.62	60.77	30.50	-3.07	9.49	0.99	-0.29	3.06	-0.62	26.55	0.89	163.28	-0.13
SB22	OC11a124	16.51	7942.35	0.48	9.95	82.46	16.42	-1.98	1.43	-0.05	0.27	4.57	-0.60	39.94	-0.98	345.40	-0.21
SB22	OC11a125	14.49	8200.36	0.27	13.76	54.43	8.57	-1.47	1.31	0.04	0.29	2.96	-0.41	54.17	-0.97	359.71	-0.09
SB22	OC11a126	8.46	2484.31	-0.51	3.27	226.56	7.30	-2.14	1.44	0.07	0.09	1.52	-0.58	25.82	-1.12	318.47	-0.11
SB22	OC11a127	13.17	4735.51	0.75	8.65	59.06	27.39	-1.20	33.21	0.30	0.43	4.59	-0.65	31.97	-0.74	193.93	0.07
SB22	OC11a128	19.26	13129.79	0.38	3.09	19.18	5.85	-1.93	5.32	0.01	1.10	11.30	-0.51	26.33	-1.00	404.88	-0.14
SB22	OC11a129	50.43	11585.58	2.03	10.25	34.32	47.04	-2.55	643.66	58.95	1.29	31.80	-1.06	44.82	-1.44	187.07	17.33
SB22	OC11a130	20.27	11560.54	0.28	4.86	6.19	4.60	-2.07	3.10	-0.05	0.64	9.41	-0.57	24.25	-0.87	573.26	-0.10
SB22	OC11a131	22.03	11859.67	-0.24	3.13	4.09	-2.29	-2.67	4.07	-0.09	0.75	6.15	-0.51	17.90	-0.95	730.86	-0.15
SB22	OC11a132	14.97	9223.88	-0.45	4.04	15.81	7.81	0.95	3.40	0.03	0.81	4.86	-0.59	27.70	-0.73	662.60	0.02
SB22	OC11a133	18.40	13877.41	0.32	3.50	20.26	5.07	-1.98	3.84	0.01	1.64	8.96	-0.74	28.49	-0.90	300.21	-0.10
SB22	OC11a134	53.28	5573.23	1.04	15.86	35.04	27.37	-2.23	7.29	0.07	0.13	1.91	-0.48	14.68	-1.21	70.43	0.04
SB22	OC11a135	39.23	11712.12	1.21	12.55	15.85	5.42	-1.33	2.47	0.03	0.44	2.37	-0.55	24.82	-1.07	112.64	0.03
SB22	OC11a136	27.39	15052.58	0.35	4.67	5.79	8.68	-2.13	4.25	0.05	1.50	11.58	-0.49	25.23	-0.97	150.11	0.03
SB22	OC11a137	14.01	8164.37	0.91	6.10	1176.40	24.23	-2.12	2.32	0.06	0.37	2.03	-0.85	13.70	-0.97	952.37	0.02
SB22	OC11a138	18.15	9059.21	5.14	5.83	5692.57	8.72	-2.53	1.82	-0.05	-0.23	4.43	-0.73	17.19	-1.07	872.75	0.05
SB22	OC11a139	16.87	18939.71	8.12	48.44	137.54	293.08	-2.48	5.79	0.29	0.54	2.53	-0.86	19.43	-1.11	788.63	0.05
SB22	OC11a140	8.74	4988.86	-0.51	2.53	2.46	3.52	-3.52	17.04	0.02	0.23	1.10	-0.84	7.76	-1.26	702.31	0.03
SB22	OC11a141	15.87	11173.75	-0.36	7.48	8.26	6.07	-1.71	3.12	0.17	0.54	1.03	-0.41	9.55	-1.15	536.73	0.03
SB22	OC11a148	10.26	4119.87	-0.50	1.54	1.75	1.98	-5.47	25.81	0.29	0.11	0.95	-1.23	7.41	-1.58	608.65	0.06
SB22	OC11a149	14.20	8805.18	-0.61	4.03	-2.70	7.33	-2.69	20.17	0.29	0.82	1.65	-1.03	19.36	-1.65	415.79	0.02
SB22	OC11a150	8.55	3336.49	-0.28	2.62	2.94	2.90	-3.36	40.63	1.18	0.19	0.49	-0.75	6.18	-1.43	605.96	0.59
SB22	OC11a151	20.93	8170.38	0.46	9.90	2.68	3.43	-2.48	14.73	0.14	-0.27	2.58	-0.66	10.23	-1.17	497.19	-0.17
SB23	OC10a199	11.07	8764.56	2.37	-0.63	35.70	3.94	-2.47	7.16	1.12	0.19	2.28	-0.70	9.56	-1.04	274.97	-0.15
SB23	OC10a200	64.99	26228.00	0.72	5.39	4.43	6.05	-2.06	3.73	0.04	0.11	1.95	-0.50	39.27	-0.84	1297.44	0.01
SB23	OC10a201	33.95	11531.99	0.25	-1.20	2.24	4.69	0.89	2.93	0.06	0.34	5.34	-0.56	16.84	-0.57	1003.51	-0.19
SB23	OC10a203	85.68	16570.55	0.42	15.98	5.20	4.47	-1.54	3.85	-0.09	-0.30	2.62	-0.65	21.34	-0.69	648.64	0.02
SB23	OC10a204	70.77	17330.11	0.47	8.62	-2.52	3.27	-2.28	3.11	-0.09	0.36	2.50	-1.03	13.55	-1.86	322.98	-0.26
SB23	OC10a205	35.35	25682.78	1.23	-1.65	-1.78	2.28	-1.63	3.15	-0.05	1.35	7.51	-0.55	31.29	-1.13	351.41	-0.10
SB23	OC10a206	204.19	16617.68	1.09	18.00	14.01	5.44	-1.68	7.13	0.08	0.26	1.10	-0.58	18.46	-0.87	832.59	-0.13
SB23	OC10a207	115.61	11657.12	0.64	21.44	2.10	3.21	-3.16	1.56	1.26	0.11	0.25	-0.44	6.65	-1.00	265.47	0.25
SB23	OC10a208	194.48	13451.16	0.60	6.20	4.30	9.12	1.14	3.87	0.17	0.07	0.60	-0.63	4.71	-0.80	963.91	-0.09
SB23	OC10a209	47.24	22067.38	1.38	2.07	10.50	4.79	-2.40	4.09	-0.10	0.23	0.83	-0.58	43.24	-0.98	930.62	-0.15
SB23	OC10a210	157.92	15411.62	0.49	1.04	3.93	3.34	-1.80	3.85	0.01	0.40	1.45	-0.60	2.02	-0.97	431.23	0.09
SB24	OC10a003	14.63	8705.18	0.71	9.02	3.15	-2.20	-4.75	96.72	7.47	22.48	2.85	-1.06	24.00	-1.16	801.27	4.17
SB24	OC10a004	14.03	14530.33	0.84	3.59	7.29	-2.16	-3.28	3.65	0.83	16.13	7.14	-0.71	21.02	-1.03	535.05	-0.08
SB24	OC10a005	6.18	5429.15	-0.21	3.46	6.54	-4.42	-3.58	11.51	0.01	-0.50	0.66	-0.82	10.76	-1.83	607.76	0.03
SB24	OC10a008	9.88	9570.63	-0.51	5.66	4.63	3.21	-3.40	7.86	0.03	0.29	1.83	-0.67	18.41	-1.23	728.71	0.04
SB24	OC10a009	13.01	8150.84	-0.49	4.26	5.51	-2.54	-2.09	12.26	-0.11	0.34	1.50	-0.93	21.92	-1.34	778.22	-0.10

Table A2.1: LA-ICPMS normalised analytical results for ablated sericite sites

Sample	Measurement	Ce_ppm	Eu_ppm	Gd_ppm	Yb_ppm	Lu_ppm	Hf_ppm	Ta_ppm	Au_ppm	Tl_ppm	Pb_ppm	Bi_ppm	Th_ppm	U_ppm
SB22	OC11a123	0.83	-0.09	-0.34	-0.48	-0.08	-0.41	-0.25	-0.23	-0.74	-0.38	-0.25	0.13	-0.16
SB22	OC11a124	-0.09	-0.15	-0.36	-0.25	-0.04	0.10	-0.22	-0.27	-0.50	-0.42	-0.19	-0.15	0.04
SB22	OC11a125	0.02	0.06	-0.56	-0.30	-0.09	-0.41	0.06	-0.17	-0.45	-0.31	-0.18	-0.06	-0.07
SB22	OC11a126	0.09	-0.08	-0.49	-0.20	0.01	0.12	-0.14	-0.56	-0.36	0.34	-0.21	-0.13	-0.06
SB22	OC11a127	0.39	0.11	0.16	-0.45	-0.06	-0.32	0.26	-0.19	-0.55	0.34	-0.19	-0.13	-0.10
SB22	OC11a128	-0.20	0.01	-0.39	-0.28	-0.04	-0.31	0.34	-0.19	0.48	0.73	-0.26	-0.16	-0.08
SB22	OC11a129	40.56	2.47	9.23	2.45	0.10	-0.41	0.67	-0.65	-0.53	-0.54	-0.36	0.49	-0.13
SB22	OC11a130	0.39	-0.10	-0.37	-0.26	-0.10	0.15	0.47	-0.28	-0.56	0.37	-0.12	0.02	-0.05
SB22	OC11a131	-0.15	0.04	-0.53	-0.31	0.01	0.26	0.30	-0.18	0.47	0.48	-0.12	-0.09	-0.12
SB22	OC11a132	0.03	0.02	0.15	-0.47	-0.07	-0.62	0.14	-0.43	-0.46	0.33	-0.26	-0.07	-0.08
SB22	OC11a133	-0.10	0.06	-0.54	0.03	-0.04	0.10	0.28	-0.22	0.38	0.53	-0.15	0.04	-0.08
SB22	OC11a134	0.12	0.05	-0.66	-0.42	-0.09	0.11	0.15	-0.20	-0.40	0.59	-0.34	0.12	0.17
SB22	OC11a135	-0.20	-0.18	-0.39	-0.39	-0.07	-0.30	0.11	-0.25	-0.48	-0.40	-0.26	0.05	0.12
SB22	OC11a136	-0.14	-0.07	0.19	-0.26	-0.09	0.26	0.24	-0.13	0.50	0.39	-0.19	-0.20	-0.08
SB22	OC11a137	-0.10	-0.15	-0.28	-0.27	0.02	-0.41	0.17	-0.45	-0.57	-0.36	0.17	-0.11	-0.13
SB22	OC11a138	0.03	-0.07	-0.46	0.13	-0.07	0.05	-0.22	-0.26	-0.34	0.54	-0.23	-0.14	-0.11
SB22	OC11a139	0.36	0.05	-0.34	-0.33	-0.05	-0.41	0.20	-0.36	0.39	0.92	0.13	-0.16	-0.15
SB22	OC11a140	-0.13	0.08	-0.63	-0.58	0.04	-0.41	0.14	-0.55	0.48	2.22	-0.40	-0.12	-0.08
SB22	OC11a141	0.02	0.02	-0.46	-0.50	0.02	-0.43	-0.10	-0.32	0.44	0.56	-0.26	0.03	-0.06
SB22	OC11a148	0.23	0.12	-0.46	-0.27	-0.06	-0.42	-0.19	-0.56	-0.95	3.78	-0.45	-0.09	-0.11
SB22	OC11a149	0.38	-0.10	-0.37	0.12	-0.12	0.06	-0.27	-0.30	-0.77	1.94	-0.36	-0.09	0.05
SB22	OC11a150	0.98	-0.23	-0.54	-0.31	0.02	0.15	0.16	-0.48	-0.76	3.61	-0.33	-0.21	-0.16
SB22	OC11a151	0.17	0.07	-0.33	-0.82	-0.05	-0.80	0.30	-0.47	0.64	1.88	-0.33	-0.20	-0.07
SB23	OC10a199	0.23	-0.22	-0.51	-0.30	0.05	0.10	0.36	-0.31	0.56	0.82	0.15	0.33	0.16
SB23	OC10a200	-0.15	0.08	-0.51	0.17	0.03	-0.27	0.23	0.20	0.34	0.36	-0.12	-0.06	-0.18
SB23	OC10a201	-0.09	-0.14	-0.62	-0.25	-0.10	-0.56	0.26	-0.23	-0.54	0.94	-0.20	-0.10	-0.12
SB23	OC10a203	-0.15	-0.10	-0.26	0.09	0.03	-0.56	0.26	-0.41	-0.42	0.77	-0.14	-0.14	-0.07
SB23	OC10a204	0.07	-0.09	-0.71	-0.31	-0.12	-0.41	0.11	0.17	-0.65	0.42	-0.18	0.05	-0.10
SB23	OC10a205	0.05	-0.10	-0.26	-0.44	-0.04	0.15	0.14	-0.19	-0.47	0.31	-0.17	-0.10	-0.05
SB23	OC10a206	-0.09	-0.10	-0.76	-0.18	-0.04	-0.28	0.09	-0.14	0.49	1.21	-0.15	-0.08	0.08
SB23	OC10a207	0.90	0.08	-0.53	-0.41	0.01	-0.57	0.03	-0.43	0.51	0.33	-0.28	-0.08	0.15
SB23	OC10a208	0.07	-0.14	0.09	-0.31	-0.04	-0.28	0.22	-0.32	0.71	2.56	-0.16	-0.15	-0.10
SB23	OC10a209	-0.15	-0.11	-0.51	-0.18	-0.12	0.09	-0.12	-0.31	0.43	0.68	-0.19	-0.19	-0.05
SB23	OC10a210	-0.09	0.05	-0.45	-0.19	0.06	-0.41	-0.19	-0.33	0.45	0.56	-0.13	-0.13	0.08
SB24	OC10a003	11.37	0.30	1.24	0.48	0.11	1.50	0.40	0.02	-0.70	0.61	-0.39	-0.15	0.36
SB24	OC10a004	0.06	-0.08	-0.23	-0.38	0.05	1.39	0.91	-0.15	0.58	0.45	-0.32	0.09	0.36
SB24	OC10a005	-0.24	0.06	-0.31	-0.21	0.03	-0.46	0.13	-0.35	0.54	1.24	-0.29	-0.07	-0.10
SB24	OC10a008	0.19	-0.10	-0.74	0.08	-0.07	0.21	0.24	-0.21	-0.43	0.85	-0.26	0.05	-0.19
SB24	OC10a009	-0.09	0.05	0.12	-0.19	0.01	0.17	0.14	-0.32	-0.76	1.32	-0.37	-0.06	0.05

Table A2.1: LA-ICPMS normalised analytical results for ablated sericite sites

Sample	Measurement	Host Rock	Alteration	Sulfides	Mineral	Li_ppm	B_ppm	Na_ppm	Mg_ppm	Al_ppm	Si_ppm	K_ppm	Ca_ppm	Ti_ppm	V_ppm	Cr_ppm
SB24	OC10a010	IGR	GS	Cpy-HS	Sericite	7.61	5.75	3625.14	7436.66	184075.75	216721.35	87498.36	-2059.51	2293.19	310.28	-12.75
SB24	OC10a011	IGR	GS	Cpy-HS	Sericite	7.57	5.41	4309.77	4546.59	146701.08	251601.97	97847.12	-2051.27	875.86	229.75	4.65
SB24	OC10a012	IGR	GS	Cpy-HS	Sericite	10.68	3.92	3953.43	6132.13	182569.21	214612.25	89717.48	-1435.84	2706.96	517.08	9.71
SB24	OC10a013	IGR	GS	Cpy-HS	Sericite	8.50	-6.91	3884.00	5908.72	187083.03	214590.13	89434.71	-1784.65	2296.72	363.20	8.49
SB24	OC10a014	IGR	GS	Cpy-HS	Sericite	6.45	-8.23	4053.74	4775.95	171422.39	228365.10	93950.42	-1712.24	1727.73	287.93	-7.81
SB24	OC10a015	IGR	GS	Cpy-HS	Sericite	10.75	-9.02	3445.00	9126.01	175086.75	224132.60	91358.29	-1430.41	1083.52	261.54	-5.33

Table A2.1: LA-ICPMS normalised analytical results for ablated sericite sites

Sample	Measurement	Mn_ppm	Fe_ppm	Co_ppm	Ni_ppm	Cu_ppm	Zn_ppm	As_ppm	Sr_ppm	Y_ppm	Zr_ppm	Nb_ppm	Ag_ppm	Sn_ppm	Sb_ppm	Ba_ppm	La_ppm
SB24	OC10a010	11.03	11573.19	0.78	2.98	3.74	2.64	-3.81	2.71	-0.07	1.13	4.67	-1.14	25.51	-1.49	971.29	0.05
SB24	OC10a011	11.49	6441.71	0.35	5.69	5.25	2.53	-2.82	7.18	0.14	0.22	1.50	-0.94	13.88	-1.25	685.91	-0.21
SB24	OC10a012	14.04	15142.15	0.78	2.96	4.12	-2.75	-2.19	2.60	0.05	1.08	5.07	-0.80	25.51	-0.87	454.55	-0.15
SB24	OC10a013	11.13	10947.21	0.34	1.47	5.55	-2.49	-1.45	5.13	0.03	0.57	4.43	-0.71	22.13	-0.87	641.15	-0.09
SB24	OC10a014	11.44	9784.40	0.51	2.97	6.42	-3.63	-3.51	3.40	0.05	0.85	2.77	-0.79	17.18	-1.50	665.31	-0.09
SB24	OC10a015	20.35	10469.94	1.39	10.15	12.77	2.18	-2.80	5.51	-0.10	0.47	2.19	-0.80	24.93	-1.28	709.59	0.08

Table A2.1: LA-ICPMS normalised analytical results for ablated sericite sites

Sample	Measurement	Ce_ppm	Eu_ppm	Gd_ppm	Yb_ppm	Lu_ppm	Hf_ppm	Ta_ppm	Au_ppm	Tl_ppm	Pb_ppm	Bi_ppm	Th_ppm	U_ppm
SB24	OC10a010	-0.23	-0.09	-0.46	-0.54	-0.07	0.16	-0.23	-0.39	-0.64	-0.56	-0.22	-0.07	-0.11
SB24	OC10a011	0.17	-0.17	0.04	-0.53	-0.05	0.04	-0.21	-0.39	-0.57	0.76	-0.24	-0.16	0.04
SB24	OC10a012	0.04	-0.15	-0.23	-0.16	-0.09	-0.25	0.33	-0.26	-0.48	0.32	-0.34	-0.24	0.06
SB24	OC10a013	0.03	0.04	-0.24	0.08	0.03	-0.26	0.63	-0.40	-0.53	-0.36	-0.22	-0.11	0.03
SB24	OC10a014	-0.13	-0.11	0.08	0.03	-0.09	-0.28	0.24	-0.36	-0.62	0.53	-0.27	-0.08	-0.13
SB24	OC10a015	0.08	0.07	-0.36	-0.39	-0.11	-0.27	0.21	-0.37	0.45	0.76	-0.28	-0.14	0.16

**Appendix 3: LA-ICPMS normalised analytical results for  
ablated apatite, xenotime and monazite sites.**

Table A3.1: LA-ICPMS normalised analytical results for ablated apatite, xenotime and monazite sites.

SampleName	Reading	Mg24	Ca43	V51	Mn55	Fe56	Sr88	Y89	La139	Ce140	Nd146	Sm147	Eu153	Gd157	Dy163
NIST610	1	437	81475	451	451	461	520	464	439	452	429	446	444	442	433
NIST610	2	434	81475	453	444	459	514	464	441	457	431	456	446	450	437
14971Mon	3	<0.6263	<1038.0610	<1.1303	<18.8812	<22.7563	1	47055	110653	366846	247825	76199	23	44576	12100
14971Mon	4	<0.4657	<1513.7522	2	<28.8567	<32.2917	1	60621	140399	468717	317975	97545	31	57824	15823
RGL4b	5	2	1000	0	<1.2777	139	3	3162	14356	27946	11115	1995	301	2072	961
RGL4b	6	0	1000	0	<1.1458	<1.4736	3	2762	12493	24387	9757	1748	264	1834	838
Banaeira	7	<0.0270	1000	<0.1066	<1.6952	<1.9343	0	1832	13147	32164	14178	6264	16	4209	808
Banaeira	8	<0.0548	1000	<0.1071	<1.8800	<1.9477	0	1826	13363	32654	14353	6400	16	4253	819
SB08_Monazite	9	21218	6486792	1210	<1512	18780	3554484	603	205319	386205	128438	12253	1562	10617	673
SB22_Monazite	10	2	9916	24	<42	58	311	17775	99916	306102	224770	50267	3088	34071	8441
SB17_Monazite	11	15	4307	133	<91	1895	61	20197	49811	236522	283391	91066	4635	52090	12521
SB17_Xenotime	12	11	<1777	562	<32	1500	12	363548	12	258	4057	10818	1706	39438	70322
SB17_Xenotime	13	3	<1009	1239	20	243	12	366624	23	286	3905	11266	1823	40476	69619
SB17_Xenotime	14	4	<1992	506	<45	199	12	365036	14	314	5407	13107	2136	40181	65413
SB17_Xenotime	15	4	<1622	16	<30	168	18	361535	167	870	5044	11348	2228	35381	63808
SB18_Monazite	16	22	7386	15	<33	36	104	16066	134725	304616	191681	49200	4483	35272	8522
SB12_Xenotime	17	22519	38411	691	635	50185	38	388950	178	1875	3938	4971	2159	21256	47341
SB12_Xenotime	18	674	8939	131	42	35742	639	373610	407	1392	2328	3272	1195	13383	45614
14971Mon	20	<1.3920	<4233.4628	<4.7844	<71.5766	<91.4402	2	175572	407959	1351296	930797	281801	88	168266	45067
RGL4b	21	<0.0460	1000	3	<2.7778	<3.4266	4	6764	28718	55820	22692	3886	251	4106	1852
RGL4b	22	3	1000	3	<3.1139	130	4	6658	28219	55895	23002	3895	253	4111	1849
Banaeira	23	0	1000	<0.1070	<1.5114	<1.6997	0	1694	12371	30282	13428	5879	14	3878	749
Banaeira	24	<0.0324	1000	<0.0960	<1.8521	<2.0477	0	1900	13720	33356	14731	6546	17	4399	857
14971Mon	25	<0.4175	<1035.8430	<1.2200	<18.7393	<23.6360	0	47624	110267	367197	248294	77032	21	45497	12328
14971Mon	26	<0.1472	1000	<0.9204	<15.3876	<18.1607	0	37415	88179	292306	193762	61131	18	35508	9555
NIST610	27	423	81475	443	438	453	516	457	440	452	433	454	448	454	437
NIST610	28	426	81475	448	440	453	510	460	438	446	424	444	442	450	434
NIST610	29	431	81475	447	441	454	514	463	438	452	433	458	452	450	442
NIST610	30	433	81475	452	444	464	515	460	441	451	428	455	446	443	434
OD306	31	110	393600	3	173	429	196	1423	3247	7868	3022	402	51	469	232
OD306	32	106	393600	2	175	422	190	1411	3221	7769	2970	400	51	459	224
OtterLake	33	49	393600	14	117	186	1673	893	2563	6580	2982	418	70	408	175

Table A3.1: LA-ICPMS normalised analytical results for ablated apatite, xenotime and monazite sites.

SampleName	Reading	Er166	Yb172	Hg202	Pb204	Pb206	Pb207	Pb208	Th232	U238	FileName	BG1	BG2	SG1	SG2	IS
NIST610	1	450	441	n.d.	423	422	422	423	454	458	OC14A001	1	26	36	60	Ca43
NIST610	2	455	453	n.d.	424	422	420	421	450	458	OC14A002	1	26	36	60	Ca43
14971Mon	3	1701	713	n.d.	<8.1131	1358	103	5116	61506	2253	OC14A003	1	26	36	60	Ca43
14971Mon	4	2231	965	n.d.	<9.9533	1780	136	6843	79437	2862	OC14A004	1	26	36	60	Ca43
RGL4b	5	254	90	n.d.	1	736	79	793	5221	649	OC14A005	1	26	36	60	Ca43
RGL4b	6	220	78	n.d.	<0.6041	553	59	736	4877	490	OC14A006	1	26	36	60	Ca43
Banaeira	7	45	15	n.d.	<0.7186	155	10	449	9662	477	OC14A007	1	26	36	60	Ca43
Banaeira	8	46	15	n.d.	<0.9039	160	10	457	9834	481	OC14A008	1	26	36	60	Ca43
SB08_Monazite	9	62	<20		176550	197800	184768	188841	1574	61	OC14A009	1	26	36	45	Ce140
SB22_Monazite	10	1293	408		<21	49	13	93	28356	1984	OC14A010	1	26	36	48	Ce140
SB17_Monazite	11	1658	463		<41	69	5	35	13790	3944	OC14A011	1	26	32	38	Ce140
SB17_Xenotime	12	39670	29980	n.d.	<12	57	4	9	3296	3339	OC14A012	1	26	40	52	Y89
SB17_Xenotime	13	37952	24864	n.d.	<9	26	2	4	1329	1250	OC14A013	1	26	36	60	Y89
SB17_Xenotime	14	37725	28692	n.d.	<19	41	2	8	2843	2209	OC14A014	1	26	36	45	Y89
SB17_Xenotime	15	41930	39620	n.d.	<14	92	5	2	837	5497	OC14A015	1	26	36	45	Y89
SB18_Monazite	16	1117	324		<16	32	2	9	2989	1709	OC14A016	1	26	36	50	Ce140
SB12_Xenotime	17	34523	34489	n.d.	<231	3996	286	469	10650	16509	OC14A017	1	26	36	60	Y89
SB12_Xenotime	18	49034	65124	n.d.	24	718	56	1248	487988	38912	OC14A018	1	26	36	60	Y89
14971Mon	20	6382	2708	n.d.	<34.0711	5313	405	21223	253220	8792	OC14A020	1	26	36	60	Ca43
RGL4b	21	570	188	n.d.	<1.3846	212	23	1743	11607	191	OC14A021	1	26	36	60	Ca43
RGL4b	22	552	180	n.d.	<1.3381	209	22	1691	11398	183	OC14A022	1	26	36	60	Ca43
Banaeira	23	41	14	n.d.	<0.7090	143	9	412	8908	441	OC14A023	1	26	36	60	Ca43
Banaeira	24	47	16	n.d.	<0.7987	163	10	464	9887	486	OC14A024	1	26	36	60	Ca43
14971Mon	25	1761	763	n.d.	<9.9720	1467	111	5747	67739	2353	OC14A025	1	26	36	60	Ca43
14971Mon	26	1377	584	n.d.	<6.6750	1133	87	4506	53330	1858	OC14A026	1	26	36	60	Ca43
NIST610	27	460	452	n.d.	429	424	420	420	448	455	OC14A027	1	26	36	60	Ca43
NIST610	28	450	441	n.d.	414	420	424	426	462	463	OC14A028	1	26	36	60	Ca43
NIST610	29	459	460	n.d.	434	438	436	431	461	461	OC14B029	1	26	36	60	Ca43
NIST610	30	451	450	n.d.	428	428	432	433	463	468	OC14B030	1	26	36	60	Ca43
OD306	31	128	104	n.d.	<1.7321	19	2	13	93	18	OC14B031	1	26	36	60	Ca43
OD306	32	125	103	n.d.	<1.5436	18	2	12	91	18	OC14B032	1	26	36	60	Ca43
OtterLake	33	86	62	n.d.	9	72	12	78	903	110	OC14B033	1	26	36	60	Ca43

Table A3.1: LA-ICPMS normalised analytical results for ablated apatite, xenotime and monazite sites.

SampleName	Reading	Mg24	Ca43	V51	Mn55	Fe56	Sr88	Y89	La139	Ce140	Nd146	Sm147	Eu153	Gd157	Dy163
McClureMnt	34	22	393600	25	77	54	4213	185	1523	2444	747	88	31	107	37
SB01_Apatite	35	60168	393600	148	4639	139805	70	2384	617	2007	1422	359	14	454	390
SB01_Apatite	36	43	393600	9	1256	291	55	2693	689	2511	1927	507	10	535	444
SB01_Apatite	37	94	393600	20	1110	422	51	2269	523	1780	1281	352	11	412	349
SB01_Apatite	38	68	393600	6	1239	2260	49	3676	878	2879	2018	586	13	685	619
SB12_Apatite	39	446	393600	3	245	819863	12336	257	969	1503	418	61	11	84	43
SB01_Apatite	40	36	393600	3	1170	235	58	6615	814	2741	2434	880	21	1156	1095
SB01_Apatite	41	53	393600	4	1305	249	54	1197	223	702	545	163	8	213	176
SB01_Apatite	42	23	393600	17	977	162	73	1568	550	1757	1221	296	23	341	269
SB01_Apatite	43	57	393600	12	1437	404	52	2123	745	2471	1772	416	9	444	361
SB01_Apatite	44	39	393600	5	1060	353	51	2994	803	2865	2283	580	12	643	510
SB01_Apatite	45	240	393600	<58.5886	<900.2021	10583	2313	<4.4722	2	17	<23.3739	<19.3501	4	<0.0000	<0.0000
SB01_Apatite	46	26	393600	6	1261	160	61	3514	654	2134	1603	499	28	611	551
SB21_Apatite	47	43	393600	<1.5465	6994	87	1089	44	21	54	41	12	12	13	8
OD306	48	111	393600	3	176	430	196	1454	3256	7902	3013	409	52	481	233
OD306	49	115	393600	3	178	439	198	1435	3157	7722	2955	399	51	468	231
NIST610	50	443	81475	456	449	460	521	467	444	463	435	464	455	458	448
OtterLake	51	50	393600	14	118	198	1677	883	2573	6561	3012	421	70	406	174
McClureMnt	52	17	393600	18	70	33	4166	162	1359	2143	640	76	27	96	31
SB21_Apatite	53	204	393600	5	1382	163	736	135	65	175	134	44	19	45	28
SB21_Apatite	54	19	393600	<1.7526	4258	<33.5950	883	36	16	41	27	8	6	10	5
SB08_Apatite	55	3463	393600	143	<59.0427	2951	216753	59	2806	5322	1853	178	26	190	28
SB08_Apatite	56	130	393600	<5.9171	4877	<95.5985	1310	246	39	163	192	66	21	85	58
SB08_Apatite	57	29903	<1197815.6341	<1836.7768	<25079.2416	57694	1044	29	25	<0.0000	<0.0000	<0.0000	34	<0.0000	<0.0000
SB08_Apatite	58	51	393600	<1.9513	1989	46	1165	193	29	103	115	51	12	57	40
SB08_Apatite	59	4204	393600	97	2738	2134	880	120	19	59	54	25	7	34	23
SB08_Apatite	60	14	393600	<1.2983	6032	<25.8986	1611	90	13	24	15	6	2	15	12
SB08_Apatite	61	20	393600	<1.5844	2554	<27.3058	1521	113	18	47	32	9	3	19	16
SB08_Apatite	62	13	393600	<1.5362	3697	<22.2626	1410	178	26	60	39	19	5	30	28
SB08_Apatite	63	152	393600	<5.8946	3341	<121.4872	1175	159	34	143	149	49	18	57	24
SB17_Apatite	64	435	393600	<1.2665	3617	3369	360	888	252	753	585	199	81	219	194
SB17_Apatite	65	458	393600	<2.1935	7636	1483	535	317	112	413	426	163	98	159	93

Table A3.1: LA-ICPMS normalised analytical results for ablated apatite, xenotime and monazite sites.

SampleName	Reading	Er166	Yb172	Hg202	Pb204	Pb206	Pb207	Pb208	Th232	U238	FileName	BG1	BG2	SG1	SG2	IS
McClureMnt	34	18	13	n.d.	6	5	2	3	33	12	OC14B034	1	26	36	60	Ca43
SB01_Apatite	35	221	213	n.d.	<27.9720	22	12	16	74	29	OC14B035	1	26	36	45	Ca43
SB01_Apatite	36	278	254	n.d.	<9.2425	16	6	9	70	31	OC14B036	1	26	36	60	Ca43
SB01_Apatite	37	224	204	n.d.	13	15	9	11	47	19	OC14B037	1	26	36	60	Ca43
SB01_Apatite	38	366	330	n.d.	13	24	7	10	108	55	OC14B038	1	26	36	48	Ca43
SB12_Apatite	39	15	11	n.d.	99	109	97	101	64	87	OC14B039	1	26	36	45	Ca43
SB01_Apatite	40	638	539	n.d.	<9.5566	31	7	11	130	85	OC14B040	1	26	36	54	Ca43
SB01_Apatite	41	114	110	n.d.	<7.9756	10	4	7	12	13	OC14B041	1	26	36	60	Ca43
SB01_Apatite	42	151	135	n.d.	<9.1891	7	3	4	33	13	OC14B042	1	26	36	60	Ca43
SB01_Apatite	43	216	211	n.d.	<8.7409	11	6	8	46	17	OC14B043	1	26	36	60	Ca43
SB01_Apatite	44	305	267	n.d.	<8.1558	14	5	8	88	33	OC14B044	1	26	36	48	Ca43
SB01_Apatite	45	<7.7975	6	n.d.	<390.8842	257	242	248	<0.7883	1	OC14B045	1	26	40	60	Ca43
SB01_Apatite	46	351	326	n.d.	<10.4522	24	7	9	60	59	OC14B046	1	26	36	60	Ca43
SB21_Apatite	47	2	2	n.d.	22	20	19	20	2	1	OC14B047	1	26	36	60	Ca43
OD306	48	130	105	n.d.	<1.4588	18	2	12	92	18	OC14B048	1	26	36	60	Ca43
OD306	49	128	105	n.d.	<1.2632	18	2	12	91	18	OC14B049	1	26	36	60	Ca43
NIST610	50	466	458	n.d.	435	435	438	440	473	478	OC14B050	1	26	36	60	Ca43
OtterLake	51	85	65	n.d.	8	71	13	79	908	111	OC14B051	1	26	36	60	Ca43
McClureMnt	52	15	11	n.d.	5	5	2	3	33	11	OC14B052	1	26	36	60	Ca43
SB21_Apatite	53	12	6	n.d.	10	2	2	2	28	1	OC14B053	1	26	34	42	Ca43
SB21_Apatite	54	2	3	n.d.	<12.8990	6	4	5	3	0	OC14B054	1	26	48	60	Ca43
SB08_Apatite	55	4	1	n.d.	4805	5286	4847	4964	8	2	OC14B055	1	26	36	60	Ca43
SB08_Apatite	56	23	14	n.d.	<40.6027	14	14	14	36	11	OC14B056	1	26	36	60	Ca43
SB08_Apatite	57	102	<0.0000	n.d.	<11960.8688	<102.1464	193	232	33	<11.3748	OC14B057	1	26	36	60	Ca43
SB08_Apatite	58	20	11	n.d.	14	9	10	10	15	4	OC14B058	1	26	36	50	Ca43
SB08_Apatite	59	10	7	n.d.	<13.1803	7	7	7	17	3	OC14B059	1	26	36	50	Ca43
SB08_Apatite	60	7	6	n.d.	14	18	17	18	0	3	OC14B060	1	26	36	60	Ca43
SB08_Apatite	61	10	9	n.d.	11	13	11	12	0	3	OC14B061	1	26	36	46	Ca43
SB08_Apatite	62	15	10	n.d.	<9.2557	15	14	14	0	4	OC14B062	1	26	36	50	Ca43
SB08_Apatite	63	9	5	n.d.	<58.1461	10	9	10	12	5	OC14B063	1	26	36	48	Ca43
SB17_Apatite	64	93	74	n.d.	8	2	1	1	1	3	OC14B064	1	26	36	60	Ca43
SB17_Apatite	65	30	20	n.d.	<13.2803	8	7	7	0	0	OC14B065	1	26	46	60	Ca43

Table A3.1: LA-ICPMS normalised analytical results for ablated apatite, xenotime and monazite sites.

SampleName	Reading	Mg24	Ca43	V51	Mn55	Fe56	Sr88	Y89	La139	Ce140	Nd146	Sm147	Eu153	Gd157	Dy163
OD306	66	64	393600	3	143	310	171	1346	2955	7203	2754	372	47	439	211
NIST610	67	426	81475	451	444	458	517	464	440	454	430	455	450	456	438
OtterLake	68	51	393600	14	122	202	1702	902	2586	6626	3024	421	70	403	173
McClureMnt	69	17	393600	11	81	39	4233	244	1994	3147	947	112	45	138	46
SB17_Apatite	70	795	393600	<1.6989	4190	3908	363	319	174	483	327	109	67	111	75
SB17_Apatite	71	481	393600	<1.4229	3897	3195	389	392	150	464	352	110	44	102	76
SB17_Apatite	72	250	393600	6	16829	1433	429	122	55	175	158	56	41	53	34
SB17_Apatite	73	333	393600	<1.4577	3248	2922	360	942	212	729	694	253	74	270	213
SB17_Apatite	74	130	393600	<1.2465	12128	458	353	125	22	86	81	31	37	28	20
SB17_Apatite	75	355	393600	<394.1055	39308	6406303	379	1367	<25.9385	141	213	107	122	<170.6888	250
SB18_Apatite	76	4606	393600	104	<96.3426	1635	161650	104	135	330	221	47	26	38	34
SB18_Apatite	77	5424	393600	245	<83.8156	11044	189332	279	1789	5207	2315	456	112	502	135
SB23_Apatite	78	1456	393600	<174.2016	16533	5276	11158	216	105	444	320	153	93	<104.0900	67
SB23_Apatite	79	174	393600	<1.6747	56719	420	698	65	66	151	91	24	14	26	13
SB22_Apatite	80	123	393600	8	1576	121	467	396	73	265	269	100	29	120	77
OtterLake	81	51	393600	14	120	200	1704	911	2596	6647	3013	425	71	407	176
McClureMnt	82	24	393600	12	105	65	4728	197	1294	2115	753	101	25	109	40
OD306	83	103	393600	2	169	389	189	1153	2410	6000	2303	312	40	356	178
OD306	84	97	393600	2	166	379	183	1126	2372	5872	2262	312	41	355	180
NIST610	85	432	81475	449	442	455	510	458	437	449	426	445	438	437	425
NIST610	86	435	81475	450	447	462	519	464	441	454	431	454	449	450	442
NIST610-zr	87	1	400	10	13	2	11	12	11	13	10	11	10	10	41
NIST610-zr	88	1	400	10	13	2	11	12	11	13	10	11	10	10	41

Table A3.1: LA-ICPMS normalised analytical results for ablated apatite, xenotime and monazite sites.

SampleName	Reading	Er166	Yb172	Hg202	Pb204	Pb206	Pb207	Pb208	Th232	U238	FileName	BG1	BG2	SG1	SG2	IS
OD306	66	118	96	n.d.	<1.3252	18	2	12	86	18	OC14B066	1	26	36	60	Ca43
NIST610	67	455	451	n.d.	432	428	423	421	452	456	OC14B067	1	26	36	60	Ca43
OtterLake	68	86	63	n.d.	10	70	12	75	880	109	OC14B068	1	26	36	60	Ca43
McClureMnt	69	22	18	n.d.	4	8	2	4	53	18	OC14B069	1	26	36	60	Ca43
SB17_Apatite	70	33	26	n.d.	<10.2906	2	2	2	0	5	OC14B070	1	26	46	60	Ca43
SB17_Apatite	71	36	31	n.d.	<8.0588	3	3	3	1	2	OC14B071	1	26	36	47	Ca43
SB17_Apatite	72	12	6	n.d.	34	33	29	31	0	0	OC14B072	1	26	36	60	Ca43
SB17_Apatite	73	96	63	n.d.	<9.2750	2	1	2	0	0	OC14B073	1	26	40	60	Ca43
SB17_Apatite	74	11	6	n.d.	33	36	33	33	0	0	OC14B074	1	26	36	46	Ca43
SB17_Apatite	75	160	110	n.d.	<2182.9245	130	129	117	11	25	OC14B075	1	26	40	60	Ca43
SB18_Apatite	76	9	6	n.d.	233	253	224	236	3	1	OC14B076	1	26	49	60	Ca43
SB18_Apatite	77	22	13	n.d.	414	442	382	384	2711	54	OC14B077	1	26	36	60	Ca43
SB23_Apatite	78	17	<38.2027	n.d.	<1374.1148	601	504	553	52	122	OC14B078	1	26	44	60	Ca43
SB23_Apatite	79	4	2	n.d.	121	139	130	136	0	1	OC14B079	1	26	36	60	Ca43
SB22_Apatite	80	35	15	n.d.	<22.9930	8	6	5	15	26	OC14B080	1	26	36	45	Ca43
OtterLake	81	89	64	n.d.	7	71	12	79	919	113	OC14B081	1	26	36	60	Ca43
McClureMnt	82	18	13	n.d.	3	3	1	2	18	6	OC14B082	1	26	36	60	Ca43
OD306	83	100	79	n.d.	<1.4918	14	2	7	50	14	OC14B083	1	26	36	60	Ca43
OD306	84	100	80	n.d.	<1.3864	14	2	7	50	14	OC14B084	1	26	36	60	Ca43
NIST610	85	447	440	n.d.	418	415	418	422	451	457	OC14B085	1	26	36	60	Ca43
NIST610	86	457	454	n.d.	423	429	427	424	456	461	OC14B086	1	26	36	60	Ca43
NIST610-zr	87	7	47	n.d.	843	11	52	6	11	0	OC14C087	1	26	36	60	Ca43
NIST610-zr	88	8	47	n.d.	849	11	52	6	11	0	OC14C088	1	26	36	60	Ca43